Future ecosystem services of temperate grasslands

bridging scales towards high-resolution spatio-temporal monitoring

Wolfgang Alexander Obermeier

2018

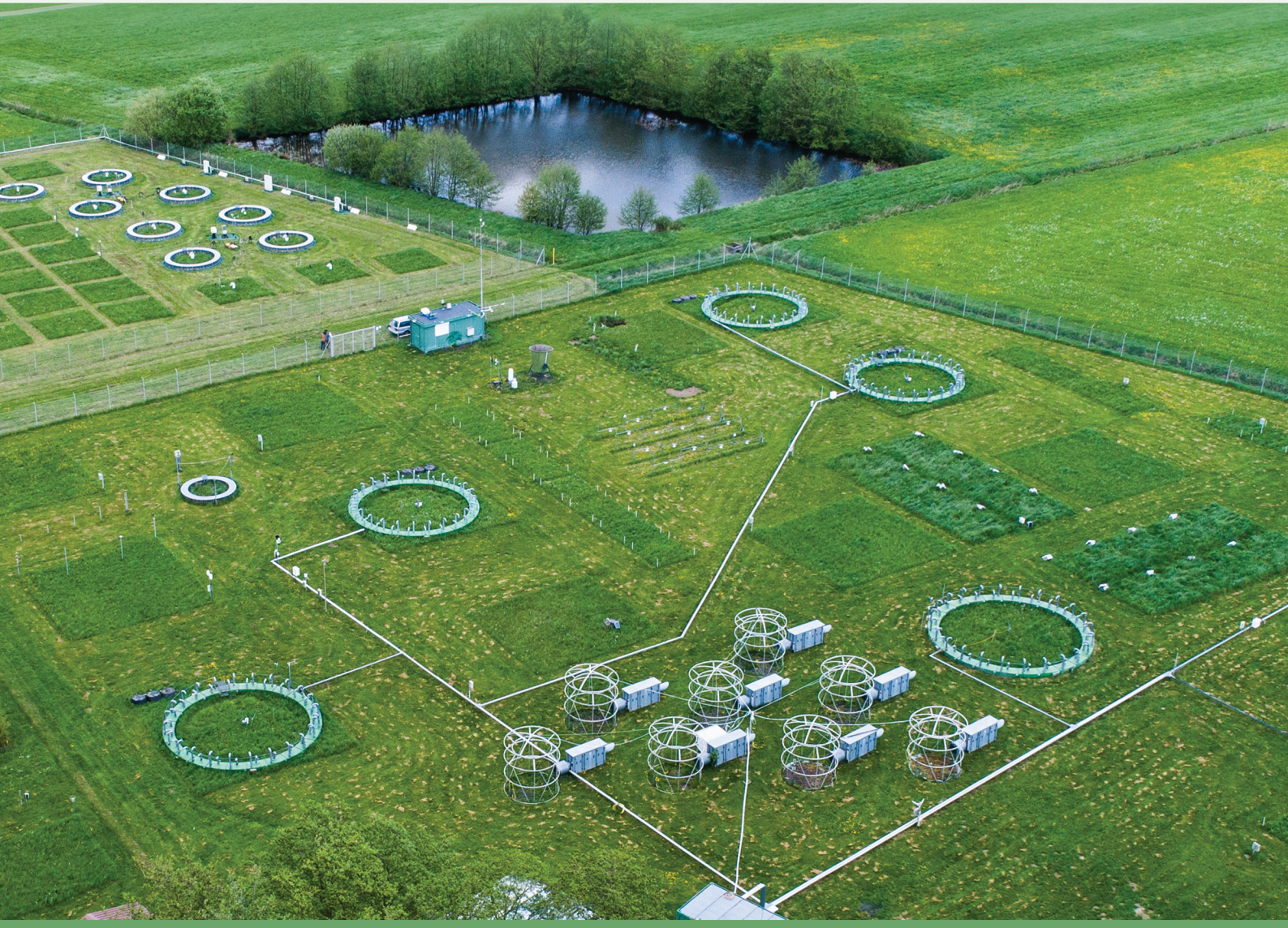

Cover: Aerial view of the Giessen Free Air Carbon dioxide Enrichment (GiFACE) experiment (photograph and cover design by Sebastian Egli, 2018)

Future ecosystem services of temperate grasslands:

bridging scales towards high-resolution spatio-temporal monitoring

kumulative Dissertation
zur
Erlangung des Doktorgrades der
Naturwissenschaften
(Dr. rer. nat.)

dem Fachbereich Geographie
der Philipps-Universität Marburg
vorgelegt von

Diplom Geograph

Wolfgang Alexander Obermeier

aus Ebersberg

Marburg / Lahn, Oktober 2018

Vom Fachbereich Geographie
der Philipps-Universität Marburg als Dissertation
am 21.01.2019 angenommen.

Erstgutachter: Prof. Dr. Jörg Bendix
Zweitgutachter: Prof. Dr. Jürg Luterbacher
Drittgutachter: Prof. Dr. Karsten Wesche

Tag der mündlichen Prüfung: 14.02.2019
Hochschulkennziffer: 1180

Table of contents

List of Figures

List of Tables

Summary

Temperate grasslands cover approximately 38% of the European agricultural area and provide various ecosystem services such as forage production, biodiversity conservation and carbon sequestration. These ecosystem services strongly depend on the biomass productivity, which with future global changes remains uncertain. Above all, an increasing atmospheric CO_2 concentration ($[CO_2]$) is assumed to enhance biomass productivity (called the CO_2 fertilization effect; CFE) in particular under dry and hot conditions, while such probable future environmental conditions rather decrease the grassland productivity in general. However, recent doubts about the classic view on the CFE call for in-depth analysis of the interacting effects of the CFE and varying environmental conditions on grassland productivity, which is usually done by CO_2 enrichment studies. Here, Free Air Carbon dioxide Enrichment (FACE) experiments have proven to be the most suitable approaches due to their minimal invasive character. Consequently, this study uses the worldwide longest operating FACE experiment on grassland, the Giessen FACE facility (GiFACE), to improve the assessment of the potential future of ecosystem services under global change.

Initially, it was tested whether the CFE in the GiFACE grassland is reduced under more extreme average weather conditions and after single extreme climatic events. To cope with the real-world conditions, a specific approach, called moving subset analysis, was developed to enable the quantification of the CFE in dependence of average weather conditions under varying $[CO_2]$s. Additionally, a time series analysis was developed to link single extreme climatic events (ECEs) with the strength of the CFE. It was found that the CFE was significant and strong under local average environmental conditions (defined by ± 1 SD of long-term average conditions), but decreased under more extreme weather conditions. The strongest decrease in the CFE under ECEs was associated with intensive and long heat waves,

and could be quantified to a large extent by calculating the Killing Degree Days (∼30% variance of the magnitude of the CFE).

Since the CFE was found to be reduced under unfavourable environmental conditions, the potential of future grassland productivity was assessed in a further step. Therefore, potential future climate regimes and statistical models of biomass were created using the long-term experimental observations. Biomass was predicted using climate variable alterations within the potential climate regimes. The comparison of the potential regimes with the climate model projections for the years with a similar [CO_2] compared to enriched [CO_2]s revealed that biomass is likely to be reduced in the mid of 21st century despite the increase in [CO_2], and thus that the CFE cannot compensate yield losses due to unfavourable environmental conditions.

Short-term environmental changes such as ECEs were shown to affect the grassland productivity while their influence might be elusive to the traditional destructive sampling approaches at harvest dates. To overcome these sampling restrictions, in the final step of this study, the feasibility of the non-invasive hyperspectral monitoring of the GiFACE grassland on a high spatio-temporal resolution was investigated. Thus, methods were developed to work with hyperspectral data and the comprehensive statistical software CRAN R. The methods developed were used to derive transfer functions between hyperspectral measurements and various laboratory-derived grassland traits by applying machine learning approaches. Good to very good leave-one-out prediction results revealed that the most important ecosystem services can precisely be predicted by hyperspectral approaches. Hyperspectral predictions of the most important grassland traits during the vegetation period highlighted how remote sensing approaches can improve grassland management in future.

Alarmingly, the reduced CFE and biomass productivity in grasslands under unfavourable future environmental conditions as detected in this thesis, suggest decreasing ecosystem services such as carbon sequestration and related climate mitigation function in future. This may – in a vicious circle – lead to a further aggravation of expected global changes and urgently calls for better mitigation and adaptation strategies. Measures necessary for this could be instructed and monitored by remote sensing methods, as was shown by the present thesis.

Zusammenfassung

Grünländer bedecken etwa 38% der europäischen Agrarfläche und bieten verschiedene Ökosystemdienstleistungen wie Futterproduktion, Biodiversitätsschutz und Kohlenstoffbindung. Diese Ökosystemleistungen hängen stark von der Biomasseproduktion ab, welche aufgrund des globalen Wandels in Zukunft ungewiss ist. Allem voran wird davon ausgegangen, dass eine steigende atmosphärische CO_2-Konzentration ($[CO_2]$) die Biomasseproduktivität insbesondere unter trockenen und heißen Bedingungen erhöht (genannt CO_2-Düngeeffekt; CFE), während im Allgemeinen solche wahrscheinlichen zukünftigen Umweltbedingungen die Grünlandproduktivität eher verringern. Jüngst aufgekommene Zweifel an der klassischen Sichtweise auf den CFE erfordern jedoch eine gründliche Analyse der Wechselwirkungen des CFE mit unterschiedlichen Umgebungsbedingungen auf die Grünlandproduktivität, welche in der Regel mittels CO_2-Anreicherungsstudien erreicht wird. Hier haben sich Free Air Carbon dioxide Enrichment (FACE) Experimente aufgrund ihres minimal-invasiven Charakters als am besten geeignete Ansätze bewiesen. Folglich verwendet diese Studie das weltweit am längsten laufende FACE-Experiment auf Grünland, das Giessen FACE (GiFACE), um den potentiellen, zukünftigen Wert verschiedener Ökosystemleistungen unter Einfluss des globalen Wandels besser abschätzen zu können.

Zunächst wurde getestet, ob der CFE im GiFACE-Grünland unter extremeren durchschnittlichen Wetterbedingungen und nach extremen Klimaereignissen reduziert ist. Für die Quantifizierung des CFE in Abhängigkeit von durchschnittlichen Wetterbedingungen unter verschiedenen $[CO_2]$s wurde ein spezifischer Ansatz, genannt Moving Subset Analyse, entwickelt, um den realen Bedingungen Rechnung zu tragen. Zusätzlich wurde eine Zeitreihenanalyse entwickelt, um einzelne extreme Klimaereignisse (ECEs) mit der Stärke des CFE zu korrelieren. Es wurde festgestellt, dass der CFE unter den lokal durchschnittlichen Wetterbedingungen

signifikant und stark ausfiel (definiert durch ±1 SD der langfristigen durchschnittlichen Wetterbedingungen), unter extremeren Wetterbedingungen sich jedoch stark verringerte. Der stärkste Rückgang des CFE unter ECEs war mit intensiven und langen Hitzewellen verbunden und konnte weitgehend durch die Berechnung der Killing Degree Days quantifiziert werden (∼30% der Varianz des CFE).

Da festgestellt wurde, dass der CFE unter ungünstigen Umweltbedingungen reduziert ist, wurde das zukünftige Potenzial der Grünlandproduktivität in einem weiteren Schritt bewertet. Hierfür sind potenzielle zukünftige Klimaregime und statistische Modelle für den Biomassezuwachs auf Basis der langfristigen experimentellen Beobachtungen erstellt worden. Der Biomassezuwachs wurde mit leicht veränderten Klimavariablen innerhalb der potenziellen Klimaregime vorhergesagt. Der Vergleich der potentiellen Klimaregime mit den Prognosen von Klimamodellen für die Jahre mit einer ähnlichen [CO_2] im Vergleich zu der angereicherten [CO_2] ergab, dass die Biomasse in der Mitte des 21. Jahrhunderts trotz der Zunahme von [CO_2] voraussichtlich reduziert sein wird. Dies zeigt, dass der CFE Ertragsausfälle durch ungünstige Umgebungsbedingungen nicht kompensieren kann.

Kurzfristige Umweltveränderungen wie ECEs wirkten sich nachweislich auf die Produktivität des Grünlandes aus, während ihr Einfluss mittels traditioneller destruktiver Stichprobenverfahren zu den Erntezeiten schwer zu erheben ist. Um diese Einschränkungen durch die Probenahme zu überwinden, wurde im letzten Schritt dieser Studie die Machbarkeit des nicht-invasiven hyperspektralen Monitoring des GiFACE-Grünlands mit einer hohen raum-zeitlichen Auflösung untersucht. Um mit den hyperspektralen Daten und der umfassenden Statistiksoftware CRAN R zu arbeiten wurden spezifische Methoden entwickelt. Mit diesen Methoden wurden Transferfunktionen zwischen hyperspektralen Messungen und verschiedenen im Labor gemessenen Grünlandmerkmalen unter Anwendung maschineller Lernansätze abgeleitet. Gute bis sehr gute Leave-One-Out-Kreuzvalidierung Ergebnisse zeigten, dass die wichtigsten Ökosystemleistungen durch hyperspektrale Ansätze präzise vorhergesagt werden können. Hyperspektrale Vorhersagen der wichtigsten Grünlandmerkmale während der Vegetationsperiode zeigten, wie Fernerkundungsansätze das Grünlandmanagement in Zukunft verbessern können.

Alarmierend ist, dass ein reduzierter CFE und eine reduzierte Biomasseproduktivität in Grünland unter ungünstigen zukünftigen Umweltbedingungen, wie

sie in dieser Arbeit festgestellt wurden, einen abnehmenden Wert an Ökosystemdienstleistungen wie der Kohlenstoffsequestrierung und der damit verbundenen Klimaschutzfunktionen in Zukunft erwarten lassen. Dies kann – einem Teufelskreis ähnlich – zu einer weiteren Verschärfung der erwarteten globalen Veränderungen führen und erfordert dringend bessere Minderungs- und Anpassungsstrategien. Hierfür notwendige Maßnahmen könnten, wie die vorliegende Arbeit zeigt, durch Fernerkundungsmethoden angeleitet und überwacht werden.

1 Introduction

Grassland ecosystems, characterised by an extensive cover of grasses and other graminoid vegetation and little or no cover of trees and shrubs, are one of the world's major biome types (Blair et al., 2014). Grasslands cover approximately 26% of the terrestrial area (Foley et al., 2011), and approximately 50% of the worldwide grassland area is used as pastures (Ramankutty et al., 2008).

This enormous extent highlights the importance of grasslands for the provision of multiple ecosystem services like forage for wildlife and ruminants (globally supplying almost 50% of biomass for animals, Herrero et al. 2013), maintenance of hydrological cycles, provision of recreational space and biodiversity conservation (Christensen et al., 1996; Lemaire et al., 2011; Millennium Ecosystem Assessment, 2005). In total, the livelihood of an estimated 1.3 billion people depends directly on the goods and services derived from pastures (Herrero et al., 2013). Additionally, grasslands provide key functions within the global carbon cycle through the assimilation of carbon dioxide (CO_2), storing approximately 20% of the world's carbon pool (Schlesinger & Andrews, 2000; White et al., 2000). Thereby, grasslands are assumed to function as a sink for atmospheric CO_2, and consequently to mitigate climate change (the latter assumed to be "the single greatest threat to a sustainable future" as stated by United Nations Secretary-General Ban Ki-Moon at the Climate Leaders Summit 2014).

The CO_2 sink and adherent climate regulation functions of grasslands mainly depend on the carbon uptake in plants which is defined by biomass productivity (Parton et al., 2012; Peters et al., 2017). But, grassland productivity is uncertain under future global change conditions (Blair et al., 2014; Booth et al., 2012; Friedlingstein et al., 2006; Gao et al., 2016; IPCC, 2013; Reichstein et al., 2013; Schimel et al., 2015). Along with a globally increasing atmospheric CO_2 concentration ($[CO_2]$), climate models for central Europe project increases in the

mean air temperature, the variability of air temperature and of precipitation, and the occurrence of extreme weather events (Beniston et al., 2007; Easterling et al., 2000; IPCC, 2013; Meehl & Tebaldi, 2004; Sillmann et al., 2013). These alterations in the environmental conditions may have contrasting effects on the grassland productivity in future. As a result, the maintenance of the ecosystem services provided by grasslands remains unclear, and the strength of the future terrestrial carbon sink has been questioned (Booth et al., 2012; Cox et al., 2000; Fung et al., 2005; Huntzinger et al., 2017; IPCC, 2013; Reichstein et al., 2013; Schimel et al., 2015; Smith et al., 2016; Zhao & Running, 2010).

1.1 Motivation

In the most recent decades, steadily increasing extreme weather conditions have been observed around the globe, and strong evidence links the increase of heat waves and precipitation extremes to the human influence on climate (Coumou & Rahmstorf, 2012). For example, a particularly extreme climate event in Europe during the summer of 2003 is probably the consequence of anthropogenic global warming (Stott et al., 2004). In the summer of 2003, air temperatures up to 6°C above the long-term average and precipitation deficits up to 300 mm (50% below the average) occurred over Europe (Ciais et al., 2005; Fink et al., 2004; García-Herrera et al., 2010; Tubiello et al., 2007). This heat and drought event led to enormous adverse social, economic and environmental effects, with an estimate of 70 000 deaths mostly of the elderly (Robine et al., 2008), a loss of 10% of mass in alpine glaciers, record-breaking forest fires in Portugal, and estimated economic losses exceeding 10 billion US$ (García-Herrera et al., 2010). Regarding the terrestrial ecosystems, the summer heat and drought in 2003 caused a reduction by approximately 30% in the primary productivity across Europe and resulted in a very anomalous net source of CO_2 for the atmosphere, reversing the effect of four years of net ecosystem CO_2 sequestration (Ciais et al., 2005). Notably, such a reduction in Europe's primary productivity was unprecedented during the last century (Ciais et al., 2005), and the synoptic conditions that caused its emergence are assumed statistically extremely unlikely (Schär et al., 2004). Nevertheless, the next record-breaking droughts combined with heat waves were observed only a

few years later in Europe, in the summer 2015 (Ionita et al., 2017; Laaha et al., 2017; NOAA National Centers for Environmental Information, 2016; Orth et al., 2016) and in the summer 2018 (NOAA National Centers for Environmental Information, 2018).

Consistent with the observed trend for the past decades, it is projected that along with increasing [CO_2] and rising air temperatures, the intensity, frequency and duration of heat waves will increase in future summers in Central Europe (Beniston et al., 2007; Meehl & Tebaldi, 2004; Schär et al., 2004; Seneviratne et al., 2014; Sillmann et al., 2013). Additionally, Orth et al. (2016) showed that a future drying out in the summer is very likely for Central Europe. Independent from such changes in the precipitation totals, the frequency of meteorological droughts (medium confidence) and heavy precipitation events (high confidence) is likely to increase in Europe, and the intervening dry spells between precipitation events are projected to become longer (Easterling et al., 2000; Hov et al., 2013; IPCC, 2013; Seneviratne et al., 2012; Sillmann et al., 2013; Solomon et al., 2007; Tebaldi et al., 2006). Consequently, single extreme climatic events (ECEs) such as heat-waves, droughts, heavy rainfall, and frosts will increase in both frequency and intensity (Beniston et al., 2007; Christidis et al., 2015; Easterling et al., 2000; IPCC, 2013; Jentsch et al., 2007; Seneviratne et al., 2012; Sillmann et al., 2013; Williams et al., 2014). Christidis et al. (2015) even predicted that summers similar to the record-breaking hot and dry summer 2003 will be very common by the mid 21st century.

Considering projected global changes, it is conceivable that the terrestrial ecosystems in Europe will be subject to much more extreme weather conditions, a higher frequency and intensity of extreme climatic events, and increased [CO_2] in future (IPCC, 2013; Jentsch et al., 2007). Consequently, the productivity of European grasslands, which consist mainly of permanent meadows and pastures composed of C3 species, will be modified under global change-related environmental alterations. This is of particular interest since grasslands are one of the major biomes, covering approximately 38% of the whole agricultural area within Europe (Food and Agriculture Organization of the United Nations Statistics Division, 2015). Thus, the value of various ecosystem services provided by grasslands, such as a considerable share of Europe's green fodder supply and the livestock sector,

is uncertain. Additionally, this may feedback into climate change since European grasslands acted as carbon sinks in the past five decades (1961-2010; Chang et al., 2016, 2015), and it is estimated that Europe's terrestrial biosphere absorbs 7 to 12% of the anthropogenic CO_2 emissions of Europe (Janssens et al., 2003).

Since the plant species of European grasslands feature the C3 photosynthetic pathway (most common carbon fixation process in plants growing under temperate climate conditions), it is expected that a reduced CO_2 limitation in plants growing under increased [CO_2] ([eCO_2]) enhances the biomass productivity, which is usually termed the CO_2 fertilization effect (CFE). The CFE is assumed to be particularly strong under hot and dry conditions (described more in detail in section 2.1.3; Ainsworth & Rogers, 2007; Coughenour & Chen, 1997; Drake et al., 1997; Idso et al., 1987; Jordan & Ogren, 1984; Long et al., 2004; Morgan et al., 2004; Owensby et al., 1999; Soussana & Lüscher, 2007; Volk et al., 2000; Wullschleger et al., 2002). Moreover, [eCO_2] may enhance the recovery of plants after extreme climatic events (Roy et al., 2016). In line with this **carbon-centric view**, many numerical models predict an increasing trend for future European grassland productivity which is mainly explained by a strong CFE (e.g., Chang et al. 2017; Gu et al. 2014; Hufkens et al. 2016; Huntzinger et al. 2017; Rounsevell et al. 2005; Williams et al. 2014). However, the projections from numerical models should be circumspectly perceived since there is a large model disagreement attributed to the models' sensitivity to rising atmospheric CO_2 (Huntzinger et al., 2017) and the too simplified implementation of experimentally observed physiological responses to global change-related variables (Tubiello et al., 2007). This was highlighted by a large divergence within satellite and model estimates of the CFE in terrestrial areas across the globe (Smith et al., 2016). Additional doubts about the classical view on the CFE have arisen from recent studies based on long-term CO_2 enrichment experiments revealing that the CFE might be reduced under drier conditions, which was explained by resource limitation due to water scarcity (Hovenden et al., 2014), or a joint water and nitrogen limitation that generally limited plant growth (Reich et al., 2014).

The controversial experimental results and the high uncertainty within numerical models reveal that the interaction of the effects of increased [CO_2] and environmental

conditions on grassland productivity, an indicator for plant and ecosystem carbon storage, is poorly understood (Hovenden et al., 2014; IPCC, 2013; Reich et al., 2014; Smith et al., 2016; Tubiello et al., 2007; White et al., 2011). Consequently, the potential of grassland productivity under global change, and thus, the value of the future ecosystem services provided by grasslands, is highly uncertain. To reduce this uncertainty, and allow for a better parametrisation e.g. within dynamic global vegetation models, suitable long-term experiments providing continuous and high quality data are urgently required (Frank et al., 2015; Lüscher et al., 2004; Norby & Luo, 2004; Rustad, 2008). Here, free air carbon dioxide enrichment (FACE) experiments are the culmination of efforts to investigate ecosystems in a manner that is minimally invasive. Therefore, the longest worldwide available time series of data acquired on a FACE experiment, the Giessen FACE facility (GiFACE), is used in this study to analyse the interacting effects of increased [CO_2] and environmental conditions on grassland productivity.

Long-term investigations are traditionally confined to destructive sampling approaches at certain sampling plots and harvest dates with consecutive, costly and labour-intensive laboratory analysis. Due to the restricted temporal resolution of the conventional sampling methods at single harvest dates, no short-term changes in the grassland productivity are captured in datasets acquired by such sampling strategies. This is problematic because it has been shown that the quantification of the effects of extreme climatic events on grassland poses a mayor challenge for ecosystem analysis (Jentsch et al., 2007; Niu et al., 2014; van der Molen et al., 2011). Therefore, FACE experiments should be monitored with a higher temporal resolution and possibly more cost-effectively procedure. Here, remote sensing approaches might have a great potential because they are rapid, non-destructive and allow high temporal resolutions with spatially explicit information. Recent advances in remote sensing have lead to the development of hyperspectral sensors which are capable of recording contiguous spectral bands with a fine spectral resolution covering a wide range of the electromagnetic spectrum. Thereby, hyperspectral approaches are expected to advance the remote estimation of e.g., grassland properties as compared to the commonly applied multispectral approaches, that cover fewer bands with a coarser spectral resolution. Consequently, this study wants to bridge scales to overcome the conventional sampling restrictions by investigating

the feasibility of the hyperspectral monitoring of the GiFACE grassland. Thereby, a deeper insight into the interacting of [eCO_2] and weather conditions on the grassland productivity than is possible by conventional destructive sampling methods will be given. In addition to an enhanced grassland monitoring, future applications of remote sensing techniques might encompass an improved grassland management (Iftikhar et al., 2016), e.g. by helping farmers to adapt fertiliser input, adjust stocking rates or find optimal harvest dates.

Summarising, the motivation of the present thesis is based on knowledge deficits regarding

- the extent of the CO_2 fertilization effect in grasslands under varying environmental conditions,
- the potential of future grassland biomass productivity under global change conditions, and
- techniques for non-invasive measurements to enable a high-resolution spatio-temporal grassland monitoring.

1.2 Aims, research questions and hypotheses

The overall goal of this thesis is to improve the assessment of the value of ecosystem services provided by temperate grasslands under global change conditions. Therefore, this study investigates the influence of real-world climatic variations on the above-ground biomass of a temperate C3 grassland under different CO_2 concentrations within the globally longest operating FACE experiment on grasslands at different scales.

Based on the above mentioned gaps in knowledge, the present thesis has the following three main **aims**:

- to assess the influence of environmental conditions on the CO_2 fertilization effect in a temperate grassland,
- to improve the assessment of potential future grassland productivity under global change conditions, and
- to facilitate a high-resolution spatio-temporal monitoring of the GiFACE grassland characteristics by remote sensing techniques.

The **first key question** to be addressed is whether and how the CO_2 fertilization effect in the grassland under investigation interrelates with changing average weather conditions in summer. Since single ECEs might also influence grassland productivity, this key question will be expanded to the investigation of the influence of ECEs on the CFE.

In the **second key question**, the potential future productivity of temperate grasslands will be investigated considering increased [CO_2]s and projected future climatic conditions. Thus, it shall be assessed whether an increased grassland biomass productivity can be expected in future mainly due to rising [CO_2], or if the projected global change-related weather alterations are likely to reduce grassland productivity in future, despite increased [CO_2].

Short-term influences of ECEs on grassland productivity *per se* and the CFE in particular might fall through the relatively coarse temporal resolutions possible by conventional sampling approaches. Therefore, the **third key question** concerns the possibilities for non-invasive hyperspectral monitoring of the grassland with a

high spatio-temporal resolution. Consequently, methods will be developed which facilitate work with hyperspectral data and comprehensive statistical software (as provided by the open-source software CRAN R), and it will be examined, whether the grassland traits related to the most important ecosystem services can accurately be predicted by non-invasive, hyperspectral approaches within the GiFACE facility.

To answer the above-mentioned questions, the following three **hypotheses** will be tested:

H 1 The CO_2 fertilization effect is reduced under more extreme average weather conditions and after extreme climatic events

H 2 Future increases in above-ground biomass productivity under elevated CO_2 concentrations more than compensate for potential biomass reductions due to global change-related environmental alterations

H 3 State-of-the-art remote sensing techniques enable the monitoring of grassland ecosystem services providing high spatio-temporal resolutions within a FACE experiment

1.3 Thesis outline

The main part of the present thesis consists of five scientific articles which are either published (2), accepted (1) or under review (2) in internationally renowned journals. The general work flow is presented in Fig. 1.1.

Within the thesis, the five articles are embedded in the scientific context by summarizing the current state of the research (**chapter 2**), and outlining the conception and technical preparation of the working packages (**chapter 3**). At first, a description of the main global change-related environmental influences on grassland productivity will be given (**section 2.1**), followed by a short description of experimental facilities to investigate the effect of increased [CO_2] on plant productivity (**section 2.2**). Subsequently the conception and technical preparation of the working packages will be described (**chapter 3**), beginning with a short description of the GiFACE experiment (**section 3.1**) and followed by the preparation of the working packages, subdivided into the investigations on the three established hypotheses (**section 3.2-3.4**) and an overview of the resulting working packages for this thesis.

In the first article (**chapter 4**), a new method will be developed to investigate the influence of average weather conditions on the effect of increased [CO_2] on summer above-ground biomass productivity within the long-term time series of the GiFACE experiment, to test part one of **H 1**.

In the second article (**chapter 5**), the same 16-year time series will be used to investigate the effects of extreme climatic events on the CO_2 fertilization effect, for both, spring and summer harvests, to test part two of **H 1**.

In the third article (**chapter 6**), the potential of future C3 grassland productivity will be evaluated using statistical models and potential climate regimes created from the long-term GiFACE data series along with projected climate alterations found in global climate models, to test **H 2**.

The fourth article (**chapter 7**) presents the enhanced R-package hsdar containing methods to process hyperspectral data with open-source software, and preliminary investigations on **H 3**, the hyperspectral predictability of grassland traits within the GiFACE experiment, using the example of canopy chlorophyll concentrations.

In the fifth article (**chapter 8**), the hyperspectral predictability, and thus the potential of a high-resolution spatio-temporal monitoring, of fourteen grassland traits related to ecosystem services will be investigated under varying CO_2 concentrations, to test **H 3**.

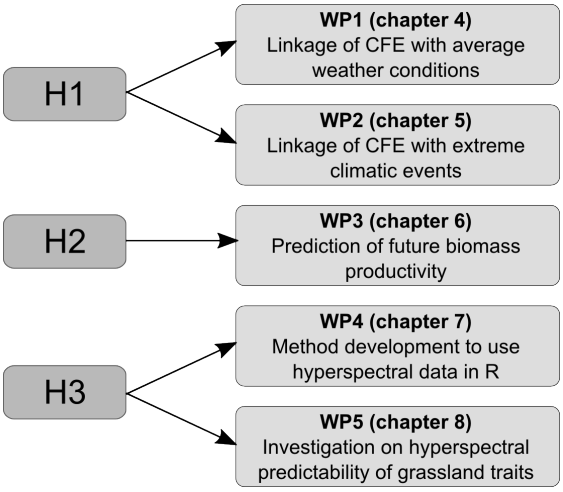

Figure 1.1: General work flow of the thesis.

Finally, the present work will end with a summary of the most important findings regarding the influence of average weather conditions and extreme climatic events on the CO_2 fertilization effect, the potential of future above-ground biomass productivity under projected global change conditions, and the hyperspectral possibilities that enhance monitoring of FACE experiments in particular and generally provide a wide range of applications (**chapter 9**). The chapter will finish with a short outlook on further research needed and a perspective on the importance of the thesis for policy makers.

References

Ainsworth, E. & Rogers, A. (2007): The response of photosynthesis and stomatal conductance to rising [CO_2]: Mechanisms and environmental interactions. *Plant, Cell and Environment*, 30, 3, 258–270.

Beniston, M., Stephenson, D.B., Christensen, O.B., Ferro, C.A., Frei, C., Goyette, S., Halsnaes, K., Holt, T., Jylhä, K., Koffi, B. et al. (2007): Future extreme events in European climate: an exploration of regional climate model projections. *Climatic Change*, 81, 1, 71–95.

Blair, J., Nippert, J., & Briggs, J. (2014): Grassland ecology. In: Ecology and the Environment. Springer, pp. 389–423.

Booth, B.B.B., Jones, C.D., Collins, M., Totterdell, I.J., Cox, P.M., Sitch, S., Huntingford, C., Betts, R.a., Harris, G.R., & Lloyd, J. (2012): High sensitivity of future global warming to land carbon cycle processes. *Environmental Research Letters*, 7, 2, 1–8.

Chang, J., Ciais, P., Viovy, N., Soussana, J.F., Klumpp, K., & Sultan, B. (2017): Future productivity and phenology changes in European grasslands for different warming levels: implications for grassland management and carbon balance. *Carbon Balance and Management*, 12, 11.

Chang, J., Ciais, P., Viovy, N., Vuichard, N., Herrero, M., Havlík, P., Wang, X., Sultan, B., & Soussana, J.F. (2016): Effect of climate change, CO_2 trends, nitrogen addition, and land-cover and management intensity changes on the carbon balance of European grasslands. *Global Change Biology*, 22, 1, 338–350.

Chang, J., Ciais, P., Viovy, N., Vuichard, N., Sultan, B., & Soussana, J.F. (2015): The greenhouse gas balance of European grasslands. *Global Change Biology*, 21, 10, 3748–3761.

Christensen, N.L., Bartuska, A.M., Brown, J.H., Carpenter, S., D'Antonio, C., Francis, R., Franklin, J.F., MacMahon, J.A., Noss,

R.F., Parsons, D.J. et al. (1996): The report of the Ecological Society of America committee on the scientific basis for ecosystem management. *Ecological Applications*, 6, 3, 665–691.

Christidis, N., Jones, G.S., & Stott, P.A. (2015): Dramatically increasing chance of extremely hot summers since the 2003 European heatwave. *Nature Climate Change*, 5, 1, 46.

Ciais, P., Reichstein, M., Viovy, N., Granier, A., Ogée, J., Allard, V., Aubinet, M., Buchmann, N., Bernhofer, C., Carrara, A., Chevallier, F., De Noblet, N., Friend, a.D., Friedlingstein, P., Grünwald, T., Heinesch, B., Keronen, P., Knohl, A., Krinner, G., Loustau, D., Manca, G., Matteucci, G., Miglietta, F., Ourcival, J.M., Papale, D., Pilegaard, K., Rambal, S., Seufert, G., Soussana, J.F., Sanz, M.J., Schulze, E.D., Vesala, T., & Valentini, R. (2005): Europe-wide reduction in primary productivity caused by the heat and drought in 2003. *Nature*, 437, 7058, 529–533.

Coughenour, M. & Chen, D.X. (1997): Assessment of Grassland and Ecosystem Responses to Atmospheric Change Using Linked Plant-Soil Process Models. *Ecological Applications*, 7, 3, 802–827.

Coumou, D. & Rahmstorf, S. (2012): A decade of weather extremes. *Nature Climate Change*, 2, 7, 491.

Cox, P.M., Betts, R.A., Jones, C.D., Spall, S.A., & Totterdell, I.J. (2000): Acceleration of global warming due to carbon-cycle feedbacks in a coupled climate model. *Nature*, 408, 184–187.

Drake, B.G., Gonzalez-Meler, M.a., & Long, S.P. (1997): MORE EFFICIENT PLANTS: A Consequence of Rising Atmospheric CO_2? *Annual Review of Plant Physiology and Plant Molecular Biology*, 48, 609–639.

Easterling, D.R., Evans, J., Groisman, P.Y., Karl, T.R., Kunkel, K.E., & Ambenje, P. (2000): Observed variability and trends in extreme climate events: a brief review. *Bulletin of the American Meteorological Society*, 81, 3, 417–426.

Fink, A.H., Brücher, T., Krüger, A., Leckebusch, G.C., Pinto, J.G., & Ulbrich, U. (2004): The 2003 European summer heatwaves and drought – synoptic diagnosis and impacts. *Weather*, 59, 8, 209–216.

Foley, J.A., Ramankutty, N., Brauman, K.A., Cassidy, E.S., Gerber, J.S., Johnston, M., Mueller, N.D., O'Connell, C., Ray, D.K., West, P.C., Balzer, C., Bennett, E.M., Carpenter, S.R., Hill, J., Monfreda, C., Polasky, S., Rockström, J., Sheehan, J., Siebert, S., Tilman, D., Zaks, D.P.M., & O'Connell, C. (2011): Solutions for a cultivated planet. *Nature*, 478, 7369, 337–42.

Food and Agriculture Organization of the United Nations Statistics Division (2015): FAOSTAT. (last access: 2017-07-27).
URL `http://faostat3.fao.org/browse/E/EL/E`

Frank, D., Reichstein, M., Bahn, M., Frank, D., Mahecha, M.D., Smith, P., Thonicke, K., van der Velde, M., Vicca, S., Babst, F., Beer, C., Buchmann, N., Canadell, J.G., Ciais, P., Cramer, W., Ibrom, A., Miglietta, F., Poulter, B., Rammig, A., Seneviratne, S.I., Walz, A., Wattenbach, M., Zavala, M.a., & Zscheischler, J. (2015): Effects of climate extremes on the terrestrial carbon cycle: concepts, processes and potential future impacts. *Global Change Biology*, 21, 8, 2861–2880.

Friedlingstein, P., Cox, P., Betts, R., Bopp, L., von Bloh, W., Brovkin, V., Cadule, P., Doney, S., Eby, M., Fung, I., Bala, G., John, J., Jones, C., Joos, F., Kato, T., Kawamiya, M., Knorr, W., Lindsay, K., Matthews, H.D., Raddatz, T., Rayner, P., Reick, C., Roeckner, E., Schnitzler, K.G., Schnur, R., Strassmann, K., Weaver, a.J., Yoshikawa, C., & Zeng, N. (2006): Climate–Carbon Cycle Feedback Analysis: Results from the C^4MIP Model Intercomparison. *Journal of Climate*, 19, 14, 3337–3353.

Fung, I.Y., Doney, S.C., Lindsay, K., & John, J. (2005): Evolution of carbon sinks in a changing climate. *Proceedings of the National Academy of Sciences*, 102, 32, 11 201–11 206.

Gao, Q., Zhu, W., Schwartz, M.W., Ganjurjav, H., Wan, Y., Qin, X., Ma, X., Williamson, M.A., & Li, Y. (2016): Climatic change controls productivity variation in global grasslands. *Scientific Reports*, 6, 26 958.

García-Herrera, R., Díaz, J., Trigo, R.M., Luterbacher, J., & Fischer, E.M. (2010): A review of the European summer heat wave of 2003. *Critical Reviews in Environmental Science and Technology*, 40, 4, 267–306.

Gu, Y., Wylie, B.K., Boyte, S.P., & Phuyal, K.P. (2014): Projecting future grassland productivity to assess the sustainability of potential biofuel feedstock areas in the greater platte river basin. *GCB Bioenergy*, 6, 1, 35–43.

Herrero, M., Havlík, P., Valin, H., Notenbaert, A., Rufino, M.C., Thornton, P.K., Blümmel, M., Weiss, F., Grace, D., & Obersteiner, M. (2013): Biomass use, production, feed efficiencies, and greenhouse gas emissions from global livestock systems. *Proceedings of the National Academy of Sciences*, 110, 52, 20 888–20 893.

Hov, Ø., Cubasch, U., Fischer, E., Höppe, P., Iversen, T., Gunnar Kvamstø, N., Kundzewicz, W., Rezacova, D., Rios, D., Duarte Santos, F., Schädler, B., Veisz, O., Zerefos, C., Benestad, R., Murlis, J., Leckebusch, G.C., & Ulbrich, U. (2013): Extreme Weather Events in Europe: preparing for climate change adaptation. Norwegian Meteorological Institute.

Hovenden, M.J., Newton, P.C.D., & Wills, K.E. (2014): Seasonal not annual rainfall determines grassland biomass response to carbon dioxide. *Nature*, 511, 7511, 583–586.

Hufkens, K., Keenan, T.F., Flanagan, L.B., Scott, R.L., Bernacchi, C.J., Joo, E., Brunsell, N.A., Verfaillie, J., & Richardson, A.D. (2016): Productivity of North American grasslands is increased under future climate scenarios despite rising aridity. *Nature Climate Change*, 6, 7, 710.

Huntzinger, D.N., Michalak, A.M., Schwalm, C., Ciais, P., King, A.W., Fang, Y., Schaefer, K., Wei, Y., Cook, R.B., Fisher, J.B., Hayes, D.,

Huang, M., Ito, A., Jain, A.K., Lei, H., Lu, C., Maignan, F., Mao, J., Parazoo, N., Peng, S., Poulter, B., Ricciuto, D., Shi, X., Tian, H., Wang, W., Zeng, N., & Zhao, F. (2017): Uncertainty in the response of terrestrial carbon sink to environmental drivers undermines carbon-climate feedback predictions. *Scientific Reports*, 7, 1, 4765.

Idso, S.B., Kimball, B.A., Anderson, M., & Mauney, J.R. (1987): Effects of atmospheric CO_2 enrichment on plant growth: the interactive role of air temperature. *Agriculture, Ecosystems & Environment*, 20, 1, 1–10.

Iftikhar, A., Cawkwell, F., Dwyer, E., Barrett, B., & Green, S. (2016): Satellite remote sensing of grasslands: from observation to management. *Journal of Plant Ecology*, 9, 6, 649–671.

Ionita, M., Tallaksen, L.M., Kingston, D.G., Stagge, J.H., Laaha, G., Van Lanen, H.A.J., Scholz, P., Chelcea, S.M., & Haslinger, K. (2017): The European 2015 drought from a climatological perspective. *Hydrology and Earth System Sciences*, 21, 3, 1397–1419.

IPCC (2013): Climate Change 2013: The Physical Science Basis. Contribution of Working Group I to the Fifth Assessment Report of the Intergovernmental Panel on Climate Change. *Intergovernmental Panel on Climate Change, Working Group I Contribution to the IPCC Fifth Assessment Report (AR5)(Cambridge Univ Press, New York).*

Janssens, I.A., Freibauer, A., Ciais, P., Smith, P., Nabuurs, G.J., Folberth, G., Schlamadinger, B., Hutjes, R.W., Ceulemans, R., Schulze, E.D. et al. (2003): Europe's terrestrial biosphere absorbs 7 to 12% of European anthropogenic CO_2 emissions. *Science*, 300, 5625, 1538–1542.

Jentsch, A., Kreyling, J., & Beierkuhnlein, C. (2007): A new generation of climate-change experiments: events, not trends. *Frontiers in Ecology and the Environment*, 5, 7, 365–374.

Jordan, D.B. & Ogren, W.L. (1984): The CO_2 /O2 specificity of ribulose 1,5-bisphosphate carboxylase/oxygenase - Dependence on ribulosebisphosphate concentration, pH and temperature. *Planta*, 161, 4, 308–313.

Laaha, G., Gauster, T., Tallaksen, L.M., Vidal, J.P., Stahl, K., Prudhomme, C., Heudorfer, B., Vlnas, R., Ionita, M., Van Lanen, H.A.J., Adler, M.J., Caillouet, L., Delus, C., Fendekova, M., Gailliez, S., Hannaford, J., Kingston, D., Van Loon, A.F., Mediero, L., Osuch, M., Romanowicz, R., Sauquet, E., Stagge, J.H., & Wong, W.K. (2017): The European 2015 drought from a hydrological perspective. *Hydrology and Earth System Sciences*, 21, 6, 3001–3024.

Lemaire, G., Hodgson, J., & Chabbi, A. (2011): Grassland Productivity and Ecosystem Services. Cabi.

Long, S.P., Ainsworth, E.a., Rogers, A., & Ort, D.R. (2004): Rising atmospheric carbon dioxide: plants FACE the future. *Annual Review of Plant Biology*, 55, 591–628.

Lüscher, A., Daepp, M., Blum, H., Hartwig, U.A., & Nösberger, J. (2004): Fertile temperate grassland under elevated atmospheric CO_2 - Role of feed-back mechanisms and availability of growth resources. *European Journal of Agronomy*, 21, 3, 379–398.

Meehl, G.A. & Tebaldi, C. (2004): More intense, more frequent, and longer lasting heat waves in the 21st century. *Science*, 305, 5686, 994–997.

Millennium Ecosystem Assessment (2005): Ecosystems and Human Well-being: Synthesis. Synthesis Reports. Island Press.

Morgan, J.a., Pataki, D.E., Körner, C., Clark, H., Del Grosso, S.J., Grünzweig, J.M., Knapp, A.K., Mosier, A.R., Newton, P.C.D., Niklaus, P.A., Nippert, J.B., Nowak, R.S., Parton, W.J., Polley, H.W., & Shaw, M.R. (2004): Water relations in grassland and desert ecosystems exposed to elevated atmospheric CO_2. *Oecologia*, 140, 1, 11–25.

Niu, S., Luo, Y., Li, D., Cao, S., Xia, J., Li, J., & Smith, M.D. (2014): Plant growth and mortality under climatic extremes: An overview. *Environmental and Experimental Botany*, 98, 13–19.

NOAA National Centers for Environmental Information (2016): State of the Climate: Global Climate Report-Annual 2015.
URL `https://www.ncdc.noaa.gov/sotc/global/201513`

NOAA National Centers for Environmental Information (2018): State of the Climate: Global Climate Report for July 2018.
URL `https://www.ncdc.noaa.gov/sotc/global/201807`

Norby, R.J. & Luo, Y. (2004): Evaluating ecosystem responses to rising atmospheric CO_2 and global warming in a multi-factor world. *New Phytologist*, 162, 2, 281–293.

Orth, R., Zscheischler, J., & Seneviratne, S.I. (2016): Record dry summer in 2015 challenges precipitation projections in Central Europe. *Scientific Reports*, 6, 28 334.

Owensby, C.E., Ham, J.M., Knapp, a.K., & Auen, L.M. (1999): Biomass production and species composition change in a tallgrass prairie ecosystem after long-term exposure to elevated atmospheric CO_2. *Global Change Biology*, 5, 497–506.

Parton, W., Morgan, J., Smith, D., Del Grosso, S., Prihodko, L., Lecain, D., Kelly, R., & Lutz, S. (2012): Impact of precipitation dynamics on net ecosystem productivity. *Global Change Biology*, 18, 3, 915–927.

Peters, G.P., Le Quéré, C., Andrew, R.M., Canadell, J.G., Friedlingstein, P., Ilyina, T., Jackson, R.B., Joos, F., Korsbakken, J.I., McKinley, G.A., Sitch, S., & Tans, P. (2017): Towards real-time verification of CO_2 emissions. *Nature Climate Change*, 7, 12, 848.

Ramankutty, N., Evan, A.T., Monfreda, C., & Foley, J.A. (2008): Farming the planet: 1. Geographic distribution of global agricultural lands in the year 2000. *Global Biogeochemical Cycles*, 22, 1.

Reich, P.B., Hobbie, S.E., & Lee, T.D. (2014): Plant growth enhancement by elevated CO_2 eliminated by joint water and nitrogen limitation. *Nature Geoscience*, 7, 2–6.

Reichstein, M., Bahn, M., Ciais, P., Frank, D.C.D., Mahecha, M.D., Seneviratne, S.I., Zscheischler, J., Beer, C., Buchmann, N., Papale, D., Rammig, A., Smith, P., Thonicke, K., van der Velde, M., Vicca, S., Walz, A., Wattenbach, M., Frank, D.C.D., Papale, D., Rammig, A., Smith, P., Thonicke, K., van der Velde, M., Vicca, S., Walz, A., & Wattenbach, M. (2013): Climate extremes and the carbon cycle. *Nature*, 500, 7462, 287–95.

Robine, J.M., Cheung, S.L.K., Le Roy, S., Van Oyen, H., Griffiths, C., Michel, J.P., & Herrmann, F.R. (2008): Death toll exceeded 70,000 in Europe during the summer of 2003. *Comptes rendus biologies*, 331, 2, 171–178.

Rounsevell, M., Ewert, F., Reginster, I., Leemans, R., & Carter, T. (2005): Future scenarios of European agricultural land use: II. Projecting changes in cropland and grassland. *Agriculture, Ecosystems & Environment*, 107, 2-3, 117–135.

Roy, J., Picon-Cochard, C., Augusti, A., Benot, M.L., Thiery, L., Darsonville, O., Landais, D., Piel, C., Defossez, M., Devidal, S., Escape, C., Ravel, O., Fromin, N., Volaire, F., Milcu, A., Bahn, M., & Soussana, J.F. (2016): Elevated CO_2 maintains grassland net carbon uptake under a future heat and drought extreme. *Proceedings of the National Academy of Sciences of the United States of America*, 113, 22, 6224–6229.

Rustad, L.E. (2008): The response of terrestrial ecosystems to global climate change: towards an integrated approach. *Science of the Total Environment*, 404, 2-3, 222–235.

Schär, C., Vidale, P.L., Lüthi, D., Frei, C., Häberli, C., Liniger, M.A., & Appenzeller, C. (2004): The role of increasing temperature variability in european summer heatwaves. *Nature*, 427, 6972, 332.

Schimel, D., Stephens, B.B., & Fisher, J.B. (2015): Effect of increasing CO_2 on the terrestrial carbon cycle. *Proceedings of the National Academy of Sciences*, 112, 2, 436–441.

Schlesinger, W.H. & Andrews, J.A. (2000): Soil respiration and the global carbon cycle. *Biogeochemistry*, 48, 1, 7–20.

Seneviratne, S.I., Donat, M.G., Mueller, B., & Alexander, L.V. (2014): No pause in the increase of hot temperature extremes. *Nature Climate Change*, 4, 3, 161.

Seneviratne, S.I., Nicholls, N., Easterling, D., Goodess, C.M., Kanae, S., Kossin, J., Luo, Y., Marengo, J., McInnes, K., Rahimi, M., Reichstein, M., Sorteberg, A., Vera, C., & Zhang, X. (2012): Changes in climate extremes and their impacts on the natural physical environment. Technical Report, Intergovernmental Panel on Climate Change.

Sillmann, J., Kharin, V., Zwiers, F., Zhang, X., & Bronaugh, D. (2013): Climate extremes indices in the CMIP5 multimodel ensemble: Part 2. Future climate projections. *Journal of Geophysical Research: Atmospheres*, 118, 6, 2473–2493.

Smith, W.K., Reed, S.C., Cleveland, C.C., Ballantyne, A.P., Anderegg, W.R., Wieder, W.R., Liu, Y.Y., & Running, S.W. (2016): Large divergence of satellite and earth system model estimates of global terrestrial CO_2 fertilization. *Nature Climate Change*, 6, 3, 306.

Solomon, S., Qin, D., Manning, M., Chen, Z., Marquis, M., Averyt, K.B., Tignor, M., Miller, H.L. et al. (Eds.) (2007): Climate change 2007: The Physical Science Basis: Contribution of Working Group I to the Fourth Assessment Report of the Intergovernmental Panel on Climate Change, volume 4. Cambridge University Press.

Soussana, J.F. & Lüscher, A. (2007): Temperate grasslands and global atmospheric change: A review. *Grass and Forage Science*, 62, 2, 127–134.

Stott, P.A., Stone, D.A., & Allen, M.R. (2004): Human contribution to the european heatwave of 2003. *Nature*, 432, 7017, 610.

Tebaldi, C., Hayhoe, K., Arblaster, J.M., & Meehl, G.A. (2006): Going to the extremes. *Climatic change*, 79, 3-4, 185–211.

Tubiello, F.N., Soussana, J.F., & Howden, S.M. (2007): Crop and pasture response to climate change. *Proceedings of the National Academy of Sciences*, 104, 50, 19 686–19 690.

van der Molen, M.K., Dolman, A.J., Ciais, P., Eglin, T., Gobron, N., Law, B.E., Meir, P., Peters, W., Phillips, O.L., Reichstein, M., Chen, T., Dekker, S.C., Doubková, M., Friedls, M.A., Jung, M., van den Hurk, B.J.J.M., de Jeu, R.A.M., Kruijt, B., Ohta, T., Rebel, K.T., Plummer, S., Seneviratne, S.I., Sitch, S., Teuling, A.J., van der Werf, G.R., & Wang, G. (2011): Drought and ecosystem carbon cycling. *Agricultural and Forest Meteorology*, 151, 7, 765–773.

Volk, M., Niklaus, P.A., & Körner, C. (2000): Soil moisture effects determine CO_2 responses of grassland species. *Oecologia*, 125, 3, 380–388.

White, A., Cannell, M.G., & Friend, A.D. (2000): CO_2 stabilization, climate change and the terrestrial carbon sink. *Global Change Biology*, 6, 7, 817–833.

White, S.R., Carlyle, C.N., Fraser, L.H., & Cahill, J.F. (2011): Climate change experiments in temperate grasslands: synthesis and future directions. *Biology Letters*.

Williams, I., Torn, M., Riley, W., & Wehner, M. (2014): Impacts of climate extremes on gross primary production under global warming. *Environmental Research Letters*, 9, 9, 094 011.

Wullschleger, S., Tschaplinski, T., & Norby, R. (2002): Plant water relations at elevated CO_2 – implications for water-limited environments. *Plant, Cell and Environment*, 25, 319–331.

Zhao, M. & Running, S.W. (2010): Drought-induced reduction in global terrestrial net primary production from 2000 through 2009. *Science*, 329, 5994, 940–943.

2 State of research

As previously stated, this thesis aims to shed new light on the interacting effects of increased [CO_2] and climatic drivers on grassland biomass productivity with the most important goal to gain better estimates of the future provision of grassland ecosystem services under global change. Therefore, this chapter will start with a short overview of the main global change-related environmental factors affecting grassland productivity (**section 2.1**), considering precipitation (**section 2.1.1**), air temperature (**section 2.1.2**), CO_2 concentrations (**section 2.1.3**), and other environmental drivers (**section 2.1.4**). This will be followed by a brief description and critical examination of experimental designs used to investigate the effects of increased [CO_2] on plant productivity (**section 2.2**).

2.1 Global change-related environmental influences on European grasslands

One of the basic plant physiological principles is the exchange of gas and water between the atmosphere and plants through small pores on the epidermis of the leaves – the stomata. When stomata are open, CO_2, the main substrate for the photosynthesis enters the leaves. At the same time, via the so-called transpiration water exits the leaves. Consequently, the opening of the stomata leads to an unavoidable trade-off between water losses and CO_2 uptake, where the latter is the prerequisite for photosynthesis. This process, which permits carbon uptake by plants will be affected by altered environmental conditions under global climate change.

2.1.1 Effects of altered precipitation

Decreased water input is assumed to lower the photosynthetic activity via stomatal limitation, because plants need to close the stomata to avoid water stress. Consequently, biomass productivity is reduced under lower precipitation input while increases in the precipitation stimulate plant growth (Miranda-Apodaca et al., 2015; Nippert et al., 2006; Weltzin et al., 2003; Wu et al., 2011; Yang et al., 2008; Zhao & Running, 2010). However, the projected increases in the variability of the precipitation input will probably decrease biomass productivity irrespective of the total precipitation (Knapp et al., 2008; Nippert et al., 2006). On the one hand, very intense precipitation events can lead to a nutrient loss through fast surface runoff or if the latter is impeded cause water-logging of the soils, and thus reduce in the biomass productivity. On the other hand, particularly in summer, longer dry intervals may lead to a critical drying of the soil and thus a reduced biomass productivity which is of particular importance in grasslands with their relatively shallow roots bringing the plants water from the upper layers of the soil (Gherardi & Sala, 2015; Knapp et al., 2008).

2.1.2 Effects of increased air temperature

In contrast to the widely accepted view on the influence of altered precipitation regimes on ecosystem productivity, the influence of air temperatures is still under debate. An increased air temperature may lead to a lengthening of the growing period (Hufkens et al., 2016; Luo, 2007), an enhanced microbial activity which increases nutrient availability (Luo, 2007; Rustad et al., 2001), and a shift towards an optimum growth temperature (Luo, 2007; Myneni et al., 1997), altogether possibly enhancing biomass productivity. However, when net photosynthesis reaches a maximum at optimal temperature further temperature increases cause declines in the photosynthesis (carbon uptake) and increased respiration (carbon loss) rates, which reduces the biomass productivity in C3 plants (Brooks & Farquhar, 1985; Farquhar et al., 1980; Long, 1991; Luo, 2007). In addition to the direct effects on plant physiology, an increasing air temperature enhances evapotranspiration and thus causes earlier water depletion in soils, which will reduce biomass productivity, especially if water availability is limited. Moreover, increasing air temperatures

may increase heat stress, and thus reduce biomass productivity especially when a low water availability limits potential for evaporative cooling in plants (De Boeck & Verbeeck, 2011; De Boeck et al., 2008; Leuzinger & Körner, 2007; Morison & Lawlor, 1999). Additionally, single events such as prolonged heat waves and frosts affect or even prevent the carbon uptake in plants which reduces biomass productivity (De Boeck et al., 2008; Jentsch et al., 2007; Niu et al., 2014; van der Molen et al., 2011). Consequently, the influence of increased air temperature on grassland productivity is not certain.

Summarising, it is evident that the projected climatic changes are likely to alter grassland productivity in the future. However, the direction and magnitude of the response, especially in the interaction with an increased [CO_2] remain uncertain. To gain a better insight into the underlying physiological principles, the basics of the biomass yield stimulation under [eCO_2], namely the CO_2 fertilization effect (CFE), will be described in the following section.

2.1.3 Influence of increased CO_2 concentrations – the CO_2 fertilization effect

The CFE is expected to increase C3 grassland biomass productivity mainly via (1) the direct effects of an increased photosynthetic carbon fixation through lesser CO_2 limitation, and (2) the indirect effects of a decreased stomatal conductance since shorter stomata opening fulfils the carbon-demand in plants (Ainsworth & Rogers, 2007; Ainsworth & Long, 2005; Field et al., 1995; Körner, 2000; Lloyd & Farquhar, 2008; Soussana & Lüscher, 2007; Volk et al., 2000).

2.1.3.1 The CO_2 fertilization effect and altered water availability

Shorter stomatal opening periods and the reduced stomatal conductance lead to lower transpirational losses and an enhanced water use efficiency of plants grown under [eCO_2]. This is expected to cause soil water savings which reduce potential water stress for plants, and thus lead to a particularly strong CFE under dry conditions (Ainsworth & Rogers, 2007; Drake et al., 1997; Idso, 1994; Jordan & Ogren, 1984; Leakey et al., 2009; Morgan et al., 2004; Owensby et al., 1999; Soussana & Lüscher, 2007; Wullschleger et al., 2002). Moreover, there is

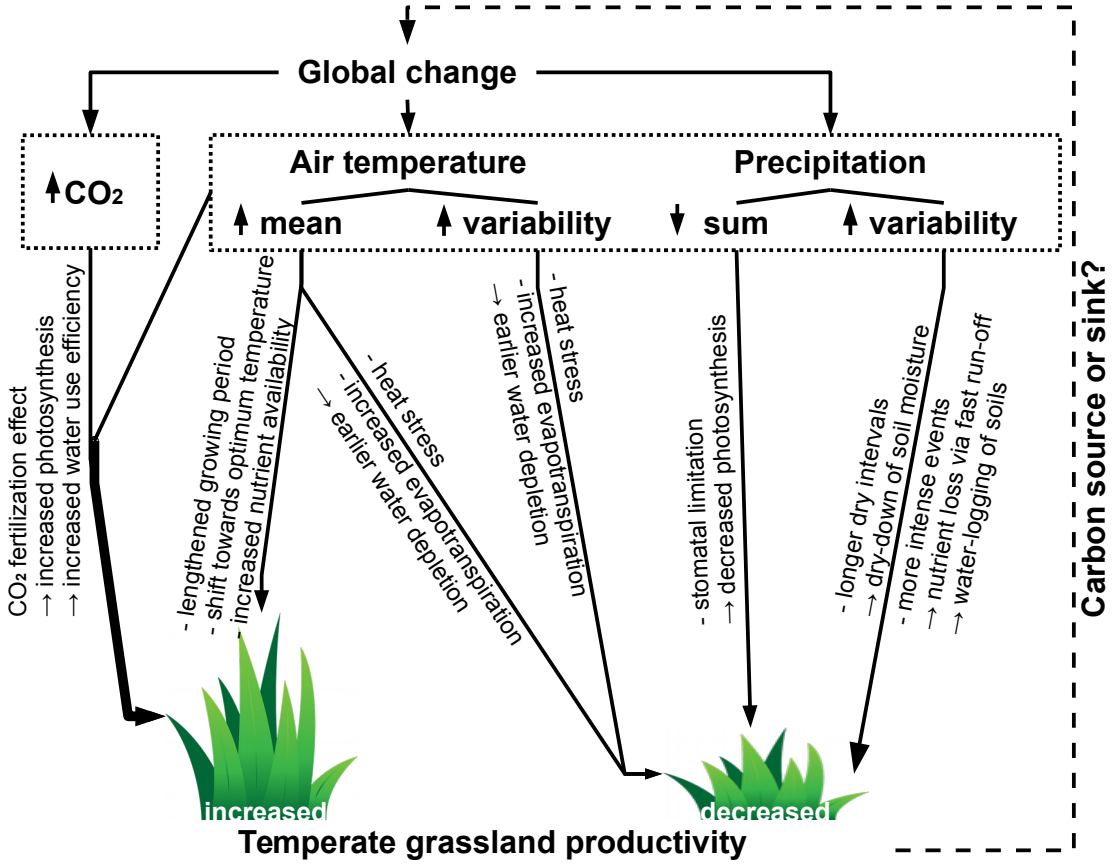

Figure 2.1: Simplified schematic of the projected global change-related environmental alterations (dashed boxes) and their widely expected influences on temperate grassland productivity. The wider arrow represents the assumption of an increased CO_2 fertilization effect under drier and warmer conditions, environmental conditions that would rather decrease the grassland biomass productivity in general.

also the possibility of an enhanced recovery after ECEs under [eCO_2], which might counterbalance biomass reductions due to global change-related environmental alterations such as a higher intensity and frequency of precipitation events (Roy et al., 2016). Nevertheless, contrasting findings in literature reported the strongest CFE under intermediate precipitation regimes (Hunt et al., 1996; Nowak et al., 2004; Volk et al., 2000), and most recent studies reported even a positive influence of summer rainfall on the CFE (Hovenden et al., 2014; Reich et al., 2014). In line with this, a long-term decline in the grassland productivity in the Northern Rocky Mountains from 1969 to 2012 was explained by increasing dryness despite

of the increases in [CO_2] (Brookshire & Weaver, 2015). And, Zhu et al. (2016) showed in a Californian grassland under long-term CO_2 enrichment that future climatic conditions are likely to push the investigated ecosystem away from conditions that maximise net primary production.

2.1.3.2 The CO_2 fertilization effect and increased air temperature

Various assumptions are also found in the scientific community regarding the effect of air temperature on the CFE. Many studies assume a particularly strong CFE under higher air temperature (Coughenour & Chen, 1997; Idso et al., 1987; Long, 1991; Long et al., 2004; Morison & Lawlor, 1999; Wang et al., 2012). This is explained by the favouring of the oxygenation (photorespiration) as the specificity of Rubisco for O_2 compared to CO_2 is increased under higher temperatures. Thereby, the ratio of photosynthesis to photorespiration is decreased under higher temperatures, which increases the relative importance of a promoted photosynthesis under [eCO_2] (Ainsworth & Rogers, 2007; Long, 1991; Long et al., 2004). In contrast, other studies revealed that the CO_2 fertilization effect might be temperature independent or even reduced under a higher air temperature (Drake et al., 1997; Jongen & Jones, 1998; Sillen & Dieleman, 2012; Ziska & Bunce, 1994). This is explained by indirect effects such as the reduced stomatal conductance, which decreases the potential for evaporative cooling in plants grown under [eCO_2] (Drake et al., 1997; McNaughton & Jarvis, 1991). Especially when water availability is limited, increased air temperature and increased [CO_2] in conjunction may thus lead to a drying of the boundary layer of the leaves which increases heat stress and results in a reduced biomass productivity (De Boeck & Verbeeck, 2011; Leuzinger & Körner, 2007; McNaughton & Jarvis, 1991; Morison & Lawlor, 1999). Moreover, Oren et al. (1999) have shown that a concomitant increase in the vapour pressure deficit with increasing air temperature results in stomatal closure, which might be more important than the direct [CO_2] effects on the photosynthetic metabolism.

2.1.4 Influence of other environmental drivers

In addition to climate and CO_2 concentration, other factors such as nutrient availability (in particular nitrogen and phosphorus), herbivores (Frank, 2007), and species diversity affect grassland productivity. An increased species diversity may for example increase biomass productivity under drought conditions, through an enhanced resistance or recovery (Kreyling et al., 2017) of ecosystems. The grazing by herbivores was shown to increase, decrease, or have no influence on productivity, depending on the type of herbivore, grassland studied, and the intensity of grazing (Frank, 2007).

Moreover, these environmental drivers are also likely to affect grassland response to [eCO_2]. For example, the CFE is thought to interact with the nutrient availability in soils, as plants grown in conditions of a high nutrient supply may respond more strongly to [eCO_2] than nutrient-stressed plants (Poorter, 1998; Reich et al., 2006b; Soussana & Lüscher, 2007). The concomitantly increased nitrogen depletion in soils under [eCO_2] causes that available soil nitrogen becomes increasingly limited and reduces the CFE which is referred to as a progressive nitrogen limitation (PNL; Leuzinger et al. 2011; Luo et al. 2004; Reich et al. 2006a).

Summarising, it was shown that global change involves simultaneously occurring alterations in environmental conditions. Due to the number of factors and the possibility of interactive effects, the prediction of ecosystem responses to these global changes remains challenging. To gain better insights on the future provision of ecosystem services by grasslands, and thus the global carbon cycle, this study will focus on the investigation of the influences of the most certain, and uniformly accepted predictions of global change.

2.2 Experimental investigation of influences of global change on grasslands

Since decades, the influence of increased atmospheric CO_2 concentrations on plant productivity has been intensively analysed in various experiments. Here, grasslands are often used for the development and testing of ecological theories, because they are sensitive to perturbations, respond relatively rapidly to environmental

alterations, and it is relatively easy to perform experiments on them (Blair et al., 2014). However, early CO_2 enrichment studies were performed in greenhouses or open-top-chambers (White et al., 2011), which may have caused unintended artificial alterations, e.g. in the micro climate of the investigated plot (Carlyle et al., 2011; Dukes et al., 2005; Porter et al., 2015). For example, increased air temperature with infrared heaters reduces the humidity of the air and causes an unrealistic vapour pressure deficit (De Boeck & Nijs, 2011; Kimball, 2005) and alters soil moisture content (Marchand et al., 2006). Therefore the derived results may be unrealistic. This was indicated by an inconsistency of the results regarding the CO_2 fertilization effect that was mainly caused by the drawbacks of the mostly short-running manipulative experiments (Carlyle et al., 2011; Körner, 2000; Long, 2006; Long et al., 2004). Additionally, long-term experiments under natural conditions revealed a weaker grassland response to [eCO_2] than expected from short-term laboratory experiments (Leakey et al., 2009; Long, 2006; Lüscher et al., 2004). Therefore, it has been advocated that the analysis of biomass responses to increased CO_2 and the interacting effects of multiple environmental factors have to be regarded for ecosystems in their natural environment (Lüscher et al., 2004; Norby & Luo, 2004; Wu et al., 2011). Consequently, to overcome the limitations of the early experimental designs, so-called Free Air Carbon dioxide Enrichment (FACE) experiments represent the most appropriate technology (Leakey et al., 2009; Long, 1991; McLeod & Long, 1999; Nowak et al., 2004; Soussana & Lüscher, 2007). Not surprisingly, results from FACE experiments are in contrast to those from open-top-chamber and greenhouse experiments and raise questions concerning the early findings of the interactions between global change and plant physiology (e.g., Hovenden et al. 2014; Reich et al. 2014). However, due to the high costs for the construction and maintenance of FACE experiments, most investigations so far were relatively short-term and long-term studies are rare.

Since biomass data from ecosystem studies is traditionally derived by destructive sampling methods at harvest dates, the analysis of changes in the grassland productivity remains confined to a relatively broad temporal resolution. However, it is assumed that also short-term changes in environmental conditions, such as ECEs, influence grassland productivity (Angert et al., 2005; Jentsch et al., 2007; Niu et al., 2014; Parmesan et al., 2000; van der Molen et al., 2011). Therefore,

the monitoring of FACE experiments should be provided by an enhanced spatial and temporal resolution at, if possible, low cost as well as non-destructive and rapid. Such enhanced monitoring is possible by hyperspectral techniques, while their application to FACE experiments have so far not been tested.

References

Ainsworth, E. & Rogers, A. (2007): The response of photosynthesis and stomatal conductance to rising [CO_2]: Mechanisms and environmental interactions. *Plant, Cell and Environment*, 30, 3, 258–270.

Ainsworth, E.A. & Long, S.P. (2005): What have we learned from 15 years of free-air CO_2 enrichment (FACE)? A meta-analytic review of the responses of photosynthesis, canopy properties and plant production to rising CO_2. *New Phytologist*, 165, 2, 351–372.

Angert, A., Biraud, S., Bonfils, C., Henning, C., Buermann, W., Pinzon, J., Tucker, C., & Fung, I. (2005): Drier summers cancel out the CO_2 uptake enhancement induced by warmer springs. *Proceedings of the National Academy of Sciences*, 102, 31, 10 823–10 827.

Blair, J., Nippert, J., & Briggs, J. (2014): Grassland ecology. In: Ecology and the Environment. Springer, pp. 389–423.

Brooks, A. & Farquhar, G.D. (1985): Effect of temperature on the CO_2 /O2 specificity of ribulose-1,5-bisphosphate carboxylase/oxygenase and the rate of respiration in the light - Estimates from gas-exchange measurements on spinach. *Planta*, 165, 3, 397–406.

Brookshire, E.N.J. & Weaver, T. (2015): Long-term decline in grassland productivity driven by increasing dryness. *Nature Communications*, 6, 7148.

Carlyle, C.N., Fraser, L.H., & Turkington, R. (2011): Tracking Soil Temperature and Moisture in a Multi-Factor Climate Experiment in Temperate Grassland: Do Climate Manipulation Methods Produce their Intended Effects? *Ecosystems*, 14, 3, 489–502.

Coughenour, M. & Chen, D.X. (1997): Assessment of Grassland and Ecosystem Responses to Atmospheric Change Using Linked Plant-Soil Process Models. *Ecological Applications*, 7, 3, 802–827.

De Boeck, H.J. & Verbeeck, H. (2011): Drought-associated changes in climate and their relevance for ecosystem experiments and models. *Biogeosciences*, 8, 5, 1121–1130.

De Boeck, H.J. & Nijs, I. (2011): An alternative approach for infrared heater control in warming and extreme event experiments in terrestrial ecosystems. *Journal of Ecology*, 99, 3, 724–728.

De Boeck, H.d., Lemmens, C., Zavalloni, C., Gielen, B., Malchair, S., Carnol, M., Merckx, R., Van den Berge, J., Ceulemans, R., & Nijs, I. (2008): Biomass production in experimental grasslands of different species richness during three years of climate warming. *Biogeosciences*, 5, 2, 585–594.

Drake, B.G., Gonzalez-Meler, M.a., & Long, S.P. (1997): MORE EFFICIENT PLANTS: A Consequence of Rising Atmospheric CO_2? *Annual Review of Plant Physiology and Plant Molecular Biology*, 48, 609–639.

Dukes, J.S., Chiariello, N.R., Cleland, E.E., Moore, L.a., Rebecca Shaw, M., Thayer, S., Tobeck, T., Mooney, H.a., & Field, C.B. (2005): Responses of grassland production to single and multiple global environmental changes. *PLoS Biology*, 3, 10.

Farquhar, G., von Caemmerer, S., & Berry, J. (1980): A biochemical model of photosynthetic CO_2 assimilation in leaves of c3 species. *Planta*, 149, 1, 78–90.

Field, C.B., Jackson, R.B., & Mooney, H.A. (1995): Stomatal responses to increased CO_2 : implications from the plant to the global scale. *Plant, Cell & Environment*, 18, 10, 1214–1225.

Frank, D.A. (2007): Drought effects on above- and belowground production of a grazed temperate grassland ecosystem. *Oecologia*, 152, 1, 131–139.

Gherardi, L.A. & Sala, O.E. (2015): Enhanced precipitation variability decreases grass- and increases shrub-productivity. *Proceedings of the National Academy of Sciences*, 112, 41, 12 735–12 740.

Hovenden, M.J., Newton, P.C.D., & Wills, K.E. (2014): Seasonal not annual rainfall determines grassland biomass response to carbon dioxide. *Nature*, 511, 7511, 583–586.

Hufkens, K., Keenan, T.F., Flanagan, L.B., Scott, R.L., Bernacchi, C.J., Joo, E., Brunsell, N.A., Verfaillie, J., & Richardson, A.D. (2016): Productivity of North American grasslands is increased under future climate scenarios despite rising aridity. *Nature Climate Change*, 6, 7, 710.

Hunt, H.W., Elliot, E.T., Detling, J.K., Morgan, J.A., & Chen, D.X. (1996): Responses of a C3 and a C4 perennial grass to elevated CO_2 and temperature under different water regimes. *Global Change Biology*, 2, 35–47.

Idso, K. (1994): Plant responses to atmospheric CO_2 enrichment in the face of environmental constraints: a review of the past 10 years' research. *Agricultural and Forest Meteorology*, 69, 3-4, 153–203.

Idso, S.B., Kimball, B.A., Anderson, M., & Mauney, J.R. (1987): Effects of atmospheric CO_2 enrichment on plant growth: the interactive role of air temperature. *Agriculture, Ecosystems & Environment*, 20, 1, 1–10.

Jentsch, A., Kreyling, J., & Beierkuhnlein, C. (2007): A new generation of climate-change experiments: events, not trends. *Frontiers in Ecology and the Environment*, 5, 7, 365–374.

Jongen, M. & Jones, M.B. (1998): Effects of elevated carbon dioxide on plant biomass production and competition in a simulated neutral grassland community. *Annals of Botany*, 82, 1, 111–123.

Jordan, D.B. & Ogren, W.L. (1984): The CO_2 /O2 specificity of ribulose 1,5-bisphosphate carboxylase/oxygenase - Dependence on ribulosebisphosphate concentration, pH and temperature. *Planta*, 161, 4, 308–313.

Kimball, B. (2005): Theory and performance of an infrared heater for ecosystem warming. *Global Change Biology*, 11, 11, 2041–2056.

Knapp, A.K., Beier, C., Briske, D.D., Classen, A.T., Luo, Y., Reichstein, M., Smith, M.D., Smith, S.D., Bell, J.E., Fay, P.A., Heisler, J.L., Leavitt, S.W., Sherry, R., Smith, B., & Weng, E. (2008): Consequences of More Extreme Precipitation Regimes for Terrestrial Ecosystems. *BioScience*, 58, 9, 811.

Körner, C. (2000): Biosphere responses to CO_2 enrichment. *Ecological Applications*, 10, 6, 1590–1619.

Kreyling, J., Dengler, J., Walter, J., Velev, N., Ugurlu, E., Sopotlieva, D., Ransijn, J., Picon-Cochard, C., Nijs, I., Hernandez, P. et al. (2017): Species richness effects on grassland recovery from drought depend on community productivity in a multisite experiment. *Ecology letters*, 20, 11, 1405–1413.

Leakey, A.D.B., Ainsworth, E.a., Bernacchi, C.J., Rogers, A., Long, S.P., & Ort, D.R. (2009): Elevated CO_2 effects on plant carbon, nitrogen, and water relations: six important lessons from FACE. *Journal of Experimental Botany*, 60, 10, 2859–76.

Leuzinger, S. & Körner, C. (2007): Water savings in mature deciduous forest trees under elevated CO_2. *Global Change Biology*, 13, 12, 2498–2508.

Leuzinger, S., Luo, Y., Beier, C., Dieleman, W., Vicca, S., & Körner, C. (2011): Do global change experiments overestimate impacts on terrestrial ecosystems? *Trends in Ecology & Evolution*, 26, 5, 236–241.

Lloyd, J. & Farquhar, G.D. (2008): Effects of rising temperatures and [CO_2] on the physiology of tropical forest trees. *Philosophical transactions of the Royal Society of London. Series B, Biological Sciences*, 363, 1498, 1811–1817.

Long, S.P. (1991): Modification of the response of photosynthetic productivity to rising temperature by atmospheric CO_2 concentrations: Has its importance been underestimated? *Plant, Cell and Environment*, 14, 729–739.

Long, S.P. (2006): Food for Thought: Lower-Than-Expected Crop Yield Stimulation with Rising CO_2 Concentrations. *Science*, 312, 5782, 1918–1921.

Long, S.P., Ainsworth, E.a., Rogers, A., & Ort, D.R. (2004): Rising atmospheric carbon dioxide: plants FACE the future. *Annual Review of Plant Biology*, 55, 591–628.

Luo, Y. (2007): Terrestrial Carbon-Cycle Feedback to Climate Warming. *Annual Review of Ecology, Evolution, and Systematics*, 38, 1, 683–712.

Luo, Y., Su, B.O., Currie, W.S., Dukes, J.S., Finzi, A., Hartwig, U., Hungate, B., Mc MURTRIE, R.E., Oren, R.A.M., Parton, W.J., Pataki, D.E., Shaw, M.R., Zak, D.R., Field, C.B., & Murtrie, R.E.M.C. (2004): Progressive Nitrogen Limitation of Ecosystem Responses to Rising Atmospheric Carbon Dioxide. *BioScience*, 54, 8, 731.

Lüscher, A., Daepp, M., Blum, H., Hartwig, U.A., & Nösberger, J. (2004): Fertile temperate grassland under elevated atmospheric CO_2 - Role of feed-back mechanisms and availability of growth resources. *European Journal of Agronomy*, 21, 3, 379–398.

Marchand, F., Verlinden, M., Kockelbergh, F., Graae, B., Beyens, L., & Nijs, I. (2006): Disentangling effects of an experimentally imposed extreme temperature event and naturally associated desiccation on arctic tundra. *Functional Ecology*, 20, 6, 917–928.

McLeod, A. & Long, S. (1999): Free-air Carbon Dioxide Enrichment (FACE) in Global Change Research: A Review. *Advances in Ecological Research*, 28, 1–56.

McNaughton, K.G. & Jarvis, P.G. (1991): Effects of spatial scale on stomatal control of traspiration. *Agricultural and Forest Meteorology*, 54, 279-301, 279–301.

Miranda-Apodaca, J., Pérez-López, U., Lacuesta, M., Mena-Petite, A., & Muñoz-Rueda, A. (2015): The type of competition modulates the ecophysiological response of grassland species to elevated CO_2 and drought. *Plant Biology*, 17, 2, 298–310.

Morgan, J.a., Pataki, D.E., Körner, C., Clark, H., Del Grosso, S.J., Grünzweig, J.M., Knapp, A.K., Mosier, A.R., Newton, P.C.D., Niklaus, P.A., Nippert, J.B., Nowak, R.S., Parton, W.J., Polley,

H.W., & Shaw, M.R. (2004): Water relations in grassland and desert ecosystems exposed to elevated atmospheric CO_2. *Oecologia*, 140, 1, 11–25.

Morison, J.I.L. & Lawlor, D.W. (1999): Interactions between increasing CO_2 concentration and temperature on plant growth. *Plant, Cell and Environment*, 22, 6, 659–682.

Myneni, R.B., Keeling, C., Tucker, C.J., Asrar, G., & Nemani, R.R. (1997): Increased plant growth in the northern high latitudes from 1981 to 1991. *Nature*, 386, 6626, 698.

Nippert, J.B., Knapp, A.K., & Briggs, J.M. (2006): Intra-annual rainfall variability and grassland productivity: can the past predict the future? *Plant Ecology*, 184, 65–74.

Niu, S., Luo, Y., Li, D., Cao, S., Xia, J., Li, J., & Smith, M.D. (2014): Plant growth and mortality under climatic extremes: An overview. *Environmental and Experimental Botany*, 98, 13–19.

Norby, R.J. & Luo, Y. (2004): Evaluating ecosystem responses to rising atmospheric CO_2 and global warming in a multi-factor world. *New Phytologist*, 162, 2, 281–293.

Nowak, R.S., Ellsworth, D.S., & Smith, S.D. (2004): Functional responses of plants to elevated atmospheric CO_2 – do photosynthetic and productivity data from face experiments support early predictions? *New Phytologist*, 162, 2, 253–280.

Oren, R., Sperry, J.S.J., Katul, G.G.G., Pataki, D.E., Ewers, B.E.B., Phillips, N., & Schäfer, K.V.R. (1999): Survey and synthesis of intra- and interspecific variation in stomatal sensitivity to vapour pressure deficit. *Plant, Cell and Environment*, 22, 12, 1515–1526.

Owensby, C.E., Ham, J.M., Knapp, a.K., & Auen, L.M. (1999): Biomass production and species composition change in a tallgrass prairie ecosystem after long-term exposure to elevated atmospheric CO_2. *Global Change Biology*, 5, 497–506.

Parmesan, C., Root, T.L., & Willig, M.R. (2000): Impacts of extreme weather and climate on terrestrial biota. *Bulletin of the American Meteorological Society*, 81, 3, 443–450.

Poorter, H. (1998): Do slow-growing species and nutrient-stressed plants respond relatively strongly to elevated CO_2? *Global Change Biology*, 4, 6, 693–697.

Porter, A.S., Gerald, C.E.F., McElwain, J.C., Yiotis, C., & Elliott-Kingston, C. (2015): How well do you know your growth chambers? testing for chamber effect using plant traits. *Plant methods*, 11, 1, 44.

Reich, P., Hobbie, S., Lee, T., & Ellsworth, D. (2006a): Nitrogen limitation constrains sustainability of ecosystem response to CO_2 . *Nature*, 440, 922–925.

Reich, P.B., Hobbie, S.E., & Lee, T.D. (2014): Plant growth enhancement by elevated CO_2 eliminated by joint water and nitrogen limitation. *Nature Geoscience*, 7, 2–6.

Reich, P.B., Hungate, B.a., & Luo, Y. (2006b): Carbon-Nitrogen Interactions in Terrestrial Ecosystems in Response to Rising Atmospheric Carbon Dioxide. *Annual Review of Ecology, Evolution, and Systematics*, 37, 1, 611–636.

Roy, J., Picon-Cochard, C., Augusti, A., Benot, M.L., Thiery, L., Darsonville, O., Landais, D., Piel, C., Defossez, M., Devidal, S., Escape, C., Ravel, O., Fromin, N., Volaire, F., Milcu, A., Bahn, M., & Soussana, J.F. (2016): Elevated CO_2 maintains grassland net carbon uptake under a future heat and drought extreme. *Proceedings of the National Academy of Sciences of the United States of America*, 113, 22, 6224–6229.

Rustad, L., Campbell, J., Marion, G., Norby, R., Mitchell, M., Hartley, A., Cornelissen, J., Gurevitch, J. et al. (2001): A meta-analysis of the response of soil respiration, net nitrogen mineralization, and aboveground plant growth to experimental ecosystem warming. *Oecologia*, 126, 4, 543–562.

Sillen, W.M.a. & Dieleman, W.I.J. (2012): Effects of elevated CO_2 and N fertilization on plant and soil carbon pools of managed grasslands: A meta-analysis. *Biogeosciences*, 9, 6, 2247–2258.

Soussana, J.F. & Lüscher, A. (2007): Temperate grasslands and global atmospheric change: A review. *Grass and Forage Science*, 62, 2, 127–134.

van der Molen, M.K., Dolman, A.J., Ciais, P., Eglin, T., Gobron, N., Law, B.E., Meir, P., Peters, W., Phillips, O.L., Reichstein, M., Chen, T., Dekker, S.C., Doubková, M., Friedls, M.A., Jung, M., van den Hurk, B.J.J.M., de Jeu, R.A.M., Kruijt, B., Ohta, T., Rebel, K.T., Plummer, S., Seneviratne, S.I., Sitch, S., Teuling, A.J., van der Werf, G.R., & Wang, G. (2011): Drought and ecosystem carbon cycling. *Agricultural and Forest Meteorology*, 151, 7, 765–773.

Volk, M., Niklaus, P.A., & Körner, C. (2000): Soil moisture effects determine CO_2 responses of grassland species. *Oecologia*, 125, 3, 380–388.

Wang, D., Heckathorn, S.A., Wang, X., & Philpott, S.M. (2012): A meta-analysis of plant physiological and growth responses to temperature and elevated CO_2 . *Oecologia*, 169, 1, 1–13.

Weltzin, J.F., Loik, M.E., Schwinning, S., Williams, D.G., Fay, P.A., Haddad, B.M., Harte, J., Huxman, T.E., Knapp, A.K., Lin, G. et al. (2003): Assessing the response of terrestrial ecosystems to potential changes in precipitation. *AIBS Bulletin*, 53, 10, 941–952.

White, S.R., Carlyle, C.N., Fraser, L.H., & Cahill, J.F. (2011): Climate change experiments in temperate grasslands: synthesis and future directions. *Biology Letters*.

Wu, Z., Dijkstra, P., Koch, G.W., Peñuelas, J., & Hungate, B.A. (2011): Responses of terrestrial ecosystems to temperature and precipitation change: a meta-analysis of experimental manipulation. *Global Change Biology*, 17, 2, 927–942.

Wullschleger, S., Tschaplinski, T., & Norby, R. (2002): Plant water relations at elevated CO_2 – implications for water-limited environments. *Plant, Cell and Environment*, 25, 319–331.

Yang, Y., Fang, J., Ma, W., & Wang, W. (2008): Relationship between variability in aboveground net primary production and precipitation in global grasslands. *Geophysical Research Letters*, 35, 23.

Zhao, M. & Running, S.W. (2010): Drought-induced reduction in global terrestrial net primary production from 2000 through 2009. *Science*, 329, 5994, 940–943.

Zhu, Z., Piao, S., Myneni, R.B., Huang, M., Zeng, Z., Canadell, J.G., Ciais, P., Sitch, S., Friedlingstein, P., Arneth, A., Liu, R., Mao, J., Pan, Y., Peng, S., Peñuelas, J., & Poulter, B. (2016): Greening of the Earth and its drivers. *Nature Climate Change*, 6, 8, 791–795.

Ziska, L.H. & Bunce, J.a. (1994): Increasing growth temperature reduces the stimulatory effect of elevated CO_2 on photosynthesis or biomass in 2 perennial species. *Physiologia Plantarum*, 91, 183–190.

3 Conception and technical preparation of the working packages

In this work, the analysis of global change-related influences on the productivity of a temperate grassland will be based on the longest globally operating FACE systems on grasslands, the GiFACE experiment. Contrasting results from earlier, mostly manipulative experiments highlighted the need for an analysis based on long-term data under natural climatic conditions. Since biomass data from long-term time series is traditionally derived by destructive sampling methods at harvest dates, short-term changes in grassland characteristics might be overseen. To overcome this limitation and bridge the scales i.e. establish a link from long-term observations to in-depth analysis by high-resolution spatio-temporal approaches, the possibilities of non-destructive grassland monitoring using hyperspectral approaches will be tested. Therefore, this chapter starts with a short description of the GiFACE experiment (**section 3.1**), followed by the methodological work flow of the thesis, divided into the working packages needed for the investigations of **H 1** (**section 3.2**), **H 2** (**section 3.3**), **H 3** (**section 3.4**), and a general overview of the working packages including a detailed overview of the work flow in Figure 3.2.

3.1 Study area - the Giessen Free Air Carbon dioxide Enrichment experiment

The investigation of the influence of global change-related environmental drivers on the grassland productivity in this study is based on the longest operating FACE

systems on grassland, the GiFACE experiment. The GiFACE facility covers a non-grazed and extensively managed species-rich grassland located near Giessen, Germany (50° 32' N and 8° 41'E; 172 m a.s.l.), and is in operation since 1998. The experimental facility comprises six FACE rings of 8 m in diameter (for a detailed description, see Andresen et al. 2018; Jäger et al. 2003). Three rings are operated under elevated CO_2 conditions by enriching the air during daylight hours to ∼20% above the ambient [CO_2] ([aCO_2]). In the other three rings (controls) the grassland vegetation grows under [aCO_2]. Due to variable wind conditions and technical limitations, the CO_2 enrichment showed slight variations within and over years. The C3 vegetation showed similar abundances within all rings, dominated by the grasses *Arrhenatherum elatius*, *Holcus lanatus* and *Poa pratensis*, accompanied by a forb fraction including one legume species present in low abundance (Kammann et al., 2005). From 1995 onwards, the grassland was fertilised with 40 kg ha^{-1} yr^{-1} calcium ammonium nitrate, which equals the annual N deposition in many intensively used agricultural regions (Reich et al., 2001), supplemented by 600 kg ha^{-1} yr^{-1} of 10% P_2 O_5 + 15% K_2O + 3% MgO and 33% CaO + MgO each spring (Kammann et al., 2005). The soil is a fluvic gleysol (Spaargaren et al., 1994) with a sandy clay loam layer above a clay layer of variable depth (Kammann et al., 2005). To maintain an undisturbed soil, the sensor installation inside the rings proceeded non-invasively.

3.2 Investigations on H 1: Reduced CO_2 fertilization effect under more extreme average weather conditions and after extreme climatic events

A general issue for the investigation of CO_2 enrichment experiments is that the mostly factorial treatment designs are used to quantify cause-effect relationships (e.g. Ainsworth & Long, 2005; Bindi et al., 2001; Casella & Soussana, 1996; Kammann et al., 2005; Shaw et al., 2002; Wullschleger et al., 2002). However, due to the complexity of CO_2 enrichment studies in general, and of FACE experiments in particular, the actual [CO_2] in the plots that are enriched with elevated CO_2 concentrations is fluctuating. Consequently, the interpretation of

Figure 3.1: Experimental plots for the CO_2 enrichment at the Giessen FACE site.

plant responses to elevated [CO_2] in interaction with e.g., environmental conditions might be misleading when constant CO_2 concentrations as defined by the factorial design are assumed. Therefore, a method has to be developed, which investigates the responses of above-ground grassland productivity to elevated [CO_2] and average weather conditions under consideration of the actual, measured CO_2 concentrations within the relevant plots. Situated in a real-world environment, the variables that describe the environmental conditions are highly correlated which complicates the disentanglement of the influence of a single environmental variable to biomass productivity. Therefore, this approach has also to depict the accompanying environmental conditions. Combining biomass measurements, the actual CO_2 concentrations, and real-world environmental conditions, **WP 1** aims to increase the understanding of the effect of average weather conditions on the CFE in the grassland under investigation. Additionally, since this approach might also be useful to reliably quantify cause-effect relationships in other experiments, the proposed method shall be made publicly available within a new R-package entitled "Moving Subset Analysis FACE" (msaFACE).

Beyond the estimated impacts from changes in the mean variables (what might be termed the "trend effect"), changes in the magnitude or frequency of extreme events ("single climatic event effect") are likely to impair plant production under climatic change, and thus are essential when investigating the response of biotic systems to climate drivers (Jentsch et al., 2007; Parmesan et al., 2000). Therefore, within **WP 2**, a time series analysis on the combined effects of increased [CO_2] and extreme climatic events on above-ground biomass production will be conducted using the long-term GiFACE data. This will be the first time that such a continuous long-term data set is used to evaluate this kind of response. The CFE in this study will be represented by the effect size of the above-ground biomass, which is defined as the relative differences in biomasses of the plots under [eCO_2] compared to the control plots under [aCO_2]. The assumptions is, that sudden changes in growing conditions such as those caused by ECEs may lead to significant changes in the effect size, while the effect size of adjacent years under similar growing conditions should not differ significantly. Thus, changes in effect size of the biomass in comparison with the previous year will be used to examine the impact of ECEs on the yield stimulating effect of [eCO_2].

3.3 Investigations on H 2: Assessment of potential future above-ground biomass productivity under projected global change conditions.

Within the subsequent working package (**WP 3**), a method has to be developed linking the experimental data from the GiFACE experiment with projected climate alterations from the IPCC model ensemble, to assess the potential of the future provision of ecosystem services by temperate grasslands. Therefore, individual statistical models will be developed that predict the biomasses within the rings under [eCO_2] and the control rings, respectively. Additionally, potential future climatic regimes will be generated based on the observed environmental conditions during the experimental period, and the derived statistical biomass models will be used to predict potential biomasses within these regimes for both, rings under [eCO_2] and rings under [aCO_2]. To assess the potential future grassland productivity,

the different potential climate regimes and their climate predictor alterations will be compared to the projected climate changes in the mid 21st century, when the atmospheric [CO_2] will be approximately at the level of the experimentally enriched [CO_2] in the GiFACE ($\sim$ 20% above the [aCO_2] under present-day conditions).

3.4 Investigations on H 3: Do hyperspectral techniques enable the monitoring of grassland ecosystem services with high spatio-temporal resolutions?

Although the analysis of the long-term time series (**WP 1 - WP 3**) will likely give important insights on the carbon-plant relationship, it is expected to be constrained by the low temporal resolution of the conventional, destructive sampling approach (e.g., two harvests in the GiFACE experiment). To overcome this restriction, methods have to be developed that are able to investigate the plant responses on a spatially and temporally higher resolution than is possible by conventional approaches. Here, approaches based on hyperspectral data have proven to be advantageous, since they allow a high temporal resolution including spatially explicit data. Additionally, they are rapid, non-destructive and cost-effective which makes them very interesting for the monitoring of ecosystem studies. The comprehensive statistical methods implemented in the open-source software CRAN R provide the ideal requirements for the processing and analysing of large datasets, such as those derived by remote sensing techniques. However, only fragmentary solutions are available to work with hyperspectral data within CRAN R, while a combination of hyperspectral techniques with the statistical power of R is straight forward. Therefore, within **WP 4**, the existing R functionality regarding the basic processing functions for hyperspectral data will be enhanced. The new functionality was made publicly available in a new R-package entitled "Hyperspectral Data Analysis in R" (hsdar).

Using the enhanced and newly developed methods of the open-source software R (**WP 4**), the investigation of the hyperspectral predictability of various grassland

traits within the GiFACE experiment will be conducted within **WP 5**. At first, various spectral normalisation techniques have to be applied to the hyperspectral data to enhance reflectance features and reduce perturbing effects that may arise e.g., from soil background, varying illumination and viewing geometry. Defined by the different normalisation approaches, various predictor feature spaces will be created, and after a careful selection of predictor variables for each grassland trait and within each feature space, the most suitable predictors will be chosen for the final models for each grassland trait. The final models will then be interpreted with regard to their predictive performances, and then used to predict the most important grassland traits related to ecosystem services to show the potential of non-destructive, hyperspectral monitoring techniques. Here, it is anticipated that the accuracy of hyperspectral approaches might be affected by different [CO_2]s, since the latter are assumed to alter plant physiology. Therefore, the investigation of the hyperspectral predictability of the grassland traits will be expanded to the analysis of potential prediction biases that might occur due to combined analysis of plots under [eCO_2] and [aCO_2].

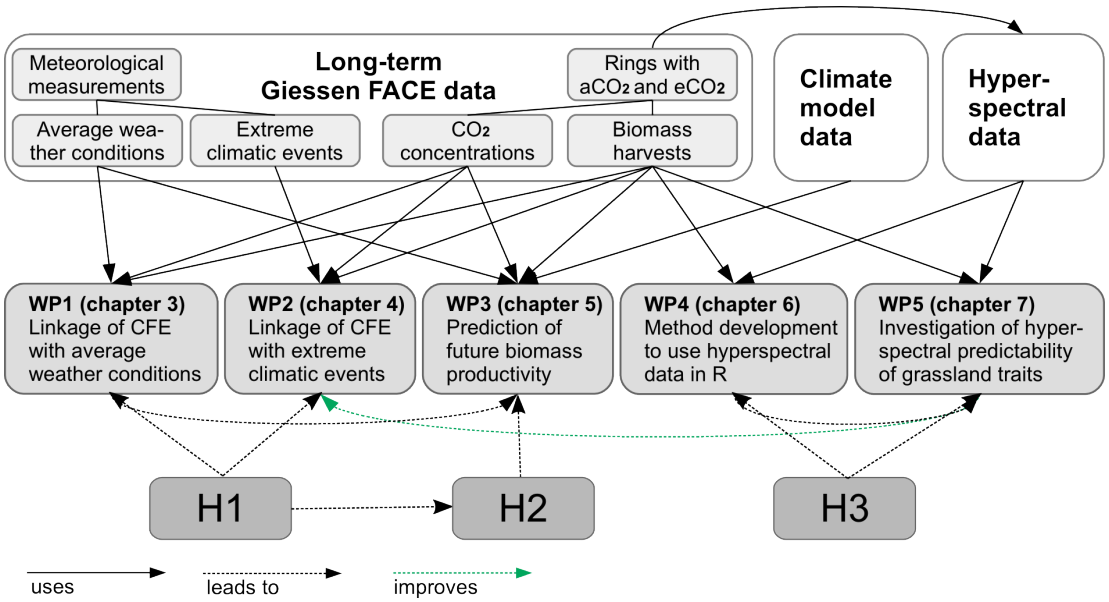

Figure 3.2: Detailed work flow of the thesis' main part. *Note.* aCO_2 and eCO_2 are ambient and elevated CO_2 concentrations, respectively. CFE is the CO_2 fertilization effect.

Due to complexity and the necessity of developing different methods for the investigation of **H 1** and **H 3**, two working packages deal with each of these hypotheses (compare Figs 1.1 and 3.2). Consequently, to test the hypotheses, the following five working packages will build the framework of the present thesis:

WP 1 Meteorological observations and CO_2 concentrations have to be aggregated to represent average conditions. Statistical models have to be developed to link different average weather conditions and varying CO_2 concentrations with above-ground biomass productivity. Model outputs will be investigated regarding if and how the CFE depends on average weather conditions to test part one of **H 1**.

WP 2 The meteorological time series has to be analysed regarding the occurrence of extreme climatic events. Changes in the response of above-ground biomass to different CO_2 concentrations between consecutive years have to be linked to intervening extreme climatic events to test part two of **H 1**.

WP 3 Statistical models to link biomass productivity with average weather conditions have to be developed for the rings under ambient and elevated [CO_2], respectively. Potential future climate regimes have to be created based on the observed weather conditions during the experimental period. Biomass productivities will be predicted within each regime and compared to projected climate change conditions in years with a similar [CO_2] compared to the experimentally enriched one, to test **H 2**.

WP 4 Functions and classes have to be developed to manage, process, and analyse hyperspectral data within the open-source software CRAN R. Using chlorophyll data from the GiFACE plots, a preliminary study on the feasibility of **H 3** will be conducted.

WP 5 Different transformations of hyperspectral reflectance data have to be delineated and linked to grassland traits related to ecosystem services that are derived in the laboratory. The spectral transformations will be investigated regarding their predictive performances for each grassland trait, and the most suitable ones used to predict on a high-resolution spatio-temporal level, and analysed regarding their performances under different CO_2 concentrations, to test **H 3**.

References

Ainsworth, E.A. & Long, S.P. (2005): What have we learned from 15 years of free-air CO_2 enrichment (FACE)? A meta-analytic review of the responses of photosynthesis, canopy properties and plant production to rising CO_2. *New Phytologist*, 165, 2, 351–372.

Andresen, L.C., Yuan, N., Seibert, R., Moser, G., Kammann, C.I., Luterbacher, J., Erbs, M., & Müller, C. (2018): Biomass responses in a temperate european grassland through 17 years of elevated CO_2. *Global Change Biology*, 24, 9, 3875–3885.

Bindi, M., Fibbi, L., & Miglietta, F. (2001): Free Air CO_2 Enrichment (FACE) of grapevine (Vitis vinifera L.): II. Growth and quality of grape and wine in response to elevated CO_2 concentrations. *European Journal of Agronomy*, 14, 145–155.

Casella, E. & Soussana, J.F. (1996): Long-term effects of CO_2 enrichment and temperature increase on a temperate grass sward. *Plant and Soil*, 182, 311, 101–114.

Jäger, H.J., Schmidt, S.W., Kammann, C., Grünhage, L., Müller, C., & Hanewald, K. (2003): The University of Giessen Free-Air Carbon Dioxide Enrichment Study: Description of the Experimental Site and of a New Enrichment System. *Journal of Applied Botany*, 77, 117–127.

Jentsch, A., Kreyling, J., & Beierkuhnlein, C. (2007): A new generation of climate-change experiments: events, not trends. *Frontiers in Ecology and the Environment*, 5, 7, 365–374.

Kammann, C., Grünhage, L., Grüters, U., Janze, S., & Jäger, H.J. (2005): Response of aboveground grassland biomass and soil moisture to moderate long-term CO_2 enrichment. *Basic and Applied Ecology*, 6, 4, 351–365.

Parmesan, C., Root, T.L., & Willig, M.R. (2000): Impacts of extreme weather and climate on terrestrial biota. *Bulletin of the American Meteorological Society*, 81, 3, 443–450.

Reich, P.B., Knops, J., Tilman, D., Craine, J., Ellsworth, D., Tjoelker, M., Lee, T., Wedin, D., Naeem, S., Bahauddin, D., Hendrey, G., Jose, S., Wrage, K., Goth, J., & Bengston, W. (2001): Plant diversity enhances ecosystem responses to elevated CO_2 and nitrogen deposition. *Nature*, 410, 6839, 809–810.

Shaw, M.R., Zavaleta, E.S., Chiariello, N.R., Cleland, E.E., Mooney, H.A., & Field, C.B. (2002): Grassland responses to global environmental changes suppressed by elevated CO_2. *Science*, 298, 5600, 1987–1990.

Spaargaren, O., Arnold, R., & Blume, H. (1994): World reference base for soil resources. *Wageningen/Rome*.

Wullschleger, S., Tschaplinski, T., & Norby, R. (2002): Plant water relations at elevated CO_2 – implications for water-limited environments. *Plant, Cell and Environment*, 25, 319–331.

4 Reduced CO_2 fertilization effect in temperate C3 grasslands under more extreme weather conditions

This chapter is published in *Nature Climate Change*, 7, 137 – 141, 2017.
Submitted: 01 February 2016, accepted: 29 November 2016

Reduced CO_2 fertilization effect in temperate C3 grasslands under more extreme weather conditions

Wolfgang A. Obermeier[1]*, Lukas W. Lehnert[1], Claudia I. Kammann[2], Christoph Müller[3,4], Ludger Grünhage[3], Juerg Luterbacher[5,6], Martin Erbs[3], Gerald Moser[3], Ruben Seibert[3], Naiming Yuan[5] and Joerg Bendix[1]

[1] Faculty of Geography, Philipps-University of Marburg, Deutschhausstraße 10, 35037 Marburg, Germany
[2] Department of Soil Science and Plant Nutrition, WG Climate Change Research for Special Crops, Hochschule Geisenheim University, Von-Lade Str. 1, 65366 Geisenheim, Germany
[3] Institute of Plant Ecology, Justus Liebig University Giessen, Heinrich-Buff-Ring 26, 35392 Giessen, Germany
[4] School of Biology and Environmental Science and Earth Institute, University College Dublin, Dublin 4, Ireland
[5] Department of Geography, Climatology, Climate Dynamics and Climate Change, Justus Liebig University, Senckenbergstraße 1, 35390 Giessen, Germany
[6] Centre for International Development and Environmental Research, Justus Liebig University Giessen, Senckenbergstraße 3, 35390 Giessen, Germany

---

Abstract The increase in atmospheric greenhouse gas concentrations from anthropogenic activities is the major driver of recent global climate change (IPCC, 2013). The stimulation of plant photosynthesis due to rising atmospheric carbon dioxide concentrations ($[CO_2]$) is widely assumed to increase the net

primary productivity (NPP) of C3 plants - the CO_2 fertilization effect (CFE; Ainsworth & Rogers 2007; Arneth et al. 2010; IPCC 2013; Long 1991; Luo 2007; Nowak et al. 2004; Soussana & Lüscher 2007). However, the magnitude and persistence of the CFE under future climates, including more frequent weather extremes, are controversial (Ainsworth & Rogers, 2007; Arneth et al., 2010; Friedlingstein et al., 2014; Hovenden et al., 2014; IPCC, 2013; Reich et al., 2014; Reichstein et al., 2013; Smith et al., 2016). Here we use data from 16 years of temperate grassland grown under 'free-air carbon dioxide enrichment' conditions to show that the CFE on above-ground biomass is strongest under local average environmental conditions. The observed CFE was reduced or disappeared under wetter, drier and/or hotter conditions when the forcing variable exceeded its intermediate regime. This is in contrast to predictions of an increased CO_2 fertilization effect under drier and warmer conditions (Wang et al., 2012). Such extreme weather conditions are projected to occur more intensely and frequently under future climate scenarios (IPCC, 2013). Consequently, current biogeochemical models might overestimate the future NPP sink capacity of temperate C3 grasslands and hence underestimate future atmospheric [CO_2] increase.

Subject terms Climate Change, Climate-change ecology, Ecophysiology, Grassland ecology

4.1 Main

Grassland covers approximately 26% of the terrestrial area (Foley et al., 2011) and approximately 70% of the global farmland (Soussana & Lüscher, 2007). In

Europe, approximately 38% of the agricultural area is covered by permanent meadows and pastures (Food and Agriculture Organization of the United Nations Statistics Division, 2011), which are mainly composed of C3 species. As the photosynthesis of C3 plants responds positively to rising [CO_2], C3 grasslands may play an important role in mitigating the increase of atmospheric [CO_2] (Ainsworth & Rogers, 2007; Arneth et al., 2010; Friedlingstein et al., 2014; IPCC, 2013; Long, 1991; Luo, 2007; Nowak et al., 2004; Soussana & Lüscher, 2007). However, the effects of elevated CO_2 ([eCO_2]) on the future terrestrial carbon balance and the [eCO_2]-induced carbon sink remain uncertain because of the scarcity of experimental long-term field data (Booth et al., 2012; Friedlingstein et al., 2014; IPCC, 2013; Schimel et al., 2015; Smith et al., 2016).

Photosynthesis, which is the central mechanism of terrestrial carbon (C) uptake, is primarily controlled by the fixation of CO_2 through carboxylation and the stomatal resistance that limits the CO_2 supply (Ainsworth & Rogers, 2007; Long, 1991; Luo, 2007; Nowak et al., 2004; Soussana & Lüscher, 2007). In C3 plants, higher CO_2 partial pressure under [eCO_2] leads to an enhanced carboxylation, concurrently reducing oxygenation and photorespiratory CO_2 losses (Long, 1991; Luo, 2007; Morison & Lawlor, 1999). As a consequence, net C uptake is enhanced if the [CO_2] increases (Ainsworth & Rogers, 2007; Long, 1991; Luo, 2007; Nowak et al., 2004; Soussana & Lüscher, 2007). Moreover, plants growing under [eCO_2] may reduce stomatal aperture since the C demand of photosynthesis is met earlier, which decreases stomatal conductance. This results in reduced transpirational water loss and increased water-use efficiency (WUE), which can translate into slower soil moisture depletion and, thus, reduced water stress for plants (Ainsworth & Rogers, 2007; Morgan et al., 2004; Owensby et al., 1999; Soussana & Lüscher, 2007; Volk et al., 2000). Therefore, in this classic carbon-centric view, the CFE can be assumed to be particularly high under drier and/or hotter weather conditions.

However, the magnitude and persistence of the CFE must be questioned under changing environmental conditions, particularly if climate extremes occur more frequently (Friedlingstein et al., 2014; Hovenden et al., 2014; Reich et al., 2014; Reichstein et al., 2013; Smith et al., 2016). Liebig's law-of-the-minimum

and the multiple-limitation hypotheses indicate that plant biomass production is not solely limited by the C supply but also by a set of cofactors including water availability, temperature and solar radiation (Farrior et al., 2013; Fatichi et al., 2014; Körner, 2015; Reich et al., 2014). Accordingly, the C uptake per unit leaf area and the plant growth rate may not strictly correlate, especially when C uptake is dependent on tissue growth (Fatichi et al., 2014; Körner, 2015). Under such circumstances, these environmental controls on tissue growth govern the C demand and, hence, the C uptake of plants (Fatichi et al., 2014; Körner, 2015). In contrast to the carbon-centric view, the greatest CFE would, therefore, be expected when environmental conditions are favourable for plant growth, that is close to the average conditions to which the plant community is adapted.

Free-air carbon dioxide enrichment (FACE) experiments represent the most appropriate technology for testing the effects of multiple environmental factors on CFE (Long, 1991; Nowak et al., 2004; Soussana & Lüscher, 2007). Few studies have addressed the CFE of grasslands with regard to the changing environmental conditions over timescales of several years (Morgan et al., 2004; Owensby et al., 1999). Those studies have primarily relied on forced manipulations (Dukes et al., 2005; Hovenden et al., 2014; Reich et al., 2014; Shaw et al., 2002) which may cause unintended artificial alterations (Dukes et al., 2005). The aim of our study was to investigate the influence of real-world climatic variations on the CFE of temperate C3 grassland by the globally longest FACE time series gathered in the Giessen FACE experiment (1998-2013, see Supplementary Figures 4.4 - 4.6). As no standard approach for such an analysis is available, we developed a new custom-tailored technique termed moving subset analysis. This approach is explained in detail in the Methods and the Supplementary Information (see Supplementary Figures 4.7 - 4.9). Briefly, the approach includes the following main features. Initially, the available time series (1998-2013) from the experiment is accumulated to averages or sums of a three-month period before harvest each year (for *experiment-support variables*, for example, average air temperature, see Supplementary Table 4.1). Then, the sequence of the years is rearranged in ascending order regarding the level of each environmental variable (forcing experiment-support variable), to form five-year subsets with similar environmental characteristics. In the next step, the CFE for each subset is derived as the slope between the total above-ground biomass (TAB)

and the average [CO_2] three months before harvest (both logarithmus naturalis (ln)-transformed). Finally, the calculated CFE values and their significance (slope and p value of the regression models) are plotted against the average of each forcing experiment-support variable in the subset (see Figures 4.1 and 4.2, and Supplementary Figures 4.8 and 4.9) to interpret the environmental influence of single and combinations of the *experiment-support variables* on the CFE. In the following, the definition of 'intermediate climatic conditions' refers to the mean $\pm$ 1 s.d. of the respective experiment-support variable three months before the harvest (vertical dashed lines in Figures 4.1 and 4.2; see Supplementary Table 4.2 for the values). More extreme environmental conditions can be assumed when the five-year averages of the *experiment-support variables* exceed the thresholds of their mean $\pm$ 1 s.d. of the entire time series.

We find the strongest CFE when intermediate environmental conditions prevail in the three months before harvest, as evidenced by the cumulative rainfall (168 mm, Fig. 4.1a), groundwater table height ($-$90 cm, Fig. 4.1b), vapour pressure deficit (0.67 kPa, Fig. 4.1c) and evapotranspiration (113 mm, Fig. 4.2d). These conditions were also characterized by low to intermediate five-year averages of air temperature and solar radiation whereas wind speed was higher than average (see the rows beneath the CFE plot for the respective environmental variable in Fig. 4.1). Likewise, the most prominent CFE was observed under conditions of intermediate air temperature (17.4°C, Fig. 4.2a) and wind speed (2.42 m s^{-1}, Fig. 4.2c), when five-year averages of rainfall and the height of the groundwater table were on an intermediate level, too. The same trend was observed for a multi-scalar drought index based on the climatic water balance (the standardized precipitation evapotranspiration index, SPEI; Fig. 4.1d), which shows the greatest CFE under weak drought conditions (negative values).

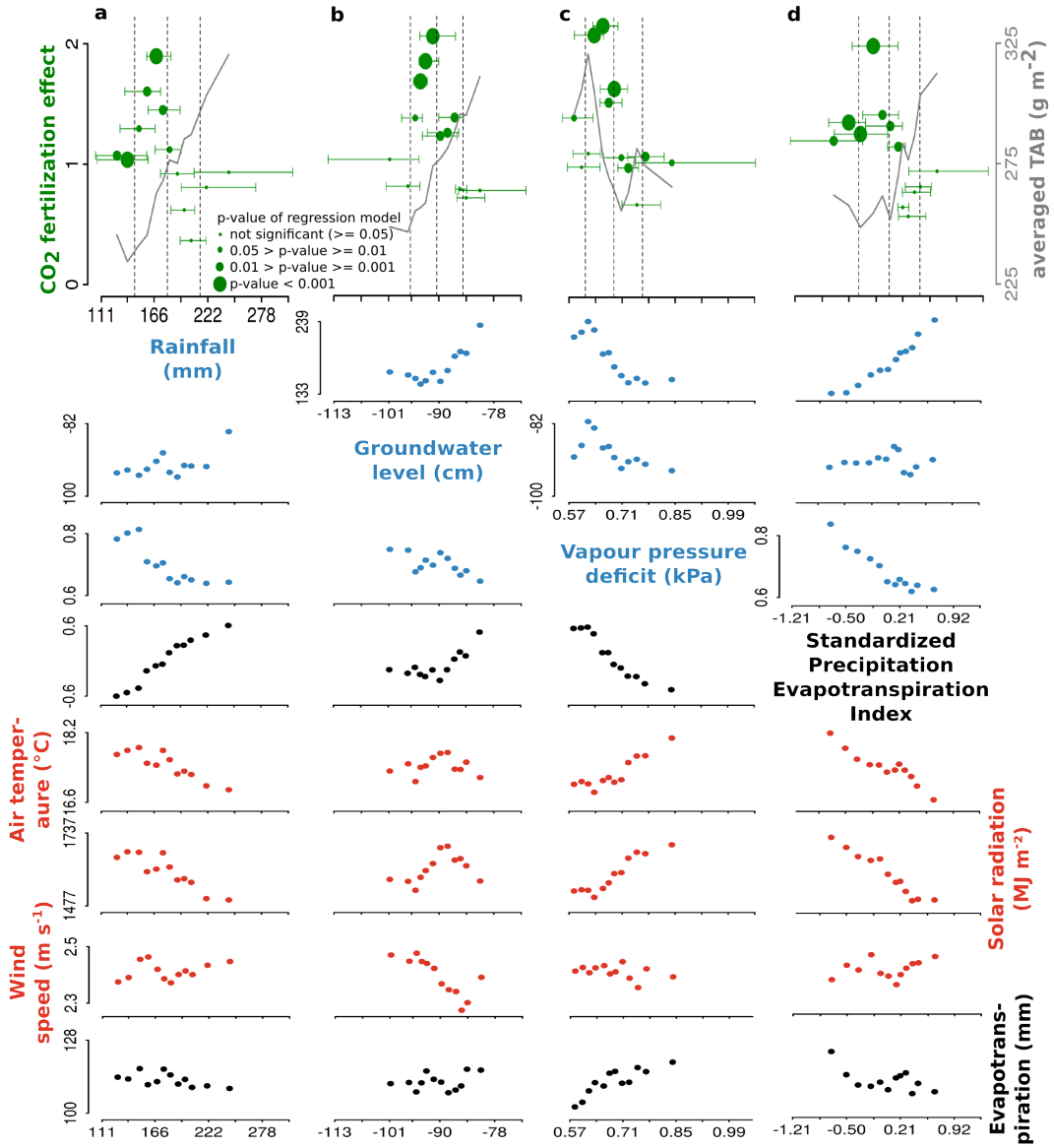

Figure 4.1: Dependence of the CO_2 fertilization effect (CFE) on drought-related variables. a-d, The upper row depicts the CFE dependent on rainfall (**a**), groundwater table height (**b**), vapour pressure deficit (**c**), and standardized precipitation evapotranspiration index (**d**); the accompanying environmental conditions are plotted in the rows underneath. See Methods and Supplementary Information for a detailed explanation of the calculations. Point sizes increase with decreasing p values as shown in the legend. Horizontal lines depict the absolute range of the experiment-support variable in the respective subset. The vertical dashed lines mark the thresholds of the intermediate and extreme environmental regimes. The solid grey line depicts the average total above-ground biomass (TAB) of all observations. Due to subset-wise aggregation regarding the forcing *experiment-support variables*, the accompanying *experiment-support variables*' values do not necessarily indicate conditions within single years.

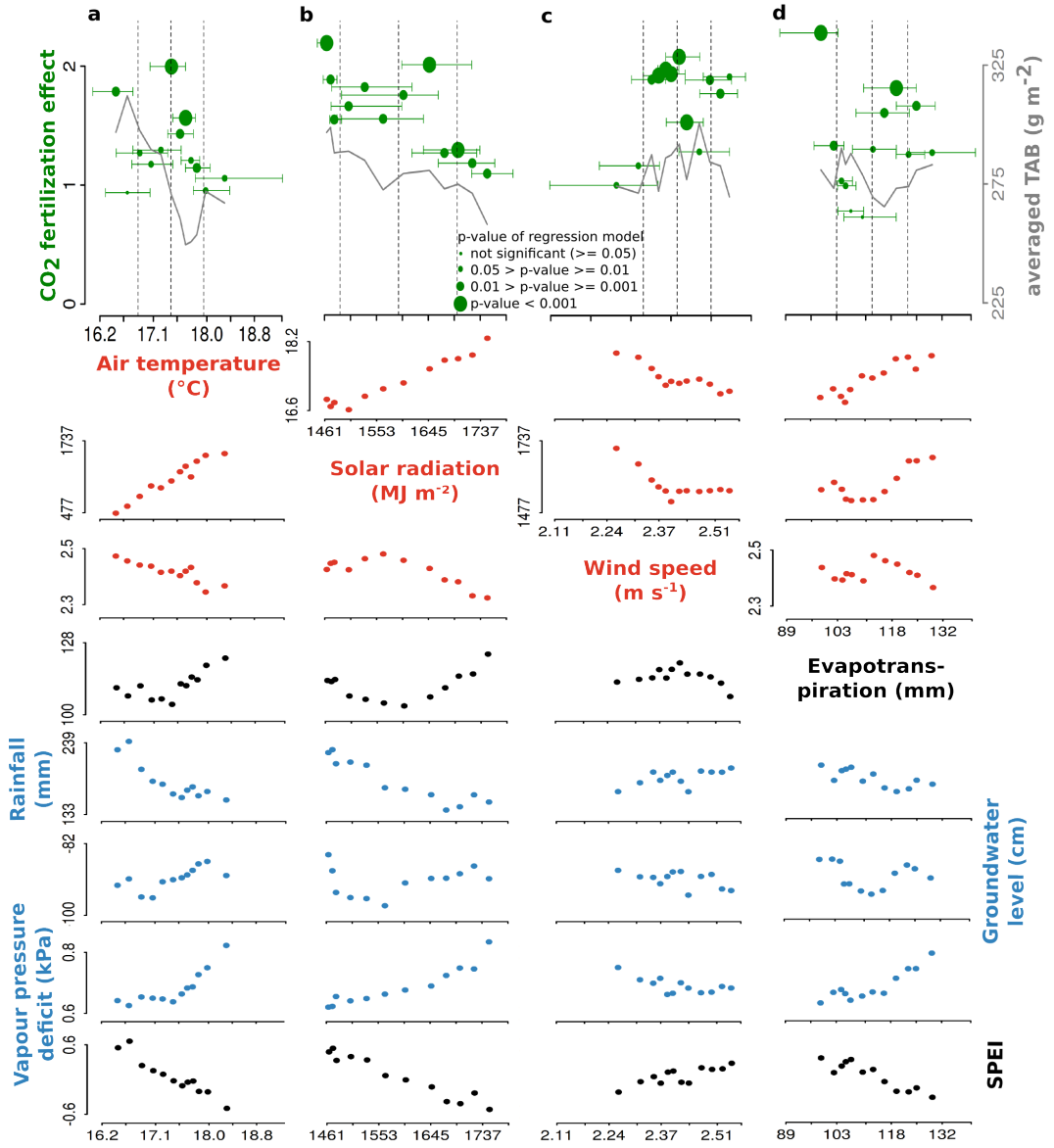

Figure 4.2: Dependence of the CO_2 fertilization effect (CFE) on heat-related variables. a-d, The upper row depicts the CFE dependent on air temperature (**a**), solar radiation (**b**), wind speed (**c**) and evapotranspiration (**d**); the accompanying environmental conditions are plotted in the rows underneath. For a description of the graphic, see the caption of Fig. 4.1.

Regarding water-related variables, the CFE is, in theory, characterized by an increased WUE of plants exposed to [eCO_2] (Morgan et al., 2004; Nowak et al., 2004; Owensby et al., 1999; Volk et al., 2000), which is advantageous if there

is the need for plants to cope with drier conditions when water scarcity may limit growth (Hovenden et al., 2014; Morgan et al., 2004; Nowak et al., 2004; Reich et al., 2014). Under ample water availability, the benefit from an increased WUE is less important. As the stomatal resistance is lower when more water is available, the sensitivity of photosynthesis to an altered [CO_2] should essentially decrease with water availability. Notably, this ability to modulate stomatal aperture appears to be important even in the strong mesic ecosystem of the current study, as suggested by the reduced CFE under conditions of water surplus (Fig. 4.3). Plants that are adapted to a good water supply should be susceptible to improved WUE under [eCO_2] in combination with reduced water availability. However, the reduced CFE found under drier conditions (Fig. 4.3) indicates a limitation of the positive effect of enhanced WUE under [eCO_2], which stays in contrast to previous studies (Ainsworth & Rogers, 2007; Morgan et al., 2004; Nowak et al., 2004; Owensby et al., 1999; Volk et al., 2000). Similar observations were reported in FACE experiments on drier temperate grasslands in Australia (Hovenden et al., 2014) and in the United States (Reich et al., 2014). These observations were explained by resource limitation if water scarcity generally limited plant growth (Hovenden et al., 2014; Reich et al., 2014) due to insufficient turgor pressure (Fatichi et al., 2014; Körner, 2015). This effect may be exacerbated by limited microbial activity and nutrient availability in dry soils, factors that contribute to multiple environmental limitations (Ainsworth & Rogers, 2007; Hovenden et al., 2014; Nowak et al., 2004).

The weak or nonsignificant CFEs under warmer conditions (Fig. 4.3) are also in contrast to the classic carbon-centric view, which assumes an enhancement of the CFE under higher air temperature when the ratio of photosynthesis to photorespiration is decreased (Long, 1991; Morison & Lawlor, 1999; Wang et al., 2012). However, for increasing air temperatures, a concomitant increase in the vapour pressure deficit (see also Supplementary Tables 4.3 and 4.4) and resulting stomatal closure was shown to be more important than the direct [CO_2] effects on the photosynthetic metabolism (Oren et al., 1999). Thus, in combination with the reduced stomatal conductance under [eCO_2], stomata closure can cause a strong reduction in transpirational cooling, which is likely to aggravate heat stress, especially under conditions of low wind speed (De Boeck & Verbeeck,

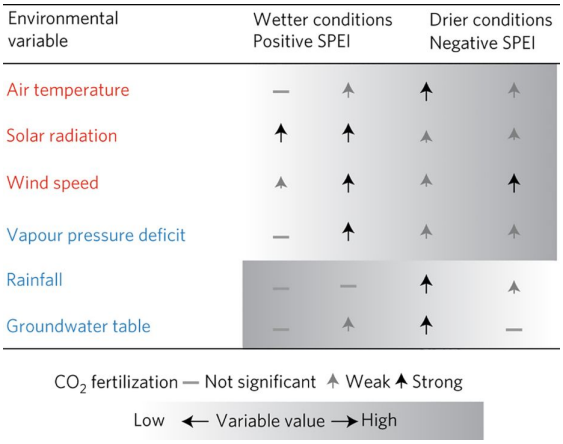

Figure 4.3: Synopsis of the CO_2 fertilization effect dependent on different environmental conditions during the three months preceding the harvest. The columns are ordered from wetter to drier on the basis of the standardized precipitation evapotranspiration index (SPEI).

2011; Morison & Lawlor, 1999) (Figure 2c). Moreover, heat stress may even be exacerbated as high air temperatures are frequently related with dry periods (Figures 4.1a and 4.2a,b and Supplementary Tables 4.3 and 4.4), thereby inducing stomatal closure (De Boeck & Verbeeck, 2011).

Irrespective of previous work on the CO_2 fertilization effect, we describe for the first time within a 16-year-long data set from a mesic grassland that environmental limitations other than CO_2 availability govern the grassland CO_2 response in both directions (low and high extremes), which is in clear contrast to the carbon-centric view on $[CO_2]$ effects. Our results do not support the assumption that the CFE is greater with lower water availability and higher air temperature (Long, 1991; Morison & Lawlor, 1999; Wang et al., 2012), conditions under which above-ground biomass production is reduced *per se* (see Figures 4.1a and 4.2a). The strongest benefit from rising $[CO_2]$ can be expected under 'average' climatic conditions (that is, those conditions to which the plant community is adapted). The CFE decreases when environmental conditions approach boundaries of 'too hot', 'too dry', or 'too wet', that is, extreme weather periods that may occur more frequently in the coming decades.

Beyond increased air temperatures (high confidence), an increased frequency of meteorological droughts (medium confidence) and heavy precipitation events

(high confidence) is projected for future summers in Central Europe (IPCC, 2013). Therefore, the CFE, which currently represents a significant global C sink (IPCC, 2013), will probably decline under future climatic conditions. As the total above-ground biomass production of the investigated grassland decreases under such conditions, terrestrial ecosystems may turn from C sinks to C sources earlier than previously projected (for the mid twenty-first century) (Cox et al., 2000). Such a change in ecosystem services was observed during a strong Europe-wide reduction of the net primary productivity, resulting in a net source of CO_2 caused by the pronounced heat and drought in 2003 (Ciais et al., 2005). Notably, in this European 'heat wave year', a negative effect of [eCO_2] on biomass production was observed in our FACE experiment (see Supplementary Figures 4.5 and 4.6), which supports our findings. A weakening of the CFE accompanied with a reduced terrestrial C sink capacity under the more frequent extreme climatic conditions in the coming decades may thus accelerate the increase of atmospheric [CO_2] and global warming.

Acknowledgements

The contribution of the following individuals to the initiation, construction, installation and long-term, ongoing maintenance of the Giessen FACE experiment is gratefully acknowledged: H.-J. Jäger (deceased 2013), S. Schmidt, J. Senkbeil, W. Stein, B. Lenz, J. Franz, T. Strohbusch, G. Mayer and A. Brück. The continued financial support of the Hessian Agency for Nature Conservation, Environment and Geology is gratefully acknowledged since it allowed an exceptionally long data set to be obtained. This research has been funded by the LOEWE excellence cluster $FACE_2FACE$ of the Hessian State Ministry of Higher Education, Research and the Arts.

4.2 Methods

4.2.1 Experiment.

The experimental site is a non-grazed and extensively managed species-rich grassland located near Giessen, Germany (50° 32' N and 8° 41'E; 172 m a.s.l.). A FACE experiment has been in operation here since 1998. In total, six FACE rings of 8 m in diameter were established (for a detailed description, see JÄGER et al. 2003 and Supplementary Fig. 4.4). To maintain an undisturbed soil, the sensor installation inside the rings proceeded non-invasively. In three rings, the grassland vegetation has been exposed to elevated CO_2 conditions by enriching the air during daylight hours to ∼20% above the ambient [CO_2]. The other three rings (controls) are operated under ambient [CO_2]. The CO_2 enrichment showed slight variations within and among years that were caused by variable wind conditions and technical failures due to material fatigue in 2012 and 2013 (see Supplementary Fig. 4.5 b). The C3 vegetation was compared in all rings and dominated by the grasses *Arrhenatherum elatius*, *Holcus lanatus* and *Poa pratensis*, accompanied by a forb fraction including one legume species present in low abundance (KAMMANN et al., 2005). The grassland was fertilized with 40 kg ha^{-1} yr^{-1} calcium ammonium nitrate, which equals the annual N deposition in many intensively used agricultural regions (REICH et al., 2001), supplemented by 600 kg ha^{-1} yr^{-1} of 10% P_2 O_5 + 15% K_2O + 3% MgO and 33% CaO + MgO each spring beginning in 1995 (KAMMANN et al., 2005). The soil is a fluvic gleysol (SPAARGAREN et al., 1994) with a sandy clay loam layer above a clay layer of variable depth (KAMMANN et al., 2005).

4.2.2 Climate and vegetation data.

Climate data were taken from meteorological stations on the field site operated by the Hessian Agency for Nature Conservation, Environment and Geology (HNLUG), the Environmental Monitoring and Climate Impact Research Station Linden (UKL) and the German Meteorological Service (DWD). Other variables were measured within each ring. All data sets cover the time period from 1998 to 2013. Data measured within each ring were TAB and [CO_2] of the air (ring-wise data). The biomass was cut each year at the beginning of September at approximately 5 cm

above ground. The yield of each ring was oven dried at 105°C to obtain TAB. [CO_2] was measured in the centre of each ring at 60 cm above ground with an infrared gas analyser (LI-COR 6252). Air temperature and relative air humidity were used to calculate the vapour pressure deficit (Allen et al., 1998). Evapotranspiration was derived on a daily basis by the FAO Penman-Monteith method (Allen et al., 1998). It was used to calculate the monthly standardized precipitation evapotranspiration index (SPEI), which is a multi-scalar drought index. Climatic and groundwater-related data are referred to as experiment-support data. The characteristics of the ring-wise and experiment-support data can be found in Supplementary Table 4.1.

4.2.3 Aggregation of variables.

[CO_2] data of each ring were aggregated from the three months preceding the harvests in September, with all values being used to calculate the average (refer to Supplementary Table 4.1, and Supplementary Figures 4.5 and 4.6). For air temperature, wind speed and vapour pressure deficit, daily average values were calculated from half-hourly measurements. For rainfall, the solar radiation and evapotranspiration, daily sums were determined. These daily values were subsequently aggregated to averages or sums for the respective three months preceding the harvest to obtain the *experiment-support variables*. The monthly values for the SPEI were averaged to obtain the respective values for the three months prior to harvest.

4.2.4 Data analysis.

Prior to the analysis of the CFE, all *experiment-support variables* were tested by cross-correlation to reveal the interactions among them. For this process, Pearson's correlation coefficient was used with a confidence interval of 0.95 (see Supplementary Table 4.3). We note that Pearson's correlation revealed a close correlation between the TAB and the [CO_2] (Pearson r: 0.46, $p < 0.001$, $n = 96$).

Due to the variable CO_2 enrichment, a methodology was developed that provides robust CFE estimates regarding the inherent variability of the CO_2 enrichment in long-term experiments such as the GiFACE (for theoretical considerations refer Supplementary Fig. 4.10; for an analysis excluding two years with distinctly

different CO_2 enrichment refer to Supplementary Fig. 4.11). The details of the moving subset analysis and data pre-/post-processing are described in the Supplementary Information. Essentially, (i) a copy of the total data set was created for each experiment-support variable (represented by the average or sum in the three months prior to the harvest) and the data were rearranged in ascending order of the respective variable (forcing experiment-support variable, for order compare Supplementary Figures 4.5 and 4.6). The resulting data sets were iteratively partitioned into subsets, each comprising five years and thus thirty ring-wise observations (both ambient and elevated rings, six rings per year), with similar characteristics for the respective variable. Consequently, the first subset contains the five years with the lowest and the last subset contains the five years with the highest levels of the forcing experiment-support variable. After the first subset was identified, the second, third, and so on subsets were compiled by dropping the year with the lowest characteristics and adding the year with the next highest characteristics of the respective variable in the subset. (ii) The relation between the ring-wise observations with the dependent variable TAB and the predictor variable [CO_2] was calculated through regression analysis within each subset. Here, the slope of the regression model is the magnitude and the p value is the significance of the CFE under the respective environmental conditions. We compared this method with frequently used approaches using only biomass yields based on a factorial treatment design (see Supplementary Fig. 4.12). (iii) In the final diagram (upper row in Figures 4.1 and 4.2), the magnitude of the CFE (y axis, slope of regression model) and its significance (point size, p value that slope is $\neq 0$) were plotted against the average and absolute range of the forcing experiment-support variable in the five-year subsets (x axis; compare Supplementary Figures 4.8 and 4.9). The grey line depicts the averaged TAB of all observations in the subset. The averaged values per subset are plotted alongside the accompanying *experiment-support variables* (see lower panels Figures 4.1 and 4.2). Here, the y tick marks indicate the minimum and maximum of the subset-wise averaged experiment-support variable. Interpreting Figures 4.1 and 4.2, the reader may keep in mind two issues regarding the *experiment-support variables*. (1) The accompanying variables' values within a subset represent the five-year average grouped according to the forcing experiment-support variable and, thus, may arise from a combination of variable years. They must not necessarily

indicate conditions within single years. (2) Given the complexity of statistical interrelations between the environmental variables (for Pearson correlations among environmental variables see Supplementary Tables 4.3 and 4.4 and Supplementary Section 4.3.3.3), any inference of the interplay between the environmental variables and the CFE must be interpreted with caution. To give an easy-to-understand summary of the CFE dependent on the various *experiment-support variables* the thresholds of the environmental regimes were used (see Fig. 4.3, for thresholds see Supplementary Table 4.2). Arrows in Fig. 4.3 generally show positive CFEs while horizontal bars represent environmental conditions without a clear CFE. The strength of the CFE indicated by the colour and the length of the arrows is assessed via the average slope of the regression models within the environmental regimes (thicker black arrows – average CFE > 1.5; smaller grey arrows – $0.25 <$ average CFE < 1.5). Environmental regimes with fewer than two significant regression models ($p < 0.05$) are defined as not significant (grey bars). To enhance readability, the *experiment-support variables* are ordered from droughty to mesic and a grey shade gradient indicates the variables' values. All statistical analyses were performed with the R statistical software version 3.1.2 (R Core Team, 2014).

Code availability.

The developed methodology is available as open source CRAN R package *'msaFACE'* (Obermeier et al., 2016).

Data availability.

The data set generated and analysed during the current study has been deposited in the Laboratory for Climatology and Remote Sensing repository (DOI: http://dx.doi.org/10.5678/LCRS/DAT.265; Obermeier 2016), and is included as an example within the CRAN R package *'msaFACE'* (Obermeier et al., 2016).

References

Ainsworth, E. & Rogers, A. (2007): The response of photosynthesis and stomatal conductance to rising [CO_2]: Mechanisms and environmental interactions. *Plant, Cell and Environment*, 30, 3, 258–270.

Allen, R., Pereira, L., Raes, D., & Smith, M. (1998): Crop evapotranspiration: Guidelines for computing crop water requirements. *Irrigation and Drainage Paper*, 56.

Arneth, A., Harrison, S.P., Zaehle, S., Tsigaridis, K., Menon, S., Bartlein, P.J., Feichter, J., Korhola, A., Kulmala, M., O'Donnell, D., Schurgers, G., Sorvari, S., & Vesala, T. (2010): Terrestrial biogeochemical feedbacks in the climate system. *Nature Geoscience*, 3, 8, 525.

Bojanowski, J.S., Donatelli, M., Skidmore, A.K., & Vrieling, A. (2013): An auto-calibration procedure for empirical solar radiation models. *Environmental Modelling & Software*, 49, 118–128.

Booth, B.B.B., Jones, C.D., Collins, M., Totterdell, I.J., Cox, P.M., Sitch, S., Huntingford, C., Betts, R.a., Harris, G.R., & Lloyd, J. (2012): High sensitivity of future global warming to land carbon cycle processes. *Environmental Research Letters*, 7, 2, 1–8.

Ciais, P., Reichstein, M., Viovy, N., Granier, A., Ogée, J., Allard, V., Aubinet, M., Buchmann, N., Bernhofer, C., Carrara, A., Chevallier, F., De Noblet, N., Friend, a.D., Friedlingstein, P., Grünwald, T., Heinesch, B., Keronen, P., Knohl, A., Krinner, G., Loustau, D., Manca, G., Matteucci, G., Miglietta, F., Ourcival, J.M., Papale, D., Pilegaard, K., Rambal, S., Seufert, G., Soussana, J.F., Sanz, M.J., Schulze, E.D., Vesala, T., & Valentini, R. (2005): Europe-wide reduction in primary productivity caused by the heat and drought in 2003. *Nature*, 437, 7058, 529–533.

Cox, P.M., Betts, R.A., Jones, C.D., Spall, S.A., & Totterdell, I.J. (2000): Acceleration of global warming due to carbon-cycle feedbacks in a coupled climate model. *Nature*, 408, 184–187.

De Boeck, H.J. & Verbeeck, H. (2011): Drought-associated changes in climate and their relevance for ecosystem experiments and models. *Biogeosciences*, 8, 5, 1121–1130.

Dukes, J.S., Chiariello, N.R., Cleland, E.E., Moore, L.a., Rebecca Shaw, M., Thayer, S., Tobeck, T., Mooney, H.a., & Field, C.B. (2005): Responses of grassland production to single and multiple global environmental changes. *PLoS Biology*, 3, 10.

Farrior, C.E., Tilman, D., Dybzinski, R., Reich, P.B., Levin, S.A., & Pacala, S.W. (2013): Resource limitation in a competitive context determines complex plant responses to experimental resource additions. *Ecology*, 94, 11, 2505–2517.

Fatichi, S., Leuzinger, S., & Körner, C. (2014): Moving beyond photosynthesis: From carbon source to sink-driven vegetation modeling. *New Phytologist*, 201, 4, 1086–1095.

Feng, Z., Rütting, T., Pleijel, H., Wallin, G., Reich, P.B., Kammann, C.I., Newton, P.C., Kobayashi, K., Luo, Y., & Uddling, J. (2015): Constraints to nitrogen acquisition of terrestrial plants under elevated CO_2. *Global Change Biology*, 21, 8, 3152–3168.

Foley, J.A., Ramankutty, N., Brauman, K.A., Cassidy, E.S., Gerber, J.S., Johnston, M., Mueller, N.D., O'Connell, C., Ray, D.K., West, P.C., Balzer, C., Bennett, E.M., Carpenter, S.R., Hill, J., Monfreda, C., Polasky, S., Rockström, J., Sheehan, J., Siebert, S., Tilman, D., Zaks, D.P.M., & O'Connell, C. (2011): Solutions for a cultivated planet. *Nature*, 478, 7369, 337–42.

Food and Agriculture Organization of the United Nations Statistics Division (2011): FAOSTAT. (last access: 2016-01-30).
URL `http://faostat3.fao.org/browse/E/EL/E`

Friedlingstein, P., Meinshausen, M., Arora, V.K., Jones, C.D., Anav, A., Liddicoat, S.K., & Knutti, R. (2014): Uncertainties in CMIP5 climate projections due to carbon cycle feedbacks. *Journal of Climate*, 27, 2, 511–526.

Hovenden, M.J., Newton, P.C.D., & Wills, K.E. (2014): Seasonal not annual rainfall determines grassland biomass response to carbon dioxide. *Nature*, 511, 7511, 583–586.

IPCC (2013): Climate Change 2013: The Physical Science Basis. Contribution of Working Group I to the Fifth Assessment Report of the Intergovernmental Panel on Climate Change. *Intergovernmental Panel on Climate Change, Working Group I Contribution to the IPCC Fifth Assessment Report (AR5)(Cambridge Univ Press, New York)*.

Jäger, H.J., Schmidt, S.W., Kammann, C., Grünhage, L., Müller, C., & Hanewald, K. (2003): The University of Giessen Free-Air Carbon Dioxide Enrichment Study: Description of the Experimental Site and of a New Enrichment System. *Journal of Applied Botany*, 77, 117–127.

Kammann, C., Grünhage, L., Grüters, U., Janze, S., & Jäger, H.J. (2005): Response of aboveground grassland biomass and soil moisture to moderate long-term CO_2 enrichment. *Basic and Applied Ecology*, 6, 4, 351–365.

Kammann, C., Müller, C., Grünhage, L., & Jäger, H.J. (2008): Elevated CO_2 stimulates N_2O emissions in permanent grassland. *Soil Biology and Biochemistry*, 40, 9, 2194–2205.

Körner, C. (2015): Paradigm shift in plant growth control. *Current Opinion in Plant Biology*, 25, 107–114.

Leuzinger, S., Luo, Y., Beier, C., Dieleman, W., Vicca, S., & Körner, C. (2011): Do global change experiments overestimate impacts on terrestrial ecosystems? *Trends in Ecology & Evolution*, 26, 5, 236–241.

Long, S.P. (1991): Modification of the response of photosynthetic productivity to rising temperature by atmospheric CO_2 concentrations: Has its importance been underestimated? *Plant, Cell and Environment*, 14, 729–739.

Luo, Y. (2007): Terrestrial Carbon-Cycle Feedback to Climate Warming. *Annual Review of Ecology, Evolution, and Systematics*, 38, 1, 683–712.

Morgan, J.a., Pataki, D.E., Körner, C., Clark, H., Del Grosso, S.J., Grünzweig, J.M., Knapp, A.K., Mosier, A.R., Newton, P.C.D., Niklaus, P.A., Nippert, J.B., Nowak, R.S., Parton, W.J., Polley, H.W., & Shaw, M.R. (2004): Water relations in grassland and desert ecosystems exposed to elevated atmospheric CO_2. *Oecologia*, 140, 1, 11–25.

Morison, J.I.L. & Lawlor, D.W. (1999): Interactions between increasing CO_2 concentration and temperature on plant growth. *Plant, Cell and Environment*, 22, 6, 659–682.

Nowak, R.S., Ellsworth, D.S., & Smith, S.D. (2004): Functional responses of plants to elevated atmospheric CO_2 – do photosynthetic and productivity data from face experiments support early predictions? *New Phytologist*, 162, 2, 253–280.

Obermeier, W. (2016): Longterm time series of the Giessen Free Air Carbon Enrichment (GiFACE) experiment.

Obermeier, W., Lehnert, L., & Bendix, J. (2016): msaFACE. R package version 0.10.0.
URL `https://CRAN.R-project.org/package=msaFACE`

Oren, R., Sperry, J.S.J., Katul, G.G.G., Pataki, D.E., Ewers, B.E.B., Phillips, N., & Schäfer, K.V.R. (1999): Survey and synthesis of intra- and interspecific variation in stomatal sensitivity to vapour pressure deficit. *Plant, Cell and Environment*, 22, 12, 1515–1526.

Owensby, C.E., Ham, J.M., Knapp, a.K., & Auen, L.M. (1999): Biomass production and species composition change in a tallgrass prairie ecosystem after long-term exposure to elevated atmospheric CO_2. *Global Change Biology*, 5, 497–506.

R Core Team (2014): R: A Language and Environment for Statistical Computing. R Foundation for Statistical Computing, Vienna, Austria. (last access:

27/01/2016).
URL `https://www.R-project.org/`

Reich, P.B., Hobbie, S.E., & Lee, T.D. (2014): Plant growth enhancement by elevated CO_2 eliminated by joint water and nitrogen limitation. *Nature Geoscience*, 7, 2–6.

Reich, P.B., Knops, J., Tilman, D., Craine, J., Ellsworth, D., Tjoelker, M., Lee, T., Wedin, D., Naeem, S., Bahauddin, D., Hendrey, G., Jose, S., Wrage, K., Goth, J., & Bengston, W. (2001): Plant diversity enhances ecosystem responses to elevated CO_2 and nitrogen deposition. *Nature*, 410, 6839, 809–810.

Reichstein, M., Bahn, M., Ciais, P., Frank, D.C.D., Mahecha, M.D., Seneviratne, S.I., Zscheischler, J., Beer, C., Buchmann, N., Papale, D., Rammig, A., Smith, P., Thonicke, K., van der Velde, M., Vicca, S., Walz, A., Wattenbach, M., Frank, D.C.D., Papale, D., Rammig, A., Smith, P., Thonicke, K., van der Velde, M., Vicca, S., Walz, A., & Wattenbach, M. (2013): Climate extremes and the carbon cycle. *Nature*, 500, 7462, 287–95.

Schimel, D., Stephens, B.B., & Fisher, J.B. (2015): Effect of increasing CO_2 on the terrestrial carbon cycle. *Proceedings of the National Academy of Sciences*, 112, 2, 436–441.

Shaw, M.R., Zavaleta, E.S., Chiariello, N.R., Cleland, E.E., Mooney, H.A., & Field, C.B. (2002): Grassland responses to global environmental changes suppressed by elevated CO_2. *Science*, 298, 5600, 1987–1990.

Smith, W.K., Reed, S.C., Cleveland, C.C., Ballantyne, A.P., Anderegg, W.R., Wieder, W.R., Liu, Y.Y., & Running, S.W. (2016): Large divergence of satellite and earth system model estimates of global terrestrial CO_2 fertilization. *Nature Climate Change*, 6, 3, 306.

Soussana, J.F. & Lüscher, A. (2007): Temperate grasslands and global atmospheric change: A review. *Grass and Forage Science*, 62, 2, 127–134.

Spaargaren, O., Arnold, R., & Blume, H. (1994): World reference base for soil resources. *Wageningen/Rome*.

Stiling, P., Moon, D., Rossi, A., Forkner, R., Hungate, B.A., Day, F.P., Schroeder, R.E., & Drake, B. (2013): Direct and legacy effects of long-term elevated CO_2 on fine root growth and plant-insect interactions. *New Phytologist*, 200, 3, 788–795.

Vicente-Serrano, S.M., Beguería, S., & López-Moreno, J.I. (2010): A multiscalar drought index sensitive to global warming: The standardized precipitation evapotranspiration index. *Journal of Climate*, 23, 7, 1696–1718.

Volk, M., Niklaus, P.A., & Körner, C. (2000): Soil moisture effects determine CO_2 responses of grassland species. *Oecologia*, 125, 3, 380–388.

Wang, D., Heckathorn, S.A., Wang, X., & Philpott, S.M. (2012): A meta-analysis of plant physiological and growth responses to temperature and elevated CO_2 . *Oecologia*, 169, 1, 1–13.

4.3 Supplementary Information

The Supplementary Information contains figures, tables and text (in respective order). The sequence of the figures follows the order of citation in the main text. The text is structured as follows: data, methods and a combined results and discussion section. Initially, additional information on the aggregation and derivation of the *experiment-support variables* is provided (Supplementary Section 4.3.1). We continue with a supporting explanation of how we have derived the CO_2 fertilization effect (CFE) in our study termed CFE_{Slope} (Supplementary Section 4.3.2.1). Refer to Supplementary Section 4.3.3.1 for the distribution characteristics of the dependent and independent variables of the underlying regression model. The new method (CFE_{Slope}) is compared to several approaches that derive the CFE based on a factorial treatment design (Supplementary Section 4.3.2.2 and Supplementary Section 4.3.3.2). Furthermore, we show the high-order correlations of the *experiment-support variables* aggregated within the subsets (Supplementary Section 4.3.2.3 and Supplementary Section 4.3.3.3). Finally, we analyse and discuss a possible time dependence of the CFE in our study (Supplementary Section 4.3.2.4).

Supplementary Figure 4.4: Experimental site. Aerial photograph provided by Thomas Wißner (© 2013).

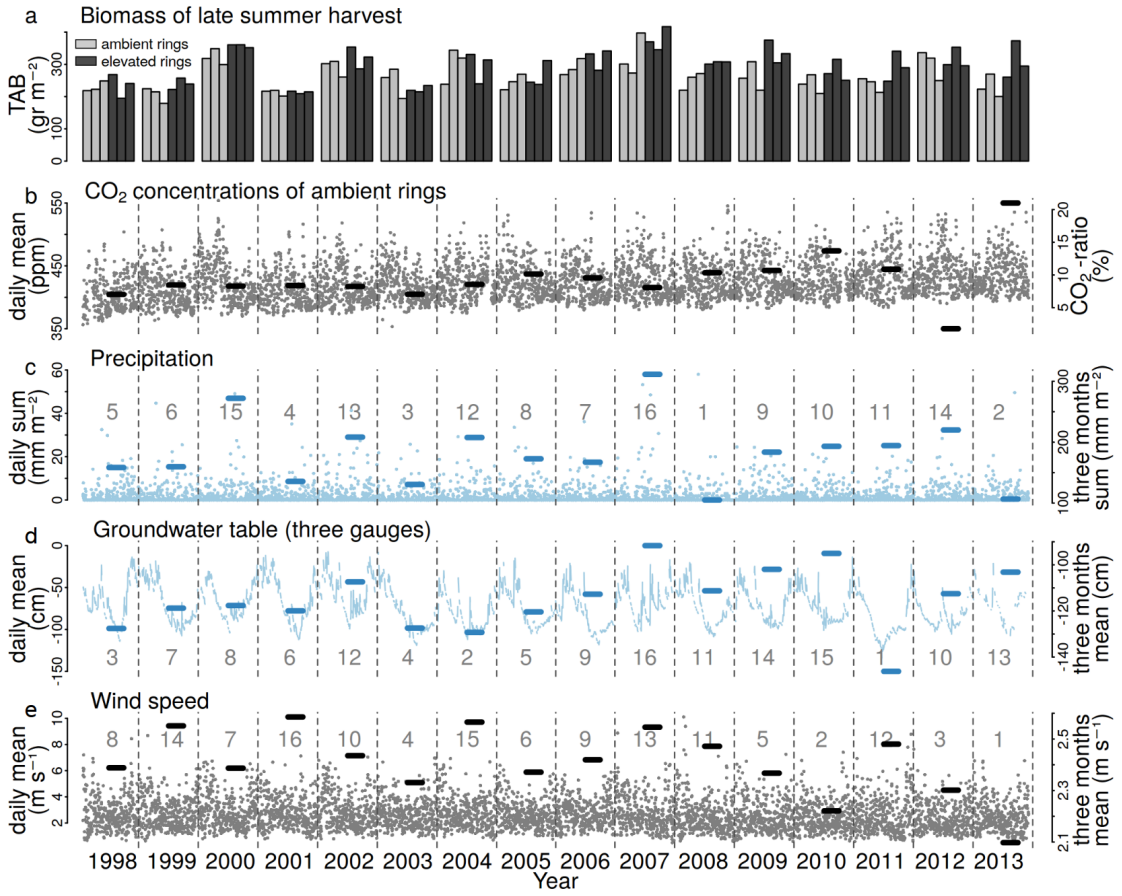

Supplementary Figure 4.5: Long-term time series of the GiFACE. Barplot of the late-summer total aboveground biomass (TAB) in the different rings (**a**), the [CO_2] of the ambient rings (**b**) and selected *experiment-support variables* (**c** - **e**). Points depict daily values (left y-axis), line segments in (**b**) and (**c** - **e**) show the CO_2-ratio between the elevated and ambient rings (right y-axis) and the aggregated values used for the moving subset analysis (three months preceding harvest, right y-axis), respectively. The daily means of the [CO_2] in the ambient rings were derived by averaging all measured values (24 h at 60 cm above ground). The CO_2-ratios were calculated as the percentage change of the three-months averaged [CO_2] of all measured values from the elevated rings compared to the ambient rings. The grey numbers in the lower panels indicate the index of the year when the data were rearranged in ascending order of the respective *experiment-support variables*.

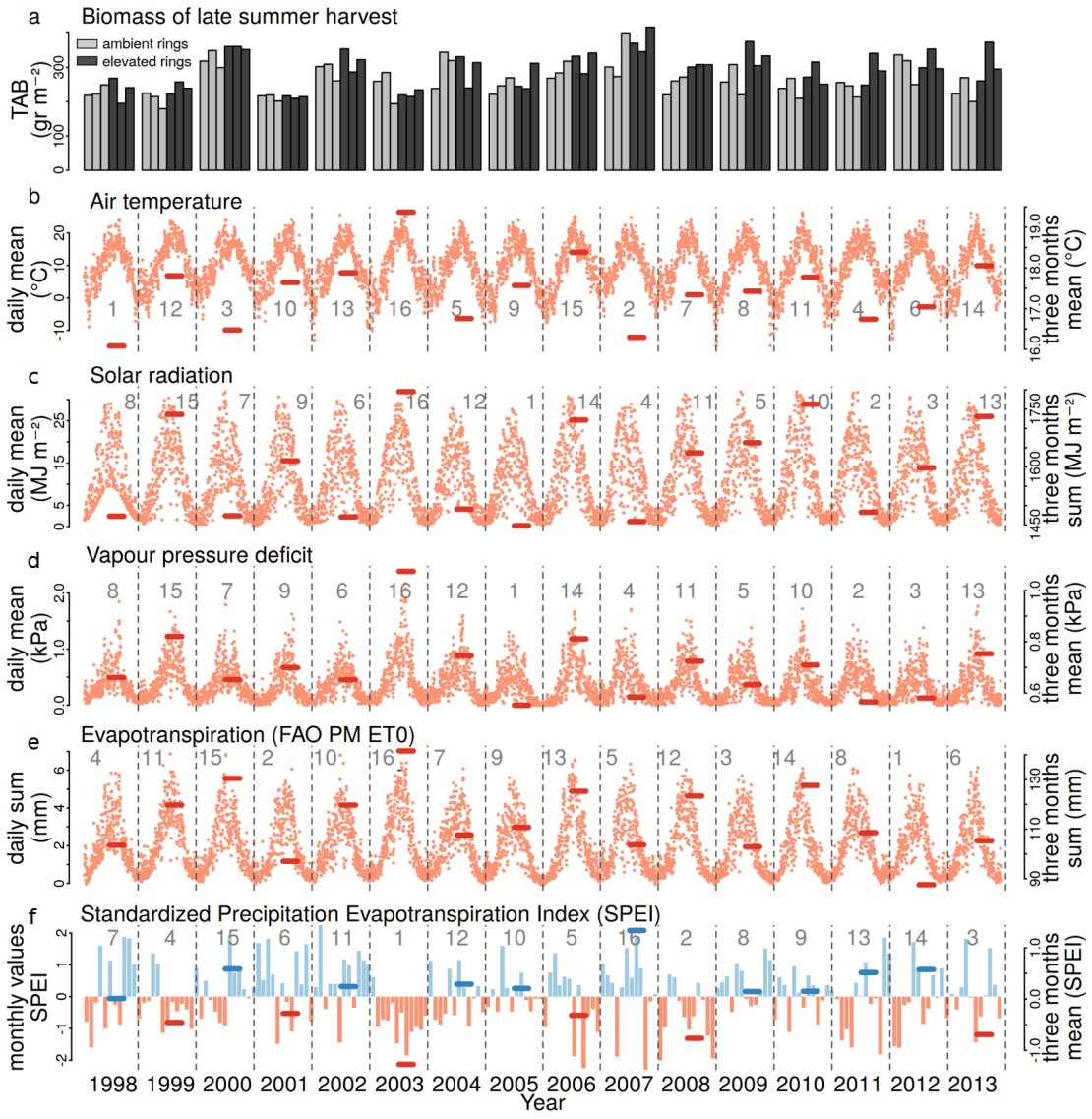

Supplementary Figure 4.6: Long-term time series of the GiFACE. (**a**) Barplot of the late-summer total aboveground biomass (TAB) in the different rings and (**b** - **f**) selected *experiment-support variables*. For the description, see the caption for Supplementary Fig. 4.5.

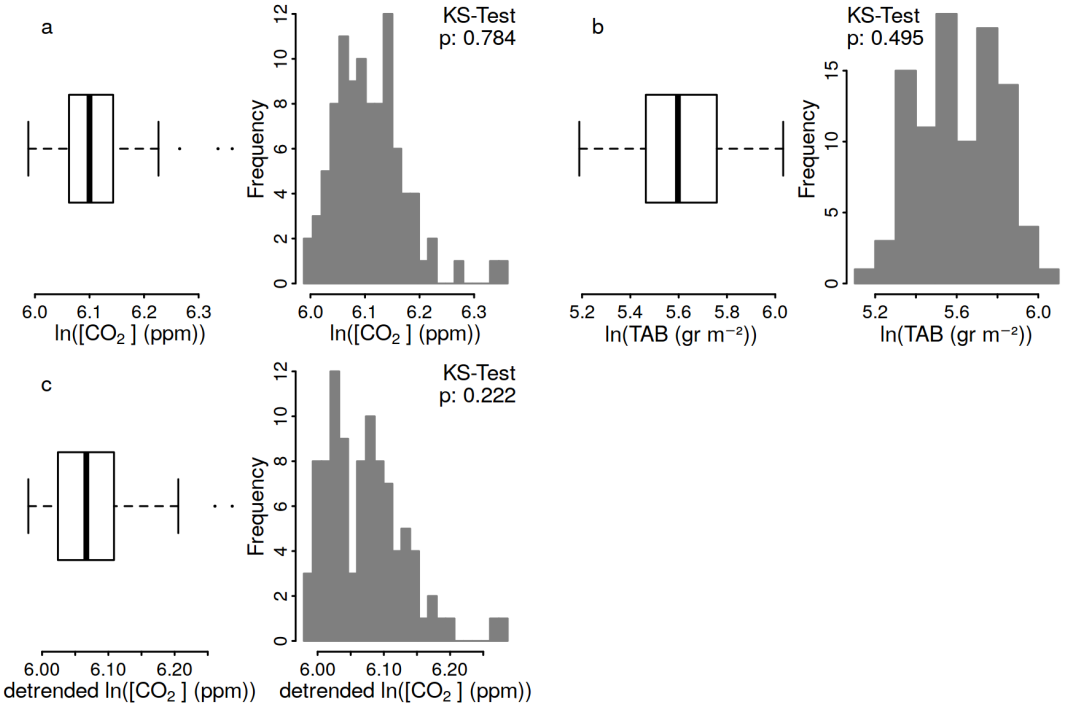

Supplementary Figure 4.7: Distribution characteristics of the dependent and independent ring-wise variables (six rings, 16 years, n = 96). Box plot with the median and the 1st and 3rd quartiles; the lowest value is within 1.5 interquartile range of the lower quartile and the highest value is within 1.5 interquartile range of the upper quartile, extreme outliers (first and third column), and the frequency distribution with the results of the Kolmogorov-Smirnov test on normality (KS-Test; second and fourth column) for (**a**) the logarithmus naturalis of $[CO_2]$, (**b**) the logarithmus naturalis of TAB, and (**c**) the detrended logarithmus naturalis of $[CO_2]$.

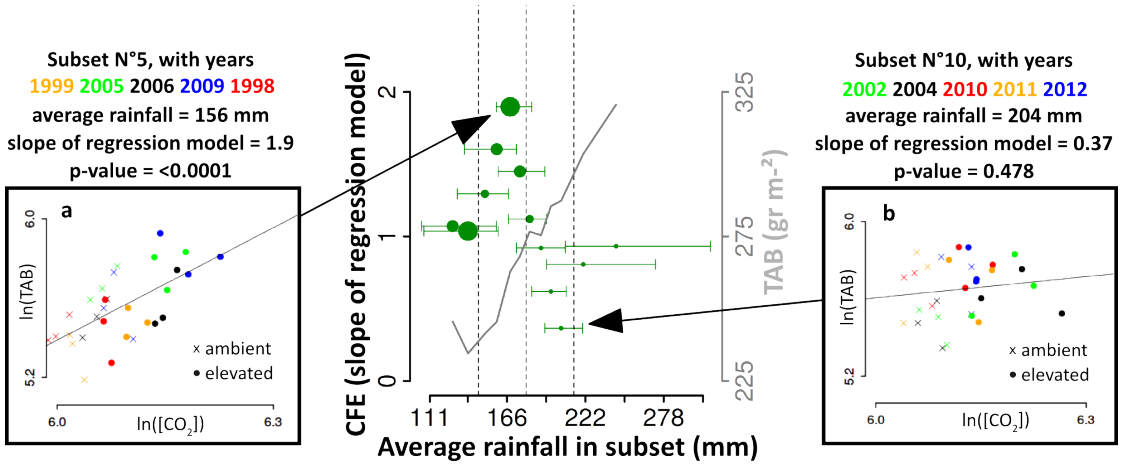

Supplementary Figure 4.8: Extended explanation plot describing how the CO_2 fertilization effect is determined on the basis of the moving subset analysis. To illustrate, the forcing *experiment-support variable* rainfall is used as an example. Two exemplary subsets are presented in detail: (**a**) the strongest and (**b**) the weakest CO_2 fertilization effect (CFE), which correspond to the 5-years moving subset N° 5 (left regression plot) and N° 10 (right regression plot).

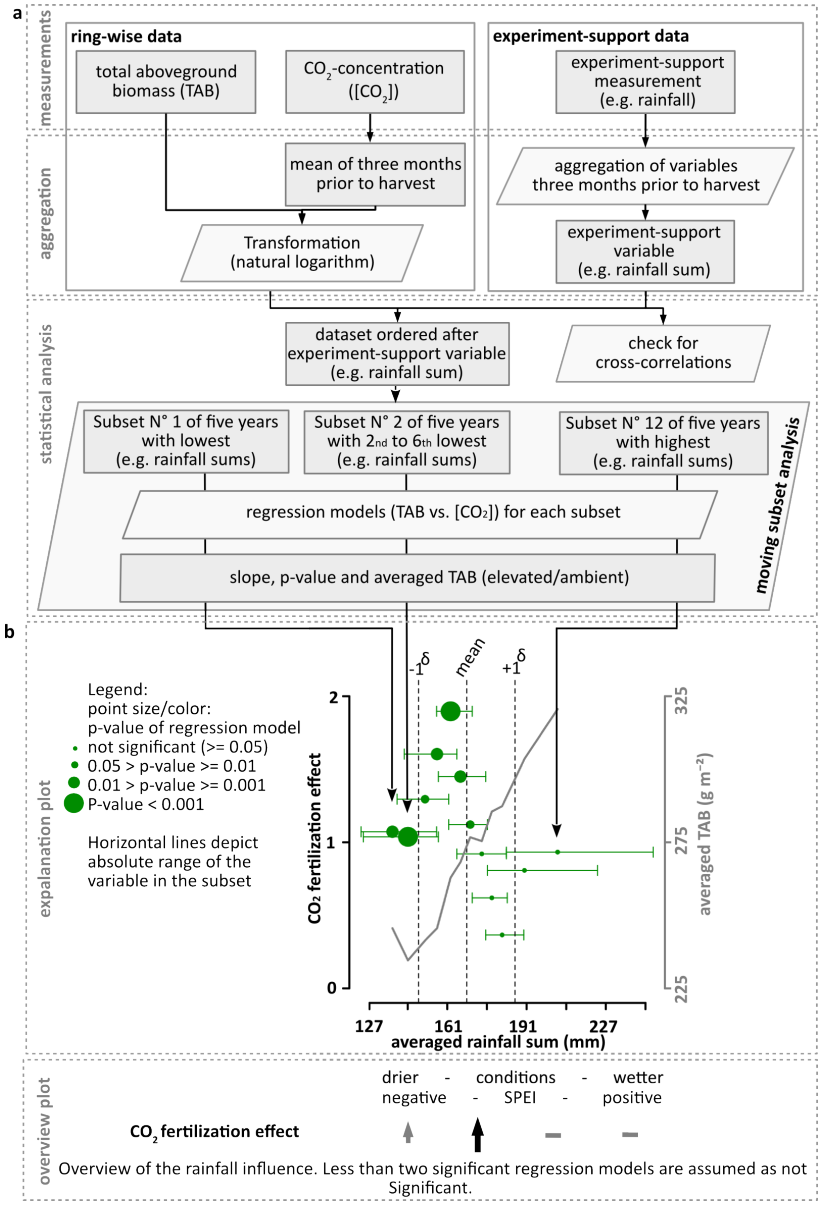

Supplementary Figure 4.9: Overview of the processing steps and an example plot using rainfall sums. Rectangles in (**a**) outline data types and parallelograms depict methods. The results in (**b**) depict the influence of the rainfall sum on the relation between CO_2 concentration ($[CO_2]$) and the total aboveground biomass. It shows the strength of the CO_2 fertilization effect (CFE) (y-axis) plotted against the average (points) and the absolute range (horizontal lines) of the variable in the respective subset. Here, the size of the points shows the significance of the CFE, indicated by the p-value of the regression model in the subset within four classes. To depict the general response of the biomass to the respective *experiment-support variable*, the average total aboveground biomass (TAB) of all rings in the subsets is plotted in grey. Dashed vertical lines depict the arithmetic mean ± 1 standard deviation (δ) of the *experiment-support variable* over the entire time series to reveal the intermediate environmental conditions that have occurred during the experiment.

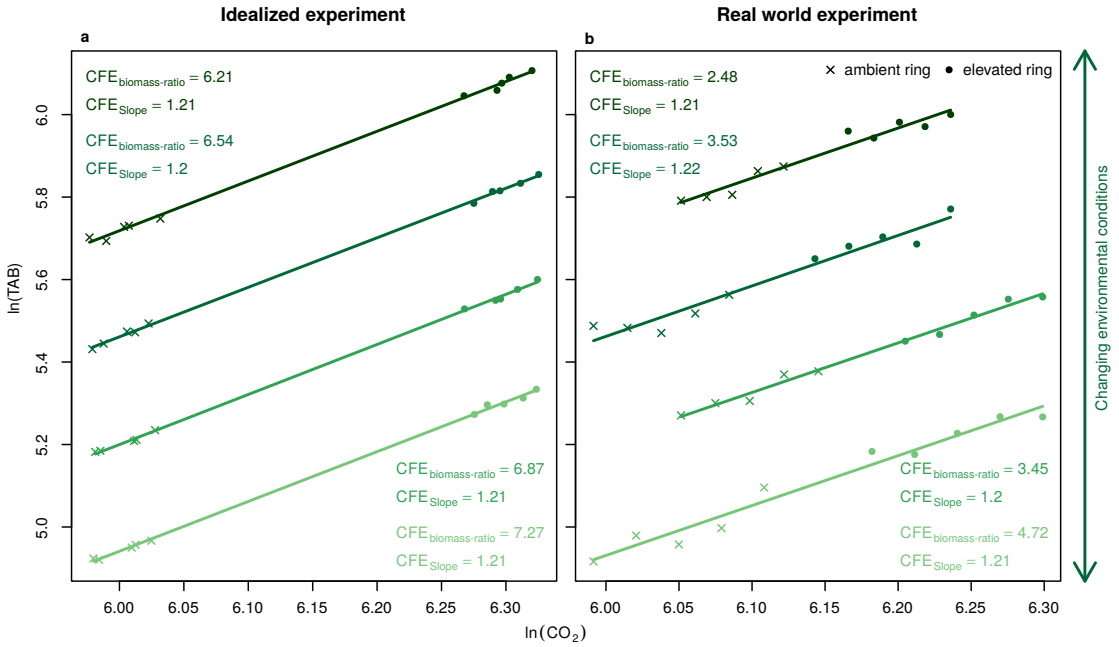

Supplementary Figure 4.10: Schematic description of the CO_2 fertilization effect under idealized (**a**) and real-world (**b**) conditions. Under idealized conditions (**a**), the CO_2 enrichment is constant over time. Consequently, the biomass depends only on environmental conditions (four different conditions are exemplary depicted by colour in the figure). In this case, the CO_2 fertilization effects (CFE) calculated with the new method (slope) and calculated as the ratio between ambient and elevated biomass yield are similar for all time slides. However, since the experiment has been conducted under natural environmental conditions, the CO_2 fertilization is not constant (**b**, see Supplementary Fig. 4.8 for actual CO_2-concentrations in the moving subsets). This causes varying CO_2-concentrations over time, which do not affect the CFE derived as the slope of the linear regression but have a considerably high effect on the ratio between ambient and elevated biomass yields.

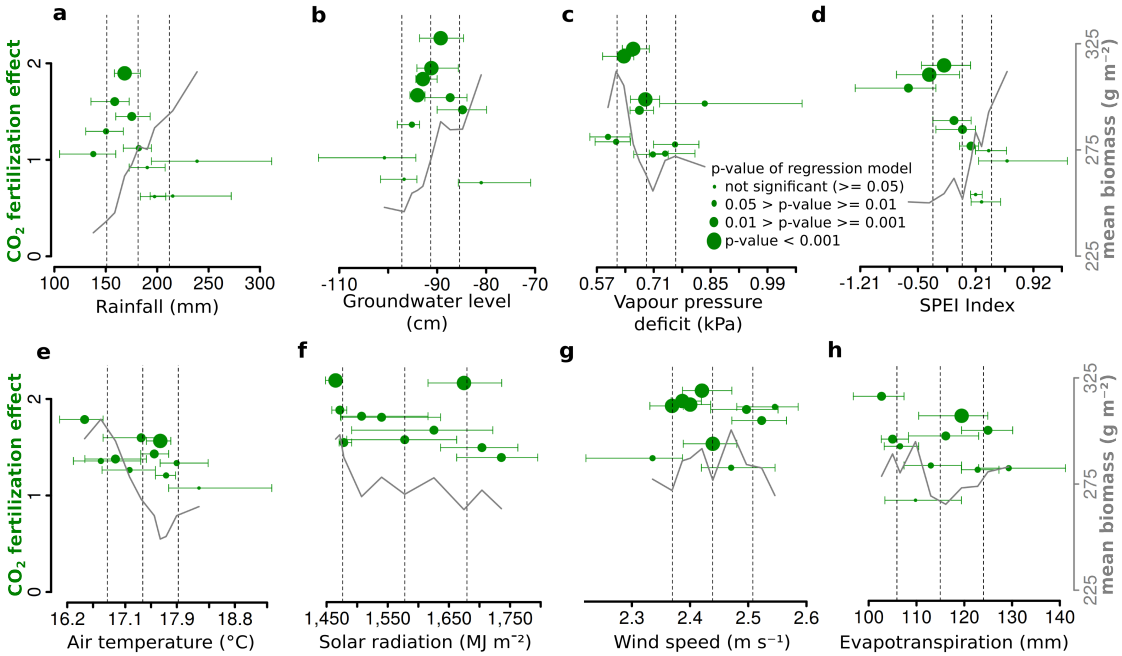

Supplementary Figure 4.11: Analysis of the CO_2 fertilization effect dependent on various *experiment-support variables* exluding the years with exceptional low and high CO_2 enrichment (2012, 2013, see Supplementary Fig. 4.5 for actual CO_2-ratios in the years). The results reveal very similar trends compared to those including all available years (1998-2013, Figures 4.1 and 4.2). This highlights that the used method is stable against occurring variations in the CO_2 enrichment and thus, that the CO_2 fertilization effect of this study could be analysed using the whole time series.

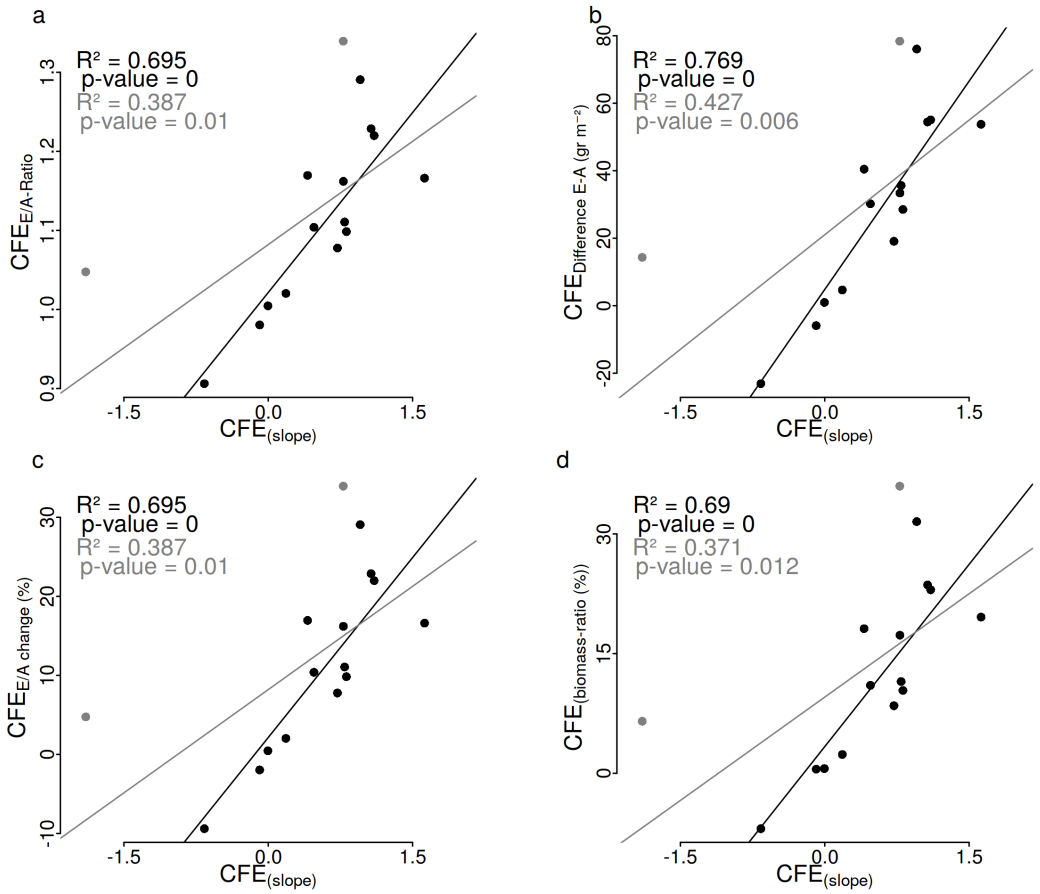

Supplementary Figure 4.12: Comparison of different approaches to derive the CO_2 fertilization effect (CFE) with the approach used in the present study (x-axis). The y-axis shows, (**a**) the difference of the aboveground biomass in the elevated rings minus the aboveground biomass in the ambient rings, (**b**) the ratio of the aboveground biomass in the elevated rings to the aboveground biomass in the ambient rings, (**c**) the relative change of aboveground biomass in the elevated rings compared to aboveground biomass in the ambient rings and (**d**) the adapted biomass-ratio approach using all possible combinations of the change in aboveground biomass in the elevated rings relative to aboveground biomass in the ambient rings. The grey lines depict the linear regression models between the dependent and independent variables using all observations. The black lines present the regression models excluding the two outliers in grey color.

Supplementary Table 4.1: Ring-wise and experiment-support data.

Measurements	Temporal resolution	No. of measurements	Sensors	Aggregation (three months prior to harvest)
TAB	on harvest	1 each ring	-	-
CO_2 concentration	hourly	1 each ring	Infrared gas analyser (LI-COR 6252)	mean of all values
Air temperature	half-hourly	1	Pt-100 resistance thermometer	mean of daily means
Wind speed	half-hourly	1	Cup Anemometer	mean of daily means
Solar radiation	half-hourly	1	Pyranometer	sum of all values
Relative humidity	half-hourly	1	Hygro-thermo transmitter	mean of daily means
Rainfall	half-hourly	3	Hellmann samplers	sum of all values
Groundwater	daily	3	gauges	mean of daily values
VPD	half-hourly	-	-	mean of daily means
FAO PM ET0	daily	-	-	mean of daily means
SPEI	monthly	-	-	mean of monthly values

TAB – Total Aboveground Biomass; VPD – Vapour Pressure Deficit; FAO PM ET0 – Evapotranspiration (calculated by the FAO Penman-Monteith method); SPEI – Standardized Precipitation Evapotranspiration Index

Supplementary Table 4.2: Thresholds for the environmental regimes.

Experiment-support variable	low	moderate intermediate	elevated intermediate	high
Rainfall (mm)	< 145.6	145.6 – 179.7	179.7 – 213.8	> 213.8
Groundwater (cm)	$<$ -96.2	-96.2 – -90.5	-90.5 – -84.7	$>$ -84.7
VPD (kPa)	< 0.61	0.61 – 0.69	0.69 – 0.76	> 0.76
Air temperature (°C)	< 16.8	16.8 – 17.4	17.4 – 17.9	> 17.9
Solar radiation (MJ m^{-2})	$< 1{,}488$	1,488 – 1,592	1,592 – 1,695	$> 1{,}695$
Wind speed (m^{-1})	< 2.33	2.33 – 2.42	2.42 – 2.50	> 2.5
FAO PM ET0 (mm)	< 103.3	103.3 – 113.1	113.1 – 122.9	> 122.9
SPEI	$<$ -0.37	-0.37 – 0.03	0.03 – 0.44	> 0.44

VPD – Vapour Pressure Deficit; FAO PM ET0 – Evapotranspiration (calculated by the FAO Penman-Monteith method); SPEI – Standardized Precipitation Evapotranspiration Index
Thresholds are defined by the mean and mean ± 1 standard deviation for the respective *experiment-support variable* when averaged in the different subsets.

Supplementary Table 4.3: Pearson's correlation coefficients (lower triangle) and p-values (upper triangle) of the *experiment-support variables*.

Experiment-support variable	Rainfall	Ground-water	VPD	Air temperature	Solar radiation	Wind speed	FAO PM ET0	SPEI
Rainfall		0.59	0.05	<0.05	<0.05	0.35	0.63	<0.0001
Groundwater	−0.15		0.55	0.24	0.45	0.83	0.14	0.50
VPD	−0.49	0.16		<0.01	<0.01	0.72	<0.01	<0.001
Air temperature	−0.57	0.31	0.74		<0.001	0.23	<0.05	<0.001
Solar radiation	−0.57	0.2	0.72	0.76		0.12	0.16	<0.01
Wind speed	0.25	−0.06	−0.1	−0.32	−0.4		0.70	0.36
FAO PM ET0	−0.13	0.35	0.64	0.51	0.37	−0.1		0.08
SPEI	0.9	−0.18	−0.8	−0.75	−0.72	0.24	−0.45	

VPD – Vapour Pressure Deficit; FAO PM ET0 – Evapotranspiration (calculated by the FAO Penman-Monteith method); SPEI – Standardized Precipitation Evapotranspiration Index

Supplementary Table 4.4: High-order correlation matrix of the *experiment-support variables* within the subset-wise aggregations. Please note that the two triangles are not identical because of the aggregation of the variables for different temporal subsets.

	AT			WND			GWL			SR		
	Trans	p	R^2	Trans	p	R^2	Trans	p	R^2	Trans	p	R^2
AT	–	–	–	exp	<0.001	0.8	ln	n.s.	0.03	ln	<0.001	0.96
WND	no	<0.001	0.78	–	–	–	no	<0.01	0.64	ln	<0.01	0.62
GWL	no	<0.05	0.46	ln	n.s.	0.28	–	–	–	ln	n.s.	0.05
SR	exp	<0.001	0.95	exp	<0.01	0.52	no	n.s.	0.18	–	–	–
PPT	exp	<0.001	0.77	exp	<0.05	0.38	exp	<0.01	0.63	exp	<0.001	0.87
VPD	ln	<0.001	0.9	exp	<0.05	0.45	exp	<0.01	0.5	ln	<0.001	0.88
SPEI	exp	<0.001	0.92	exp	<0.01	0.66	exp	<0.01	0.55	exp	<0.001	0.94
ET0	ln	<0.01	0.67	ln	n.s.	0.11	exp	n.s.	0.1	ln	n.s.	0.19

	PPT			VPD			SPEI			ET0		
	Trans	p	R^2	Trans	p	R^2	Trans	p	R^2	Trans	p	R^2
AT	no	<0.001	0.79	ln	<0.001	0.84	no	<0.001	0.88	exp	<0.001	0.84
WND	ln	n.s.	0.12	ln	n.s.	0.16	exp	n.s.	0.13	ln	n.s.	0.26
GWL	ln	<0.001	0.72	ln	<0.05	0.46	exp	n.s.	0.18	exp	n.s.	0.04
SR	no	<0.001	0.8	no	<0.001	0.88	no	<0.001	0.94	no	<0.01	0.56
PPT	–	–	–	exp	<0.001	0.77	no	<0.001	0.95	exp	<0.01	0.53
VPD	exp	<0.001	0.78	–	–	–	no	<0.001	0.9	no	<0.001	0.79
SPEI	exp	<0.001	0.97	exp	<0.001	0.93	–	–	–	no	<0.001	0.84
ET0	no	<0.05	0.33	exp	<0.001	0.77	no	<0.05	0.38	–	–	–

AT – Air Temperature; WND – Wind Speed; GWL – Groundwater Level; SR – Solar Radiation; PPT – Rainfall; VPD – Vapour Pressure Deficit; SPEI – Standardized Precipitation Evapotranspiration Index; ET0 – Evapotranspiration (calculated by the FAO Penman-Monteith method)

Trans column indicates the transformation (no – not transformed; ln – logarithm naturalis; exp – exponential) for the aggregated accompanying variables (row-wise) with the best fit to the aggregated forcing experiment-support variable.

4.3.1 Supplementary Data

We have supplemented the *experiment-support variables* by two multi-factorial variables: (i) evapotranspiration and (ii) the standardised precipitation evapotranspiration index (SPEI) for drought indication.

The evapotranspiration for a homogeneous grass canopy was estimated on a daily basis using the FAO Penman-Monteith method (FAO PM ET0; Allen et al. 1998), implemented in the *sirad* package (CRAN R; Bojanowski et al. 2013; R Core Team 2014). The input variables were the daily minimum and maximum air temperature (°C), daily mean wind speed (m s^{-1}), daily solar radiation sum (MJ m^{-2} d^{-1}), and the mean daily vapour pressure (kPa). The latter was derived as (Allen et al., 1998):

$$es = 0.6108 \cdot \exp\left(\frac{17.27 \cdot T_{mean}}{T_{mean} + 237.3}\right) \tag{4.1}$$

$$vap\_pres = RH_{mean}/100 \cdot es, \tag{4.2}$$

where T_{mean} is the mean daily air temperature in°C, RH_{mean} is the mean daily relative humidity in %, and *vap_pres* is the mean daily vapour pressure in kPa. Additional input parameters were the clear sky transmissivity (cst), altitude above sea level (165 m), height of the wind speed measurement (2 m), and the latitude of the study site (50.053°N). The cst, which is the ratio between the measured solar radiation and the extra-terrestrial irradiance for clear sky days, was derived (cst = 0.725) by means of the reference solar radiation (*sirad*, CRAN R; Bojanowski et al. 2013; R Core Team 2014).

The FAO PM ET0 was used to derive the standardised precipitation evapotranspiration index (SPEI; Vicente-Serrano et al. 2010) on a monthly basis, which is a multi-scalar drought index. The SPEI is based on the climatic water balance defined by the total amount of precipitation minus evapotranspiration. The *SPEI* package (CRAN R; R Core Team 2014; Vicente-Serrano et al. 2010) was used for its calculation. Essentially, the data are transformed to a Gaussian standard distribution with zero mean and a standard deviation of one, assuming a Log-logistic distribution and using probability weighted moments for parameter estimation. Thus, a self-calibrating and standardized index for a given location is

obtained (negative values indicate dry conditions and positive values indicate wet conditions).

4.3.2 Supplementary Methods

4.3.2.1 Extended explanation of the method used to derive the CO_2 fertilization effect

In our study, the CFE was calculated by the regression of the ln (logarithmus naturalis) transformed total aboveground biomass (TAB in grams dry weight per square meter) with the actual ln transformed [CO_2] measured in the centre of each ring (parts per million, average of three months preceding the harvest) (see the Methods section and Supplementary Figures 4.8 and 4.9). Here, all observations (both treatments, ambient and elevated) were used. For a better understanding, Supplementary Fig. 4.8 shows the determination of the CFE, which is the basis of the entire moving subset analysis presented in Supplementary Fig. 4.9, with rainfall as an example of an *experiment-support variable*.

1. In the first step, the dataset containing ring-wise and *experiment-support variables* is rearranged in ascending order of the rainfall sum (forcing experiment-support variable) in the three months before harvest (Supplementary Fig. 4.9). The total dataset is then partitioned into subsets where each contains 5 years featuring similar environmental characteristics. In case of the rainfall, the first subset encompasses the five driest years. For the second one, the year with the lowest rainfall sum is dropped and replaced by the year with the sixth lowest rainfall sum to achieve a four years overlap of adjacent subsets. This is repeated until the last subset is reached which encompasses the five wettest years. With 16 years (1998-2013) of available data and the four-year overlap 12 subsets are created. Please note that by not grouping consecutively but ordered according to their numerical characteristics we are able to analyse the CFE-environment relationship starting from low via moderate to high values of the forcing *experiment-support variable*.

2. Supplementary Fig. 4.8 reveals that the CFE represents the amount of change in the TAB concomitant with the amount of change in the [CO_2]. The CFE is

derived as the slope of the regression model between [CO_2] and TAB, which are calculated separately within each of the subsets defined above (presented for two rainfall subsets in Supplementary Fig. 4.8). Before regression modelling, the dependent variable (TAB) and the explanatory variable ([CO_2]) were transformed to their logarithmus naturalis to strengthen the statistical validity of the regression models (see Supplementary Results and Supplementary Fig. 4.7). By considering six rings for each year and a 5-year subset, every regression is based on 30 samples (Supplementary Fig. 4.8). Consequently, the significance of the CFE was derived as the p-value of the slope in the regression model for each subset.

3. By presenting the slope and its significance against the sum of the rainfall in the respective subset, the influence of rainfall on the CFE is revealed. The results are presented in a comprehensive way in Figures 4.1 and 4.2. For a more detailed description of the Figures, see Supplementary Fig. 4.9 b and its caption.

4.3.2.2 Determination of the CFE: novel approach of this study compared to common approaches

We compare the yearly CFE derived as the slope of the regression model (CFE_{Slope}, newly developed approach, this study) with the most common options to derive the CFE on the basis of a factorial treatment design (results are presented in Supplementary Fig. 4.10). These approaches include the calculation of the CFE based on (1) the simple difference of the TAB in the elevated rings (eTAB) minus the TAB in the ambient rings (aTAB) (CFE_{E-A}), (2) the averaged eTAB divided by the averaged aTAB ($CFE_{E/A-Ratio}$) and (3) the difference of the eTAB minus aTAB divided by the aTAB ($CFE_{E/A-change}$). Moreover, (4) we have slightly adapted the latter approach by using the relative change in the eTAB compared to the aTAB for each possible combination in one year. Encompassing three elevated and

three ambient rings, nine values result for one year, whose average represents the percentage change of eTAB relative to aTAB for one year ($CFE_{biomass-ratio}$):

$$ratio = \sum_{i=1}^{3} \sum_{k=1}^{3} \frac{e_i - a_k}{a_k} \tag{4.3}$$

where:

e_i = biomass yield in elevated ring (i)

a_k = biomass yield in ambient ring (k)

$$CFE_{biomass-ratio} = \frac{ratio}{3^2} \tag{4.4}$$

In the final plots (see Supplementary Fig. 4.10), the CFE-values of the different approaches are plotted against the CFE_{Slope} of the linear regression models, including and excluding outliers. Aware that expected differences might be explained by variations of the actual CO_2 enrichment, we have complemented this analysis with an schematic overview of the CFE calculation based on different calculations (see Supplementary Fig. 4.12). Therefore, we compare the $CFE_{biomass-ratio}$ with the CFE_{Slope}, under idealized experimental conditions and under more realistic conditions which included a varying [CO_2].

4.3.2.3 Method to derive a high-order correlation matrix

Situated in a real-world environment, most of the *experiment-support variables* are highly correlated (see the Methods section and Supplementary Table 4.3). Because of frequently non-linear relationships of such environmental variables, we have determined the correlations of the *experiment-support variables* using different transformations. To this end, the subset-wise aggregations of the *experiment-support variables* were used, because we describe the CFE-environment relations within these. For each subset defined by the forcing *experiment-support variable* (columns in Supplementary Table 4.4, and compare the upper panels in Figures 4.1 and 4.2) the average of the accompanying *experiment-support variables* within the subset was derived (compare lower panels Figures 4.1 and 4.2). Three transformation modes (logarithmus naturalis, unchanged and exponential) were applied to the averaged accompanying *experiment-support variables*. To highlight any strong interactions

of the subsets, the correlations between the transformations of the accompanying and forcing *experiment-support variables* (subset-wise aggregated) were examined, with the best results indicated by Pearson's product moment correlation coefficient presented in Supplementary Table 4.4.

4.3.2.4 Analysis of the time dependence of the CFE

Some studies have shown time dependences of the CFE, either as the result of a declining trend, for example because of progressive nitrogen limitation (PNL; Leuzinger et al. 2011), or an increasing trend, for example by legacy effects caused by fertilization through artificial ploughing during the experimental setup (Stiling et al., 2013). To check for a potential time dependence of the CFE in our study, we calculated the rank correlation between the CFE and years by means of Kendall's tau.

4.3.3 Supplementary Results and Discussion

4.3.3.1 Characteristics of the dependent and independent variables

Neither a bimodal distribution of the [CO_2] data, which may be expected because of the factorial treatment design, nor TAB are visible in the data (see the Methods section and Supplementary Fig. 4.7). The Kolmogorov-Smirnov (KS) test on normality for both variables (transformed to their logarithmus naturalis) showed good results. Thus, the statistical validity of regression techniques for the derivation of the CFE is not constrained, for example, by the occurrence of two clouds of points. We explain this by the low CO_2 enrichment level (20% during daylight hours, which, on average, caused a 9.5% higher [CO_2] in the elevated rings compared to ambient rings for the three month average, and the long-term time series with an associated increasing atmospheric [CO_2], which caused an 8% higher [CO_2] in the ambient rings of 2013 compared to 1998. This relationship is clearly shown by detrending the [CO_2] data. Therefore, we subtracted the atmospheric background [CO_2] increase, which we derived by the linear model through the ambient [CO_2]. The remaining distribution of the residual [CO_2] values reveals a bimodal distribution as defined by the factorial treatment design. This highlights that a similar magnitude of the

inter- and intra-annual differences in the $[CO_2]$ prevented a bimodal distribution of the $[CO_2]$.

4.3.3.2 Comparison of the CFE derived by the different approaches

We compared the yearly CFE_{Slope} (method used in the present study) with various approaches that derive the CFE on basis of a factorial treatment design (see Supplementary Fig. 4.10). The results show positive linear relations between the CFE_{Slope} and all tested alternative methods (all significant on 0.05 level), that were enhanced by excluding the outliers (p-value < 0.001). However, differences between the CFE_{Slope} and the other approaches occur. We explain this by a varying CO_2 enrichment over time (compare Supplementary Fig. 4.5 b). This relation is clearly depicted in a schematic overview (Supplementary Fig. 4.12). Supplementary Fig. 4.12 a shows an idealized experimental setup with the CFE_{Slope} and the $CFE_{biomass-ratio}$ calculated for four different dates, which differ in that varying environmental conditions lead to different biomass yields. Here, the CO_2 enrichment within the four different dates remains stable. Consequently, the CFE derived by both approaches CFE_{Slope} and $CFE_{biomass-ratio}$) remains stable for the different dates. In Supplementary Fig. 4.12 b the CO_2 enrichment is not constant for all dates, which depicts a more realistic picture of the real-world conditions observed in our experiment (compare Supplementary Fig. 4.5 b). Consequently, the $CFE_{biomass-ratio}$ strongly varies whereas the CFE_{Slope} remains stable. This is because the $CFE_{biomass-ratio}$ approach assumes a stable CO_2 enrichment defined by the factorial design. In contrast, the CFE_{Slope} accounts for the occurring variations in the CO_2 enrichment because it considers the actual $[CO_2]$, which has been measured in the centre of each ring in our experiment. This shows the necessity for considering the actual $[CO_2]$ to derive the CFE, especially under a variable CO_2 enrichment over time, which we believe is the normal case in such long-term field experiments.

4.3.3.3 High-order correlation matrix

Located in a real-world environment, strong correlations were found between the *experiment-support variables* (see Supplementary Table 4.3). A strong statistical

connection was also found for the different transformations of the subset-wise aggregated *experiment-support variables* (see Supplementary Table 4.4). Highly significant strong correlations were found for air temperature with all other *experiment-support variables*, for rainfall and vapour pressure deficit to all variables except wind speed, and for the SPEI as well as the PET to all variables except wind speed and groundwater table. Weak and partly non-significant correlations were observed for wind speed and groundwater table height with the other *experiment-support variables*. Overall, strong correlations indicate the difficulties in allocating the actual influences of each individual *experiment-support variables* on the CFE. However, the non-significant correlations between groundwater table and the FAO PM ET0 and SPEI highlights the utility of analysing single environmental variables because even a multi-factorial climatic drought index, for example, does not reflect the actual amount of available water in an ecosystem.

4.3.3.4 Time-independence of the CFE

The inter-annual variability of the CFE was much higher than the long-term changes (see Supplementary Figures 4.5a and 4.6a). Thus, applying a Kendall rank correlation test did not reveal a temporal trend of the CFE (p-value = 0.35, T = 71, tau = 0.183). We believe that the constant fertilization of our experimental site with mineral nutrients (N fertilization approximately equals the annual N deposition in intensively used agricultural regions; Reich et al. 2001) inhibited a depletion of the mineral nutrients in the soil, and thus PNL. Feng et al. (Feng et al., 2015) did not find any evidence of PNL constraints on the CFE at a decennial timescale in their meta-analysis, including an eight year data series from our experiment. They report a significantly decreasing trend of eCO_2-induced decreases in plant N concentration that diminished over time. Additionally, we are convinced that legacy effects did not cause a bias in our results, as the site has not been ploughed for more than 100 years (Kammann et al., 2008). Moreover, the permanent grassland has been fertilized consistently with 40 kg $ha^{-1}a^{-1}$ N and cut twice a year for decades (Kammann et al., 2005). The soil beneath the harvested vegetation was never markedly disturbed and the sensor installation was carefully implemented.

5 Extreme climatic events down-regulate the grassland biomass response to elevated carbon dioxide

This chapter is under review in *Nature Scientific Reports*.
Submitted: 23 May 2018

Extreme climatic events down-regulate the grassland biomass response to elevated carbon dioxide

Naiming Yuan[1,2*], Gerald Moser[3], Christoph Müller[3,4], Wolfgang A. Obermeier[5], Joerg Bendix[5] and Juerg Luterbacher[1,6]

[1] Department of Geography, Climatology, Climate Dynamics and Climate Change, Justus Liebig University, Senckenbergstraße 1, 35390 Giessen, Germany
[2] CAS Key laboratory of Regional Climate-Environment for Temperate East Asia, Institute of Atmospheric Physics, Chinese Academy of Sciences, Beijing, 100029, China
[3] Department of Plant Ecology, Justus Liebig University Giessen, Heinrich-Buff-Ring 26, 35392 Giessen, Germany
[4] School of Biology and Environmental Science and Earth Institute, University College Dublin, Dublin 4, Ireland
[5] Faculty of Geography, Philipps-University of Marburg, Deutschhausstraße 10, 35037 Marburg, Germany
[6] Centre for International Development and Environmental Research, Justus Liebig University Giessen, Senckenbergstraße 3, 35390 Giessen, Germany

---

Abstract Terrestrial ecosystems are considered as carbon sinks that may mitigate the impacts of increased atmospheric CO_2 concentration ($[CO_2]$). However, it is not clear what their carbon sink capacity will be under extreme climatic conditions. In this study, we used long-term (1998-2013) data from a C3 grassland Free Air CO_2 Enrichment (FACE) experiment in Germany to study the combined effects of elevated $[CO_2]$

and extreme climatic events (ECEs) on aboveground biomass production. CO_2 fertilization effect (CFE), which represents the promoted plant photosynthesis and water use efficiency under higher [CO_2], was quantified by calculating the relative differences in biomass between the plots with [CO_2] enrichment and the plots with ambient [CO_2]. Down-regulated CFEs were found when ECEs occurred during the growing season, and the CFE decreases were statistically significant with p well below 0.05 (t-test). Of all the observed ECEs, the strongest CFE decreases were associated with intensive and prolonged heat waves. These findings suggest that more frequent ECEs in the future are likely to restrict the mitigatory effects of C3 grassland ecosystems, leading to an accelerated warming trend. To reduce the uncertainties of future projections, the atmosphere-vegetation interactions, especially the ECEs effects, are emphasized and need to be better accounted.

Subject terms Climate-change impacts, Climate-change mitigation, Climate-change ecology, Grassland ecology

5.1 Main

Atmospheric carbon dioxide concentration [CO_2] has increased substantially since industrialization and is projected to rise by 40% from approx. 400 ppm in early 2017 to 550 ppm by 2050 (RCP8.5 scenario; Dlugokencky & Tans 2017; IPCC 2013). The rising atmospheric CO_2 concentration contributes largely to global warming, and also stimulates ecosystem productivity (Ainsworth & Long, 2005; Leakey et al., 2009; Long et al., 2004). It has been estimated that terrestrial ecosystems have sequestered about 25% of the anthropogenic carbon emissions over the past half-century (Le Quéré et al., 2009). Therefore, most ecosystems potentially act as carbon (C) sinks and mitigate the effects of increased [CO_2] (Hörtnagl

et al., 2018; Schimel et al., 2001). Concerns regarding the future capacity of ecosystems as C sinks have been raised due to the negative effects of extreme climatic events (ECEs; Williams et al. 2014). Extreme events such as prolonged heat waves, droughts, and frosts can significantly reduce ecosystem carbon uptake and productivity, thereby influencing the regional carbon cycle (Ciais et al., 2005; Reichstein et al., 2013; Zhao & Running, 2010) and gradually shifting the ecosystems from a C sink towards a C source (Ciais et al., 2005). Since ECEs have been projected to increase in both frequency and intensity (Christidis et al., 2015; Sillmann et al., 2013), studying the combined effects of ECEs and elevated atmospheric [CO_2] ([eCO_2]) on the carbon cycle of ecosystems is important for both understanding mechanisms (Zhu et al., 2017) and reducing predictive uncertainty (Huntzinger et al., 2017).

Elevated [CO_2] stimulates ecosystem productivity (termed the CO_2 fertilization effect, CFE) directly through i) enhanced photosynthesis (Long, 1991; Long et al., 2004), or indirectly through ii) reduced stomatal conductance (Ainsworth & Rogers, 2007; Ding et al., 2018; Kellner et al., 2017; Morgan et al., 2004) and iii) reduced respiration (Haworth et al., 2016). Accordingly, one may expect stronger CFEs at higher temperatures or in drier conditions (Bernacchi et al., 2006; Bishop et al., 2014), and the negative effects of ECEs may be ameliorated through improving water use efficiency (WUE; Robredo et al. 2007), increasing the plant carbon uptake (Yu et al., 2012), and enhancing recovery after ECEs (Roy et al., 2016). However, different studies have demonstrated that these theories are not applicable to all ecosystems (Hovenden et al., 2014; Reich et al., 2014). In some experiments, [eCO_2] was found to have no alleviating effect against ECEs (Brookshire & Weaver, 2015; Duan et al., 2014). On the contrary, [eCO_2] may increase the risk of exposure to ECEs by extending the growing season length (Liu et al., 2018). Meanwhile, ECEs can prevent plants from benefiting from [eCO_2] (Fitzgerald et al., 2016). The CFEs may be strongest under intermediate environmental conditions and vanish under more extreme weather conditions (Obermeier et al., 2017). The inconsistencies in these results indicate an important role for ECEs in altering CFEs, and emphasize the necessity for more detailed studies, which have thus far been prevented due to the lack of suitable long-term continuous and high quality data (Frank et al., 2015).

5 Extreme climatic events down-regulate the grassland biomass response to elevated carbon dioxide

In this study, we analyzed data from one of the longest Free Air Carbon dioxide Enrichment (FACE) experiments (Gi-FACE, 1998-2013) in the world and studied the combined effects of [eCO_2] and ECEs on aboveground biomass production. The Gi-FACE experiment was carried out on a permanent grassland in the German federal state of Hesse, near Giessen (50°32'N and 8°41'E) at 172 m a.s.l. (Fig. S5.8). Three circular plots were subjected to [eCO_2], while another three circular plots served as controls at ambient [CO_2] ([aCO_2]). They were arranged in a randomized block design (three blocks). The CO_2 fumigation began in May 1998 with an enrichment level of +20% [CO_2] above the ambient level during daylight hours (Fig. S5.9). The vegetation comprised species-rich grassland where aboveground grass biomass contributed more than 2/3 of the harvest in most years (Tab. S5.2-S5.3). Biomass was harvested twice a year before the end of spring (H1) and summer (H2) (JÄGER et al., 2003) (Tab. S5.4).

In contrast to recent work by OBERMEIER et al. (2017), that used the summer growing season data from the Gi-FACE only, we here focused on both growing seasons and defined ECEs directly using various environmental datasets including semi-hourly 2m-air temperature records, semi-hourly precipitation records, daily soil moisture, etc. We determined extreme dry events for both growing seasons, anomalous cold events including hard frost in spring, and extreme hot events including heat waves in summer. The definitions are provided in the "Material and Method" section, and corresponding figures can be found in the supplementary materials (Figs. S5.10- S5.15). The CFE in this study is represented by the effect size (ES) of the aboveground biomass, which is defined as the relative differences in biomass between the eCO_2 plots and the aCO_2 plots. We assumed that the ES of adjacent years under similar growing conditions did not differ significantly, i.e., sudden changes in growing conditions, such as those caused by ECEs, may lead to significant changes in ES. Therefore, by investigating the changes in ES of the biomass in comparison with the previous year we were able to examine the impact of ECEs on the yield stimulating effect of [eCO_2].

Before the connections between extreme climatic events and the CO_2 fertilization effects on the aboveground biomass can be studied, we first need to check whether the calculated effect size represented the true CO_2 effect. By setting a repeated measures analysis of variance (rmANOVA) model with factors time, CO_2, block,

time × CO_2 , and time × block included, the treatment effects for different plant functional groups were studied. As shown in Tab. 5.1, there were significant CO_2 fertilization effects on grass (H1, 1998-2005, 1998-2013; H2, 1998-2005), but the differences of the forbs (incl. legumes) biomass cannot be explained by the [CO_2] treatment. As a result, when considering total biomass, the treatment effect was only statistically significant for H2 when the second time section (2007-2013) was considered. This is reasonable as large initial biases of the forbs (incl. legumes) existed in the first few years of the experiment. As discussed in (Andresen et al., 2018), since 1997 before the start of the FACE up to the years before 2006/2007, there were more forbs and legumes harvested in the aCO_2 plots than in the eCO_2 plots. Benefited from the higher [CO_2] in eCO_2 plots, an increasing trend of ES was observed from 2001 to 2008 (see Fig. 5.3 in Andresen et al. 2018), but the positive effects of elevated [CO_2] were still covered especially for the first time section (1998-2005/2006). Therefore, the ES of forbs (incl. legumes) is not a good indicator for the CFEs. In the following analysis, we will mainly focus on the reactions of the aboveground total biomass, as well as grass biomass to the emergence of ECEs. The results regarding forbs (incl. legumes) will be shown in the supplementary materials (Fig. S5.16).

Using various environmental and meteorological datasets (see "Material and Method" section), different ECEs were identified. For the spring growing periods, we identified extreme cold events in 2003, 2005, and 2013; spring hard frost events in 2005, 2010, and 2013; as well as extreme dry events in 2007 (Fig. 5.1; Luterbacher et al. 2007). For each year with ECEs, see Fig. 5.2a, the ES of total biomass in H1 was found to be lower than in the previous year, while for most non-extreme years, the ES in H1 was higher than in the previous year or remained unchanged. There were only two years (1999 and 2012) where lower ES values were found but not related to ECEs. For 1999, one explanation for the relatively low ES may be attributed to the initial unbalanced effects of the FACE experiment, as the Gi-FACE experiment started in 1998. For 2012, the low ES were most probably related to the extremely low [CO_2] enrichment, which was caused by technical problems (Fig. S5.9). In fact, due to the low [CO_2] enrichment in 2013, together with the extreme cold events, an even lower ES was found in 2013 than in 2012 (Fig. 5.2a), indicating a combined effect of low [CO_2] enrichment and ECEs. Similar

Table 5.1: *P*-values for effect of the factors: Time, CO_2 treatment, block, time × CO_2, and time × block, on the biomass (Total, Grasses, and Forbs & Legumes) examined by repeated measures ANOVA. The effect was assessed for each harvest (H1 and H2) and the rmANOVA model was used at the full time series, as well as the two half time sections as suggested by Andresen et al. (2018). For significant effect at $P < 0.05$, one asterisk was marked, while for $P < 0.01$, we use two asterisks. '*n.s.*' indicated non-significant effect at $P > 0.1$.

PFG	Factors	H1			H2		
		1998-2005	2006-2013	1998-2013	1998-2005	2006-2013	1998-2013
Total	Time	0.033*	0.019*	0.015*	0.026*	0.099	0.051
	CO_2	*n.s.*	0.108	*n.s.*	*n.s.*	0.007**	*n.s.*
	Block	0.047*	*n.s.*	*n.s.*	*n.s.*	0.054	*n.s.*
	Time × CO_2	*n.s.*	*n.s.*	*n.s.*	*n.s.*	*n.s.*	*n.s.*
	Time × Block	*n.s.*	*n.s.*	*n.s.*	*n.s.*	*n.s.*	*n.s.*
Grasses	Time	0.026*	0.032*	0.006**	0.023*	0.013*	0.032*
	CO_2	0.004**	0.053	0.005**	0.016*	*n.s.*	0.070
	Block	0.002**	0.032*	0.002**	0.047*	*n.s.*	*n.s.*
	Time × CO_2	*n.s.*	*n.s.*	*n.s.*	*n.s.*	*n.s.*	*n.s.*
	Time × Block	*n.s.*	*n.s.*	*n.s.*	*n.s.*	0.039*	*n.s.*
Forbs & Legume	Time	0.016*	0.017*	0.019*	0.071	*n.s.*	0.039*
	CO_2	*n.s.*	*n.s.*	*n.s.*	*n.s.*	*n.s.*	*n.s.*
	Block	*n.s.*	*n.s.*	*n.s.*	*n.s.*	*n.s.*	*n.s.*
	Time × CO_2	*n.s.*	*n.s.*	*n.s.*	*n.s.*	*n.s.*	*n.s.*
	Time × Block	*n.s.*	*n.s.*	*n.s.*	*n.s.*	*n.s.*	*n.s.*

results were found for the grass biomass (Fig. 5.2b). If we remove the potential effects of extremely low [CO_2] enrichment, and classify the ES changes (compared to the previous year) from 1999-2011 into two groups according to the occurrence of ECEs, the ES changes were well separated (Fig. 5.3a, b). For the years with ECEs, the ES decrease were statistically significant with $p = 0.01$ for the total biomass and $p = 0.007$ for the grass biomass. Therefore, the ECEs in spring played a major role in decreasing the ES.

For the summer growing period, prolonged heat wave events were detected in 2003 and 2006 (Fig. 5.1), with twelve and nine consecutive days with daily maximum temperature T_{max} higher than 30°C, respectively (Fig. S5.12). By calculating the sum of maximum temperatures exceeding 30°C (killing degree days [KDDs], see "Material and Method" section, similar to the definition in Butler & Huybers 2013), we found also high values in 2010 and 2013 (Fig. S5.11c), suggesting potential damages from high temperature in these years. Considering that there were four consecutive days with $T_{max} > 0$°C in 2010 (Fig. S5.12), which could almost be classified as a heat wave event (see Fig. 5.1, the light red color), we determine that

Year	Spring Growing Period				Summer Growing Period			
	Hard Frost in spring	Extremely Cold	Extremely Dry	Extreme [eCO_2]	Heat wave events	High KDDs	Extremely Dry	Extreme [eCO_2]
1998	–	–	–	–	–	–	–	–
1999	–	–	–	–	–	–	–	–
2000	–	–	–	–	–	–	–	–
2001	–	–	–	–	–	–	–	–
2002	–	–	–	–	–	–	–	–
2003	–	√	–	–	√	√	–	–
2004	–	–	–	–	–	–	–	–
2005	√	√	–	–	–	–	–	–
2006	–	–	–	–	√	√	–	–
2007	–	–	√	–	–	–	–	–
2008	–	–	–	–	–	–	–	–
2009	–	–	–	–	–	–	–	–
2010	√	–	–	–	√	√	–	–
2011	–	–	–	–	–	–	–	–
2012	–	–	–	LOW	√	–	–	LOW
2013	√	√	–	LOW	–	√	–	HIGH

Figure 5.1: Detected extreme climate events (ECEs) in the spring and summer growing periods for years from 1998 to 2013. The colored boxes with check marks depict the occurrence of ECEs in the corresponding years. For the spring growing period, ECEs including hard frost in spring, extreme cold and dry events are shown, while for the summer growing period, heat wave events, high KDDs, and extreme dry events are detected. For the years that experienced a strong heat wave event, we used a dark red color. For the years that did not experience a strong heat wave event, but are very close to satisfying the conditions for being a heat wave event (4 days in a row with $T_{max} > 30°C$), we used a light red color. Besides ECEs, extreme [CO_2] enrichment events are also shown.

the summer growing period in 2010 also experienced extreme hot events. While for 2012 and 2013, extreme low and high [CO_2] enrichments were observed, respectively (Fig. 5.1 and Fig. S5.9). Therefore, to remove the potential side effects from the extreme [CO_2] enrichments, we only consider the ECEs in 2003, 2006, and 2010. For the total biomass in H2, ES decreases were found in two of the three years (2003, 2010; Fig. 5.4a). Only in 2006, the ES was not decreased, which was most probably due to the sudden increase of ES of forbs (Fig. S5.16b). After removing

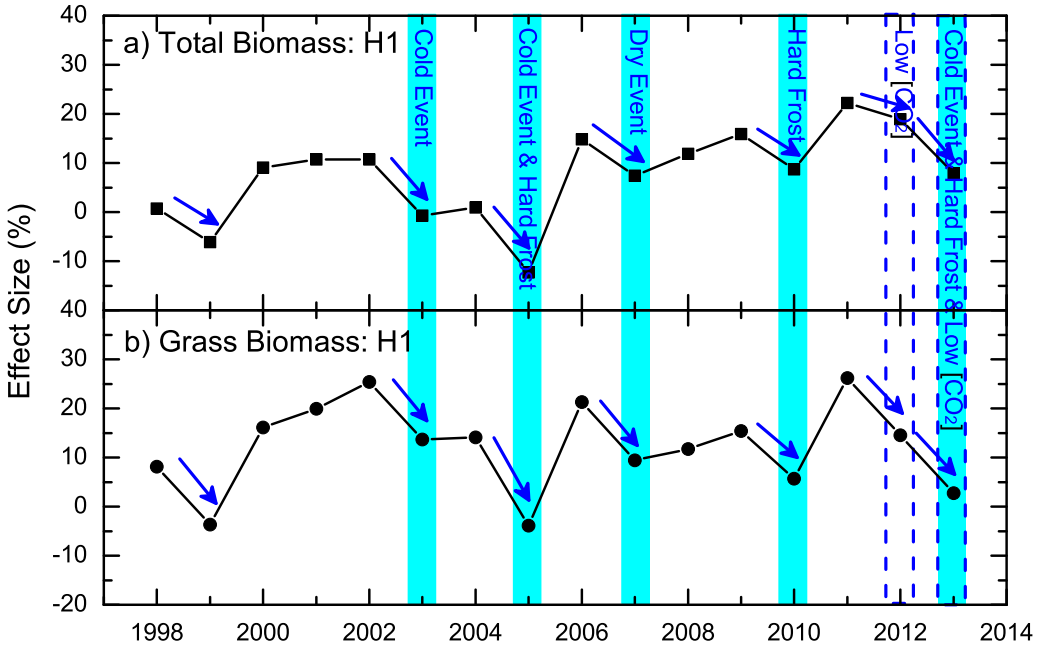

Figure 5.2: Connections between ECEs and the effect size (ES) of aboveground biomass in the spring harvest (H1). a) shows the ES of the aboveground total biomass, b) shows the ES of the aboveground grass biomass. The blue columns mark the years with ECEs, and the type of ECEs are shown within each column. For years with extreme [CO_2] enrichment events, the columns are in dashed-borders. In both a) and b), the decreases of ES are marked by blue arrows. As one can see, for all the years with ECEs, the ES of both total biomass and grass biomass decreased.

the forbs from the total biomass, ES decreases were observed in all the three years (Fig. 5.4b). Conversely, for the majority of the other years without ECEs, the ES was higher than in the previous year or remained unchanged (Fig. 5.4). If we classify the ES changes (compare to the previous year) into two groups according to the occurrence of ECEs, clear separations were again revealed (Fig. 5.3c, d). For the years with ECEs, the ES decreases are statistically significant with $p = 0.04$ for the total biomass and $p = 0.002$ for the grass biomass. Therefore, the CFEs in H2 also decreased significantly under the effects of ECEs.

To confirm these findings, we further compared the different CFEs using a new method proposed by Obermeier et al. (2017), who quantified CFEs as the slopes of productivity versus [CO_2]. Although the enrichment level of [CO_2] was set as 20% above the ambient level, the actually measured [CO_2] varied over the six

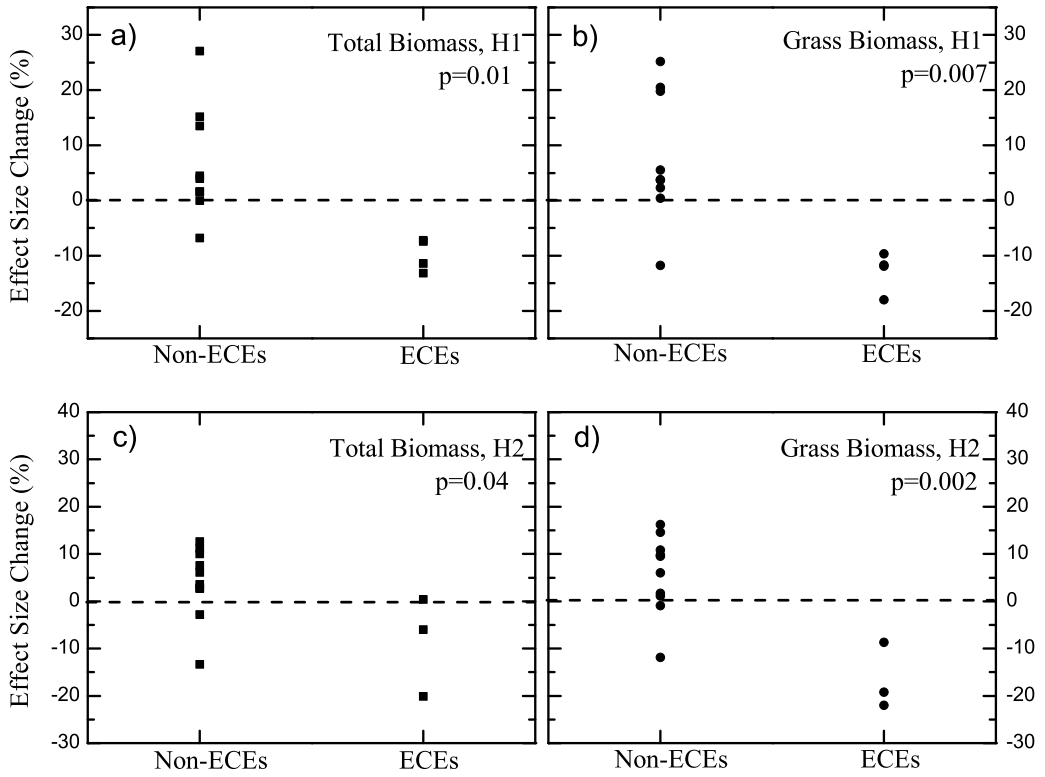

Figure 5.3: ES changes under different environmental conditions The ES changes (compared to the previous year) were classified into two groups according to the occurrence of ECEs. a), c) show the results for the total biomass, for H1 and H2 respectively; while b), d) show the results for the grass biomass. The dashed line in each sub-figure is the zero line. The two groups in each figure are well separated. By applying student's t-test (two sided), the differences are statistically significant with $p = 0.01$, 0.007, 0.04, and 0.002 for the sub-figures from a)-d), respectively

rings, which enabled to analyze productivity changes dependent on different CO_2 concentrations. Fig. 5.5 indicates the case in 2002 versus 2003 (H1, H2) and the case in 2009 versus 2010 (H1, H2) for total biomass, while Fig. 5.6 shows the results for grass biomass. In 2002 and 2009, no ECE was observed in both spring and summer growing periods. While in 2003, we found extreme cold events in spring, heat waves in summer; and in 2010, we found hard frost events in spring, high KDDs in summer (Fig. 5.1). Therefore, these two pairs were suitable examples to show the effects of ECEs on ES. For the years without ECEs (2002 and 2009, red), stronger responses of the total productivity to increased [CO_2] were found in Fig. 5.5. The steeper slope indicates higher CFEs. While for years with ECEs

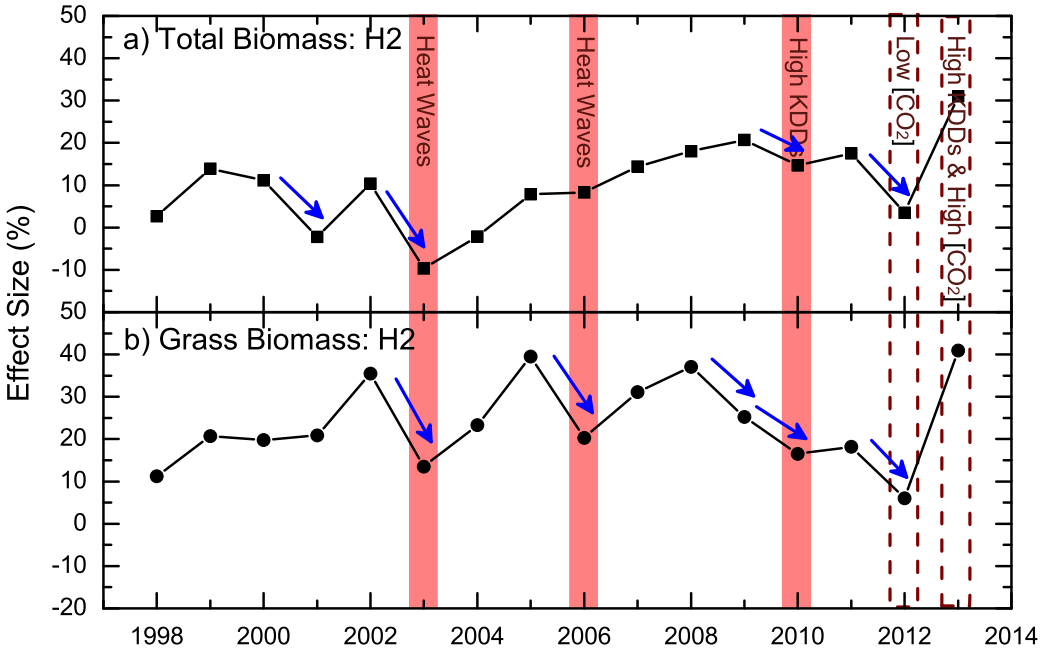

Figure 5.4: Connections between ECEs and ES of aboveground biomass in the summer harvest (H2). a) shows the ES of the aboveground total biomass, b) shows the ES of the aboveground grass biomass. Similar to Fig. 5.2, the ECEs are marked with red columns. For years with extreme $[CO_2]$ enrichment events, the columns have red dashed-borders. In both a) and b), the decreases of ES are marked by blue arrows. As one can see, for most years with ECEs, the ES of both total biomass and grass biomass decreased. Only one exception was found in 2006 for the total biomass.

(2003 and 2010, blue), the slope decreased, vanished, or even became negative, suggesting smaller CFEs under the stress of ECEs. Similar results were obtained for the grass biomass. As shown in Fig. 5.6, after removing the biomass of forbs from the calculation, the results became even clearer. Since the regression analysis was based on the measurements of only six rings, due to the large fluctuations, the differences in the slopes between 2002 and 2003 (or 2009 and 2010) were not all statistically significant (see p-values in the figure captions). However, from this simple comparison, we can still observe clear down-regulations of CFEs under the effects of ECEs.

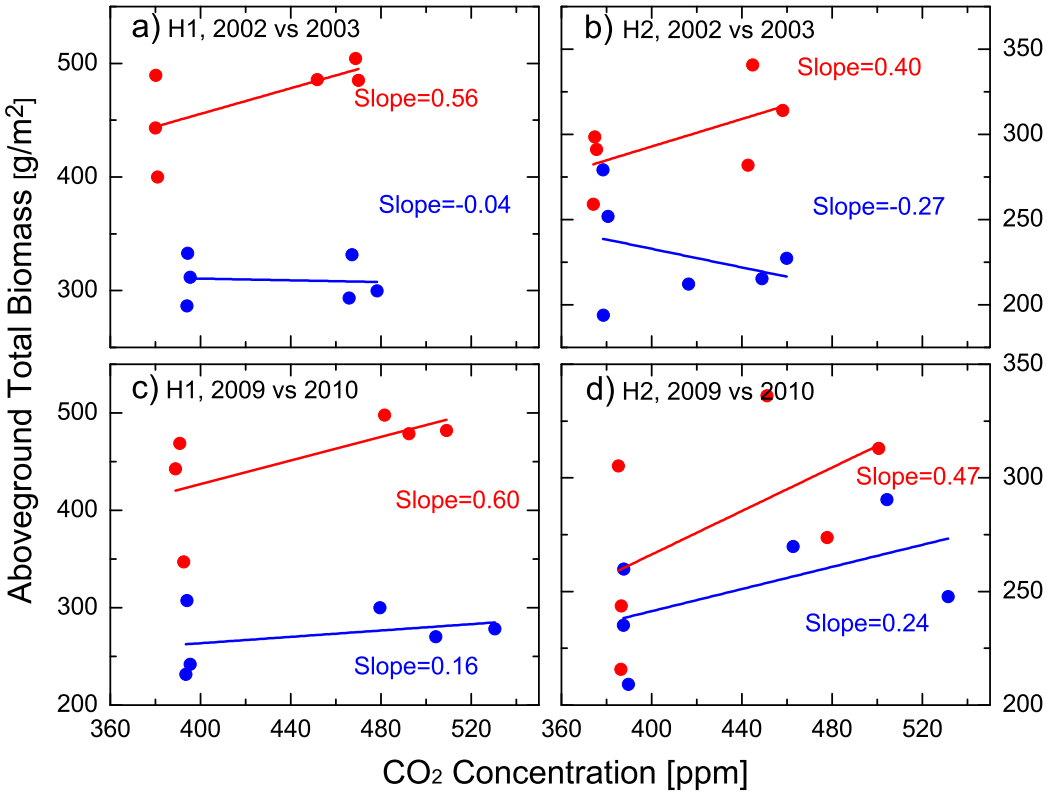

Figure 5.5: Regression analysis of the aboveground total biomass versus CO_2 concentrations for growing periods with/without ECEs. a-b) indicate the results of 2002 (red) and 2003 (blue) for H1 and H2, respectively. c-d) show the results of 2009 (red) and 2010 (blue). For the growing periods without ECEs (2002 and 2009), steeper slopes are obtained indicating stronger links between biomass and $[CO_2]$. Conversely, for the growing periods with ECEs (2003 and 2010), the slopes are lower, indicating weaker CFEs. The difference in the slopes in each sub-figure is clear, with $p = 0.13$, 0.16, 0.31, and 0.57 for (a-d), respectively.

5.2 Discussion and Conclusion

In this study, we investigated the combined effects of extreme climatic events (e.g. heat wave events, extremely hot/cold events, extremely dry events, as well as hard frost events, etc.) and elevated $[CO_2]$ on aboveground biomass production. For both spring and summer, down-regulated effect size of aboveground biomass was observed when extreme climatic events occurred during the growing season, and the strongest decreases were associated with intensive and prolonged heat waves. In contrast to previous theories that suggest that stronger CO_2 fertilization effects

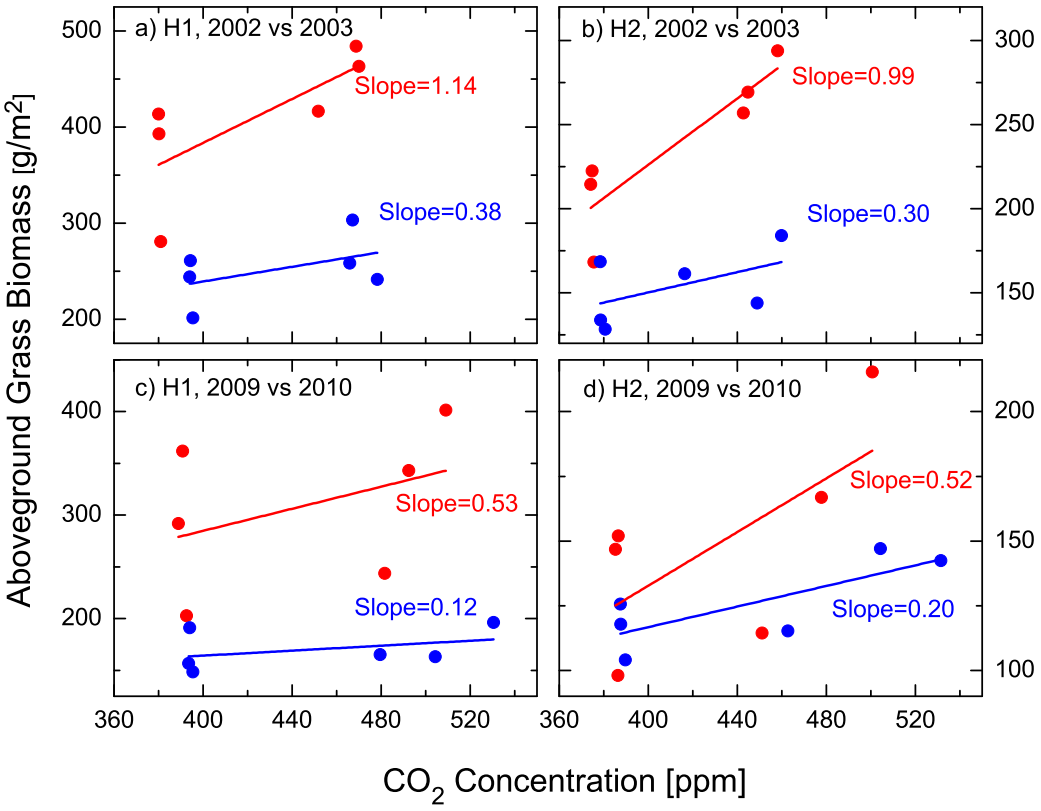

Figure 5.6: Regression analysis of the aboveground grass biomass versus CO_2 concentrations for growing periods with/without ECEs. Similar to Fig. 5.5, but for the grass biomass. The difference in the slopes in each sub-figure is clear, with $p = 0.23$, 0.05, 0.50, and 0.31 for (a-d), respectively.

may be expected under higher temperatures and drier conditions (Ainsworth & Rogers, 2007; Long, 1991; Long et al., 2004; Morgan et al., 2004), our results suggest the CO_2 fertilization effects can be lower if the growth conditions are too harsh, e.g., when heat wave events and droughts occur. This is reasonable as plant growth is influenced by multiple factors. Besides water, CO_2, and light, plants also depend on factors including nutrient availability, temperature, pathogens, and herbivores. Stress from ECEs may limit plant growth via reduced enzyme activity, increased vulnerability to pathogens and herbivores, increased respiratory losses, etc. Accordingly, the high availability of CO_2 cannot be fully utilized by plants. Our results are different to previous theories, but do not violate them. We argue that the previous theories (Ainsworth & Rogers, 2007; Long, 1991; Long

et al., 2004; Morgan et al., 2004) are only applicable within a certain range, which may be determined by the local average environmental conditions (Obermeier et al., 2017, 2018). Exceeding this optimal range, e.g., under extreme climatic events, the CO_2 fertilization will no longer overrule the plant growth.

Besides the growing periods with ECEs, there are also few cases (e.g., 1999 and 2012 for both total biomass and grass biomass in H1; 2009 and 2012 for grass biomass in H2) where the decreased ES were not related to ECEs. Accordingly, the occurrence of ECEs is only a sufficient condition for the decrease of ES, not a prerequisite. The changes of ES can be influenced by other factors such as anomalous low [CO_2] enrichment, or PFG competitions. For instance, the decreased ES in both harvest of 2012 were most probably related to the extremely low [CO_2] enrichment (Fig. S5.9), which was caused by technical problems. For H2 in 2009, the competition between grass and other plant functional types (forbs, legumes) may have contributed to the decreased ES of grass biomass (Fig. S5.17). The interactions between plants also plays an important role, e.g., in dry growing periods, one of the dominant grasses and biomass builder (Arrhenaterum elatius) reduces significantly its growth but is only in parts replaced by other species. This was part of other studies (Andresen et al., 2018). In our analysis, only the abiotic climatic factors were considered, biotic factors and species interactions were disregarded.

In view of the non-negligible effect of ECEs, it is necessary to include the effects of ECEs for the understanding of ecosystem responses to increased [CO_2]. Properly quantified indexes that present the effects of ECEs may be important for future projections. In our work, we calculated the killing degree days (KDDs) as one measure of the extreme events. Actually, it can also serve as an useful indicator of the negative effects of high temperatures in summer. As shown in Fig. 5.7, a significant negative correlation between KDDs and ES of grass biomass was found. For high KDDs, the ES dropped, while when the KDDs were low, the effect size increased. Due to the unstable [CO_2] enrichment in 2012 and 2013, we calculated the correlation between ES and KDDs using the early 14-year data (1998-2011), which yielded a coefficient r of -0.52 with $p = 0.056$. The regression analysis indicated that 28% of the variance in the natural logarithm ES could be explained by the natural logarithm KDDs, which was significant with $p = 0.031$ (Fig. 5.7b; see Fig. S5.18 for the same result but without natural logarithm transformation).

Therefore, we have reason to believe the extremely high temperatures may control the ES of the grass biomass during summer, which may be associated with the reduced transpiration caused by reduced stomatal conductance (De Boeck & Verbeeck, 2011) and increased respiration (Haworth et al., 2016). In this case, KDDs could potentially be used for development as an index for future projections of the response of the grassland to increased [CO_2].

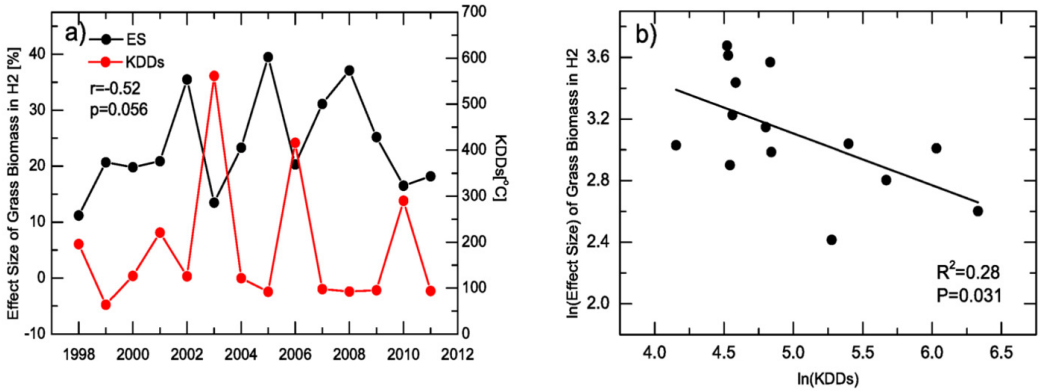

Figure 5.7: Relationships between the killing degree days (KDDs) and the effect size (ES) of grass biomass in the summer harvest (H2). To remove the side effects of extreme [CO_2] enrichment events in 2012 and 2013, only the early 14 years data (1998-2011) were used for this figure. a) Time series of KDDs (red curve, refer to right axis) and the ES (black curve, refer to left axis). b) Regression analysis, 28% variance of the natural logarithm effect size can be explained by the natural logarithm KDDs, which is significant with $p = 0.031$. For the results without logarithmic transformation, please refer to Fig. S11.

Our work focused on a grassland in central Europe. For other ecosystems, although different ECEs may occur and play different roles, we believe that the findings should be similar, in that i) the ECEs can down-regulate the CFEs, and ii) a properly quantified index (e.g. KDDs) may help explain the changes in CFEs. As extreme climatic events such as drought, heat waves, etc., are projected to increase in both frequency and intensity (Christidis et al., 2015; Sillmann et al., 2013), the mitigatory effects of C3 grassland ecosystems are likely to be restricted, leading to an accelerated warming trend in the future. To better understand atmosphere-vegetation interactions and further alleviate the uncertainties of future projections, additional results from other long-term studies over different climate zones are required.

5.3 Materials and Methods

5.3.1 Site description

The Gi-FACE experiment was carried out at a field site with an area of 1.5 ha in the German federal state of Hesse, near the town Giessen (50°32'N and 8°41'E) at 172 m a.s.l. The local annual mean precipitation over the research period was 558 ± 92mm and the annual mean 2m-air temperature was 9.4 ± 0.1°C. The research area has been managed as a meadow. It was mowed twice a year and not ploughed for at least 100 years. The old, non-grazed grassland has been fertilized with 50-80 kg N ha^{-1} yr^{-1} up to 1995. Afterwards nitrogen fertilization was reduced to 40 kg N ha^{-1} yr^{-1}. The harvested biomass of this species rich grassland is dominated by grass, with small amounts of forb and legume included. The FACE experiment started in May 1998 and the mean $[CO_2]$ enrichment is +20% above ambient during daylight hours. There are three circular plots (rings) subjected to elevated $[CO_2]$ (eCO_2), while another three circular plots (rings) served as controls with ambient $[CO_2]$ (aCO_2) (see Fig. S5.8). They were arranged in a randomized block design (three blocks). Each ring had an inner diameter of 8m with an inner circular buffer-zone of 0.9m. Biomass was harvested twice a year before the end of spring (H1) and summer (H2). In each harvest from 1998 on, the vegetation was cut manually with garden scissors at 3-5 cm above the soil surface. The harvested aboveground biomass was stored at 4°C and sorted by hand into three functional groups: grasses, forbs and legumes. For more details of the site, please refer to (Andresen et al., 2018; Jäger et al., 2003).

5.3.2 Data description

Aboveground biomass harvested from both spring (H1) and summer (H2) were used in this study. The spring harvest date was around the end of May (beginning of June) each year, while the summer harvest date was around the beginning of September (see Tab. S5.4). Mean biomass calculated over the three elevated $[CO_2]$ plots and biomass averaged over the three ambient $[CO_2]$ plots were used to quantitatively show the CO_2 fertilization effects. Besides biomass, daily soil moisture (volumetric water content in 10 cm soil depth, averaged from the measurements of 4 probes

in each plot), semi-hourly 2m-air temperature, semi-hourly precipitation, as well as the hourly mean of CO_2 concentration measured in the center of each ring, were used in this study. The soil moisture (averaged over the six rings) and precipitation are used for the determination of extreme dry events, while the 2m-air temperature records are used for the determination of extreme cold/hot events (as well as hard frost events and heat wave events), and also the calculation of Killing Degree Days (KDDs). With the measured CO_2 concentration in each ring, we investigated the true [CO_2] enrichment (see Fig. S5.9). Before determining extreme events, new data such as the number of days with daily maximum temperature higher than 30°C, the number of consecutive rain free days, the averaged daily minimum temperatures, etc., were derived for each growing period, to better show the environmental properties (see Tab. S5.5 and Tab. S5.6).

5.3.3 Statistical Analysis

5.3.3.1 Determination of the growing periods.

For spring, the start of growing season was defined as the first day after winter, when the daily mean air temperature is higher than 5°C (Tab. S5.5), as phenological observations showed significant aboveground growth from that day onwards and CO_2 flux measurements show a net CO_2 assimilation. The end of growing season thus was the harvest day of H1 (Tab. S5.4). For summer, the start of growing season was the first day after H1, while the end of growing season was the harvest day of H2 (around the beginning of September).

5.3.3.2 Calculation of Effect Size (ES).

The CO_2 fertilization effects in this study are represented by the effect size (ES) of aboveground biomass, which is defined as:

$$ES = \frac{Bio(eCO_2) - Bio(aCO_2)}{Bio(aCO_2)} * 100\%, \tag{5.1}$$

where Bio(eCO_2) stands for the dry biomass matter obtained from eCO_2 plots, while Bio(aCO_2) represents the dry biomass matter obtained from the aCO_2 plots. It is worth to note that there are three blocks in the experiment, and each block

consist of two plots (one eCO_2 plots and one aCO_2 plots). Although the plots within each block are closely located (Fig. S5.8), they may still carry different background information which could further affect the productivity. Besides, from the rmANOVA (Tab. 5.1), the factor "Block" has significant effects for both the total biomass and the grass biomass, indicating inter-replicate discrepancies. To remove this background information, we used the averaged biomass (over the 3 replicates) to better estimate the CO_2 fertilization effects.

5.3.3.3 Repeated-measures ANOVA (rmANOVA).

To check whether the effect size (ES) was indeed induced by the elevated [CO_2], the treatment effect was assessed by rmANOVA. Aboveground total biomass, grass biomass, and the forbs (incl. legumes) measured from the six plots (three blocks) were analyzed, respectively. Factors including time, CO_2 treatment, block, as well as the interactions time $\times$ CO_2 , time $\times$ block were considered in the model. For each harvest (H1 and H2), the rmANOVA model was run for the full time period of 1998-2013. Meanwhile, as suggested by the break point analysis in (Andresen et al., 2018), two half time sections, 1998-2005 and 2006-2013, were also analyzed by rmANOVA. If the p-values for the CO_2 treatment is smaller than 0.05, we consider there were significant treatment effect and ES can be used to represent the CO_2 fertilization effect.

5.3.3.4 Competition of Plant Functional Groups (PFGs).

To quantify the competition of grass with other plant functional groups (forb+legume), the Relative Changes (RCs) of grass percentage compared with that in the previous year were calculated (Tab. S5.2-S5.3). To quantitatively test for the different RCs in eCO_2 rings and in aCO_2 rings, the product of RC in eCO_2 rings and RC in aCO_2 rings were calculated for each year (Fig. S5.17). Positive products indicate that the grass percentages in eCO_2 rings and in aCO_2 rings changed towards the same direction (increased or decreased) compared with the previous year, while negative products depict different changing directions (increase and decrease). By definition, increased grass percentage in eCO_2 rings and decreased grass percentage in aCO_2 rings may contribute to an increasing ES of grass biomass (e.g., H1 in 2011), while

a decreased grass percentage in eCO_2 rings associated with an increased grass percentage in aCO_2 rings lead to a decreasing ES of grass biomass (e.g., H2 in 2009).

5.3.3.5 Definition of Extreme Climatic Events (ECEs).

We have defined different ECEs, including extreme cold and hot events, extreme dry events, hard frost in spring, as well as heat wave events. Their definitions are shown below. It is worth to note that i) two times standard deviation (2SD) was widely used for the determination of ECEs, but other threshold (e.g. 1.5SD) has also been checked, which gives robust results; ii) when studying the period-averaged (accumulated) temperature (precipitation), linear trends over 1997-2013 were removed before the analysis.

Extreme cold events: For a given growing period, if i) the minimum temperature averaged over this period was exceptionally low (exceeds 2SD, based on the data from 1997-2013); or ii) the number of days with below-zero daily air mean temperature ($T_{mean} < 0°C$) was exceptionally high (exceeds 2SD, based on the data from 1997-2013); or iii) the consecutive days with $T_{mean} < 0°C$ was exceptionally long (exceeds 2SD, based on the data from 1997-2013), we defined this growing period had experienced an extreme cold event (Fig. S5.10).

Extreme hot events: For a given growing period, if i) the maximum temperature averaged over this period was exceptionally high (exceeds 2SD, based on the data from 1997-2013); or ii) the number of days with $T_{max} > 30°C$ was exceptionally high (exceeds 2SD, based on the data from 1997-2013); or iii) the consecutive days with $T_{max} > 30°C$ was longer than 5 days, we considered this growing period had experienced an extreme hot event (Figs. S5.11-S5.12). Especially, when the condition iii) was satisfied, we define a heat wave event (Fig. S5.12). The threshold 30°C was determined according to the 95th percentile of the daily maximum temperature distribution, a definition similar to those used previously (Anderson & Bell, 2011).

Extreme dry events: For a given growing period, if i) the precipitation accumulated over this period was exceptionally low (exceeds 2SD, based on the data from 1997-2013); or ii) the soil moisture averaged over this period was exceptionally low

(exceeds 2SD, based on the data from 1997-2013); or iii) the consecutive rain free days were long enough to exceed 2SD, we say this growing period had experienced an extreme dry event (Figs. S5.13- S5.14).

Hard frost in spring: If in spring (March, April, and May) after the first day of the growing season, the daily minimum temperature dropped below -10°C, we defined it as a hard frost event in spring (Fig. S5.15), which is believed to cause severe damages to vegetation (Frank et al., 2015).

5.3.3.6 Calculation of Killing Degree Days (KDDs).

KDDs is the sum of maximum temperatures in excess of 30°C, as shown below,

$$KDDs = \sum_{i=1}^{n} aT_i,\ a = \begin{cases} 1 & T_i \geq 30°\text{C} \\ 0 & T_i < 30°\text{C} \end{cases} \tag{5.2}$$

where T_i, $i = 1, 2, \cdots, n$ represent the daily maximum temperatures from the beginning to the end of the growing period. KDDs is one indicator that represent the negative impacts of high temperature. Different from (Butler & Huybers, 2013), where the threshold was 29°C, here in this study we use 30°C, as this is the threshold we used to determine heat wave events. Fig. S5.11c shows the KDDs calculated for each year.

Acknowledgement:

This work is funded by the LOEWE excellence cluster FACE2FACE of the Hessen State Ministry of Higher Education, Research and the Arts. We also acknowledge the long-term funding of the GiFACE infrastructure by the Hessian Agency for Nature Conservation, Environment and Geology (HLNUG). N. Y. acknowledges the supports from National Natural Science Foundation of China (No.41675088), and the CAS Pioneer Hundred Talents Program. We thank LetPub (www.letpub.com) for its linguistic assistance during the preparation of this manuscript.

References

Ainsworth, E. & Rogers, A. (2007): The response of photosynthesis and stomatal conductance to rising [CO_2]: Mechanisms and environmental interactions. *Plant, Cell and Environment*, 30, 3, 258–270.

Ainsworth, E.A. & Long, S.P. (2005): What have we learned from 15 years of free-air CO_2 enrichment (FACE)? A meta-analytic review of the responses of photosynthesis, canopy properties and plant production to rising CO_2. *New Phytologist*, 165, 2, 351–372.

Anderson, G.B. & Bell, M.L. (2011): Heat waves in the united states: mortality risk during heat waves and effect modification by heat wave characteristics in 43 us communities. *Environmental Health Perspectives*, 119, 2, 210.

Andresen, L.C., Yuan, N., Seibert, R., Moser, G., Kammann, C.I., Luterbacher, J., Erbs, M., & Müller, C. (2018): Biomass responses in a temperate european grassland through 17 years of elevated CO_2. *Global Change Biology*, 24, 9, 3875–3885.

Bernacchi, C.J., Leakey, A.D., Heady, L.E., Morgan, P.B., Dohleman, F.G., McGrath, J.M., Gillespie, K.M., Wittig, V.E., Rogers, A., Long, S.P. et al. (2006): Hourly and seasonal variation in photosynthesis and stomatal conductance of soybean grown at future CO_2 and ozone concentrations for 3 years under fully open-air field conditions. *Plant, Cell & Environment*, 29, 11, 2077–2090.

Bishop, K.a., Leakey, A.D.B., & Ainsworth, E.a. (2014): How seasonal temperature or water inputs affect the relative response of C 3 crops to elevated [CO_2]: a global analysis of open top chamber and free air CO_2 enrichment studies. *Food and Energy Security*, 33–45.

Brookshire, E.N.J. & Weaver, T. (2015): Long-term decline in grassland productivity driven by increasing dryness. *Nature Communications*, 6, 7148.

Butler, E.E. & Huybers, P. (2013): Adaptation of us maize to temperature variations. *Nature Climate Change*, 3, 1, 68.

Christidis, N., Jones, G.S., & Stott, P.A. (2015): Dramatically increasing chance of extremely hot summers since the 2003 European heatwave. *Nature Climate Change*, 5, 1, 46.

Ciais, P., Reichstein, M., Viovy, N., Granier, A., Ogée, J., Allard, V., Aubinet, M., Buchmann, N., Bernhofer, C., Carrara, A., Chevallier, F., De Noblet, N., Friend, a.D., Friedlingstein, P., Grünwald, T., Heinesch, B., Keronen, P., Knohl, A., Krinner, G., Loustau, D., Manca, G., Matteucci, G., Miglietta, F., Ourcival, J.M., Papale, D., Pilegaard, K., Rambal, S., Seufert, G., Soussana, J.F., Sanz, M.J., Schulze, E.D., Vesala, T., & Valentini, R. (2005): Europe-wide reduction in primary productivity caused by the heat and drought in 2003. *Nature*, 437, 7058, 529–533.

De Boeck, H.J. & Verbeeck, H. (2011): Drought-associated changes in climate and their relevance for ecosystem experiments and models. *Biogeosciences*, 8, 5, 1121–1130.

Ding, J., Yang, T., Zhao, Y., Liu, D., Wang, X., Yao, Y., Peng, S., Wang, T., & Piao, S. (2018): Increasingly important role of atmospheric aridity on tibetan alpine grasslands. *Geophysical Research Letters*, 45, 6, 2852–2859.

Dlugokencky, E. & Tans, P. (2017): NOAA/ESRL.
URL `http://www.esrl.noaa.gov/gmd/ccgg/trends/`

Duan, H., Duursma, R.A., Huang, G., Smith, R.A., Choat, B., O'Grady, A.P., & Tissue, D.T. (2014): Elevated [CO_2] does not ameliorate the negative effects of elevated temperature on drought-induced mortality in Eucalyptus radiata seedlings. *Plant, Cell and Environment*, 37, 7, 1598–1613.

Fitzgerald, G.J., Tausz, M., O'Leary, G., Mollah, M.R., Tausz-Posch, S., Seneweera, S., Mock, I., Löw, M., Partington, D.L., McNeil, D. et al. (2016): Elevated atmospheric [CO_2] can dramatically increase wheat yields in semi-arid environments and buffer against heat waves. *Global Change Biology*, 22, 6, 2269–2284.

Frank, D., Reichstein, M., Bahn, M., Frank, D., Mahecha, M.D., Smith, P., Thonicke, K., van der Velde, M., Vicca, S., Babst, F., Beer, C., Buchmann, N., Canadell, J.G., Ciais, P., Cramer, W., Ibrom, A., Miglietta, F., Poulter, B., Rammig, A., Seneviratne, S.I., Walz, A., Wattenbach, M., Zavala, M.a., & Zscheischler, J. (2015): Effects of climate extremes on the terrestrial carbon cycle: concepts, processes and potential future impacts. *Global Change Biology*, 21, 8, 2861–2880.

Haworth, M., Moser, G., Raschi, A., Kammann, C., Grünhage, L., & Müller, C. (2016): Carbon dioxide fertilisation and supressed respiration induce enhanced spring biomass production in a mixed species temperate meadow exposed to moderate carbon dioxide enrichment. *Functional Plant Biology*, 43, 1, 26–39.

Hörtnagl, L., Barthel, M., Buchmann, N., Eugster, W., Butterbach-Bahl, K., Díaz-Pinés, E., Zeeman, M., Klumpp, K., Kiese, R., Bahn, M., Hammerle, A., Lu, H., Ladreiter-Knauss, T., Burri, S., & Merbold, L. (2018): Greenhouse gas fluxes over managed grasslands in central europe. *Global Change Biology*, 24, 5, 1843–1872.

Hovenden, M.J., Newton, P.C.D., & Wills, K.E. (2014): Seasonal not annual rainfall determines grassland biomass response to carbon dioxide. *Nature*, 511, 7511, 583–586.

Huntzinger, D.N., Michalak, A.M., Schwalm, C., Ciais, P., King, A.W., Fang, Y., Schaefer, K., Wei, Y., Cook, R.B., Fisher, J.B., Hayes, D., Huang, M., Ito, A., Jain, A.K., Lei, H., Lu, C., Maignan, F., Mao, J., Parazoo, N., Peng, S., Poulter, B., Ricciuto, D., Shi, X., Tian, H., Wang, W., Zeng, N., & Zhao, F. (2017): Uncertainty in the response of terrestrial carbon sink to environmental drivers undermines carbon-climate feedback predictions. *Scientific Reports*, 7, 1, 4765.

IPCC (2013): Climate Change 2013: The Physical Science Basis. Contribution of Working Group I to the Fifth Assessment Report of the Intergovernmental Panel on Climate Change. *Intergovernmental Panel on Climate Change, Working*

Group I Contribution to the IPCC Fifth Assessment Report (AR5)(Cambridge Univ Press, New York).

Jäger, H.J., Schmidt, S.W., Kammann, C., Grünhage, L., Müller, C., & Hanewald, K. (2003): The University of Giessen Free-Air Carbon Dioxide Enrichment Study: Description of the Experimental Site and of a New Enrichment System. *Journal of Applied Botany*, 77, 117–127.

Kellner, J., Multsch, S., Houska, T., Kraft, P., Müller, C., & Breuer, L. (2017): A coupled hydrological-plant growth model for simulating the effect of elevated CO_2 on a temperate grassland. *Agricultural and Forest Meteorology*, 246, 42–50.

Le Quéré, C., Raupach, M.R., Canadell, J.G., Marland, G., Bopp, L., Ciais, P., Conway, T.J., Doney, S.C., Feely, R.A., Foster, P. et al. (2009): Trends in the sources and sinks of carbon dioxide. *Nature Geoscience*, 2, 12, 831.

Leakey, A.D.B., Ainsworth, E.a., Bernacchi, C.J., Rogers, A., Long, S.P., & Ort, D.R. (2009): Elevated CO_2 effects on plant carbon, nitrogen, and water relations: six important lessons from FACE. *Journal of Experimental Botany*, 60, 10, 2859–76.

Liu, Q., Piao, S., Janssens, I.A., Fu, Y., Peng, S., Lian, X., Ciais, P., Myneni, R.B., Peñuelas, J., & Wang, T. (2018): Extension of the growing season increases vegetation exposure to frost. *Nature Communications*, 9, 1, 426.

Long, S.P. (1991): Modification of the response of photosynthetic productivity to rising temperature by atmospheric CO_2 concentrations: Has its importance been underestimated? *Plant, Cell and Environment*, 14, 729–739.

Long, S.P., Ainsworth, E.a., Rogers, A., & Ort, D.R. (2004): Rising atmospheric carbon dioxide: plants FACE the future. *Annual Review of Plant Biology*, 55, 591–628.

Luterbacher, J., Liniger, M.A., Menzel, A., Estrella, N., Della-Marta, P.M., Pfister, C., Rutishauser, T., & Xoplaki, E. (2007): Exceptional european warmth of autumn 2006 and winter 2007: Historical context, the underlying dynamics, and its phenological impacts. *Geophysical Research Letters*, 34, 12.

Morgan, J.a., Pataki, D.E., Körner, C., Clark, H., Del Grosso, S.J., Grünzweig, J.M., Knapp, A.K., Mosier, A.R., Newton, P.C.D., Niklaus, P.A., Nippert, J.B., Nowak, R.S., Parton, W.J., Polley, H.W., & Shaw, M.R. (2004): Water relations in grassland and desert ecosystems exposed to elevated atmospheric CO_2. *Oecologia*, 140, 1, 11–25.

Obermeier, W.A., Lehnert, L.W., Kammann, C.I., Müller, C., Grünhage, L., Luterbacher, J., Erbs, M., Moser, G., Seibert, R., Yuan, N., & Bendix, J. (2017): Reduced CO_2 fertilization effect in temperate C3 grasslands under more extreme weather conditions. *Nature Climate Change*, 7, 2, 137—-141.

Obermeier, W.A., Lehnert, L.W., Ivanov, M.A., Luterbacher, J., & Bendix, J. (2018): Reduced summer aboveground productivity in temperate c3 grasslands under future climate regimes. *Earth's Future*, 6, 5, 716–729.

Reich, P.B., Hobbie, S.E., & Lee, T.D. (2014): Plant growth enhancement by elevated CO_2 eliminated by joint water and nitrogen limitation. *Nature Geoscience*, 7, 2–6.

Reichstein, M., Bahn, M., Ciais, P., Frank, D.C.D., Mahecha, M.D., Seneviratne, S.I., Zscheischler, J., Beer, C., Buchmann, N., Papale, D., Rammig, A., Smith, P., Thonicke, K., van der Velde, M., Vicca, S., Walz, A., Wattenbach, M., Frank, D.C.D., Papale, D., Rammig, A., Smith, P., Thonicke, K., van der Velde, M., Vicca, S., Walz, A., & Wattenbach, M. (2013): Climate extremes and the carbon cycle. *Nature*, 500, 7462, 287–95.

Robredo, A., Pérez-López, U., de la Maza, H.S., González-Moro, B., Lacuesta, M., Mena-Petite, A., & Munoz-Rueda, A. (2007): Elevated

CO_2 alleviates the impact of drought on barley improving water status by lowering stomatal conductance and delaying its effects on photosynthesis. *Environmental and Experimental Botany*, 59, 3, 252–263.

Roy, J., Picon-Cochard, C., Augusti, A., Benot, M.L., Thiery, L., Darsonville, O., Landais, D., Piel, C., Defossez, M., Devidal, S., Escape, C., Ravel, O., Fromin, N., Volaire, F., Milcu, A., Bahn, M., & Soussana, J.F. (2016): Elevated CO_2 maintains grassland net carbon uptake under a future heat and drought extreme. *Proceedings of the National Academy of Sciences of the United States of America*, 113, 22, 6224–6229.

Schimel, D.S., House, J.I., Hibbard, K.A., Bousquet, P., Ciais, P., Peylin, P., Braswell, B.H., Apps, M.J., Baker, D., Bondeau, A. et al. (2001): Recent patterns and mechanisms of carbon exchange by terrestrial ecosystems. *Nature*, 414, 6860, 169.

Sillmann, J., Kharin, V., Zwiers, F., Zhang, X., & Bronaugh, D. (2013): Climate extremes indices in the CMIP5 multimodel ensemble: Part 2. Future climate projections. *Journal of Geophysical Research: Atmospheres*, 118, 6, 2473–2493.

Williams, I., Torn, M., Riley, W., & Wehner, M. (2014): Impacts of climate extremes on gross primary production under global warming. *Environmental Research Letters*, 9, 9, 094 011.

Yu, J., Lihua, C., Xu, M., & Huang, B. (2012): Effects of elevated CO_2 on physiological responses of tall fescue to elevated temperature, drought stress, and the combined stresses. *Crop Science*, 52, 1848–1858.

Zhao, M. & Running, S.W. (2010): Drought-induced reduction in global terrestrial net primary production from 2000 through 2009. *Science*, 329, 5994, 940–943.

Zhu, X., Huang, C., Zhang, L., Liu, H., Yu, J., Hu, Z., & Hua, W. (2017): Systematic analysis of hsf family genes in the brassica napus genome reveals novel responses to heat, drought and high CO_2 stresses. *Frontiers in Plant Science*, 8, 1174.

5.4 Supplementary Material

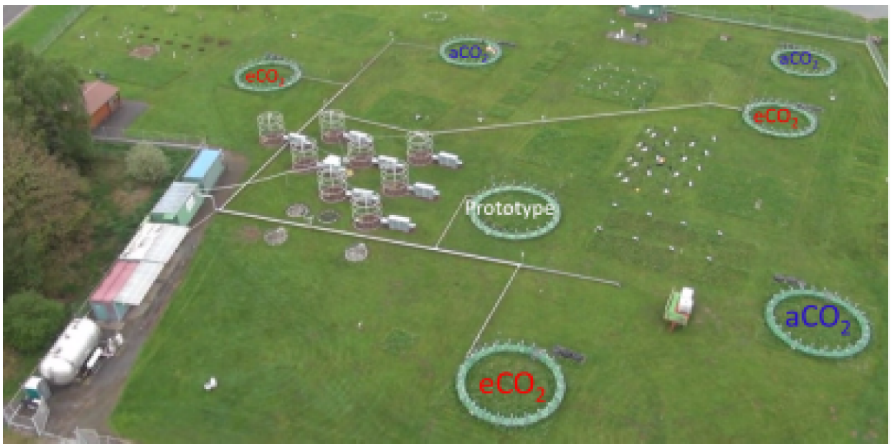

Figure 5.8: Aerial photo of the Gi-FACE field site. Locations of the rings with elevated CO_2 (eCO_2) and ambient CO_2 (aCO_2) are indicated. Inner diameter of the rings is 8m. We acknowledge the Hessian Agency for Nature Conservation, Environment and Geology (HLNUG) for providing this photo.

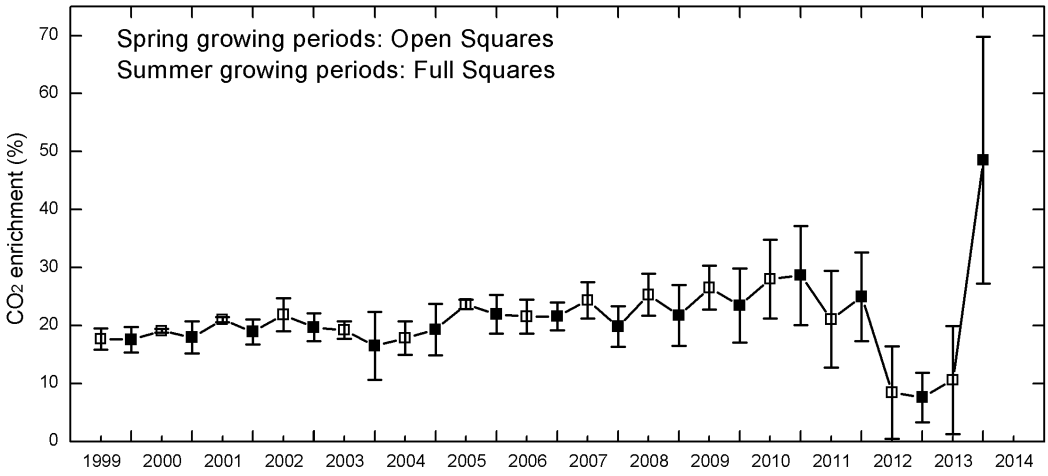

Figure 5.9: Measured $[CO_2]$ enrichment for spring and summer growing periods before the respective harvest dates. The open squares represent the $[CO_2]$ enrichment of the spring Harvest (H1), while the solid squares stand for the $[CO_2]$ enrichment of the summer Harvest (H2). The error bars are the one standard deviation calculated from the $[CO_2]$ records over different rings. For H1 in 2012 and 2013, the $[CO_2]$ enrichments were extremely low due to technical issues, while for H2 in 2012 and 2013, the $[CO_2]$ enrichments were extremely low and high, respectively.

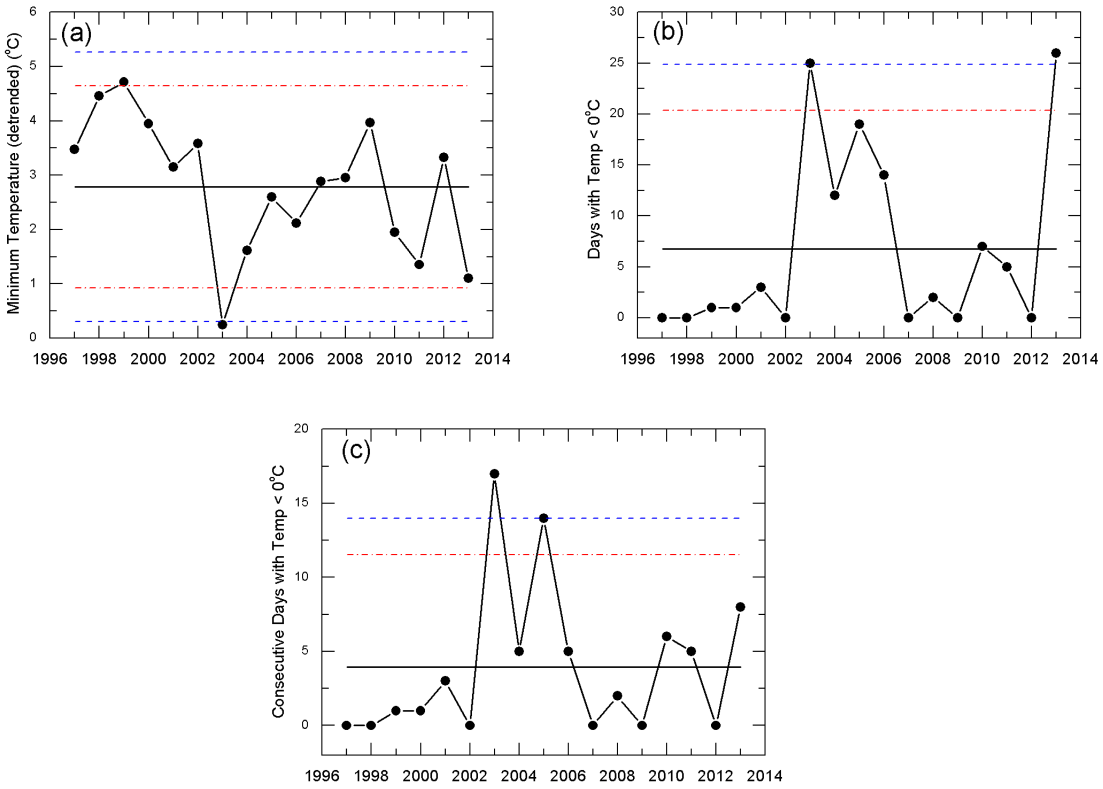

Figure 5.10: Determination of extreme cold events during spring growing period. a) shows the daily minimum temperature (with linear trend over 1997-2013 removed) averaged over the growing period for each year, b) shows the number of days with Tmean < 0°C during the growing period for each year, and c) shows the number of consecutive days with Tmean < 0°C during the growing period for each year. The red and blue dashed lines represent the 1.5 and 2 times of standard deviations. Extreme cold events were found in 2003, 2005, and 2013.

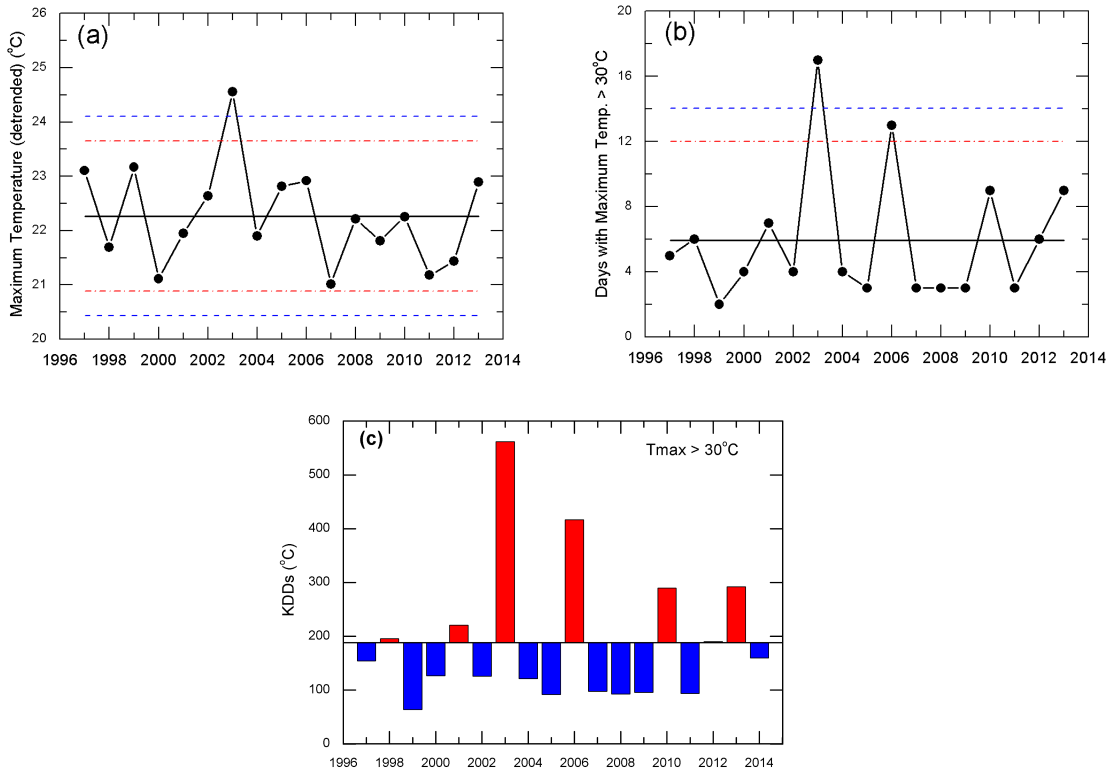

Figure 5.11: Determination of extreme hot events as well as Killing Degree Days (KDDs) during summer growing period. a) shows the daily maximum temperature (with linear trend over 1997-2013 removed) averaged over the growing period for each year, b) shows the number of days with Tmax $> 30°C$ during the growing period for each year, and c) shows the KDDs calculated for each year. In 2003 the grassland had experienced an extreme hot event.

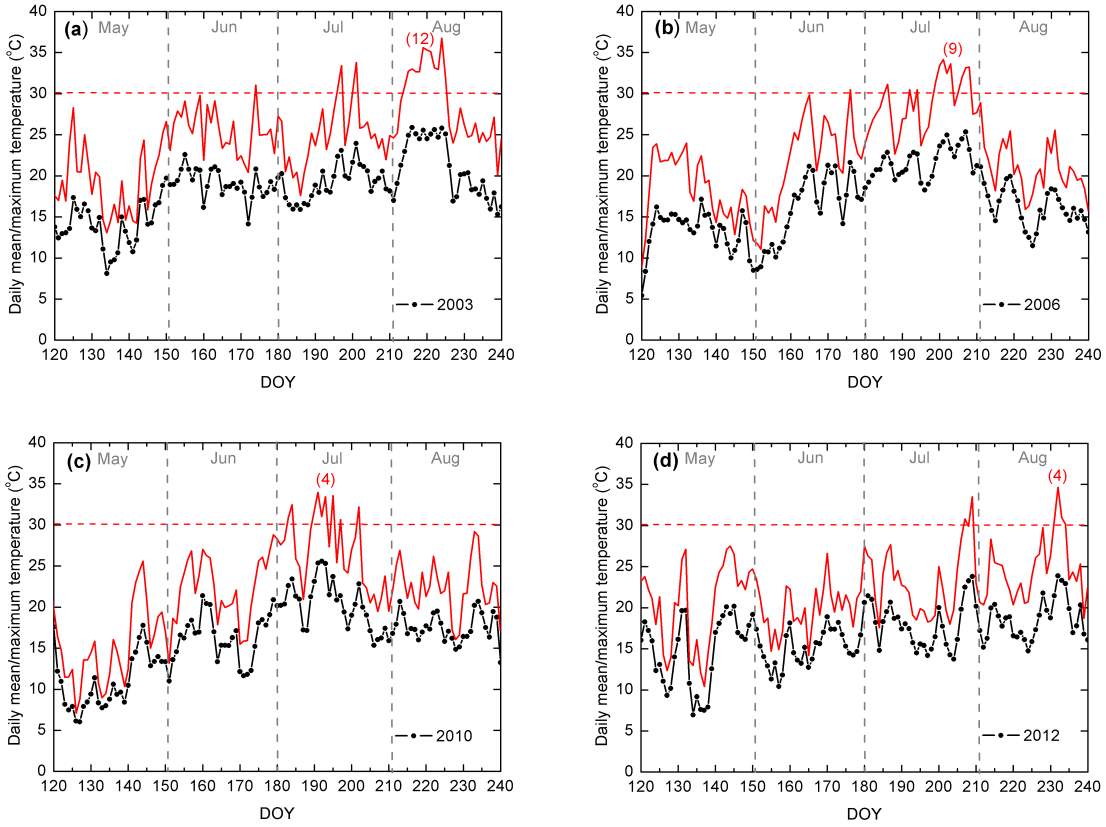

Figure 5.12: Determination of heat wave events during summer growing period. The black curve represents the daily mean temperature, while the red curve shows the daily maximum temperature. The red number in each sub-figure represents the number of consecutive days with Tmax > 30°C. a) shows the results of 2003, while b), c), d) are for 2006, 2010, and 2012. There were strong heat wave events in 2003 and 2006.

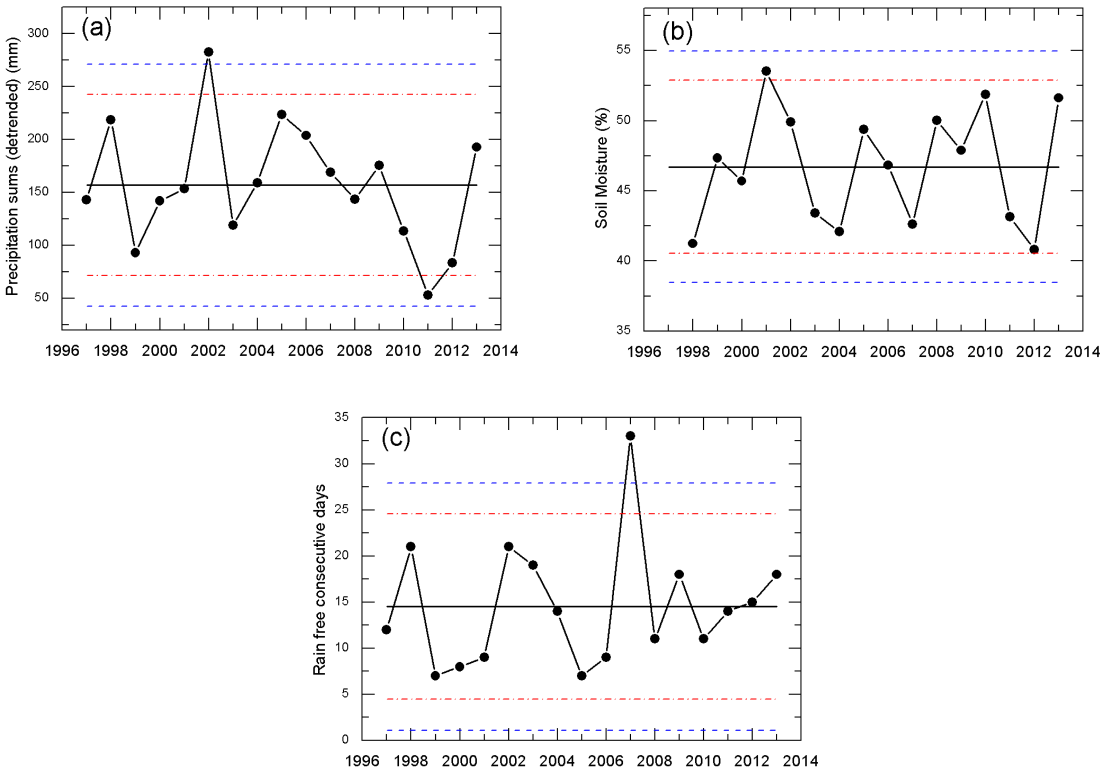

Figure 5.13: Determination of extreme dry events during spring growing period. a) shows the precipitation (with linear trend over 1997-2013 removed) accumulated over the growing period for each year, b) shows the soil moisture averaged over the growing period for each year, and c) shows the number of consecutive rain free days during the growing period for each year. The red and blue dashed lines represents the 1.5 and 2 times of standard deviations. Extreme dry events occurred in 2007.

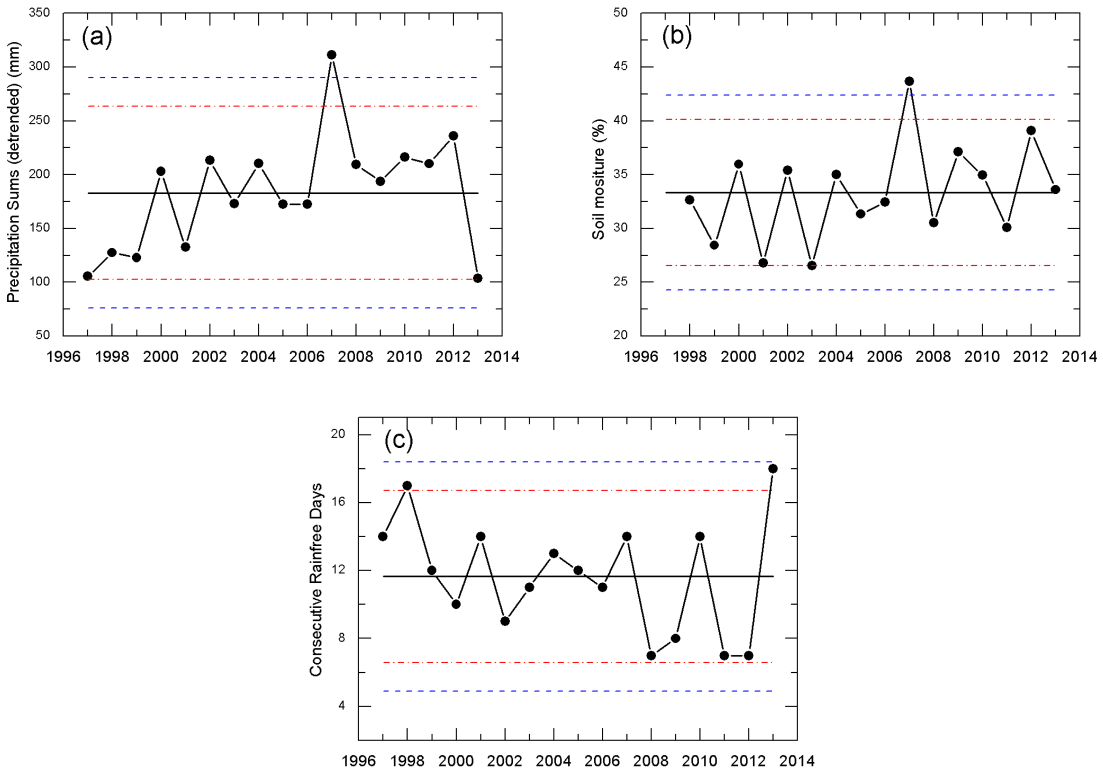

Figure 5.14: Determination of extreme dry events during summer growing period. The same as Fig. S5.13, but for the summer growing period. There was no extreme dry event in the summer growing period, but an extremely wet season in 2007.

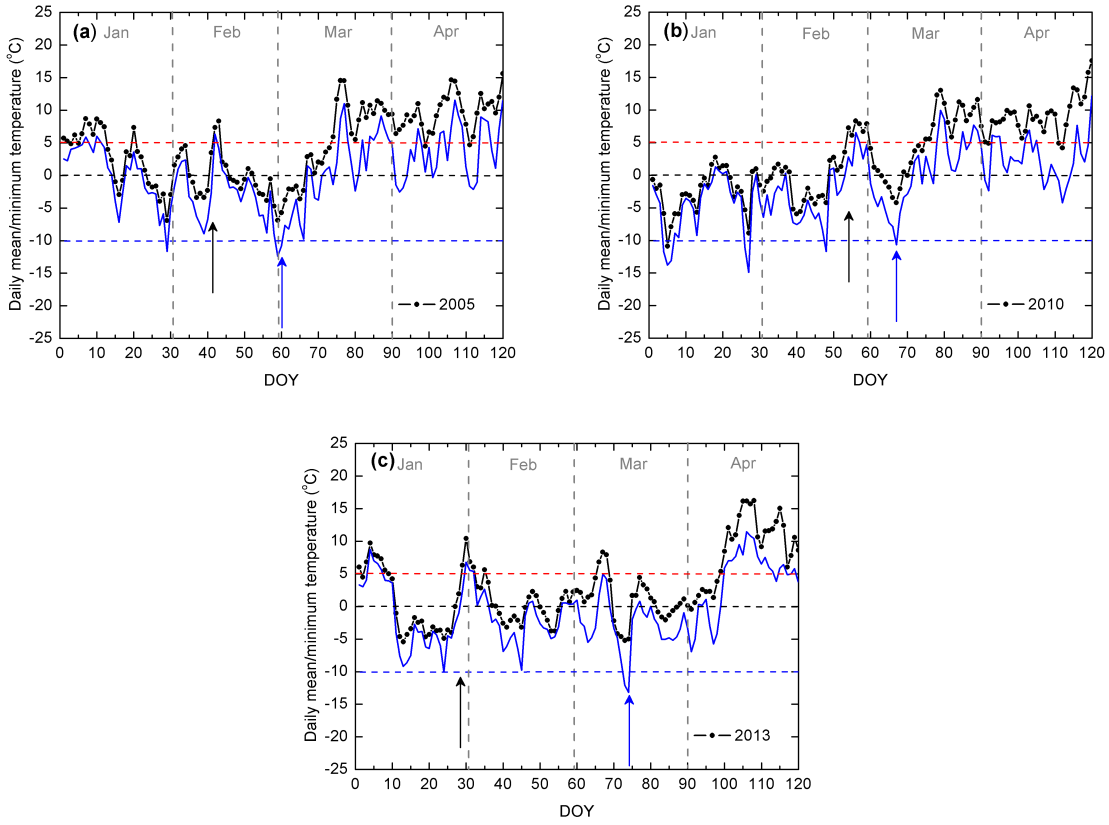

Figure 5.15: Determination of hard frost events in spring. The black curve represents the daily mean air temperature, while the blue curve shows the daily minimum temperature. The black arrow points to the day when the growing season started and the blue arrow points to the day with hard frost event. a) shows the results of 2005, and b), c) are for 2010 and 2013. After the start of growing season, these three years all experienced hard frost events in spring.

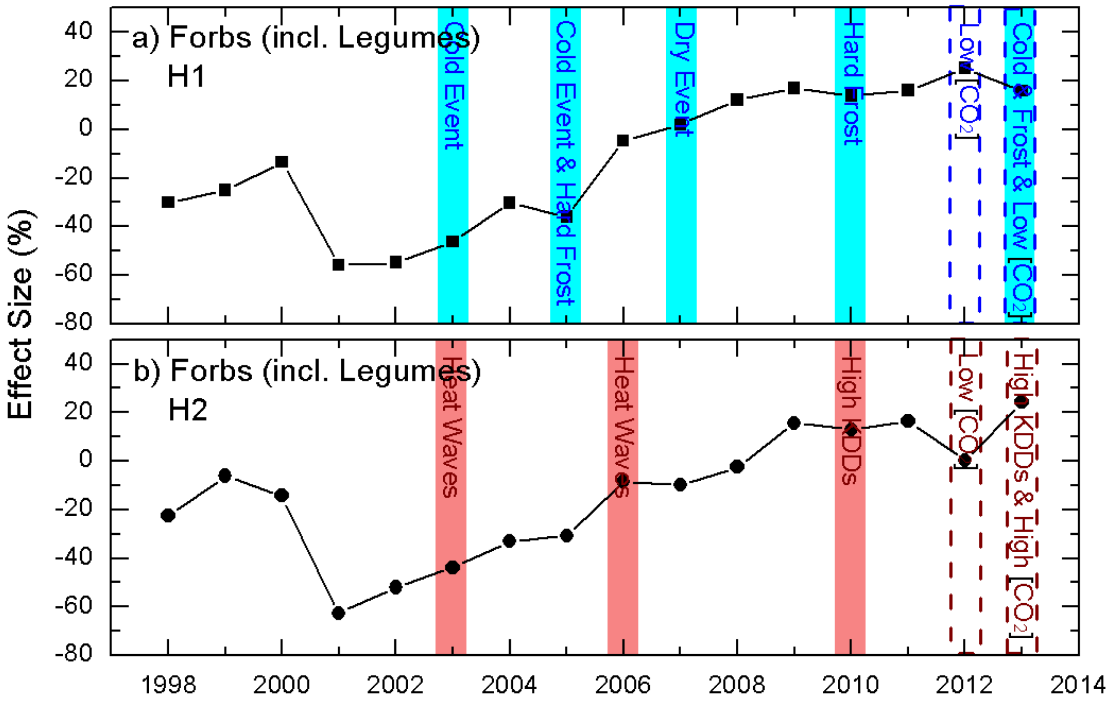

Figure 5.16: Effect size (ES) of forbs (incl. legumes). a) shows the results for H1, b) shows the results for H2. The blue columns mark the years with ECEs in spring growing period, while the red columns mark the years with ECEs in summer growing period. The type of ECEs are also shown in each column.

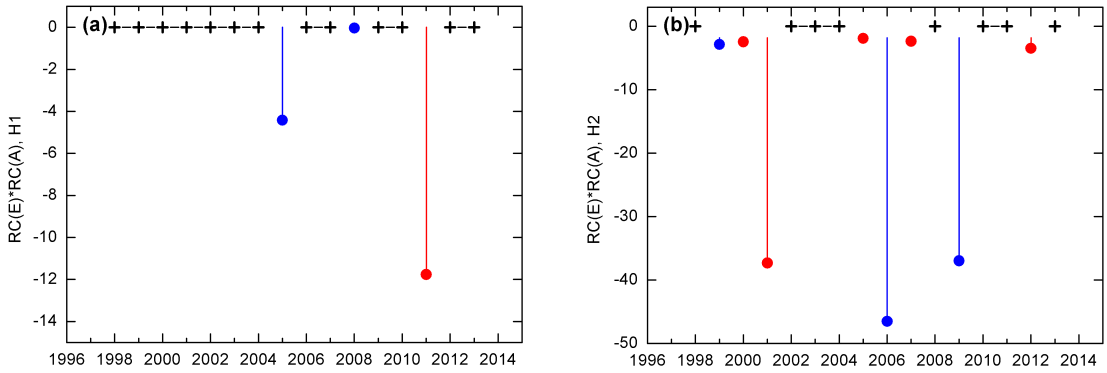

Figure 5.17: Quantitative analysis of the different changing directions of grass percentage between eCO_2 rings and aCO_2 rings, for H1 (a) and H2 (b). Using the "Relative Change" (RC) values shown in Tab. S5.2 and Tab. S5.3, we calculated the product of RC in eCO_2 rings and RC in aCO_2 rings. Positive products indicate the same changing direction (increase or decrease) of grass percentage in eCO_2 rings and aCO_2 rings. In this case, we mark a plus (+). Negative products are shown with different colors. When RC in eCO_2 rings is positive but RC in aCO_2 rings is negative, we use red color. On the contrary, when RC in eCO_2 rings is negative but RC in aCO_2 rings is positive, we use blue color.

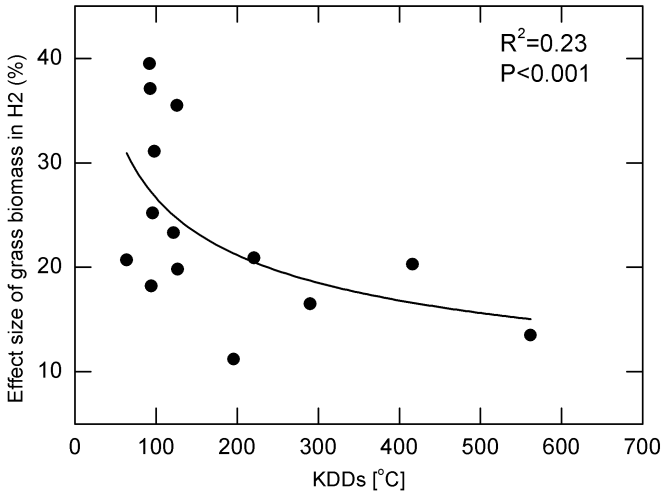

Figure 5.18: Relations between the effect size of grass biomass in H2 and the KDDs. This figure is similar to the Fig. 5.7 in the main text, but the data are not transformed by natural log. By making power-law fitting, one can find significant relations ($p < 0.001$) between the effect size of grass biomass and the KDDs.

Table 5.2: Grass Percentage measured in each year, for H1. In this table, the grass percentage (%) measured in H1 are shown in the 2nd column (for the eCO_2 rings, E rings) and the 4th column (for the aCO_2 rings, A rings). The numbers in the 3rd and the 5th columns are the relative changes (RC) of the grass percentage compared to that in the previous year.

Year (H1)	Grass Percentage in E rings (%)	Relative Change in E rings (%)	Grass Percentage in A rings (%)	Relative Change in A rings (%)
1997	88.3		83.8	
1998	86.3	−2.22	80.8	−3.62
1999	90.3	4.63	88.1	9.02
2000	81.1	−10.16	76.4	−13.28
2001	95.2	17.37	87.9	15.08
2002	92.4	−2.94	81.3	−7.55
2003	86.7	−6.15	76.1	−6.39
2004	79.4	−8.50	69.7	−8.34
2005	78.8	−0.76	73.8	5.79
2006	79.6	1.12	74.6	1.14
2007	74.5	−6.46	72.2	−3.25
2008	74.4	−0.81	72.3	0.21
2009	68.0	−8.57	67.2	−7.12
2010	62.0	−8.85	63.7	−5.14
2011	63.4	2.29	60.5	−5.13
2012	57.0	−10.11	59.1	−2.34
2013	57.3	0.56	60.4	2.26

Table 5.3: Grass Percentage measured in each year, for H2. In this table, the grass percentage (%) measured in H2 are shown in the 2nd column (for the eCO_2 rings, E rings) and the 4th column (for the aCO_2 rings, A rings). The numbers in the 3rd and the 5th columns are the relative changes (RC) of the grass percentage compared to that in the previous year.

Year (H2)	Grass Percentage in E rings (%)	Relative Change in E rings (%)	Grass Percentage in A rings (%)	Relative Change in A rings (%)
1997	77.4		83.8	
1998	80.4	3.85	80.8	11.99
1999	78.9	−1.86	88.1	0.59
2000	80.3	1.84	76.4	−0.36
2001	89.5	11.34	87.9	−3.25
2002	87.9	−1.71	81.3	−0.79
2003	74.6	−15.13	76.1	−16.16
2004	69.9	−6.37	69.7	−9.20
2005	70.6	1.09	73.8	−0.10
2006	64.9	−8.09	74.6	5.73
2007	67.7	4.23	72.2	−0.14
2008	59.6	−11.89	72.3	−13.53
2009	54.6	−8.38	67.2	4.35
2010	50.3	−7.90	63.7	−4.96
2011	55.9	11.13	60.5	13.61
2012	56.9	1.84	59.1	−0.94
2013	43.5	−22.63	60.4	−26.30

Table 5.4: Harvest dates of the Gi-FACE experiment. In this table, the harvest dates (start date and end date) of both spring harvest (H1) and summer harvest (H2) are shown.

Year	H1 Harvest Start	H1 Harvest End	H2 Harvest Start	H2 Harvest End
1998	15^{th} Jun	16^{th} Jun	3^{rd} Sep	7^{th} Sep
1999	14^{th} Jun	14^{th} Jun	25^{th} Aug	31^{th} Aug
2000	23^{rd} May	23^{rd} May	11^{th} Sep	11^{th} Sep
2001	28^{th} May	28^{th} May	10^{th} Sep	10^{th} Sep
2002	3^{rd} Jun	3^{rd} Jun	9^{th} Sep	9^{th} Sep
2003	19^{th} May	19^{th} May	8^{th} Sep	8^{th} Sep
2004	1^{st} Jun	1^{st} Jun	6^{th} Sep	6^{th} Sep
2005	13^{th} Jun	13^{th} Jun	13^{th} Sep	13^{th} Sep
2006	29^{th} May	29^{th} May	11^{th} Sep	11^{th} Sep
2007	30^{th} May	30^{th} May	10^{th} Sep	10^{th} Sep
2008	27^{th} May	27^{th} May	8^{th} Sep	8^{th} Sep
2009	25^{th} May	25^{th} May	7^{th} Sep	7^{th} Sep
2010	25^{th} May	25^{th} May	6^{th} Sep	6^{th} Sep
2011	23^{rd} May	23^{rd} May	5^{th} Sep	5^{th} Sep
2012	29^{th} May	29^{th} May	3^{rd} Sep	3^{rd} Sep
2013	3^{rd} Jun	3^{rd} Jun	2^{nd} Sep	2^{nd} Sep

Table 5.5: Data derived from the growing period of each year, for spring. Detailed data for better characterization of the properties of growing period are shown. For spring, six columns of data including the Day Of Year (DOY) of the last hard frost event, the DOY of the start of growing season, the number of days with Tmean $< 0°C$, the number of rain free days, the number of rain free consecutive days, as well as the true CO_2 Enrichment level, are presented in the table. "-" means there was no hard frost event in the corresponding year.

Year	Hard Frost DOY	Start of Growing Season	Num of Days Tmean $< 0°C$	Num of Rain free Days	Rain free Consecutive Days	CO_2 enrichment (%)
1998	35	43	0	67	21	no data
1999		50	1	60	7	17.73
2000	28	29	1	48	8	19.12
2001	56	36	3	51	9	21.05
2002	6	20	0	64	21	21.92
2003	12	20	25	70	19	19.23
2004		32	12	80	14	17.77
2005	60	42	19	66	7	23.70
2006	24	47	14	47	9	21.45
2007	26	29	0	70	33	24.45
2008		53	2	37	11	25.22
2009	16	57	0	47	18	26.45
2010	67	54	7	47	11	27.85
2011	54	35	6	77	14	21.06
2012	43	48	0	63	15	8.46
2013	74	20	26	60	18	10.61

Table 5.6: Data derived from the growing period of each year, for summer. Detailed data for better characterization of the properties of growing period are shown. For summer, five columns of data including the DOY of the start of growing season, the number of days with Tmax > 30°C, the number of rain free days, the number of rain free consecutive days, as well as the true CO_2 enrichment level, are presented in the table.

Year	Start of Growing Season	Num of Days Tmax > 30°C	Num of Rain free Days	Rain free Consecutive Days	CO_2 enrichment (%)
1998	166	6	45	17	no data
1999	165	2	45	12	17.55
2000	143	4	46	10	17.92
2001	148	7	56	14	18.97
2002	154	4	54	9	19.60
2003	139	17	64	11	16.44
2004	152	4	38	13	19.22
2005	164	3	46	12	21.91
2006	149	13	59	11	21.70
2007	150	3	50	14	19.76
2008	149	3	50	7	21.82
2009	148	3	52	8	23.44
2010	143	9	51	14	28.71
2011	144	3	43	7	24.93
2012	151	6	40	7	7.62
2013	155	9	61	18	48.53

6 Reduced Summer Aboveground Productivity in Temperate C3 Grasslands Under Future Climate Regimes

This chapter is published in *Earth's Future*, 6 (5), 715–729, 2018.
Submitted: 06 February 2018, accepted: 23 April 2018

Reduced Summer Aboveground Productivity in Temperate C3 Grasslands Under Future Climate Regimes

Wolfgang A. Obermeier[1]*, Lukas W. Lehnert[1], Martin A. Ivanov[2], Juerg Luterbacher[2,3] and Joerg Bendix[1]

[1] Faculty of Geography, Philipps-University of Marburg, Deutschhausstraße 10, 35037 Marburg, Germany
[2] School of Biology and Environmental Science and Earth Institute, University College Dublin, Dublin 4, Ireland
[3] Department of Geography, Climatology, Climate Dynamics and Climate Change, Justus Liebig University, Senckenbergstraße 1, 35390 Giessen, Germany

Abstract Temperate grasslands play globally an important role, for example, for biodiversity conservation, livestock forage production, and carbon storage. The latter two are primarily controlled by biomass production, which is assumed to decrease with lower amounts and higher variability of precipitation, while increasing air temperature might either foster or suppress biomass production. Additionally, a higher atmospheric CO_2 concentration ($[CO_2]$) is supposed to increase biomass productivity either by directly stimulating photosynthesis or

indirectly by inducing water savings (CO_2 fertilization effect). Consequently, future biomass productivity is controlled by the partially contrasting effects of changing climatic conditions and [CO_2], which to date are only marginally understood. This results in high uncertainties of future biomass production and carbon storage estimates. Consequently, this study aims at statistically estimating mid-21st century grassland aboveground biomass (AGB) based on 18 years of data (1998-2015) from a free air carbon enrichment experiment. We found that lower precipitation totals and a higher precipitation variability reduced AGB. Under drier conditions accompanied by increasing air temperature, AGB further decreased. Here AGB under elevated [CO_2] was partly even lower compared to AGB under ambient [CO_2], probably because elevated [CO_2] reduced evaporative cooling of plants, increasing heat stress. This indicates a higher susceptibility of AGB to increased air temperature under future atmospheric [CO_2]. Since climate models for Central Europe project increasing air temperature and decreasing total summer precipitation associated with an increasing variability, our results suggest that grassland summer AGB will be reduced in the future, contradicting the widely expected positive yield anomalies from increasing [CO_2].

Keywords Free Air Carbon Enrichment (FACE), climate extremes, climate change, temperate grassland, aboveground biomass, future yields

6.1 Introduction

On a global scale, approximately 26% of the terrestrial areas (Foley et al., 2011) and 70% of farmland (Soussana & Lüscher, 2007) are covered by grasslands. In

Europe, permanent meadows and pastures (mainly composed of C3 species) cover approximately 38% of the agricultural area (Food and Agriculture Organization of the United Nations Statistics Division, 2015). The enormous extent highlights the importance of grasslands for biodiversity conservation and forage supply for wildlife and livestock. Additionally, grasslands play an important role within the global carbon cycle through carbon assimilation, today harboring approximately 20% of the world's carbon pool (Schlesinger & Andrews, 2000; White et al., 2000) and potentially maintaining its CO_2 sink function under future climate conditions (Schimel et al., 2015), depending upon future biomass productivity (Parton et al., 2012).

Biomass productivity, in respect to climate variables, is claimed to be mainly controlled by air temperature and precipitation inputs (Andresen et al., 2016; Luo, 2007; Mowll et al., 2015; Nippert et al., 2006; Parton et al., 2012; Weltzin et al., 2003). However, the effect of air temperature on biomass productivity is still under debate. With increasing air temperature, a shift towards an optimum growth temperature (Luo, 2007; Myneni et al., 1997), lengthening of the growing season through earlier spring emergence and later autumn senescence (Hufkens et al., 2016; Luo, 2007), and increased nutrient availability due to higher microbial activity (Luo, 2007; Rustad et al., 2001) may foster aboveground biomass (AGB) production. In contrast, if atmospheric water availability remains constant, rising air temperature increases evaporation, decreases soil moisture availability (Niu et al., 2008), and increases midday heat stress (De Boeck et al., 2008), altogether hampering AGB productivity. The current view on the expected influences of changes in precipitation on grassland AGB is more uniform. Since the productivity of most temperate grasslands is positively influenced by rainfall, increases in total summer precipitation will concomitantly increase grassland productivity (Nippert et al., 2006; Weltzin et al., 2003; Yang et al., 2008). However, changes in precipitation variability alter grassland productivity independent of the total precipitation (Fay et al., 2011, 2003; Gherardi & Sala, 2015; Knapp et al., 2008; Nippert et al., 2006). Especially during the summer, decreased AGB with increasing precipitation variability has been related to a critical dry-down of soil moisture (Nippert et al., 2006). This effect of precipitation variability on productivity is particularly evident for grasslands that feature relatively shallow

roots feeding the plant water demand from the upper layers of soil (Gherardi & Sala, 2015; Knapp et al., 2008).

Despite climate-induced changes in AGB productivity, it is widely accepted that increasing [CO_2] will enhance future biomass productivity through reduced CO_2 limitation of (C3) plants, which is usually referred to as the CO_2 fertilization effect (Ainsworth & Rogers, 2007; Ainsworth & Long, 2005; Lloyd & Farquhar, 2008; Soussana & Lüscher, 2007). As a consequence of reduced CO_2 limitation, water-use efficiency of plants increases because stomata need less be opened to obtain CO_2 (Kellner et al., 2017). Thus, it is expected that the CO_2 fertilization effect is particularly strong under drier conditions (Morgan et al., 2004; Soussana & Lüscher, 2007; Volk et al., 2000). Likewise, a strong CO_2 fertilization effect is anticipated under warm conditions, when the ratio of photosynthesis to photorespiration is decreased, since photosynthesis is promoted by elevated [CO_2] (Long, 1991; Luo, 2007; Morison & Lawlor, 1999). However, field studies have shown that the CO_2 fertilization effect is reduced under more extreme conditions (e.g., drier and/or hotter; Hovenden et al. 2014; Obermeier et al. 2017; Reich et al. 2014). In agreement with those findings, recent studies suggest that plants benefit from increasing CO_2 only if carbon demand is high, the latter depending on processes of tissue formation and cell growth (Fatichi et al., 2014; Körner, 2015).

As a result, changing climate and increasing atmospheric [CO_2] interact and may have contrasting effects on biomass productivity in the future, which is currently poorly understood and is mainly studied by numerical models (e.g., Chang et al. 2017; Gu et al. 2014; Hufkens et al. 2016; Huntzinger et al. 2017; Rounsevell et al. 2005). To overcome model uncertainties, a field data-driven assessment of the future AGB productivity is urgently needed, for example, to estimate future vulnerability of livestock forage, biodiversity conservation, and carbon storage. Large-scale and long-term experiments under natural conditions provide the best possibility to test AGB response to the multitude of interactions under climate change (De Boeck et al., 2008; Zhu et al., 2016). Therefore, free air carbon enrichment (FACE) experiments represent a state-of-the-art technique. Here we use one of the longest continuously operating FACE experiments on grasslands to estimate, for the first time, future biomass production, combining

field measurements, simulated future climate regimes, and a variable atmospheric [CO_2]. To construct future climate regimes, we modified the ranges and relations of the climate variables during the experimental period, to coincide with the general findings of IPCC projections. By comparing the AGB under the different climate regimes, we quantified changes of biomass production in the mid of the 21st century in relation to current yields. To achieve this, we (1) generated potential future climatic regimes, by slightly altering the ranges and relations of climate variables selected during an exhaustive AGB model selection approach, and (2) estimated the AGB productivity under ambient and elevated [CO_2] within the potential future climate regimes. Significant changes among climatic regimes and [CO_2] were evaluated to quantify the relative changes and the uncertainties of future biomass production in C3 grasslands of Central Europe.

6.2 Materials and Methods

6.2.1 Study site

The large-scale FACE field experiment near Giessen, Germany (GiFACE; 50°32'N and 8°41'E; 172 m a.s.l.) has been running since 1998. The main purpose of the GiFACE experiment is to study the effects of higher [CO_2] on a temperate, nongrazed and extensively managed, species-rich grassland ecosystem. Six FACE rings of 8-m diameter were established (for a detailed description of the study site see Andresen et al. 2018; Jäger et al. 2003. In three of the rings (control rings) plants grew under ambient CO_2 conditions. In the other three rings, the vegetation has been exposed to elevated CO_2 conditions (∼20% above ambient [CO_2] during daylight hours), roughly simulating the CO_2 conditions expected for the period from 2021 to 2050. Compared to other FACE studies, such a low CO_2 enrichment was chosen to prevent artifacts that may arise from a sudden stepwise increase in [CO_2] (Luo, 2001; Newton et al., 2001). The soil is a Fluvic Gleysol (Food and Agriculture Organization of the United Nations Statistics Division, 1994) with a sandy clay loam layer above a clay layer of variable depth (Kammann et al., 2005). The grassland composition is comparable within all rings and is dominated by the C3 grasses *Arrhenaterum elatium*, *Galium mollugo*,

Holcus lanatus, and *Poa pratensis*, accompanied by a forb fraction and legumes, the latter at low abundance (Kammann et al., 2005). Throughout the experimental period, the vegetation has been steadily fertilized with 40-kg nitrogen·ha^{-1}·year^{-1} and 600 kg·ha^{-1}·year^{-1} of 10% phosphorus pentoxide +15% potassium oxide +3% magnesium oxide and 33% calcium oxide + magnesium oxide in spring (Kammann et al., 2005).

6.2.2 Meteorological Data, Vegetation, and CO_2 Data

The meteorological data were measured at the field site from climate stations run by the Hessian Agency of Nature Conservation, Environment and Geology (HLNUG) and the Environmental Monitoring and Climate Impact Research Station Linden (UKL). For air temperature, a Pt-100 resistance thermometer at 2-m height was used. Precipitation was measured using three Hellmann samplers, randomly distributed over the experimental area.

The AGB (dry matter) was derived at the time of peak biomass accumulation (beginning of September) by cutting the vegetation approximately 5 cm above ground and subsequently oven drying at 105°C. To enable a comparison of climate-induced changes on AGB productivity, we investigated the AGB in the control rings under ambient [CO_2] (aAGB) and in the rings exposed to elevated CO_2 (eAGB). Mean values of AGB were calculated for both treatments and each year.

To model AGB productivity depending on environmental conditions, we generated various climate predictors (refer to section 6.2.3). Therefore, we used the meteorological data sets (hourly and half-hourly measurements) and included the 90 days prior to each September harvest in the analysis, roughly corresponding to the summer months of June, July, and August. Within these 90-day periods, predictors for AGB estimation were calculated. Hourly precipitation was aggregated to daily precipitation total. Daily mean, minimum, and maximum values of air temperature were extracted from half-hourly measurements. All data sets used for current biomass modeling covered the time period from 1998 to 2015. Technical problems caused a very low CO_2 enrichment in 2012 and a very high CO_2 enrichment in 2013 (Obermeier et al., 2017). Thus, both years were excluded from further analysis. Data analysis was conducted using the CRAN R version 3.3.3 (R Core Team,

Table 6.1: Overview of the predictors derived from air temperature (2 m) measurement.

Abbreviation	Long form	Unit	Formula
AT_Mean	Mean air temperature	°C	$\sum_{i=h-90}^{h} \frac{\text{Tmean}_i}{90}$
AT_MeanTrans	Transformed mean air temperature	°C	$\text{Tmean}_{all} = \frac{\sum \text{ATMean}}{18}$ $\text{Tmean}_{all} = \sqrt{(\sum_{i=h-90}^{h} \frac{\text{Tmean}_i}{90} - \text{Tmean}_{all})^2}$
AT_MaxMean	Mean of the daily maximum air temperature	°C	$\sum_{i=h-90}^{h} \frac{\text{Tmax}_i}{90}$
GDD	Growing degree-days	°C	$\sum_{i=h-90}^{h} \frac{Tmin_i + Tmax_i}{2} - 5$, $Tmin_i = \begin{cases} 5°\text{C if } Tmin_i < 5°\text{C}, \\ Tmin_i \text{ otherwise} \end{cases}$ $Tmax_i = \begin{cases} 30°\text{C if } Tmax_i > 30°\text{C}, \\ Tmax_i \text{ otherwise} \end{cases}$
KDD	Killing degree-days	°C	$\sum_{i=h-90}^{h} Tmax_i$ $Tmax_i = \begin{cases} 0°\text{C if } Tmax_i < 30°\text{C}, \\ Tmax_i \text{ otherwise} \end{cases}$

Note. h denotes the day of year of harvest. $Tmean_i$, $Tmax_i$, and $Tmin_i$ refer to the aggregated average, maximum, and minimum air temperature of day i, respectively; $Tmean_{all}$ is the long-term average air temperature within the investigated 90-day periods.

2018). An overview of the processing steps is given in the Supporting Information (Supplementary Fig. 6.7).

6.2.3 Predictors for AGB

The estimation of future grassland AGB requires a wide set of variables to account for both changes in absolute air temperature and precipitation values and shifts in their variability. While simple statistical models depend on basic climate variables, such as the mean annual temperature and total annual precipitation (e.g., Lee et al. 2011), other studies suggest that additional attributes such as the timing and frequency of precipitation events influence ecosystem productivity and thus should be included in the analysis (Craine et al., 2012; Heisler-White et al., 2009; Knapp et al., 2015; Nippert et al., 2006; Parton et al., 2012; Pierre et al., 2011; Swemmer et al., 2007; Yang et al., 2008). To depict a realistic image of the most important ecophysiological conditions, we created various predictors based on air temperature (Table 6.1) and precipitation (Table 6.2) data. Further details on the predictor variables used in this study can be found in 6.1.

Table 6.2: Overview of the predictors derived from precipitation measurements.

Abbreviation	Long form	Unit	Formula
PPT_Sum	Total summer precipitation	mm	$\sum_{i=h-90}^{h} \mathrm{PPT}_i$
N° dry days	Number of days with less than 1 mm of precipitation	days	$\sum_{i=h-90}^{h} \mathrm{DD}$, $DD = \begin{cases} 0 \text{ if } PPT_i \geq 1\text{mm} \\ 1 \text{ if } PPT_i < 1\text{mm} \end{cases}$
Mean dry-interval length	Mean dry-interval length	days	A dry-interval is defined by at least six consecutive days with less than 1 mm precipitation. The average length of the dry-intervals is calculated.
Max dry-interval length	Maximum dry-interval length	days	Number of days in the longest period of consecutive dry days with less than 1 mm precipitation.
N° rain events	Number of rain events	events	Number of rain events, where consecutive days with precipitation > 1 mm are counted as one event.
Mean event size	Mean precipitation total for one rain event	mm	$\frac{\sum_{i=h-90}^{h} \mathrm{PPT}_i}{\mathrm{N}^\circ \text{ rain events}}$
PPT_Max	Maximum of the daily precipitation totals	mm	$\max(\mathrm{PPT}_i)$

Note. h denotes the Day of Year of harvest. PPT_i is the sum of the daily precipitation in day i.

6.2.4 Creation of Predictor Subsets

To ensure that, regardless of the result of the variable selection (refer to section 6.2.5), biomass alterations can be attributed to either changes in air temperature or the variability of precipitation inputs, two separate predictor subsets were created: The first subset consisted of temperature-related variables, and the second one was based on precipitation-related variables. However, since the total summer precipitation is expected to dominate the influence on the AGB production, it is included as predictor in both subsets. Consequently, the precipitation amount and air temperature subset includes the mean air temperature, mean daily maximum air temperature, growing degree-days, killing degree-days, and the transformed mean air temperature, along with the total summer precipitation. The precipitation amount and variability subset contains the variables of total summer precipitation, maximum daily precipitation, number of dry days, number of rain events, mean event size, maximum dry-interval length, and the mean dry-interval length.

6.2.5 Selection of Final Predictors and Final Model Creation

Two separate partial least squares regression (PLSR) models were fitted to estimate aAGB and eAGB in relation to the predictors included in the precipitation amount

and air temperature and the precipitation amount and variability subsets. The final set of predictor variables within each subset was selected applying an exhaustive information-theoretic model-selection approach based on the Akaike information criterion (Akaike, 1998), supported by PLSR regression outputs. The selection of the optimal set of predictor variables was performed using the averaged AGB of all rings, resulting in an identical predictor space for eAGB and aAGB. For further information on predictor selection, model tuning and validation of the biomass estimation, see Supplementary Section 6.5.2.

6.2.6 Future Climate Regime Creation and Regime-Based AGB Estimations

For each subset, we created the most plausible future climate regimes by altering the selected predictor variables. Since neither air temperature nor precipitation regimes have experimentally been altered, we extracted potential future regimes (e.g., low precipitation input with high air temperature) within the ranges and inherent relations of the climatic variables measured during the experimental period. The methodology is described briefly in the following; for a detailed description with the example of the dry regime in the precipitation amount and air temperature subset refer to Supplementary Fig. 6.7 and Supplementary Section 6.5.3.

Since total summer precipitation is the most important predictor for summer AGB, all climatic regimes were primarily defined by means of the total summer precipitation (precipitation amount regime; compare Fig. 6.1). Dry regimes are located within the lower quartile and medium precipitation regimes within the interquartile range of the observed 90-day precipitation amount measured during the 18 years of the experiment. To account for other variables that influence the biomass productivity, we defined three subregimes for each main precipitation amount regime by altering the remaining predictors. This resulted in two main regimes and six subregimes for each of the two subsets (precipitation amount and air temperature, and precipitation amount and variability subset; Figures 6.1, 6.3, and 6.4).

For the creation of subregimes we used the empirical relationship between the climatic drivers during the experimental period assuming that the qualitative

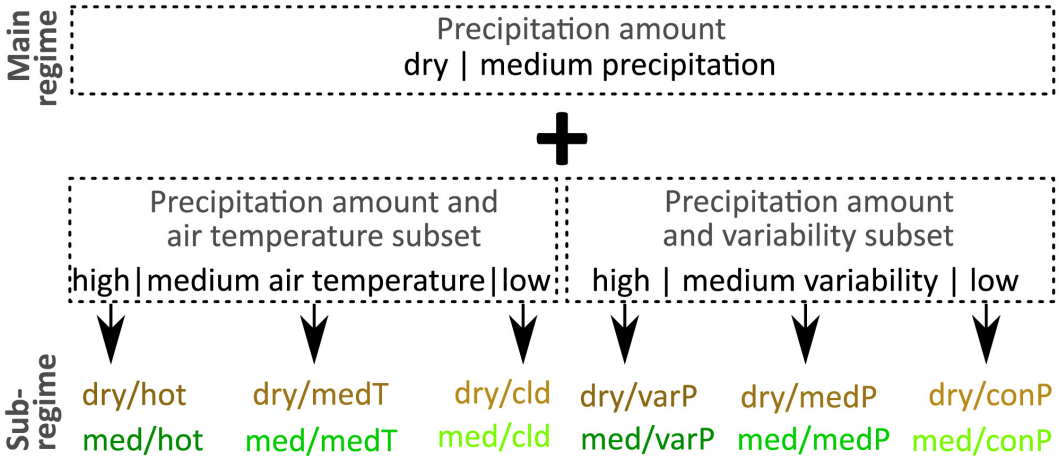

Figure 6.1: Schematic overview of the regimes and subregimes for the precipitation amount and air temperature subset and the precipitation amount and variability subset. Main regimes were primarily defined by the precipitation amounts. For each main regime and subset, three subregimes were defined by modifying the related predictor variables. The predictor ranges for the different subregimes can be found in Supplementary Tables 6.9 and 6.10. Med stands for medium precipitation amount, medT stands for medium air temperature, medP stands for medium precipitation variability, cld stands for cold, varP stands for a high precipitation variability, and conP stands for a low variability in the precipitation inputs.

relationships between the climate variables will persist despite of climate change. Therefore, linear regression models between the total summer precipitation and each predictor variable were calculated. To account for possible stronger variations of the climatic conditions in the future, 1,000 precipitation sample values were uniformly drawn within the respective precipitation amount regime boundaries (e.g., a total summer precipitation between 105 and 155 mm for the dry regime). For each precipitation value, the regression estimates were used to interpolate the corresponding predictor values. Since lower correlations between climatic variables enlarge the uncertainty of the regression results, the estimates were not directly used. Instead, 1,000 normal distributions were fitted to the sampled precipitation values, with the corresponding predictor estimate as mean value, and a standard deviation calculated according to the 0.05 and 0.95 confidence interval of the linear regression model. From each of the 1,000 distributions, one single value was randomly sampled and used as the predictor value corresponding to the respective precipitation sample value. For the hot (hot in Fig. 6.1) and

variable precipitation (varP in Fig. 6.1) subregimes, the mean values of the normal distributions were shifted by plus one standard deviation. For the cold (cld in Fig. 6.1) and constant precipitation variability (conP in Fig. 6.1) subregimes, the mean values of the normal distributions were reduced by one standard deviation accordingly. The resulting boundaries of the subregimes are depicted in Figures 6.3 and 6.4, respectively (thresholds of the climate variables within the subregimes can be found in Supplementary Tables 6.9 and 6.10, respectively). Within each of these subregimes, eAGB and aAGB were estimated by means of the 1,000 samples for each predictor and the final PLSR models. To compare the biomass estimations, we also calculated the relative AGB change in the elevated compared to the ambient rings for each subregime (100*(eAGB-aAGB)/aAGB).

6.2.7 Assessment of Future Climate Conditions

To assess the climate regimes that are most likely to depict frequent future conditions, we compared the projected predictor alterations to various climate model results. Due to the well-known, nonlinear relationship between [CO_2] and photosynthesis (Farquhar et al., 1980), we constrained our analysis to the years 2021 to 2050 with a predicted atmospheric [CO_2] in the range of the experimentally enriched [CO_2] in the elevated rings. One hundred twenty-three numerical regional climate models based on different global models and emission scenarios publicly available in the Regionaler Klimaatlas Deutschland (Regionale Klimabüros in der Helmholtz-Gemeinschaft, 2017) were used. Here various climate calculations based on the Special Report on Emissions Scenarios A1B (total number = 24; Hollweg et al. 2008; Jacob et al. 2007; van der Linden & Mitchell 2009), A2 (20; Christensen et al. 2005; Jacob et al. 2008), B1 (3; Hollweg et al. 2008; Jacob et al. 2008), and B2 (4; Christensen et al. 2005), as well as based on representative concentration pathways (RCP) 2.6 (10; Jacob et al. 2014, RCP), 4.5 (30; Jacob et al. 2014), and RCP8.5 (32, Jacob et al. 2014) were included. To assess the most probable predictor alterations for the years 2021 to 2050, we considered model runs that depict the minimum, mean, and maximum changes of the respective variable in the ensemble in Germany. Moreover, we depicted the mean change of the respective variable in the ensemble and selected future time

period for the experimental area in Linden. For ease of assignment, we refer to the climate calculations always in the form of "emission scenario/global model/regional model".

6.3 Results

To unravel the relations between predictor variables and biomass productivity, Pearson's correlation coefficients were calculated (Supplementary Table 6.4). For total summer precipitation, Pearson's correlation coefficient was greater than 0.8 for the mean size of rain events, which we therefore excluded from further analysis to enable a proper predictor selection. Very high correlations were found between mean air temperature, growing degree-days, killing degree-days, and mean of daily maximum air temperature. The strongest correlation with AGB was observed for total summer precipitation. Significant correlations with summer AGB were found for all predictors except growing degree-days, number of dry days, maximum dry-interval length, and transformed mean air temperature.

The combined approach using information theory and PLSR technique revealed predictors for the finals models for AGB estimation within the two subsets (Supplementary Tables 6.5 and 6.6, and Supplementary Section 6.5.1). For the precipitation amount and air temperature subset, final predictors were total summer precipitation and transformed mean air temperature. For the precipitation amount and variability subset, total summer precipitation, number of rain events, number of dry days, and mean dry-interval length were chosen as final predictors.

The predictive performance of the final PLSR model for the precipitation amount and air temperature subset was generally high, except for 2 years (2008 and 2015, Figures 6.2a and 6.2b). The best performances were yielded for aAGB if one latent vector was used and for eAGB if two latent vectors were used (Supplementary Table 6.7). Within the precipitation amount and variability subset three latent vectors were used for the estimation of aAGB as well as for eAGB (Supplementary Table 6.8). Here differences between estimated and measured AGB values were very small (Figures 6.2c and 6.2d). The model residuals did not tend to change towards the more extreme AGB yields (e.g., very high yields in 2000, 2007, and 2014; and very low yields in 2003 and 2015).

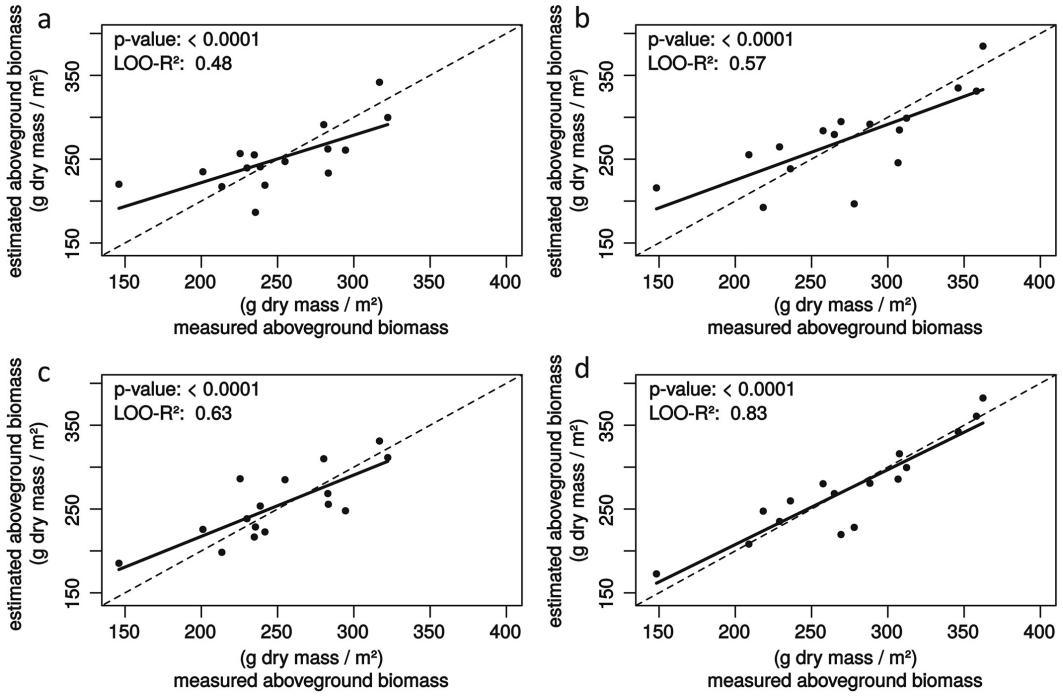

Figure 6.2: Leave-one-out cross-validation of summer aboveground biomass (AGB) estimation in the ambient (a and c) and the elevated rings (b and d) for the precipitation amount and air temperature subset (a and b), and the precipitation amount and variability subset (c and d). Each point represents the treatment-wise AGB per square meter and harvest date. The solid and dashed lines depict the linear regression line and the 1:1 line, respectively.

The ranges of the predictor values within the future subregimes of the precipitation amount and air temperature subset, as well as the precipitation amount and variability subset, can be found in Supplementary Tables 6.9 and 6.10, respectively. Within the precipitation amount and air temperature subset, lower precipitation totals coincided with higher air temperature (Fig. 6.3). Air temperature changes were higher within the dry subregimes (dry) than in the medium precipitation subregimes (medP). Within the precipitation amount and variability subset, a higher variability in rainfall (varP) coincided with a higher number of dry days, a longer mean dry-interval length, and a lower number of rain events (Fig. 6.4). The regimes with comparable constant precipitation inputs (conP) were characterized by a lower number of dry days, a shorter mean dry-interval length, and a higher number of rain events.

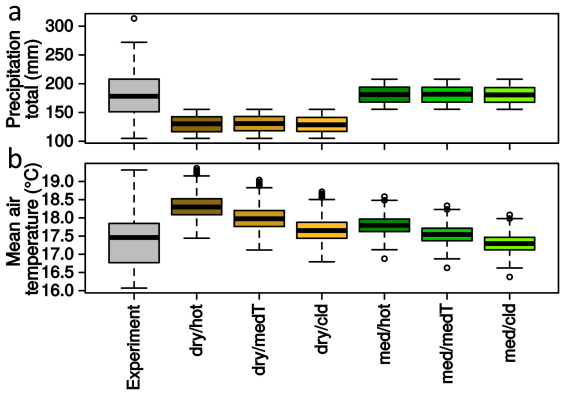

Figure 6.3: Box plots of experimental (gray) and regime-wise (colored) precipitation total (a) and mean air temperature (b) of the precipitation amount and air temperature-related subset. Median, first and third quartiles, and the lowest/highest value within the 1.5 interquartile range of the lower/upper quartile are shown. Please note that variable mean air temperature shows the original air temperature values, while the model input is the transformed mean air temperature variable (with growth optimum assumed at long-term average of 17.4°C).

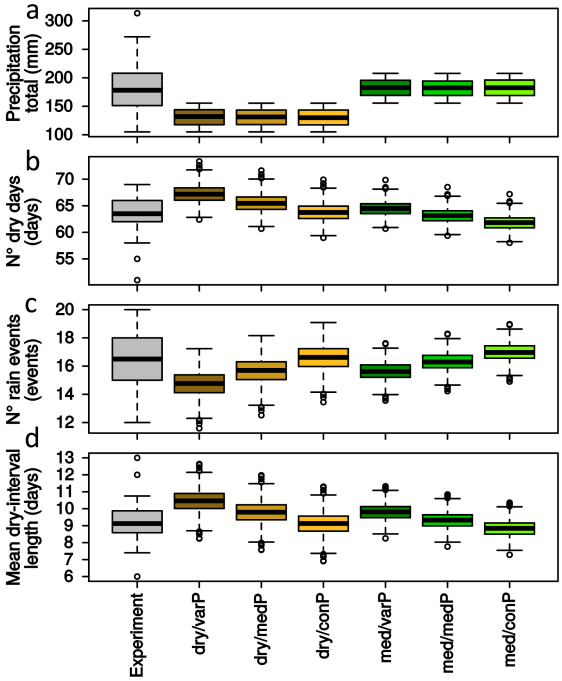

Figure 6.4: Box plots of experimental (gray) and regime-wise (colored) precipitation sum (a), number of dry days (b), number of rain events (c), and mean dry-interval length (d) of the precipitation amount and variability-related subset. For a description, refer to Figure 6.3.

The results of the estimation of biomass under future conditions will be outlined first for the air temperature-related subset, followed by the precipitation variability-related subset. AGB productivity was lowest in the dry main regime with a biomass yield lower than the average during the experimental period, for both rings with elevated [CO_2] and rings under ambient atmospheric [CO_2] (Fig. 6.5a). With an increase in air temperature, eAGB was significantly further decreased within the dry regime, and the dry and hot subregime (dry/hot) showed the overall lowest summer AGB. Accordingly, the highest AGB within the dry regime was estimated in the dry and cold subregime (dry/cld). The medium precipitation regime revealed an eAGB in the range of the elevated [CO_2] rings during the experimental period, while changes in the air temperature caused slightly significant changes only between the hot (med/hot) and medium temperature (med/medT) subregimes. Significantly higher eAGB compared to aAGB was found for all subregimes (<0.001; Fig. 6.5b). This relative AGB change was highest for the medium precipitation and medium air temperature subregime (med/medT) and hardly altered by air temperature in the medium precipitation regime. In the dry regime, increasing air temperature reduced the relative AGB change. Here even negative values were observed, representing lower AGB values under elevated compared to ambient conditions.

Within the precipitation amount and variability subset, the estimated AGB was lowest in the dry regime (Fig. 6.6a), with AGB lower than the mean AGB of the experimental period. For the medium precipitation regime, AGB was in the range of the average AGB during the experimental period. Over the full range of the predictors appearances, summer AGB increased with total summer precipitation and number of rain events, while an increase in the number of dry days and mean dry-interval length significantly reduced summer eAGB. With a more even distribution of rainfall events, eAGB productivity was significantly enhanced, which was more pronounced in the dry (dry/conP) compared to the medium precipitation (med/conP) regime. For all subregimes, the relative AGB change was strongly significant (<0.001; Fig. 6.6b), with the highest AGB change in the medium precipitation regime. Here increases in precipitation variability decreased relative AGB change only slightly. For the dry regime, increases in the variability of precipitation inputs (dry/varP) led to strong reductions in eAGB productivity and relative AGB changes.

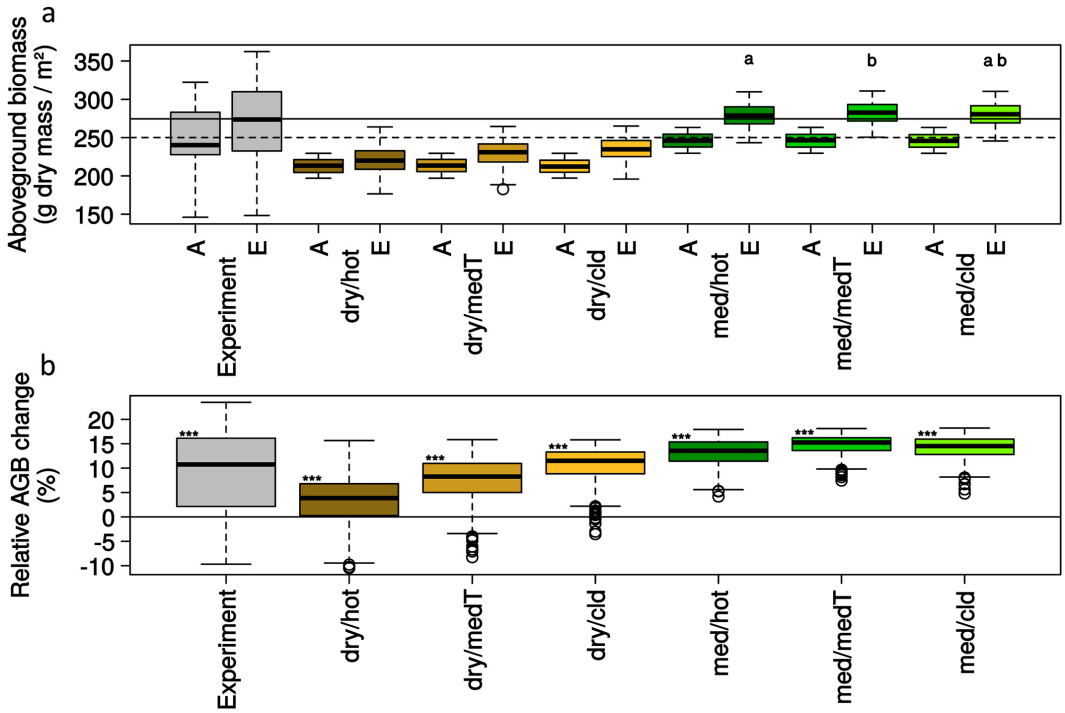

Figure 6.5: Box plots of experimental (gray) and regime-wise (colored) summer aboveground biomass (AGB, a) and relative change in AGB (b) for the precipitation amount and air temperature-related subsets. For AGB (a, upper row), A denotes under normal atmospheric [CO_2], and E stands for elevated [CO_2] conditions; the solid line represents mean AGB in the elevated rings (eAGB), and the dashed line depicts mean AGB under ambient [CO2] (aAGB). Differences among eAGB estimates in the different subregimes were all significant except those pairs indicated by the same lower case letter (a, upper row). "***" (b, lower row) highlights a significantly higher eAGB compared to aAGB.

Projected future summer precipitation totals in Germany ranged broadly, from an increase of 23% to a decrease of 28%, with a mean decrease in the experimental area of 0% to 10% (Table 6.3). Similarly, the number of rainy days in summer (an indicator for the number of rain events used in our study) ranged from an increase of 4 days to a decrease of 5 days in Germany, with a mean decrease of 0 to 3 days for the experimental area (Table 6.3). Projected air temperature changes for Germany in summer were very constant among the models with a mean increase of 1.3°C and a range from 0.2°C to 3°C across the models. The number of dry days and mean dry-interval length were not modeled by the investigated global and regional climate models.

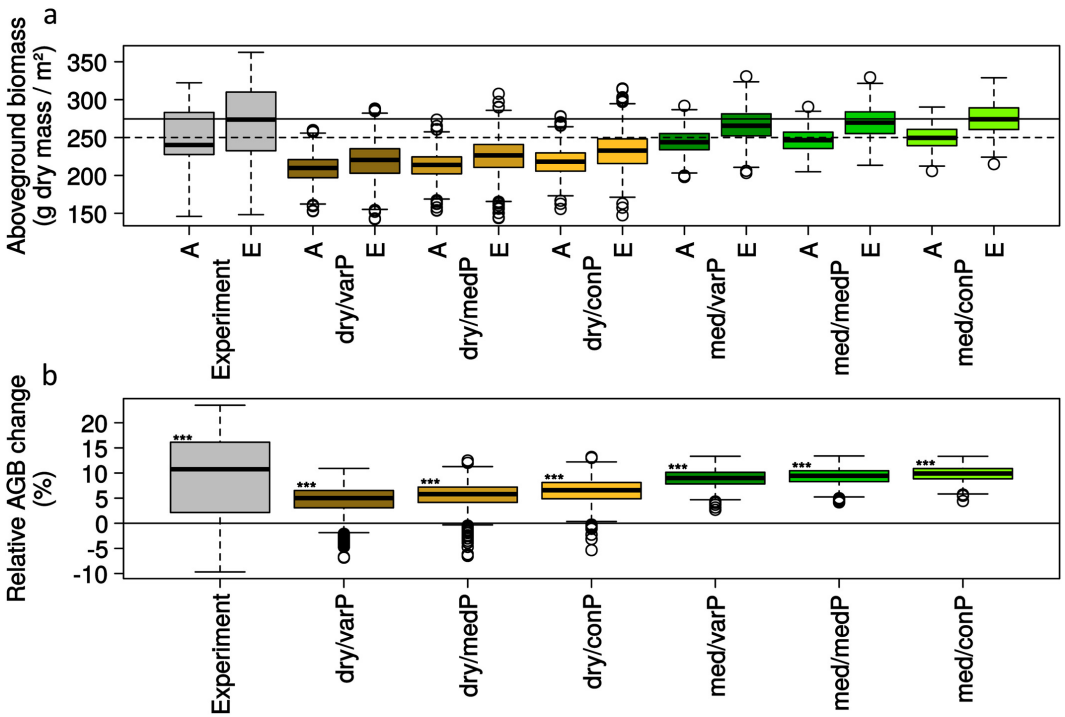

Figure 6.6: Box plots of experimental (gray) and regime-wise (colored) summer aboveground biomass (AGB, a) and relative change in AGB (b) for the precipitation amount and variability-related subset. For a description, refer to Fig. 6.5.

6.4 Discussion

To evaluate potential changes in biomass productivity under future climatic and atmospheric conditions, we estimated summer AGB under ambient and elevated CO_2 by means of climate predictors and 18 years of the GiFACE climate manipulation experiment. Despite a distinct overestimation of the most extreme AGB values, the PLSR models for the precipitation amount and air temperature-related models yielded good results. However, the PLSR models based on the precipitation amount and variability-related variables outperformed the best precipitation amount and air temperature-related model by far. Here the nearly perfect fit of the regression line between the measured and estimated summer AGB and the 1:1 line revealed that eAGB in particular was accurately estimated. Even under the most extreme conditions, in the record dry and hot summers of 2003 (Ciais et al., 2005) and 2015 (Orth et al., 2016), AGB yields were estimated very well. Therefore, we conclude that the combination of the selected predictors realistically reflects

Table 6.3: Projected changes of the climatic variables during summer for the period 2021-2050 compared to 1961-1990.

		Germany						Study area
Climatic variable	Unit of change	Minimum		Mean		Maximum		Mean
PPT_Sum	%	-28	RCP8.5/NorESM1-M/ HIRHAM5	0	RCP2.6/MPI-ESM-LR/ REMO2009	+23	RCP8.5/HadGEM2-ES/ RegCM4-3	0 to -10
AT_Mean	°C	+0.2	A1B/BCM2/ HIRHAM5	+1.3	RCP8.5/MIROC5/ RC4	+3	RCP8.5/HadGEM2-ES/ CCLM4-8-17	+1 to +1.5
N° rainy days	days	-5	RCP2.6/EC-EARTH/ RCA4	-1	RCP4.5/MPI-ESM-LR/ REMO2009	+4	RCP4.5/IPSL-CM5A-MR/ WRF331F	0 to -3 0 to -3

Note. Minimum, mean, and maximum values of 123 climate models are given, averaged over all grid cells in Germany. The mean change for the experimental area is derived from the climate model run with the smallest absolute deviation to the mean of all 123 model runs. The climate model runs are referred to in form of "emission scenario/global model/regional model."

the ecophysiological importance especially of the precipitation variability-related variables. The results prove that aAGB and eAGB can be estimated accurately by means of the selected climate predictors and long-term (18 years) field observations.

We used the selected climate predictors to simulate potential future climate regimes on the basis of the predictor relations during the experimental period and their expected alterations under different climate model runs. Irrespective of the high uncertainty especially regarding precipitation trends in Central Europe in IPCC AR5 model ensemble, those climate models that captured past droughts (1901-2015) best, suggested a future drying in the summer (Orth et al., 2016). Therefore, we conclude that the dry regime seems to depict environmental conditions that will frequently occur in Central Europe in the mid of the 21st century.

Air temperature is widely projected to increase with a high certainty; thus, the hot subregimes are considered to reflect dominant conditions in the near future. Therefore, the dry and hot subregime (dry/hot) is assumed to be the most realistic future scenario within the precipitation amount and air temperature subset.

In concert with rising air temperature, the intervening dry spells between precipitation events may become longer (Easterling et al., 2000; Hov et al., 2013; Seneviratne et al., 2012; Sillmann et al., 2013; Solomon et al., 2007). Therefore, the number of dry days and the mean dry-interval length will most likely increase, which is supported by the projected decrease in the number of rain events for the study area. Thus, we conclude that the subregimes with a high variability of rainfall inputs (dry/varP and med/varP) are most likely representing dominant future conditions. Due to the concomitant reductions in total precipitation, the dry and variable precipitation subregime (dry/varP) is likely to present the most dominant future conditions within the precipitation amount and variability subset.

Using the potential future climate regimes and the PLSR models, we were able to estimate regime-wise AGB under ambient and elevated [CO_2] and thus compare potential future alterations in AGB productivity. Regime-wise AGB alterations will be first discussed for the dry regimes, followed by the hot subregimes (hot) and finally the variable precipitation subregimes (varP).

The strong reduction in AGB productivity in the dry regimes was not surprising, since total summer precipitation is widely recognized as the main driver of biomass productivity (Mowll et al., 2015; Nippert et al., 2006; Weltzin et al., 2003). Lower aAGB and eAGB in the dry regimes compared to average AGB in the experimental period indicated that precipitation-related biomass reduction outperforms the yield-stimulating effects of higher [CO_2]. This is in line with the observed long-term decline in grassland productivity due to increasing dryness despite increasing atmospheric [CO_2] (Brookshire & Weaver, 2015). However, the stronger reduction in eAGB compared to aAGB (low relative AGB change) in the dry regimes was unexpected, since increased water-use efficiency of plants grown under elevated CO_2 leads to the widespread assumption that plants profit from elevated CO_2 particularly under drier conditions (Morgan et al., 2004; Soussana & Lüscher, 2007; Volk et al., 2000). Nevertheless, this is in line with a recent paradigm change, which states that plants may only profit from elevated CO_2 if the carbon demand is high, which depends on processes of tissue formation and cell growth (Fatichi et al., 2014; Körner, 2015). The results are in clear contrast to the expectations of a strongly enhanced AGB productivity in the future (Gu et al., 2014; Hufkens et al., 2016; Li et al., 2014), which is mainly attributed to increasing atmospheric [CO_2] (Chang et al., 2017; Rounsevell et al., 2005).

In the dry regime where air temperature is generally high, the pronounced decrease in AGB productivity with increasing air temperature may result from heat stress and indicates that the optimum temperature of this plant community is already exceeded (Luo, 2007; Mowll et al., 2015). The concept of an optimum growth temperature to which vegetation is adapted is also suggested by the low influence of air temperature on AGB in the medium precipitation regime, where air temperature is near the optimum growth temperature. Remarkably, in the dry regime, the influence of air temperature on eAGB was way beyond its influence on aAGB. This can be explained by the increased water-use efficiency of plants

grown under elevated CO_2, which reduces transpiration cooling, and thus may lead to intensified heat stress. Thus, negative impacts of rising air temperature on biomass productivity have especially to be assumed for plants grown under elevated CO_2. This is supported by the additional negative relative AGB changes estimated in the dry subregimes with increasing air temperature, and the negative CO_2 fertilization effect observed in the experiment during the record hot summer of 2003. Therefore, we conclude that the negative influence of high air temperature on biomass productivity is likely to increase with increasing [CO_2] and that strong reductions in biomass productivity in dry summers will be further aggravated by higher air temperature.

In the dry regime with high variability in precipitation inputs (dry/varP), lower AGB indicates the importance of soil moisture variability. Here increases in the number of dry days and mean dry-interval length, combined with the decreasing number of rain events, reduced AGB production independently of changes in total summer precipitation. This highlights the importance of the direct effects of soil moisture variability on root activity, plant water status, and photosynthesis (Fay et al., 2011), especially when soil water becomes limited. Such a strong influence of timing and variability of precipitation inputs on biomass productivity (Craine et al., 2012; Fay et al., 2011, 2003; Gherardi & Sala, 2015) is supported by the strongly improved model performance when variability-related variables were included. However, since changes in air temperature often translates to altered water balance (De Boeck et al., 2008; Mowll et al., 2015; Niu et al., 2008), it is difficult to disentangle temperature from precipitation variability-related effects on biomass productivity. Increasing air temperature positively affects carbon gain several days after a substantial rain event (more likely in the medium precipitation main regime and constant precipitation variability subregimes), while causing negative effects when soil water is low during dry periods (more likely in the dry main regime and variable precipitation subregimes; Niu et al. 2008. Nevertheless, the lower relative AGB change with higher precipitation variability is in line with the new paradigm that plants profit from elevated CO_2 only if carbon demand is high (Fatichi et al., 2014; Körner, 2015). Therefore, we conclude that further reductions in grassland AGB are likely due to increasing variability in precipitation in the near future.

Our study clearly reveals that grassland biomass productivity is reduced under more extreme climate regimes, despite higher [CO_2]. Such conditions, namely, reduced total precipitation and increased air temperature and precipitation variability, are very likely to occur more frequently in the near future (Easterling et al., 2000; Seneviratne et al., 2012; Solomon et al., 2007). Importantly, under such unfavorable environmental conditions, elevated CO_2 might even reduce AGB productivity, probably due to reduced transpiration, which weakens evaporative cooling. Therefore, the importance of air temperature to AGB productivity might increase in future. The results are in clear contrast to the expected strong positive yield anomalies owing to increases in [CO_2] and its widely expected mitigating effect on negative climate-change impacts. Moreover, our results are in contrast to a single-year study, which simulated near-future climate and concluded that higher [CO_2] might mitigate the effects of extreme drought and heat waves on ecosystem net carbon uptake (Roy et al., 2016). Given the high species diversity in the investigated grassland, the results seem even more noticeable, since it has been shown that a high biodiversity should stabilize ecosystem productivity during more extreme climatic events (Isbell et al., 2015). Therefore, we assume an overestimation of the yield-stimulating effect of higher [CO_2] by model simulations, because biomass reductions due to altered climatic conditions are not sufficiently considered. Thus, the amount of livestock and wildlife forage per area in the temperate grassland of our study area and similar ecosystems are expected to decrease in the future. Assuming constant respiration rates, reduced biomass productivity will also translate into reduced terrestrial carbon uptake, the latter characterized by large uncertainties mainly due to model disagreement for their sensitivity to rising atmospheric [CO_2] (Huntzinger et al., 2017; Luo et al., 2008; Solomon et al., 2007). This will further strengthen global climate change via ecosystem feedback.

Acknowledgments

The contribution of the following individuals to the initiation, construction, installation, and long-term, ongoing maintenance of the Giessen FACE experiment is gratefully acknowledged: H.-J. Jäger (deceased 2013), S. Schmidt, J. Senkbeil, W. Stein, B. Lenz, J. Franz, T. Strohbusch, G. Mayer, and A. Brück. We also want to thank

M. Schulz for his artwork. The continued financial support of the Hessian Agency for Nature Conservation, Environment and Geology (HLNUG) is gratefully acknowledged since it allowed an exceptionally long data set to be obtained. The research has been funded by the LOEWE excellence cluster $FACE_2FACE$ of the Hessian State Ministry of Higher Education, Research and the Arts. The data set generated and analyzed during the current study is deposited in the Laboratory for Climatology and Remote Sensing repository (DOI: https://doi.org/10.5678/lcrs/DAT.309).

References

Ainsworth, E. & Rogers, A. (2007): The response of photosynthesis and stomatal conductance to rising [CO_2]: Mechanisms and environmental interactions. *Plant, Cell and Environment*, 30, 3, 258–270.

Ainsworth, E.A. & Long, S.P. (2005): What have we learned from 15 years of free-air CO_2 enrichment (FACE)? A meta-analytic review of the responses of photosynthesis, canopy properties and plant production to rising CO_2. *New Phytologist*, 165, 2, 351–372.

Akaike, H. (1998): Information theory and an extension of the maximum likelihood principle. In: E. Parzen, K. Tanabe, & G. Kitagawa (Eds.), Selected Papers of Hirotugu Akaike. Springer New York, New York, NY, pp. 199–213.

Andresen, L.C., Müller, C., de Dato, G., Dukes, J.S., Emmett, B.A., Estiarte, M., Jentsch, A., Kröel-Dulay, G., Lüscher, A., Niu, S., Peñuelas, J., Reich, p.B., Reinsch, S., Ogaya, R., Schmidt, I.K., Schneider, M.K., Sternberg, M., Tietema, A., Zhu, K., & Bilton, M. (2016): Shifting impacts of climate change: Long-term patterns of plant response to elevated CO_2, drought, and warming across ecosystems. In: Advances in ecological research, volume 55. Elsevier, pp. 437–473.

Andresen, L.C., Yuan, N., Seibert, R., Moser, G., Kammann, C.I., Luterbacher, J., Erbs, M., & Müller, C. (2018): Biomass responses in a temperate european grassland through 17 years of elevated CO_2. *Global Change Biology*, 24, 9, 3875–3885.

Beier, C., Emmett, B., Gundersen, P., Tietema, A., Peñuelas, J., Estiarte, M., Gordon, C., Gorissen, A., Llorens, L., Roda, F., & Williams, D. (2004): Novel approaches to study climate change effects on terrestrial ecosystems in the field: Drought and passive nighttime warming. *Ecosystems*, 7, 6, 583–597.

Brookshire, E.N.J. & Weaver, T. (2015): Long-term decline in grassland productivity driven by increasing dryness. *Nature Communications*, 6, 7148.

Burnham, K.P., Anderson, D.R., & Huyvaert, K.P. (2011): AIC model selection and multimodel inference in behavioral ecology: some background, observations, and comparisons. *Behavioral Ecology and Sociobiology*, 65, 1, 23–35.

Butler, E.E. & Huybers, P. (2013): Adaptation of us maize to temperature variations. *Nature Climate Change*, 3, 1, 68.

Calcagno, V., de Mazancourt, C. et al. (2010): glmulti: an r package for easy automated model selection with (generalized) linear models. *Journal of statistical software*, 34, 12, 1–29.

Chang, J., Ciais, P., Viovy, N., Soussana, J.F., Klumpp, K., & Sultan, B. (2017): Future productivity and phenology changes in European grasslands for different warming levels: implications for grassland management and carbon balance. *Carbon Balance and Management*, 12, 11.

Christensen, J., Corti, S., Déqué, M., Heimann, D., Zemsch, M., Jones, R., Rowell, D., Hassell, D., Hein, D., Schär, C. et al. (2005): Prediction of Regional scenarios and Uncertainties for Defining European Climate change risks and Effects (PRUDENCE). Technical Report, Danish Meteorological Institute, Copenhagen.

Ciais, P., Reichstein, M., Viovy, N., Granier, A., Ogée, J., Allard, V., Aubinet, M., Buchmann, N., Bernhofer, C., Carrara, A., Chevallier, F., De Noblet, N., Friend, a.D., Friedlingstein, P., Grünwald, T., Heinesch, B., Keronen, P., Knohl, A., Krinner, G., Loustau, D., Manca, G., Matteucci, G., Miglietta, F., Ourcival, J.M., Papale, D., Pilegaard, K., Rambal, S., Seufert, G., Soussana, J.F., Sanz, M.J., Schulze, E.D., Vesala, T., & Valentini, R. (2005): Europe-wide reduction in primary productivity caused by the heat and drought in 2003. *Nature*, 437, 7058, 529–533.

Craine, J.M., Nippert, J.B., Elmore, A.J., Skibbe, A.M., Hutchinson, S.L., & Brunsell, N.A. (2012): Timing of climate variability and grassland

productivity. *Proceedings of the National Academy of Sciences of the United States of America*, 109, 9, 3401–3405.

De Boeck, H.d., Lemmens, C., Zavalloni, C., Gielen, B., Malchair, S., Carnol, M., Merckx, R., Van den Berge, J., Ceulemans, R., & Nijs, I. (2008): Biomass production in experimental grasslands of different species richness during three years of climate warming. *Biogeosciences*, 5, 2, 585–594.

Easterling, D.R., Evans, J., Groisman, P.Y., Karl, T.R., Kunkel, K.E., & Ambenje, P. (2000): Observed variability and trends in extreme climate events: a brief review. *Bulletin of the American Meteorological Society*, 81, 3, 417–426.

Farquhar, G., von Caemmerer, S., & Berry, J. (1980): A biochemical model of photosynthetic CO_2 assimilation in leaves of c3 species. *Planta*, 149, 1, 78–90.

Fatichi, S., Leuzinger, S., & Körner, C. (2014): Moving beyond photosynthesis: From carbon source to sink-driven vegetation modeling. *New Phytologist*, 201, 4, 1086–1095.

Fay, P., Blair, J., Smith, M., Nippert, J., Carlisle, J., & Knapp, A. (2011): Relative effects of precipitation variability and warming on tallgrass prairie ecosystem function. *Biogeosciences*, 8, 10, 3053–3068.

Fay, P.A., Carlisle, J.D., Knapp, A.K., Blair, J.M., & Collins, S.L. (2003): Productivity responses to altered rainfall patterns in a C4-dominated grassland. *Oecologia*, 137, 2, 245–251.

Foley, J.A., Ramankutty, N., Brauman, K.A., Cassidy, E.S., Gerber, J.S., Johnston, M., Mueller, N.D., O'Connell, C., Ray, D.K., West, P.C., Balzer, C., Bennett, E.M., Carpenter, S.R., Hill, J., Monfreda, C., Polasky, S., Rockström, J., Sheehan, J., Siebert, S., Tilman, D., Zaks, D.P.M., & O'Connell, C. (2011): Solutions for a cultivated planet. *Nature*, 478, 7369, 337–42.

Food and Agriculture Organization of the United Nations Statistics Division (1994): Draft world reference base for soil resources. (last access: 2017-07-27).

Food and Agriculture Organization of the United Nations Statistics Division (2015): FAOSTAT. (last access: 2017-07-27).
URL http://faostat3.fao.org/browse/E/EL/E

Gherardi, L.A. & Sala, O.E. (2015): Enhanced precipitation variability decreases grass- and increases shrub-productivity. *Proceedings of the National Academy of Sciences*, 112, 41, 12 735–12 740.

Gu, Y., Wylie, B.K., Boyte, S.P., & Phuyal, K.P. (2014): Projecting future grassland productivity to assess the sustainability of potential biofuel feedstock areas in the greater platte river basin. *GCB Bioenergy*, 6, 1, 35–43.

Heisler-White, J.L., Blair, J.M., Kelly, E.F., Harmoney, K., & Knapp, A.K. (2009): Contingent productivity responses to more extreme rainfall regimes across a grassland biome. *Global Change Biology*, 15, 12, 2894–2904.

Hollweg, H.D., Böhm, U., Fast, I., Hennemuth, B., Keuler, K., Keup-Thiel, E., Lautenschlager, M., Legutke, S., Radtke, K., Rockel, B., Schubert, M., Will, A., Woldt, M., & Wunram, C. (2008): Ensemble Simulations over Europe with the Regional Climate Model CLM forced with IPCC AR4 global scenarios. *M & D Technical Report*, 3, 154.

Hov, Ø., Cubasch, U., Fischer, E., Höppe, P., Iversen, T., Gunnar Kvamstø, N., Kundzewicz, W., Rezacova, D., Rios, D., Duarte Santos, F., Schädler, B., Veisz, O., Zerefos, C., Benestad, R., Murlis, J., Leckebusch, G.C., & Ulbrich, U. (2013): Extreme Weather Events in Europe: preparing for climate change adaptation. Norwegian Meteorological Institute.

Hovenden, M.J., Newton, P.C.D., & Wills, K.E. (2014): Seasonal not annual rainfall determines grassland biomass response to carbon dioxide. *Nature*, 511, 7511, 583–586.

Hufkens, K., Keenan, T.F., Flanagan, L.B., Scott, R.L., Bernacchi, C.J., Joo, E., Brunsell, N.A., Verfaillie, J., & Richardson, A.D. (2016): Productivity of North American grasslands is increased under future climate scenarios despite rising aridity. *Nature Climate Change*, 6, 7, 710.

Huntzinger, D.N., Michalak, A.M., Schwalm, C., Ciais, P., King, A.W., Fang, Y., Schaefer, K., Wei, Y., Cook, R.B., Fisher, J.B., Hayes, D., Huang, M., Ito, A., Jain, A.K., Lei, H., Lu, C., Maignan, F., Mao, J., Parazoo, N., Peng, S., Poulter, B., Ricciuto, D., Shi, X., Tian, H., Wang, W., Zeng, N., & Zhao, F. (2017): Uncertainty in the response of terrestrial carbon sink to environmental drivers undermines carbon-climate feedback predictions. *Scientific Reports*, 7, 1, 4765.

Hurvich, C.M. & Tsai, C.L. (1989): Regression and time series model selection in small samples. *Biometrika*, 76, 2, 297–307.

Isbell, F., Craven, D., Connolly, J., Loreau, M., Schmid, B., Beierkuhnlein, C., Bezemer, T.M., Bonin, C., Bruelheide, H., de Luca, E., Ebeling, A., Griffin, J.N., Guo, Q., Hautier, Y., Hector, A., Jentsch, A., Kreyling, J., Lanta, V., Manning, P., Meyer, S.T., Mori, A.S., Naeem, S., Niklaus, P.a., Polley, H.W., Reich, P.B., Roscher, C., Seabloom, E.W., Smith, M.D., Thakur, M.P., Tilman, D., Tracy, B.F., van der Putten, W.H., van Ruijven, J., Weigelt, A., Weisser, W.W., Wilsey, B., & Eisenhauer, N. (2015): Biodiversity increases the resistance of ecosystem productivity to climate extremes. *Nature*, 526, 574–577.

Jacob, D., Bärring, L., Christensen, O.B., Christensen, J.H., De Castro, M., Deque, M., Giorgi, F., Hagemann, S., Hirschi, M., Jones, R., Kjellström, E., Lenderink, G., Rockel, B., Sánchez, E., Schär, C., Seneviratne, S.I., Somot, S., van Ulden, A., & van den Hurk, B. (2007): An inter-comparison of regional climate models for europe: model performance in present-day climate. *Climatic change*, 81, 1, 31–52.

Jacob, D., Göttel, H., Kotlarski, S., Lorenz, P., & Sieck, K. (2008): Klimaauswirkungen und Anpassung in Deutschland – Phase 1: Erstellung regionaler Klimaszenarien für Deutschland. Technical Report, Umweltbundesamt.

Jacob, D., Petersen, J., Eggert, B., Alias, A., Christensen, O.B., Bouwer, L.M., Braun, A., Colette, A., Déqué, M., Georgievski, G., Georgopoulou, E., Gobiet, A., Menut, L., Nikulin, G., Haensler, A., Hempelmann, N., Jones, C., Keuler, K., Kovats, S., Kröner, N., Kotlarski, S., Kriegsmann, A., Martin, E., van Meijgaard, E., Moseley, C., Pfeifer, S., Preuschmann, S., Radermacher, C., Radtke, K., Rechid, D., Rounsevell, M., Samuelsson, P., Somot, S., Sousanna, J.F., Teichmann, C., Valentini, R., Vautard, R., Weber, B., & Yiou, P. (2014): EURO-CORDEX: new high-resolution climate change projections for European impact research. *Regional Environmental Change*, 14, 2, 563–578.

Jäger, H.J., Schmidt, S.W., Kammann, C., Grünhage, L., Müller, C., & Hanewald, K. (2003): The University of Giessen Free-Air Carbon Dioxide Enrichment Study: Description of the Experimental Site and of a New Enrichment System. *Journal of Applied Botany*, 77, 117–127.

Kammann, C., Grünhage, L., Grüters, U., Janze, S., & Jäger, H.J. (2005): Response of aboveground grassland biomass and soil moisture to moderate long-term CO_2 enrichment. *Basic and Applied Ecology*, 6, 4, 351–365.

Kellner, J., Multsch, S., Houska, T., Kraft, P., Müller, C., & Breuer, L. (2017): A coupled hydrological-plant growth model for simulating the effect of elevated CO_2 on a temperate grassland. *Agricultural and Forest Meteorology*, 246, 42–50.

Knapp, A.K., Beier, C., Briske, D.D., Classen, A.T., Luo, Y., Reichstein, M., Smith, M.D., Smith, S.D., Bell, J.E., Fay, P.A., Heisler, J.L., Leavitt, S.W., Sherry, R., Smith, B., & Weng, E. (2008): Consequences of More Extreme Precipitation Regimes for Terrestrial Ecosystems. *BioScience*, 58, 9, 811.

Knapp, A.K., Fay, P.A., Blair, J.M., Collins, S.L., Smith, M.D., Carlisle, J.D., Harper, C.W., Danner, B.T., Lett, M.S., & McCarron, J.K. (2002): Rainfall variability, carbon cycling, and plant species diversity in a mesic grassland. *Science*, 298, 5601, 2202–2205.

Knapp, A.K., Hoover, D.L., Wilcox, K.R., Avolio, M.L., Koerner, S.E., La Pierre, K.J., Loik, M.E., Luo, Y., Sala, O.E., & Smith, M.D. (2015): Characterizing differences in precipitation regimes of extreme wet and dry years: implications for climate change experiments. *Global Change Biology*, 21, 7, 2624–2633.

Körner, C. (2015): Paradigm shift in plant growth control. *Current Opinion in Plant Biology*, 25, 107–114.

Lee, T.D., Barrott, S.H., & Reich, P.B. (2011): Photosynthetic responses of 13 grassland species across 11 years of free-air CO_2 enrichment is modest, consistent and independent of N supply. *Global Change Biology*, 17, 9, 2893–2904.

Li, Q., Tuo, D., Zhang, L., Wei, X., Wei, Y., Yang, N., Xu, Y., Anten, N.P., & Pan, X. (2014): Impacts of climate change on net primary productivity of grasslands in inner mongolia. *The Rangeland Journal*, 36, 5, 493–503.

Lloyd, J. & Farquhar, G.D. (2008): Effects of rising temperatures and [CO_2] on the physiology of tropical forest trees. *Philosophical transactions of the Royal Society of London. Series B, Biological Sciences*, 363, 1498, 1811–1817.

Lobell, D.B., Bänziger, M., Magorokosho, C., & Vivek, B. (2011): Nonlinear heat effects on African maize as evidenced by historical yield trials. *Nature Climate Change*, 1, 4, 42–45.

Long, S.P. (1991): Modification of the response of photosynthetic productivity to rising temperature by atmospheric CO_2 concentrations: Has its importance been underestimated? *Plant, Cell and Environment*, 14, 729–739.

Luo, Y. (2001): Transient ecosystem responses to free-air CO_2 enrichment (FACE): experimental evidence and methods of analysis. *New Phytologist*, 152, 1, 3–8.

Luo, Y. (2007): Terrestrial Carbon-Cycle Feedback to Climate Warming. *Annual Review of Ecology, Evolution, and Systematics*, 38, 1, 683–712.

Luo, Y., Gerten, D., Le Maire, G., Parton, W.J., Weng, E., Zhou, X., Keough, C., Beier, C., Ciais, P., Cramer, W., Dukes, J.S., Emmett, B., Hanson, P.J., Knapp, A., Linder, S., Nepstad, D., & Rustad, L. (2008): Modeled interactive effects of precipitation, temperature, and [CO_2] on ecosystem carbon and water dynamics in different climatic zones. *Global Change Biology*, 14, 9, 1986–1999.

Morgan, J.a., Pataki, D.E., Körner, C., Clark, H., Del Grosso, S.J., Grünzweig, J.M., Knapp, A.K., Mosier, A.R., Newton, P.C.D., Niklaus, P.A., Nippert, J.B., Nowak, R.S., Parton, W.J., Polley, H.W., & Shaw, M.R. (2004): Water relations in grassland and desert ecosystems exposed to elevated atmospheric CO_2. *Oecologia*, 140, 1, 11–25.

Morison, J.I.L. & Lawlor, D.W. (1999): Interactions between increasing CO_2 concentration and temperature on plant growth. *Plant, Cell and Environment*, 22, 6, 659–682.

Mowll, W., Blumenthal, D.M., Cherwin, K., Smith, A., Symstad, A.J., Vermeire, L.T., Collins, S.L., Smith, M.D., & Knapp, A.K. (2015): Climatic controls of aboveground net primary production in semi-arid grasslands along a latitudinal gradient portend low sensitivity to warming. *Oecologia*, 177, 4, 959–969.

Myneni, R.B., Keeling, C., Tucker, C.J., Asrar, G., & Nemani, R.R. (1997): Increased plant growth in the northern high latitudes from 1981 to 1991. *Nature*, 386, 6626, 698.

Newton, P., Clark, H., Edwards, G., & Ross, D. (2001): Experimental confirmation of ecosystem model predictions comparing transient and equilibrium plant responses to elevated atmospheric co_2. *Ecology Letters*, 4, 4, 344–347.

Nippert, J.B., Knapp, A.K., & Briggs, J.M. (2006): Intra-annual rainfall variability and grassland productivity: can the past predict the future? *Plant Ecology*, 184, 65–74.

Niu, S., Wu, M., Han, Y., Xia, J., Li, L., & Wan, S. (2008): Water-mediated responses of ecosystem carbon fluxes to climatic change in a temperate steppe. *New Phytologist*, 177, 1, 209–219.

Obermeier, W.A., Lehnert, L.W., Kammann, C.I., Müller, C., Grünhage, L., Luterbacher, J., Erbs, M., Moser, G., Seibert, R., Yuan, N., & Bendix, J. (2017): Reduced CO_2 fertilization effect in temperate C3 grasslands under more extreme weather conditions. *Nature Climate Change*, 7, 2, 137—-141.

Orth, R., Zscheischler, J., & Seneviratne, S.I. (2016): Record dry summer in 2015 challenges precipitation projections in Central Europe. *Scientific Reports*, 6, 28 334.

Parton, W., Morgan, J., Smith, D., Del Grosso, S., Prihodko, L., Lecain, D., Kelly, R., & Lutz, S. (2012): Impact of precipitation dynamics on net ecosystem productivity. *Global Change Biology*, 18, 3, 915–927.

Pierre, K.J.L., Yuan, S., Chang, C.C., Avolio, M.L., Hallett, L.M., Schreck, T., & Smith, M.D. (2011): Explaining temporal variation in aboveground productivity in a mesic grassland: the role of climate and flowering. *Journal of Ecology*, 99, 5, 1250–1262.

R Core Team (2018): R: A Language and Environment for Statistical Computing. R Foundation for Statistical Computing, Vienna, Austria. (last access: 27/07/2018).
URL `https://www.R-project.org/`

Reich, P.B., Hobbie, S.E., & Lee, T.D. (2014): Plant growth enhancement by elevated CO_2 eliminated by joint water and nitrogen limitation. *Nature Geoscience*, 7, 2–6.

Roltsch, W.J., Zalom, F.G., Strawn, A.J., Strand, J.F., & Pitcairn, M.J. (1999): Evaluation of several degree-day estimation methods in California climates. *International Journal of Biometeorology*, 42, 4, 169–176.

Rounsevell, M., Ewert, F., Reginster, I., Leemans, R., & Carter, T. (2005): Future scenarios of European agricultural land use: II. Projecting changes in cropland and grassland. *Agriculture, Ecosystems & Environment*, 107, 2-3, 117–135.

Roy, J., Picon-Cochard, C., Augusti, A., Benot, M.L., Thiery, L., Darsonville, O., Landais, D., Piel, C., Defossez, M., Devidal, S., Escape, C., Ravel, O., Fromin, N., Volaire, F., Milcu, A., Bahn, M., & Soussana, J.F. (2016): Elevated CO_2 maintains grassland net carbon uptake under a future heat and drought extreme. *Proceedings of the National Academy of Sciences of the United States of America*, 113, 22, 6224–6229.

Rustad, L., Campbell, J., Marion, G., Norby, R., Mitchell, M., Hartley, A., Cornelissen, J., Gurevitch, J. et al. (2001): A meta-analysis of the response of soil respiration, net nitrogen mineralization, and aboveground plant growth to experimental ecosystem warming. *Oecologia*, 126, 4, 543–562.

Schimel, D., Stephens, B.B., & Fisher, J.B. (2015): Effect of increasing CO_2 on the terrestrial carbon cycle. *Proceedings of the National Academy of Sciences*, 112, 2, 436–441.

Schlenker, W. & Roberts, M.J. (2009): Nonlinear temperature effects indicate severe damages to U.S. crop yields under climate change. *Proceedings of the National Academy of Sciences of the United States of America*, 106, 37, 15 594–15 598.

Schlesinger, W.H. & Andrews, J.A. (2000): Soil respiration and the global carbon cycle. *Biogeochemistry*, 48, 1, 7–20.

Seneviratne, S.I., Nicholls, N., Easterling, D., Goodess, C.M., Kanae, S., Kossin, J., Luo, Y., Marengo, J., McInnes, K., Rahimi, M., Reichstein, M., Sorteberg, A., Vera, C., & Zhang, X. (2012): Changes in climate extremes and their impacts on the natural physical environment. Technical Report, Intergovernmental Panel on Climate Change.

Sillmann, J., Kharin, V., Zwiers, F., Zhang, X., & Bronaugh, D. (2013): Climate extremes indices in the CMIP5 multimodel ensemble: Part 2. Future

climate projections. *Journal of Geophysical Research: Atmospheres*, 118, 6, 2473–2493.

Solomon, S., Qin, D., Manning, M., Chen, Z., Marquis, M., Averyt, K.B., Tignor, M., Miller, H.L. et al. (Eds.) (2007): Climate change 2007: The Physical Science Basis: Contribution of Working Group I to the Fourth Assessment Report of the Intergovernmental Panel on Climate Change, volume 4. Cambridge University Press.

Soussana, J.F. & Lüscher, A. (2007): Temperate grasslands and global atmospheric change: A review. *Grass and Forage Science*, 62, 2, 127–134.

Sugiura, N. (1978): Further analysts of the data by akaike's information criterion and the finite corrections: Further analysts of the data by akaike's. *Communications in Statistics – Theory and Methods*, 7, 1, 13–26.

Swemmer, A.M., Knapp, A.K., & Snyman, H.A. (2007): Intra-seasonal precipitation patterns and above-ground productivity in three perennial grasslands. *Journal of Ecology*, 95, 4, 780–788.

van der Linden, P. & Mitchell, J.F.B. (2009): ENSEMBLES: Climate Change and its Impacts - Summary of research and results from the ENSEMBLES project. Technical Report, Met Office Hadley Centre, Exeter, United Kingdom.

Volk, M., Niklaus, P.A., & Körner, C. (2000): Soil moisture effects determine CO_2 responses of grassland species. *Oecologia*, 125, 3, 380–388.

Weltzin, J.F., Loik, M.E., Schwinning, S., Williams, D.G., Fay, P.A., Haddad, B.M., Harte, J., Huxman, T.E., Knapp, A.K., Lin, G. et al. (2003): Assessing the response of terrestrial ecosystems to potential changes in precipitation. *AIBS Bulletin*, 53, 10, 941–952.

White, A., Cannell, M.G., & Friend, A.D. (2000): CO_2 stabilization, climate change and the terrestrial carbon sink. *Global Change Biology*, 6, 7, 817–833.

Wold, S., Sjöström, M., & Eriksson, L. (2001): PLS-regression: a basic tool of chemometrics. *Chemometrics and Intelligent Laboratory Systems*, 58, 2, 109–130.

Yan, W. & Hunt, L. (1999): An equation for modelling the temperature response of plants using only the cardinal temperatures. *Annals of Botany*, 84, 5, 607–614.

Yang, Y., Fang, J., Ma, W., & Wang, W. (2008): Relationship between variability in aboveground net primary production and precipitation in global grasslands. *Geophysical Research Letters*, 35, 23.

Zhu, Z., Piao, S., Myneni, R.B., Huang, M., Zeng, Z., Canadell, J.G., Ciais, P., Sitch, S., Friedlingstein, P., Arneth, A., Liu, R., Mao, J., Pan, Y., Peng, S., Peñuelas, J., & Poulter, B. (2016): Greening of the Earth and its drivers. *Nature Climate Change*, 6, 8, 791–795.

6.5 Supporting Information

6.5.1 Predictors for AGB

A non-linear response of aboveground biomass (AGB) to the mean air temperature (AT_Mean) can be expected due to physiological reasons. For C3 plants, it has been shown that increases in cool air temperatures promote net photosynthesis, which peaks at an optimal temperature and declines with further increases in air temperature (Luo, 2007; Mowll et al., 2015). Assuming that the growth optimum temperature is equal to the long-time local average air temperature ($Tmean_{all}$ = 17.5°C, in our study), we defined a transformed mean air temperature variable (AT_MeanTrans). Additionally, heat waves have shown to reduce AGB productivity (Craine et al., 2012), and therefore we calculated the mean of daily maximum air temperatures (AT_MaxMean). Moreover, to reflect potentially occurring heat stress, which could reduce yield, e.g., directly through damaging plant tissues or enzymes (Butler & Huybers, 2013; Lobell et al., 2011; Yan & Hunt, 1999), we also included a variable called killing degree days (KDD). To complement the indicators related to the thermal regime, we calculated the cumulative growing degree-days (GDD), which reflects the accumulated heat (or insolation) above a certain base temperature (5°C in our study) and below a defined upper threshold (30°C in our study) where plant growth is assumed to occur (Beier et al., 2004; Butler & Huybers, 2013; Roltsch et al., 1999; Schlenker & Roberts, 2009).

It is widely accepted that the main factor controlling the AGB productivity is the total summer precipitation (PPT_Total; Mowll et al. 2015; Nippert et al. 2006; Weltzin et al. 2003). As an indicator for drought stress, we derived the number of dry days (N° dry days). However, the aggregated total summer precipitation and number of dry days alone do not account for the full dynamics of plant available water because the duration and frequency of dry periods between rain events significantly alter ecosystem functioning (Knapp et al., 2008; Swemmer et al., 2007). Longer dry-intervals lead to below-average soil water content and show substantial negative impacts on aboveground productivity in mesic grasslands (Heisler-White et al., 2009; Knapp et al., 2002). To consider such drought stress induced by higher variability of water inputs, we derived the mean and maximum

dry-interval length (mean and max dry-interval length; Heisler-White et al. 2009; Swemmer et al. 2007), where a dry-interval was defined as a period of at least six consecutive dry days as defined in the Regionaler Klimaatlas Deutschland (Regional Climate Atlas of Germany; Regionale Klimabüros in der Helmholtz-Gemeinschaft, 2017). We complemented the indicators for the precipitation distribution with the number of precipitation events (N° rain events), and we included the mean size of such rain events (Mean event size) since they are claimed to significantly alter grassland productivity regardless of the total amount (Heisler-White et al., 2009; Swemmer et al., 2007). Since very high precipitation sums may lead to a water loss through fast run-off, or cause the water-logging of soils, we have also included the absolute maximum of the daily precipitation sums as a predictor (PPT_Max).

6.5.2 Final predictor selection and final model creation

At first, to enable a proper predictor selection, all predictors that were strongly correlated with the total summer precipitation (absolute Pearson correlation coefficients > 0.8) were excluded from further analysis (compare Supplementary Table 6.4). The remaining predictors were used in a second step as candidates for the selection of two independent multivariate biomass estimation models. The most relevant predictors within each subset were selected by means of Kullback-Leibler information loss, as implemented in the small-sample corrected Akaike information criteria (AICc; Hurvich & Tsai 1989; Sugiura 1978). Therefore, all possible unique multivariate linear models involving the remaining predictor candidates within both subsets were built using the CRAN R package **'glmulti'** (Calcagno et al., 2010). The AICc for each of the models is calculated, and the most favourable model within each subset is defined by the lowest AICc value (AICc_min), where Kullback-Leibler information loss is minimized. However, the model with the lowest AICc value is not necessarily the one that best represents the data, and expert knowledge has proven to be mandatory for the selection of a final model (Burnham et al., 2011). Therefore, all models can be ranked by their AICc and, in the sense of information theory, considered more or less plausible regarding their AICc change respective to AICc_min ($\triangle$AICc). While earlier literature suggested that models with a $\triangle$AICc greater than two might be dismissed, (Burnham et al., 2011)

have shown that models with a △AICc smaller than seven need to be considered as plausible. The properties of the most plausible models, as indicated by their △AICc (< 7) for the precipitation amount and air temperature subset (12 models) and the precipitation amount and variability subset (10 models), are depicted in Supplementary Tables 6.5 and 6.6, respectively. To cope with the inherent model selection uncertainty, we compared the predictors used within the most plausible models with the relative variable importance of the predictors within all possible models for each subset (compare Supplementary Fig. 6.8).

To give additional information on the quality of the models selected by the information-theoretic approach, each set of predictor variables in the best models was tested for their individual predictive performances regarding AGB. Therefore, we calculated partial least squares (PLSR) regression models (Wold et al., 2001) to cope with potentially non-linear relationships between the predictors and AGB. PLSR techniques transfer the information content of the predictor variables to independent latent vectors (LVs), which are generated with respect to a maximum representativeness of the dependent variable. Within both subsets, we chose two final PLSR models to estimate summer AGB, one for eAGB and one for aAGB. The final models and their optimum number of latent vectors (LVs) were selected by the Pearson correlation coefficient between the measured AGBs and estimated values from a leave-one-out cross validation (LOO) cross validation (compare Supplementary Tables 6.7 and 6.8). Since our focus is the estimation of future AGB productivity (eAGB, elevated rings), we attached a higher value to the model performances of eAGB compared to aAGB. The final PLSR models were then used to estimate eAGB and aAGB within different climatic regimes for the precipitation amount and air temperature as well as precipitation amount and variability subset.

6.5.3 Future climate regime creation (example dry regimes)

All climatic regimes were primarily defined by means of the total summer precipitation. Subsequently, each of the sub-regimes is defined by the empirical relationship between the climatic drivers during the 18 year experimental period. In the following, the steps for the sub-regime creation are described with the example of all sub-regimes within the dry regime. Beginning with the medium air temperature

sub-regime, the estimation of the mean air temperature values is required (refer also to Supplementary Fig. 6.7 – section 6.2.5). At first, a linear regression model between the total summer precipitation and the mean air temperature was calculated to maintain any interaction between the climatic drivers of AGB. To account for the possible stronger variations of the climatic conditions in the future, 1000 specific precipitation sample values were uniformly drawn within the boundaries of the respective precipitation amount regime, e.g., a total summer precipitation between 105 and 155 mm for the dry regime. For each of the uniformly sampled precipitation values, the above mentioned regression model was used to estimate the corresponding values of air temperature. However, the lower the correlation between climatic variables, the higher the uncertainty of the associated air temperature estimate. To account for this, the estimates were not directly used. Instead, a normal distribution was fitted to each of the randomly created air temperatures by using the estimate as the mean value of the normal distribution. The standard deviation of the distributions was calculated according to the 0.05 and 0.95 confidence interval of the linear regression model for the respective precipitation sample value. Consequently, if the correlation between climatic drivers gets weaker, as is the case towards extreme values, the wider the normal distribution is. From each of the 1000 air temperature distributions, one single value was randomly sampled and used as the mean air temperature value corresponding to the respective precipitation sample value. For the hot sub-regime, the means of the normal distributions were shifted by one standard deviation towards hotter air temperatures. The associated mean air temperature value for each precipitation sample was then randomly sampled from the shifted normal distribution. For the cold sub-regime, the means of the normal distributions were reduced by one standard deviation accordingly.

6.5.4 Detailed results for variable selection and model performances

For the precipitation amount and air temperature subset, the most plausible models ($\triangle$AICc < 7) showed different combinations of the predictor variables (Supplementary Table 6.5). The best model, according to information theory within this subset (AICc_min), included only the total summer precipitation and revealed

an AICc of 161.05 and an Akaike weight of 0.356. The second-best model included the transformed mean air temperature along with precipitation sum and revealed an AICc of 162.87 and an Akaike weight of 0.144. The PLSR models for the AGB in the rings under atmospheric [CO_2] performed equally for both sets of predictor variables with a LOO-R^2 of 0.48 and a RMSE of 32 gr dr wt / m^2 (Supplementary Table 6.8). For the AGB in the rings with enriched [CO_2], the PLSR model that included the transformed mean air temperature outperformed the best model as selected by the Akaike information criteria (LOO-R^2 of 0.57 vs. 0.52 and RMSE of 37.6 vs. 39.7 gr dr wt / m^2) and had the overall highest LOO-R^2 and smallest RMSE-value with respect to all tested models for the precipitation amount and air temperature subset. Within the precipitation amount and variability subset, the AICc values for ten models were sufficiently low and have consequently been tested ($\triangle$AICc < 7, Supplementary Table 6.6). The model with the lowest AICc included the variables of total summer precipitation, N° dry days, N° rain events and the mean dry-interval length and had an AICc of 151.36 and an Akaike weight of 0.437. The LOO cross validation of the corresponding PLSR model on eAGB resulted in the overall highest LOO-R^2 (0.83) and the smallest RMSE (23.3 gr dr wt / m^2; Supplementary Table 6.8). The coinciding results from the information-theoretic approach and the PLSR technique gave strong indications for the predictor choice for the final PLSR model within the subsets.

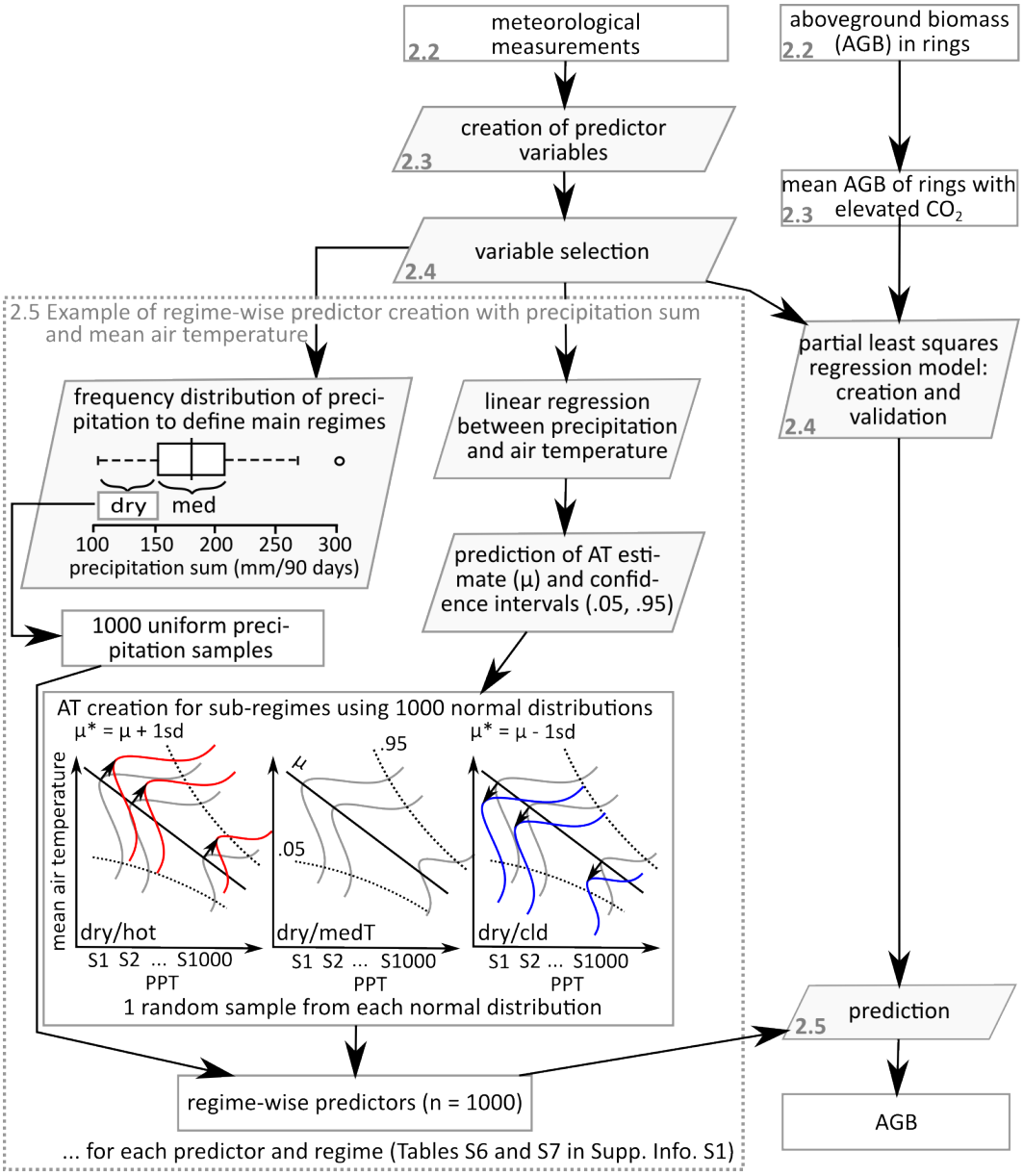

Supplementary Figure 6.7: Overview of the processing steps for the estimation of aboveground biomass in the elevated rings using the example of the dry regime. Rectangles outline data types and parallelograms depict methods. Grey numbers refer to the sections in the text. AGB is the aboveground biomass, AT is the mean air temperature, PPT is the total summer precipitation, med stands for the medium water amount regime, medT stands for the medium air temperature regime, cld stands for the cold regime, μ is the mean of the normal distribution, and sd stands for the standard deviation. S1, S2 and S1000 refer to the index of 1000 precipitation values, uniformly sampled within the dry regime.

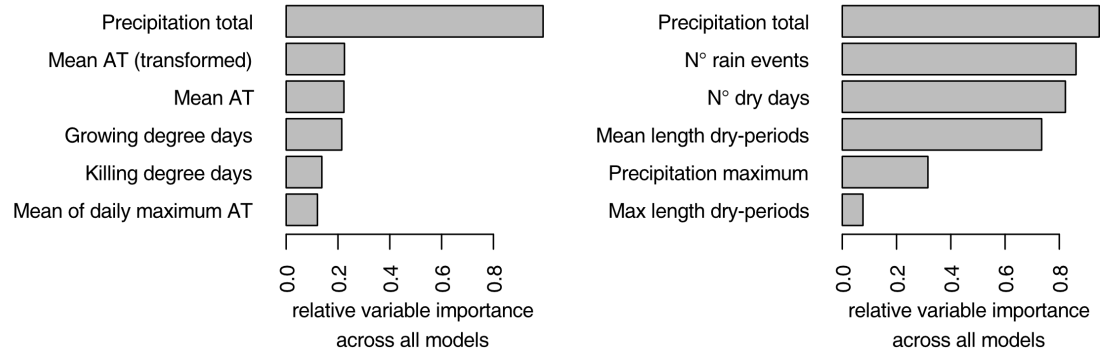

Supplementary Figure 6.8: Relative importance of the variables used within the model selection for (a) the precipitation amount and air temperature subset and (b) the precipitation amount and variability subset. The relative importance equals the sum of the relative Akaike weights of the models where the variables appear. AT is air temperature.

Supplementary Table 6.4: Pearson correlation coefficients and significance levels ($p < 0.001$ - "***"; $p < 0.01$ - "**"; and $p < 0.05$ - "*") of the predictor candidates and summer aboveground biomass in the elevated rings (eAGB) calculated for the 1998-2015 period. Due to the number of variables, the table is split into two sheets. Bold font represents variables included in the final models to estimate future biomass production. Normal fonts represent variables that were excluded either due to high correlation with the precipitation sum or information-theory based model selection (see text for details).

	PPT_Total	GDD	AT_Mean	AT_Max Mean	PPT_Max	**N° dry days**
GDD	−0.51*					
AT_Mean	−0.56*	0.99***				
AT_Max Mean	−0.55*	0.97***	0.98***			
PPT_Max	0.73**	−0.18	−0.25	−0.28		
N° dry days	−0.53*	0.58*	0.63**	0.64**	−0.21	
N° rain events	0.28	−0.45	−0.53*	−0.53*	0.21	−0.74**
Mean event size	0.86***	−0.31	−0.32	−0.31	0.58*	−0.15
Max dry-interval length	−0.19	0.19	0.26	0.23	−0.03	0.50
Mean dry-interval length	−0.29	0.32	0.38	0.33	−0.08	0.68**
KDD	−0.47	0.75***	0.82***	0.80***	−0.23	0.59*
AT_Mean Trans	0.00	−0.17	−0.24	−0.24	−0.02	−0.04
eAGB	0.81***	−0.45	−0.54*	−0.52	0.67**	−0.48

	N° rain events	Mean event size	**Dry-interval length** Max	**Mean**	KDD	**AT_Mean Trans**
Mean event size	−0.22					
Max dry-interval length	−0.54*	0.06				
Mean dry-interval length	−0.70**	0.05	0.76***			
KDD	−0.58*	−0.20	0.43	0.33		
AT_Mean Trans	0.21	−0.04	−0.34	−0.14	−0.59*	
eAGB	0.57*	0.56*	−0.43	−0.55*	−0.50*	0.27

Note. GDD – Growing degree days; AT – Air temperature; PPT – Precipitation; KDD – Killing degree days

Supplementary Table 6.5: Overview of the twelve most plausible models of summer above-ground biomass based on the **precipitation amount and air temperature** subset, as selected by the small-sample corrected Akaike information criteria (AICc). Model number indicates decreasing plausibility, and the Akaike weight represents the relative probability of the model.

Model	AICc	Akaike weight	Precipitation total	Mean AT (trans.)	Growing degree days	Killing degree days	Mean max AT	Mean AT
1	161.05	0.356	X					
2	162.87	0.144	X	X				
3	163.93	0.085	X		X			X
4	164.21	0.073	X			X		
5	164.42	0.066	X					X
6	164.55	0.062	X				X	
7	164.67	0.058	X		X			
8	167.16	0.017	X	X		X		
9	167.21	0.016	X	X				X
10	167.22	0.016	X	X	X			
11	167.23	0.016	X	X			X	
12	167.76	0.012	X		X	X		X

AT – Air temperature

Supplementary Table 6.6: Overview of the ten most plausible models of summer aboveground biomass based on the **precipitation amount and variability** subset, as selected by the small-sample corrected Akaike information criteria (AICc). Model number indicates decreasing plausibility, and the Akaike weight represents the relative probability of the model.

Model	AICc	Akaike weight	Precipitation total	Precipitation maximum	N° dry days	N° rain events	Dry-interval length mean	Dry-interval length maximum
1	151.36	0.437	X		X	X	X	
2	151.51	0.149	X		X	X		
3	153.65	0.139	X	X	X	X	X	
4	155.7	0.05	X	X			X	
5	156.63	0.031		X			X	
6	156.66	0.031	X		X	X		X
7	157.56	0.02	X	X	X	X		
8	157.57	0.02	X			X		
9	157.84	0.017	X	X		X		
10	158.00	0.016	X		X	X	X	X

Supplementary Table 6.7: Characteristics of the leave-one-out cross validation (LOO) for the best partial least squares model within selected predictor combinations in the **precipitation amount and air temperature** subset. For the specified predictors refer to Supplementary Table 6.5 and the respective model number (first column).

	PLSR model ambient rings			PLSR model elevated rings		
Model	N° latent vectors	LOO-R^2	RMSE	N° latent vectors	LOO-R^2	RMSE
1	1	0.48	32	1	0.52	39.7
2	1	0.48	32	2	0.57	37.6
3	3	0.45	33.8	3	0.54	39.1
4	2	0.34	37.2	2	0.45	42.8
5	1	0.48	32	1	0.52	39.7
6	1	0.48	32	1	0.52	39.7
7	2	0.41	34.9	2	0.43	44.1
8	2	0.34	37.2	3	0.52	40.3
9	1	0.48	32	1	0.52	39.7
10	2	0.41	34.9	3	0.52	40.2
11	1	0.48	32	1	0.52	39.7
12	4	0.45	33.7	4	0.49	41.8

RMSE – Root mean Square Error

Supplementary Table 6.8: Characteristics of the leave-one-out cross validation (LOO) for the best partial least squares model within selected for each predictor combinations in the **precipitation amount and variability** subset. For the specified predictors refer to Supplementary Table 6.6 and the respective model number (first column).

	PLSR model ambient rings			PLSR model elevated rings		
Model	N° latent vectors	LOO-R^2	RMSE	N° latent vectors	LOO-R^2	RMSE
1	3	0.63	27.8	3	0.83	23.3
2	3	0.66	26.2	3	0.71	32.1
3	4	0.75	22.9	4	0.81	25.3
4	3	0.69	25.3	3	0.6	36.8
5	2	0.73	22.8	2	0.58	36.7
6	4	0.54	31.7	4	0.8	26.0
7	4	0.69	25.7	4	0.68	34.7
8	2	0.56	29.6	2	0.62	35.9
9	3	0.64	27.7	3	0.58	38.6
10	4	0.56	31	4	0.82	24.3

RMSE – Root mean Square Error

Supplementary Table 6.9: Regimes and sub-regimes defined within the **precipitation amount and air temperature** subset. Values were rounded for clarity.

PPT amount regime	dry			medium			wet		
Temperature sub-regime	hot	medT	cld	hot	medT	cld	hot	medT	cld
PPT_Total (mm)	105-155	105-55	105-155	155-208	155-208	155-208	208-313	208-313	208-313
AT_Mean (°C)	17.4-19.5	17.1-19.2	16.8-18.8	17.0-18.5	16.8-18.3	16.5-18.0	15.6-18.7	15.1-18.2	14.6-17.8

AT – Air temperature; PPT – Precipitation

Supplementary Table 6.10: Regimes and sub-regimes defined within the **precipitation amount and variability** subset. Values were rounded for clarity.

PPT amount regime	dry			medium			wet		
PPT variability sub-regime	varP	medP	conP	varP	medP	conP	varP	medP	conP
PPT_Total (mm)	105-155	105-55	105-155	155-208	155-208	155-208	208-313	208-313	208-313
N° drydays (days)	62-74	60-72	58-70	60-68	59-67	57-66	52-68	49-65	47-63
N° rain events (events)	12-17	13-18	14-19	14-18	14-18	15-19	12-21	13-22	14-23
Mean dry-inter-val length (days)	8-13	8-12	7-11	8-12	8-11	7-11	6-12	5-11	4-11

PPT – Precipitation

7 Hyperspectral Data Analysis in R: The hsdar-Package

This chapter is accepted for publication in *Journal of Statistical Software*.
Submitted: 18 October 2016, accepted: 05 March 2018

Hyperspectral Data Analysis in R: The hsdar-Package

Lukas W. Lehnert[1]*, Hanna Meyer[1], Wolfgang A. Obermeier[1], Brenner Silva[1], Bianca Regeling[1], Boris Thies[1], Jörg Bendix[1]

[1] Faculty of Geography, Philipps-University of Marburg, Deutschhausstraße 10, 35037 Marburg, Germany

Abstract

Hyperspectral remote sensing is a promising tool for a variety of applications including ecology, geology, analytical chemistry and medical research. This article presents the new **hsdar** package for R statistical software, which performs a variety of analysis steps taken during a typical hyperspectral remote sensing approach. The package introduces a new class for efficiently storing large hyperspectral datasets such as hyperspectral cubes within R. The package includes several important hyperspectral analysis tools such as continuum removal, normalized ratio indices and integrates two widely used radiation transfer models. In addition, the package provides methods to directly use the functionality of the **caret** package for machine learning tasks.

Two case studies demonstrate the package's range of functionality: First, plant leaf chlorophyll content is estimated and second, cancer in the human larynx is detected from hyperspectral data.

Keywords hyperspectral remote sensing, hyperspectral imaging, spectroscopy, continuum removal, normalized ratio indices

7.1 Introduction

Hyperspectral data refers to measurements of reflectance, transmission or absorption of electromagnetic radiation with a very high spectral resolution. Consider photographs taken with a normal digital camera to illustrate the concept of spectral resolution. The sensors in digital cameras have three bands that cover the blue, green and red portions of the visible electromagnetic radiation. Each band is sensitive to radiation in a wavelength range of approximately 100 nm. Hyperspectral sensors, in contrast, feature hundreds of such bands that are sensitive to a very narrow wavelength range along the electromagnetic spectrum (often down to 1 nm). Together, all bands continuously cover a certain portion of the electromagnetic spectrum. Additionally, most hyperspectral sensors feature bands within the infrared or ultraviolet ranges. For instance, the hyperspectral satellite sensor Hyperion provides data with 220 bands with a spectral resolution of approximately 11 nm (wavelength range) at each 10 nm (sampling interval) from 400 nm (visible) to 2500 nm (short-wavelength infrared, Pearlman et al., 2001).

Hyperspectral imaging, also referred to as imaging spectroscopy, is used in various disciplines, such as analytical chemistry (Blanco & Villarroya, 2002), agricultural research (precision farming, Haboudane et al., 2002), ecology (Ustin et al., 2004), pedology (Gomez et al., 2008), geology (Bishop et al., 2011), and medical research (Calin et al., 2014; Regeling et al., 2015). The main advantages of hyperspectral imaging are its cost-effectiveness in spatial analysis, the non-destructive measurement of biophysical and biochemical properties of the

investigated surface and the speed of analysis (up to real-time). Hyperspectral analysis is not restricted to space-born approaches. Many of the above-mentioned fields make use of portable spectrometers or hyperspectral cameras, which can be used in the field, in the laboratory or even in a surgical suite. The choice of the measuring device and its spectral specifications depends on the surface under investigation and the aim of the analysis. For instance, vegetation has a very prominent spectral feature called the red-edge. This refers to a sharp increase of reflectance values in the near infrared wavelengths. These wavelengths, in contrast, are less informative in geological analyzes, which usually require the short- and mid-infrared wavelengths.

Currently, most hyperspectral approaches use commercial software tools such as Erdas Imagine, ENVI or the hyperspectral toolbox in MATLAB. These tools are generally expensive and have limited functionalities for statistical analysis. Therefore, we developed a new package in the open source software R (R Core Team, 2013). The **H**yper**s**pectral **D**ata **A**nalysis ("**hsdar**") package combines important hyperspectral analysis tools with the statistical power of R. This article is structured as follows: The first section summarizes the reasons why R is convenient for hyperspectral analysis. The next section outlines the main functionalities and the implementation of the **hsdar** package, and also compares it with other available software tools with a special focus on the other hyperspectral package **"hyperSpec"** in R. Finally, two examples demonstrate the effectiveness of combining hyperspectral techniques with the statistical power of R.

7.2 Why use R for hyperspectral imaging analysis

The methodology which is commonly applied in the analysis of hyperspectral datasets consists of three parts: (1) the preprocessing of spectra, (2) the extraction of the relevant information (i.e., spectral characteristics associated with biophysical properties of the target), and (3) a classification or regression analysis to predict biophysical properties in space and time. R is the most comprehensive software tool for performing statistical analyses during step (3). In this context, especially the machine learning algorithms such as support vector machines, Random forests and artificial neural networks are powerful tools for modelling different parameters

across space and time (for applications see e.g., Bacour et al., 2006; Hansen et al., 2002; Schwieder et al., 2014). However, the functionality required for steps (1) and (2) has only been partly available in R, was distributed across multiple packages and was not directly applicable to hyperspectral data.

Thus, to take advantage of the statistical power of R for hyperspectral data analysis, a new package was developed that provides a framework for handling and analyzing hyperspectral data. A special focus was set on the analysis of large datasets taken under field conditions for e.g., vegetation remote sensing. The R-package **hsdar** implements commonly used processing routines for hyperspectral data and further combines or extends the existing functionality of R to include hyperspectral data into a broad range of statistical analyses.

7.3 Overview of the functionality of hsdar

This section gives a brief technical overview on the general functionality provided by **hsdar**. The description starts with a short introduction of the classes followed by a summary of the main functions.

7.3.1 Classes

To provide a framework to handle large hyperspectral datasets, the **hsdar**-package defines a new S4-class called "Speclib". This allows the user to store hyperspectral measurements and all information associated with those measurements in a single object (Figure 7.1). The hyperspectral measurements consist of reflectance values stored in the spectra slot and their spectral specifications. The spectra are stored either as a numeric matrix or a RasterBrick-object. The matrix is intended for smaller data sets such as point measurements, whereas the RasterBrick object may contain large hyperspectral (satellite) images. If the spectra are stored as a matrix, the rows delineate between different samples while the columns represent the different spectral bands. The spectral specification consists of two numeric vectors stored in the wavelength and the **f**ull-**w**idth-**h**alf-**m**aximum (fwhm) slots. The wavelength gives the central position of each band and the fwhm value describes the difference between the wavelength values where the sensitivity of the sensor is

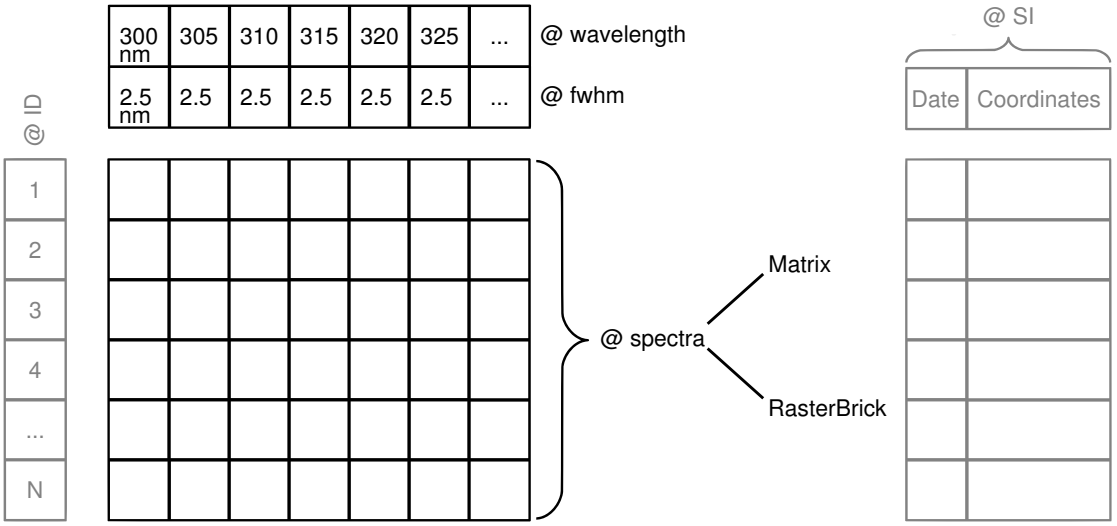

Figure 7.1: Scheme of the S4-class "Speclib" implemented in **hsdar**. Black Slots are Required and Grey Ones are Optional. The Spectra's Slot can Either be a Matrix or a RasterBrick Object. The SI Slot can Encompass Various Types of Objects Including Raster Images. Note that Functions Exist to set and return Data in Each Slot.

half of its maximum in the respective band. Both values are specifications of the sensor used to acquire the data and must be in the same unit. It is preferred to use nm but automatic conversion from other typical units such as μm is supported. If the fwhm values are unknown, the difference between neighboring bands are used as an approximation. The associated data (termed SI as an abbreviation for **s**upplementary **i**nformation), which is included as a list, may contain any type of ancillary information like the measurement setup or the geographical position. Additionally, raster images are supported as part of the SI.

Speclibs can be created through several methods. For each method, the user must at least know the wavelength values of all bands that must be available as a numeric vector. The most important method to create an object of class Speclib is using the file path pointing to a hyperspectral raster image readable by **rgdal** or **raster** (Bivand et al., 2016; Hijmans, 2016; Pebesma et al., 2015). The second option to create a Speclib is to read the reflectance values from a file (e.g., a comma-separated list) and store these in a matrix. This matrix, together with the wavelength information, can then be used to create a Speclib. In the following

short example, the example dataset "spectral_data" (which is already a Speclib) is divided into its basic components, which are then used to create a new Speclib:

```
R> library("hsdar")
R> data("spectral_data")
R> reflectance <- spectra(spectral_data)
R> class(reflectance)

[1] "matrix"

R> wv <- wavelength(spectral_data)
R> class(wv)

[1] "numeric"

R> spec_lib <- speclib(reflectance, wv)
R> class(spec_lib)

[1] "Speclib"
attr(,"package")
[1] "hsdar"
```

In this example, the spectra (**reflectance**) are stored as a matrix and the wavelength (**wv**) is stored as a numeric vector.

Aside from using local offline data, **hsdar** can search online hyperspectral databases and automatically download data. The following example searches for spectra from grass species in the USGS Digital splib04 Spectral Library and downloads the data. Note that missing data in the downloaded spectra are automatically masked out.

```
R> avl <- USGS_get_available_files()
R> grass_spectra <- USGS_retrieve_files(avl = avl,
+    pattern = "grass-fescue")
```

In the example above, the first command returns all available spectra. Users can specify a subset of spectra in a search string within the retrieve function (in this case "grass-fescue"), which is downloaded and converted to a Speclib. Note that the function supports approximate string matching so that entries similar to the search string are found.

7.3.2 Functionality

Along with the new Speclib class, **hsdar** includes several methods to summarize, plot, query and replace data in Speclib objects. Since many hyperspectral datasets are available as raster datasets (e.g., if acquired by satellite), **hsdar** provides a simple interface to the **raster** package that allows users to read and save data from and to all common raster formats via the **rgdal** interface (Bivand et al., 2016; Hijmans, 2016; Pebesma et al., 2015). On commonly used hardware, hyperspectral raster datasets often exceed the capacity of the RAM. To overcome this issue, **hsdar** provides two processing options for such large datasets. The simpler, less computational effective option is to store the spectra as a RasterBrick object in a Speclib. In this case, the spectra are read into memory only upon request and most of the functions process the spectral data block-wise. In this context, the functions automatically detect if the data should be processed block-wise or if all the data should be read before executing the function. For block-wise computation, the resulting spectra are saved as a temporary raster file and the function returns a new Speclib object pointing to the temporary file. The disadvantage of this option is that if more than one function is applied, the spectra have to be saved and re-read multiple times. Thus, a second option is available, which follows the framework of the **raster** package but requires the user to be familiar with simple programming tasks in R. Like the **raster** package, **hsdar** provides **writeStart**, **getValuesBlock**, **writeValues** and **writeStop** methods for the Speclib class so that the user can easily process a large dataset by iteratively reading parts (chunks) of the images, passing it through multiple functions and writing the result to a new raster file. Only one reading and writing process is required in this case, which considerably expedites the analysis. A typical code block would look like the following. To execute it, note that **wavelength** needs to be defined and **infile** must point to an existing file readable by the **raster** package. The result will be a new file in the GeoTIFF-format defined by **outfile** featuring the same number of bands as the existing file (option 'nl'):

```
R> ra <- speclib(infile, wavelength)
R> tr <- blockSize(ra)
R> res <- writeStart(ra, outfile, nl = nbands(ra),
+    format = "GTiff")
```

```
R> for (i in 1:tr$n)
+  {
+    v1 <- getValuesBlock(ra, row=tr$row[i],
+    nrows=tr$nrows[i])
+    v2 <- ANY_FUNCTION(v1)
+    res <- writeValues(res, v2, tr$row[i])
+  }
R> res <- writeStop(res)
```

In the loop, function(s) provided by the **hsdar** package can be applied to the Speclib **v1**. Examples of functions will be discussed in detail in the following sections. The result of the function(s) (termed **v2** in this example) is then written to the initially defined file (**res**). Note that objects **res** and **v1** are of class Speclib, while **v2** may be a vector, matrix or a Speclib depending on the return value of the functions applied in between. Please read the help files and the corresponding vignette available in the **raster** package for further information.

The functionality provided by the **hsdar** package can be divided into preprocessing, analysis and modelling stages (Table 7.1). In the following, we briefly outline the most important features except those that are part of the analysis in the section of case studies.

Noise reduction is a critical preprocessing task in hyperspectral analysis because, as a consequence of their high spectral resolution, the sensors often suffer from low signal to noise ratios, thus, an important step of each hyperspectral analysis is filtering the spectra. In **hsdar** the function **noiseFiltering** applies one of four predefined filters (Savitzky-Golay-, Lowess-, mean-, Spline-filter) or any other filter function from the **signal** package (Ligges et al., 2013). Figure 7.2 shows the effect of filtering (red lines) spectra that were artificially affected by random noise (black lines). Additionally, **hsdar** provides functions to calculate variables derived from spectral features and allows the user to integrate (bin or spectrally resample) hyperspectral datasets to sensors featuring a lower spectral resolution. Spectral resampling can be performed using predefined spectral response functions of common satellite sensors or using Gaussian spectral response functions defined by the fwhm values of the sensor with the lower resolution. Alternatively, spectral

Preprocessing	Analysis	Modeling
• Filtering • Derivations • Spectral resampling • *Continuum removal*	• Red edge parameters • $\sim$ 100 Vegetation indices • Soil indices • *Normalized ratio indices* • Spectral unmixing • *Feature selection algorithms* • *Extraction of absorption features*	• Implementation of the leaf reflectance model PROSPECT and the canopy reflectance model PROSAIL • *Link to machine learning functionality of caret (*Kuhn*, 2008)*

Table 7.1: Summary of the Main Functionalities of the **hsdar**-package. Items in Italic are Presented in Detail in the Case Studies Section.

response values may be stored in a Speclib and passed directly to the resampling function.

To analyze hyperspectral datasets, the computation of approximately 100 vegetation and soil indices is implemented in **hsdar**. The indices can be accessed via the functions **vegindex** and **soilindex** which encompass widely used indices such as the normalized difference vegetation index (NDVI, Tucker, 1979) in addition to specialized indices such as the cellulose absorption index (CAI), which is a proxy for litter amounts and plant coverage (Nagler et al., 2003). Additionally, users can easily define their own index using a simple syntax. In (hyperspectral) remote sensing of vegetation, the sharp increase in the reflectance values between 680 and 750 nm (red edge) is the most important feature, as the shape of the red edge is determined by the amount of water and chlorophyll in the vegetation. Thus, the red edge is seen as a reliable indicator for plant health in addition to leaf area index, plant coverage, chlorophyll, water and nitrogen content (e.g., Filella & Peñuelas, 1994). Different methods for extracting relevant information in the shape of the red edge are included in **hsdar**. These encompass common methods such as deriving the red edge inflection point using a Gaussian fit (Miller et al.,

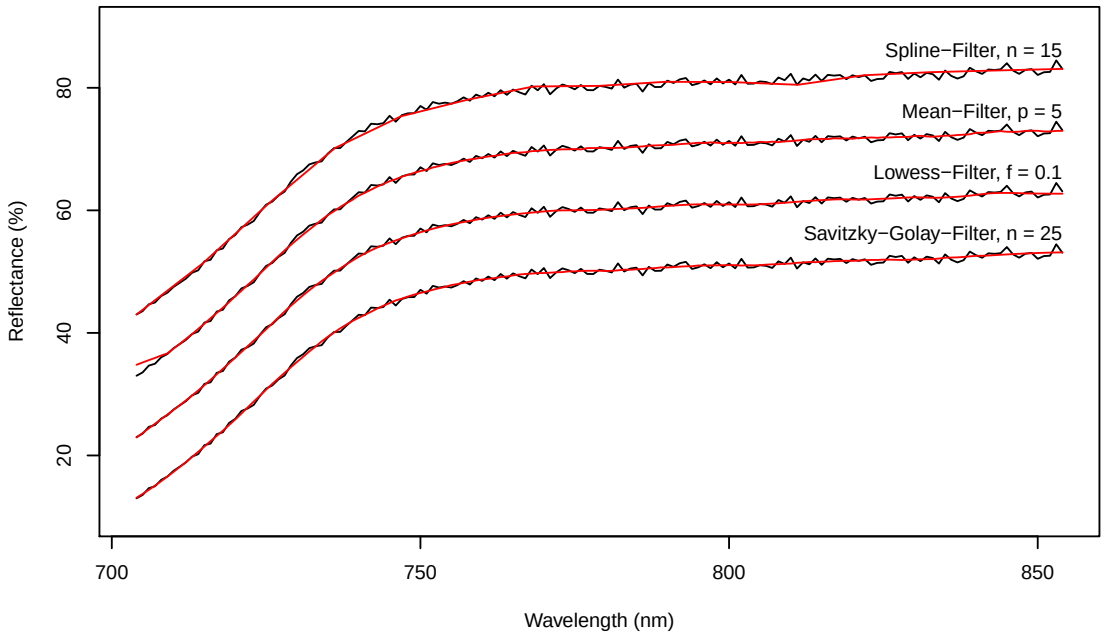

Figure 7.2: Effect of Filtering to Reduce Noise in Spectral Data. Red Lines are the Filtered Reflectance and the Black Lines the Raw Reflectance. All Filters are Applied to the Same Spectrum. Note that for Illustration Purposes, the Values of the Lowess-, Mean-, and Spline-Reflectances have been Increased by 10, 20 and 30 % After Filtering, respectively. Settings for the Filters are as follows: **n** and **p** for the Savitzky-Golay- Spline- and Meanfilters are the Filter Lengths, whereas **f** Gives the Proportion of Bands in the Spectrum that Influence the Smooth at Each Value in the Loewess-filter.

1990) or more recent advances such as the red edge position through linear extrapolation (Cho & Skidmore, 2006). Finally, **hsdar** provides functionality to perform linear spectral unmixing (LSU, Sohn & McCoy, 1997) e.g., for estimating the fractional vegetation cover.

hsdar implements two frequently used radiative transfer models to simulate the reflectance values of vegetation. The first one is the leaf reflectance model PROSPECT (vers. 5B and D, Féret et al., 2017; Jacquemoud & Baret, 1990). The second one is the canopy reflectance model PROSAIL which enhances the functionality of PROSPECT and includes canopy directional reflectance simulation (Jacquemoud et al., 2009). In addition, the inverted PROSPECT model allows the user to estimate the content of various biochemical parameters in the leaves from hyperspectral data (Jacquemoud, 1993).

7.4 Other hyperspectral imaging tools

Comparable functionality can be found in commercial software tools, i.e., MATLAB (The MathWorks, Inc., Natick, Massachusetts) and ENVI (Environment for visualizing images, Exelis Visual Information Solutions, Boulder, Colorado). A hyperspectral toolbox is available in MATLAB that provides feature extraction algorithms such as principal component analysis as well as supervised classification algorithms such as a Maximum Likelihood classifier (Arzuaga-Cruz et al., 2004). ENVI has functions for preprocessing hyperspectral images such as continuum removal and feature extraction algorithms such as the spectral angle mapper.

In the open source software R, **hsdar** completes its hyperspectral functionality together with another major hyperspectral package called **hyperSpec** (Beleites & Sergo, 2016). The primary difference between the packages is that **hsdar** is intended for analyzing datasets collected under field conditions with satellites or spectrometers with a special focus on vegetation and ecosystem remote sensing (Dechant et al., 2017; Grosse-Stoltenberg et al., 2016; Lehnert et al., 2014; Meyer et al., 2017). In contrast, the **hyperSpec** package provides many useful functions for plotting with a special focus on hyperspectral data acquired under laboratory conditions as in chemistry or medical research (Beleites et al., 2011, 2013). Functions in **hsdar** allow it to interface with the **hyperSpec** package, i.e., to convert between Speclib objects and the hyperSpec class. Consequently, **hsdar** users also have access to various import and plotting functions provided by the latter package.

7.5 Case studies

In the following sections two study cases are presented to explore the functionality of **hsdar**. The first case study uses data from a field experiment conducted in central Germany where hyperspectral images were taken from grassland vegetation exposed to enhanced CO_2 air concentrations (Figure 7.3a). The example includes spectra preprocessing, followed by the extraction of absorption features, calibration and validation of a prediction model for chlorophyll content. In the second case study, emphasis is given to the calculation of normalized ratio indices and model

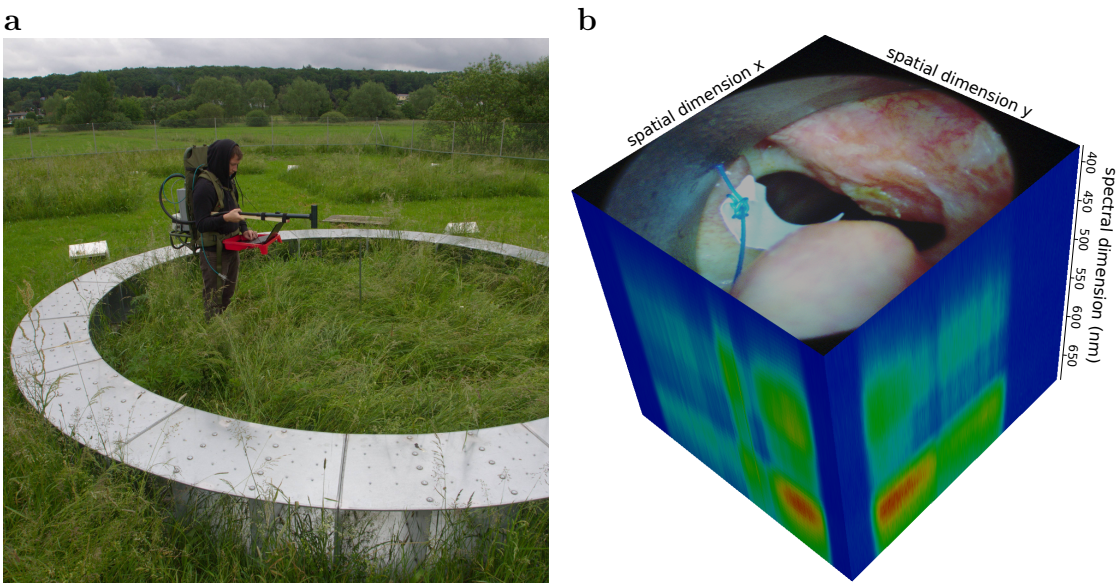

Figure 7.3: Sampling of Hyperspectral Data at the GiFACE Experimental Site with the Spectrometer (a). The Silver Ring is Part of the CO_2-Enrichment System. In (b), an Example Image Illustrates the Hyperspectral Cube of the Human Larynx Produced by the **hsdar** Function "cubePlot". The RGB-image on top of the Cube is Created from the Bands of the Hyperspectral Image Corresponding to the Center of the Red, Green and Blue Wavelengths. The Colors at the Vertical Sides of the Cube Represent the Intensity Values of the 30 Different Spectral Bands of the Sensor (blue = low to red = high).

parameterization to detect cancer cells in human larynx tissue using hyperspectral images (Figure 7.3b).

7.5.1 Remote sensing of vegetation: chlorophyll content

The first example demonstrates the applicability of **hsdar** for hyperspectral data analysis in vegetation studies. Specifically, the package is used to estimate chlorophyll content of plants from hyperspectral data. The dataset was acquired within the scope of a FACE (**f**ree **a**ir **c**arbon dioxide **e**nrichment) experiment conducted on a temperate grassland situated near Giessen, Germany (Kammann et al., 2005; Obermeier et al., 2017). On 15 plots (each 2 x 2 m), the chlorophyll content of the two most abundant grasses (*Arrhenatherum elatius* and *Trisetum flavescens*) was measured using a Konica Minolta SPAD-502Plus chlorophyll meter. The mean value of chlorophyll content of both species was calculated and weighted

by their corresponding plant coverage. Hyperspectral data were acquired at the time of the chlorophyll measurements using a HandySpec® field spectrometer, which simultaneously measures reflectance values from 305 nm to 1705 nm with a spectral resolution of 1 nm (Figure 7.3a). The field spectrometer has two sensors measuring from 305 to 1049 nm and 1050 to 1705 nm. On each plot, 24 spectra were collected under natural (solar) illumination and averaged. Each plot was visited three times, on 30.05.2014, 08.08.2014 and 13.05.2015. Thus, the dataset contains 45 observations.

The following paragraph describes the preprocessing steps that reduce measurement errors and artifacts in the spectral data. Then, the spectra are transformed to reduce the influence of the illumination at time of acquisition. Finally, the chlorophyll content is estimated with Random Forest using the transformed spectra as predictors (Breiman, 2001). Here, we use the **randomForest** package by Liaw & Wiener (2002) in combination with the **caret** package created by Kuhn (2008).

In the first preprocessing step noise is removed from the spectra using a Savitzky-Golay filter (method "sgolay") with a length of 15 nm. The filter reduces the noise of the reflectance values by fitting a polynomial function and eliminates small differences between neighboring bands, which are most likely a result of measurement inaccuracy.

```
R> data("spectral_data")
R> spectral_data <- noiseFiltering(spectral_data,
+    method = "sgolay", p = 15)
```

The result is a Speclib object, which contains a filtered spectral signature in the original sampling resolution. In addition, the empirical function of Coste et al. (2010) is used to transform the chlorophyll SPAD values to μg cm^{-2} ($C_{a,b}$) to facilitate the interpretation of the chlorophyll content values:

$$C_{a,b} = \frac{117.1 \cdot SPAD}{148.84 - SPAD} \tag{7.1}$$

Note that the SPAD chlorophyll value is shipped with the example dataset and stored in the supplementary information (SI) of the object.

```
R> SI(spectral_data)$chlorophyll <-
+    (117.1 * SI(spectral_data)$chlorophyll) /
+    (148.84 - SI(spectral_data)$chlorophyll)
```

Chlorophyll strongly absorbs light at around 460 nm in the blue and around 670 nm in the red parts of the electromagnetic radiation (e.g., Mutanga & Skidmore, 2004a). Therefore, the spectra are trimmed to their visible and near infrared part (310 - 1000 nm). The resulting spectral data after preprocessing are visualized in Figure 7.4a.

```
R> spectral_data <- spectral_data[,
+    wavelength(spectral_data) >= 310 &
+    wavelength(spectral_data) <= 1000]
```

Since the absorption of chlorophyll is not restricted to the central wavelength, but also affects the neighboring bands, the reflectance values are considerably lowered in the blue and red parts which lead to "absorption features" in the spectral signature of the reflectance (shown as gray boxes in Figure 7.4a). The form and magnitude of these absorption features are correlated to the chlorophyll content of the measured vegetation (Mutanga & Skidmore, 2004a,b). To enhance the form of the absorption features, the spectra can be transformed by constructing a continuum hull around each spectrum. In general, there are two methods for defining such a hull. In the first approach, the convex hull uses the global maximum of the reflectance values as an initial fix point. Then, additional fix points are found to create a convex hull (see red line in Figure 7.4a). The second approach is called segmented upper hull. Here, the slope of the line to the left and right of the maximum must be positive and negative, respectively (see blue line in Figure 7.4a). This does not necessarily mean the hull is convex, however. Geologic hyperspectral analyzes often use the convex hull because the distinct absorption features of minerals in the mid-infrared part of the spectrum are easily derived. In vegetation studies, the absorption features of chlorophyll are very close to one another and the reflectance maximum in the green part is considerably lower than in the near infrared. Consequently, only one absorption feature would be detectable. Therefore, a segmented upper hull (option 'sh') is used in this example to ensure that two small features are identified instead of one large feature. To enhance the chlorophyll

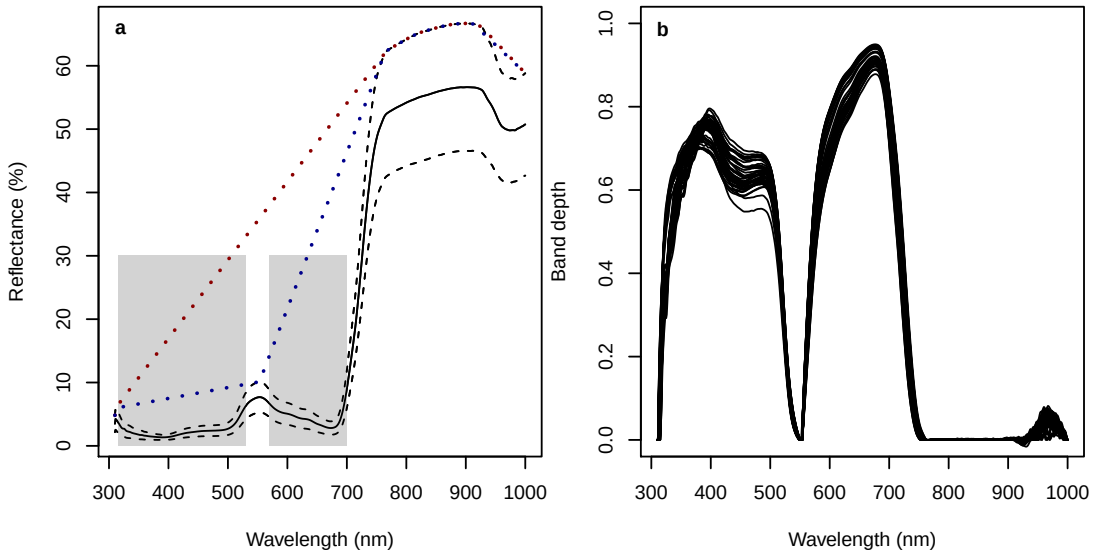

Figure 7.4: Spectral Data of the Vegetation at the 15 Plots. Black Lines Show Mean (Solid) and Mean ± one Standard Deviation (Dashed) of Reflectance Values (a). The Red and Blue Dashed Lines Symbolize the Convex and Segmented Upper Hull of the Upper Standard Deviation Spectrum, respectively. The Gray Boxes Symbolize the Absorption Wavelength of Chlorophyll. In (b) Band Depth Values are Plotted as the Result of the Segmented Upper Hull Transformation Applied to the Reflectance Spectra.

absorption features, the reflectance values are afterward transformed into band depth values (option 'bd'):

$$BD_{d,\lambda} = 1 - \frac{R_\lambda}{CV_\lambda} \tag{7.2}$$

where R is the measured reflectance and CV is the reflectance value of the constructed continuum line at wavelength λ.

```
R> spec_bd <- transformSpeclib(spectral_data,
+    method = "sh", out = "bd")
```

The band depth values in relation to the wavelength of all 45 spectra are plotted in Figure 7.4b. The chlorophyll absorption features correspond to the first two peaks of the band depth values. The absorption features are now defined as the part of the spectrum between two fix points (band depth values of 0). Since the third absorption feature centered around 980 nm is related to plant water content and biomass rather than chlorophyll (Peñuelas et al., 1993), only the absorption features at 460 nm and 670 nm are selected for further analysis.

```
R> featureSpace <- specfeat(spec_bd, c(460, 670))
```

Several parameters can be calculated from absorption features. These include the wavelength values corresponding to the maximum and the half maximum band depth values. Additionally, the area under the curve is extracted as well as the difference between an idealized Gaussian curve and the observed band depth values. See Table 7.2 for a subset of the resulting parameters of the example data set.

```
R> featureSpace <- feature_properties(featureSpace)
```

In the last part of this example, the chlorophyll contents of the measured samples are estimated using the parameters derived from the absorption feature and the band depth values within the features as predictors. Multivariate statistics and machine learning approaches are frequently used for this purpose, because prediction models based on multiple (and often correlated) variables usually out-perform the univariate approaches. To cope with multivariate and machine learning tasks, **hsdar** provides wrapper functions that enable the user to directly use the functionalities of the **caret** package. This is by far the most comprehensive multivariate package since it includes various approaches with the same syntax and functions. To use the functions of **caret**, the response variable has to be defined, which must be stored in the SI attached to the Speclib object ("featureSpace").

```
R> featureSpace <- setResponse(featureSpace, "chlorophyll")
```

The spectra are the default selection for predictors. However, additional predictor variables from the attributes of the spectra can be included. In this example, all parameters extracted above are added.

```
R> featureSpace <- setPredictor(featureSpace,
+    names(SI(featureSpace))[4:ncol(SI(featureSpace))])
```

The final model for deriving chlorophyll content is trained by tuning the required parameter for the Random Forest model (Number of randomly selected predictor variables, mtry). 10-fold cross validation is repeated 5 times for model tuning and estimating accuracy. The internal predictions of the final tuning setup are returned providing an independent data set for validation. The accuracy of the predictions

performed by the model is evaluated with the root mean square error (RMSE) and the R^2-value. For further information about strategies on model settings and cross validation see Kuhn & Johnson (2013) and Kuhn (2008).

```
R> ctrl <- trainControl(method = "repeatedcv", number = 10,
+    repeats = 5, savePredictions = "final")
R> rfe_trained <- train(featureSpace, trControl = ctrl,
+    method = "rf")
```

The number of randomly selected predictor variables at each split of the trees is set to mtry = 453. Using the repeated cross validation, the chlorophyll contents estimated by the Random Forest model fit well if compared to the measured ones (RMSE = 2.49 mg, $R^2 = 0.95$, Figure 7.5). This shows that the proposed method incorporating hyperspectral data is a valid approach for chlorophyll estimation. The resulting model can be used to predict the chlorophyll content of plots where it has not been measured in the field (e.g., Lehnert et al., 2014).

7.5.2 Hyperspectral detection of cancer

The second example shows how hyperspectral imaging can be used in non-invasive detection of cancer of the human larynx (head and neck squamous cell carcinoma; hence referred to as "HNSCC"). This is demonstrated with a data subset acquired at the University of Bonn, Germany that includes hyperspectral images from 25 patients, 10 of which have a histopathological diagnosis of HNSCC. The images were acquired using an endoscope, which was coupled with a monochromatic CCD camera. A special Polychrome V light machine allowed researchers to change the wavelength of the impinging radiation so that several images taken under different illuminations could be combined into hyperspectral cubes (Figure 7.3b). The images were preprocessed and collocated using the methodology proposed by Regeling et al. (2015). The preprocessing is key because the different bands are acquired with short time lapse as a consequence of the varying light source. Medical experts' manual classification into cancerous and non-cancerous tissue was used as reference. The following code loads the data into R and plots them to explore the differences between cancerous and non-cancerous tissue (Figure 7.6).

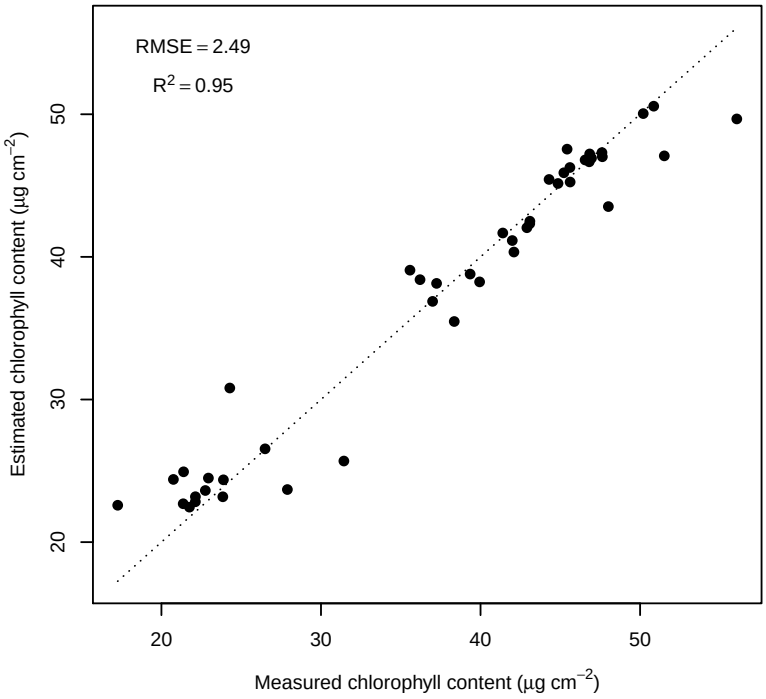

Figure 7.5: Estimated vs. Measured Chlorophyll Content.

```
R> data("cancer_spectra")
R> plot(subset(cancer_spectra, infected == 1),
+    ylim = c(0, 400), col = "darkred")
R> plot(subset(cancer_spectra, infected == 0),
+    new = FALSE)
```

Additionally, the response variable ("infected") is converted to a factor:

```
R> SI(cancer_spectra)$infected <-
+    as.factor(SI(cancer_spectra)$infected)
```

In contrast to the first example, the spectra of the human larynx are expressed in counts and not reflectance values. Thus, the absolute values highly depend on the light source, the temperature of the sensor, and the illumination geometry. To

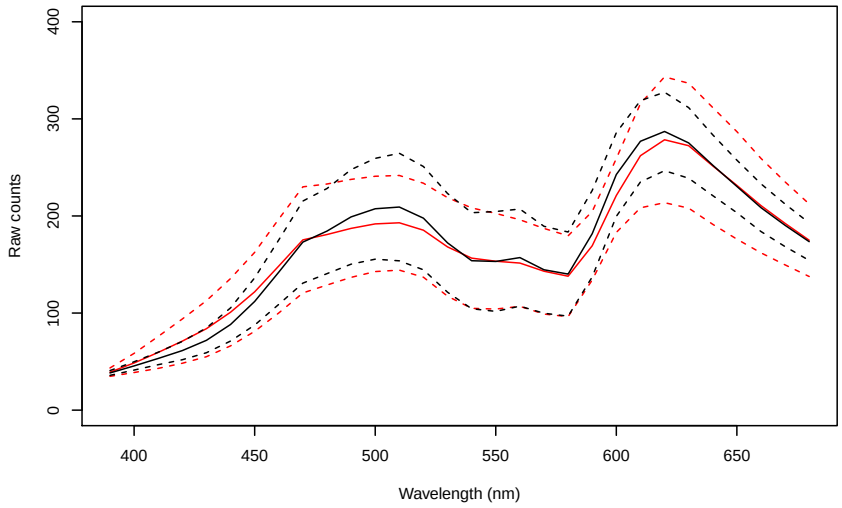

Figure 7.6: Spectral Data of the Cancerous (red) and Non-cancerous (black) Parts of the Larynx Showing the Mean (Solid Line) and Standard Deviation (Dashed Lines) of the Count Values Detected by the Monochromatic CCD Camera.

cope with this limitation, normalized ratio indices are calculated instead of using the absolute count values. Mathematically, these are defined as:

$$NRI_{i,j} = \frac{R_i - R_j}{R_i + R_j} \tag{7.3}$$

Here, R is the reflectance (or in this case the number of counts) at wavelength i or j. These indices are then calculated for all possible combinations of bands through the predefined function "nri".

```
R> nri_data <- nri(cancer_spectra, recursive = TRUE)
```

The *NRI* values can be directly used as predictors in univariate generalized linear models, for example. Note that a multitude of models must be derived depending on the number of bands in the hyperspectral dataset. Initially, it is worthwhile to resample the spectra to a coarser spectral resolution to reduce the number of models. Alternatively, some functions in **hsdar** directly support parallel processing using the **foreach** package. To execute a function on two cores in parallel, simply use the following code depending on the operating system.

For Linux/Mac OS:

```
R> library("doMC")
R> n_cores <- 2
R> registerDoMC(n_cores)
```

For Windows:

```
R> library("doMPI")
R> n_cores <- 2
R> cl <- startMPIcluster(count = n_cores)
R> registerDoMPI(cl)
```

Please note that the dataset in the current example is not large enough to benefit from parallel processing. Therefore, the previous code snippet can be skipped, and we continue by calculating the generalized linear models using the *NRI* values as predictors for infection:

```
R> glm_models <- glm.nri(infected ~ nri_data,
+    preddata = cancer_spectra, family = binomial)
```

It must be noted that the indices are highly correlated, which is a common drawback to using them in a multivariate analysis. In this example, however, each index is used as a predictor in a separate model to eliminate collinearity.

The coefficients, p-values and test statistics of the generalized linear models can now be plotted in 2-d correlograms. In such diagrams, the x-axis and the y-axis represent the two spectral bands used to calculate the index. The color in the diagram symbolizes the coefficient of the model. Thus, the diagrams provide an initial look at band combinations that might be useful for distinguishing between cancerous and non-cancerous parts of the tissue.

```
R> plot(glm_models, coefficient = "z.value",
+    legend = "outer")
R> plot(glm_models, coefficient = "p.value",
+    uppertriang = TRUE, zlog = TRUE)
```

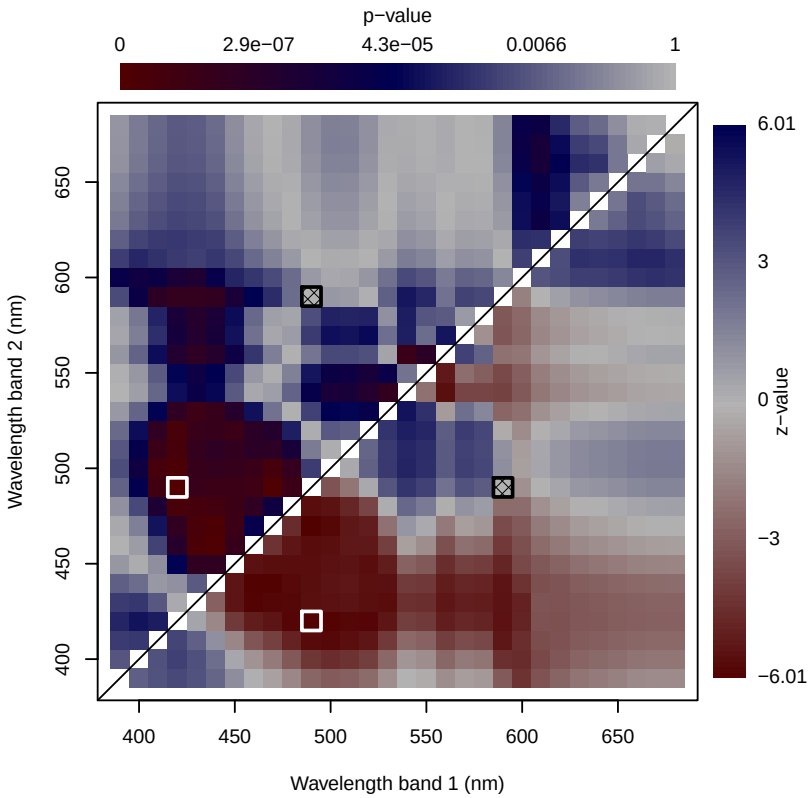

Figure 7.7: Relationship between Cancer and Normalized Ratio Indices. The Lower, Right Portion (Triangle) of the Graph Shows the z-values of the Binomial Regression and the Upper Triangle Represents the Corresponding p-values. The White Squares Mark the Positions of the Index (z- and p-values), That Perform Best, While the Black Squares Show the Index With the Worst Performance. Note that Color of p-values is Logarithmically Scaled.

The plot is shown in Figure 7.7. Almost every index calculated from wavelengths between 400 nm and 450 nm and any other band featured low p-values and, thus, had a significant effect on the distinction between cancerous and non-cancerous tissue (see white rectangle in Figure 7.7). Positive z-values were observed for *NRI* values calculated from longer wavelengths. Negative z-values were obtained for indices calculated from 450 nm to 550 nm for the first band and 400 nm to 480 nm for the second band. The index with the worst performance was calculated from bands 490 nm and 590 nm (see shaded black rectangle in Figure 7.7).

This approach, however, precludes multiple *NRI* values from being used as predictors because they are usually highly correlated, as previously mentioned. Thus, machine learning algorithms classify cancerous cells, as in the first example, because collinearity among predictor variables does not affect their predictive performance. Predictor and response variables have to be defined: As response variable, the column "infected" in the SI was used and the *NRI* values are used as predictors by default. The stage of the cancer is used as an additional predictor variable, because the spectral signal in the early stages of the cancer differs from that in later stages.

```
R> nri_data <- setResponse(nri_data, "infected")
R> nri_data <- setPredictor(nri_data, "stage")
```

Unlike the first example, highly correlated predictor variables are excluded before model training by applying a recursive feature elimination, which reduces the computational time. Afterwards, two techniques are used to classify cancerous and non-cancerous tissues: (1) support vector machine (Chang & Lin, 2011; Meyer et al., 2014) and (2) neural network classification (Ripley, 1996; Venables & Ripley, 2002).

```
R> sel_feat <- rfe(nri_data, cutoff = 0.9)
R> ctrl <- trainControl(method = "repeatedcv", number = 10,
+    repeats = 5, savePredictions = "final")
R> rfe_trained_svm  <- train(sel_feat, trControl = ctrl,
+    importance = TRUE, method = "svmRadial")
R> rfe_trained_nnet <- train(sel_feat, trControl = ctrl,
+    importance = TRUE, method = "nnet")
```

Table 7.3 shows the validation result of the final models for both methods. Support vector machine performed slightly better and yielded an overall accuracy of 93.33% as compared to 90% for the neural network classification. This shows that hyperspectral imaging and machine learning approaches may yield positive results for detecting cancer in human tissue. The data used in this case study have several drawbacks mainly due to the acquisition with a variable light source instead of a hyperspectral camera in combination with a constant light source. This causes the

count values to be dependent on movements of the patient and the illumination geometry by the light source. However, the analysis based on normalized ratio indices yielded robust results clearly highlighting its large potential. Since hyperspectral imaging is a non-invasive measurement technology, the examination is relatively comfortable for the patient. However, it has to be noted that the detection of cancer with hyperspectral imaging may only facilitate the diagnose of a medical expert. At the moment, there is no possibility to automatically diagnose cancer in the human larynx without the knowledge of a trained medical expert (Regeling et al., 2016).

7.6 Conclusions

The two case studies provide an initial impression of what hyperspectral remote sensing can be used for and how a typical approach may look. Both examples show how the **hsdar** package can be used as a powerful tool within R for remote sensing and spatial applications. Based on the widely used raster package, **hsdar** introduces new functionalities for processing hyperspectral data and gives users control over the results of univariate and multivariate modeling approaches, including machine learning techniques. Although **hsdar** is dedicated to spectral data featuring many bands, it is applicable to any multispectral satellite data including Landsat 8 (8 bands in the visible and near infrared part of the electromagnetic radiation) or MODIS (19 bands) (Lehnert et al., 2015). For example, **hsdar** can perform linear spectral unmixing or calculate spectral indices such as the NDVI. **hsdar** differentiates itself from the other hyperspectral package available for R (**hyperSpec**, Beleites & Sergo, 2016) by focusing on environmental instead of laboratory analysis. Data can easily be transferred between both packages since **hsdar** provides functions to convert to and from objects in **hyperSpec**. Both packages extend R by functions for all state of the art methods in hyperspectral imaging which have been available only in commercial software tools so far.

Acknowledgments

Initial development of the **hsdar** package was financially supported by the German Federal Ministry of Education and Research (BMBF) within the Pasture Degradation Monitoring System (PaDeMoS) project (03G0808C). Data for the first case study was taken in the framework of the LOEWE excellence cluster $FACE_2FACE$ funded by the Hessian State Ministry of Higher Education, Research and the Arts. The second case study was based on data from the project "Early Detection of Laryngeal Cancer by Hyperspectral Imaging" (German Cancer Aid, project number 109825 and 110275).

ID	Area		Width		Feature Width		Dist. to Gauss Curve f_{460}		Dist. to Gauss Curve f_{670}	
	f_{460}	f_{670}	f_{460}	f_{670}	f_{460}	f_{670}	left	right	left	right
1	23.85	131.44	518	715	0.11	0.77	191.00	0.13	139.00	0.06
2	22.13	134.01	521	716	0.12	0.76	194.00	0.11	142.00	0.06
3	31.44	136.32	520	718	0.11	0.78	194.00	0.13	144.00	0.07
4	17.26	132.26	519	715	0.11	0.77	192.00	0.12	139.00	0.06
5	21.75	135.03	520	716	0.12	0.78	193.00	0.10	142.00	0.07
6	23.88	132.46	519	717	0.11	0.76	192.00	0.12	142.00	0.06
7	21.39	136.13	519	716	0.11	0.78	193.00	0.13	141.00	0.07
8	20.75	134.76	519	720	0.11	0.79	193.00	0.12	147.00	0.07
9	22.75	138.98	520	717	0.12	0.80	194.00	0.12	143.00	0.07
10	22.94	130.43	520	716	0.11	0.76	192.00	0.11	141.00	0.06
11	27.89	135.50	520	716	0.12	0.77	193.00	0.12	142.00	0.06
12	24.28	129.25	519	718	0.11	0.76	192.00	0.12	144.00	0.06
13	26.50	135.68	520	718	0.11	0.77	195.00	0.14	145.00	0.07
14	22.13	131.74	520	718	0.11	0.77	193.00	0.11	144.00	0.07
15	21.36	134.58	520	717	0.12	0.77	193.00	0.12	143.00	0.06
16	37.25	123.95	514	718	0.11	0.77	192.00	0.13	143.00	0.06
17	36.99	131.96	519	718	0.12	0.75	193.00	0.14	146.00	0.07
18	45.60	127.86	517	719	0.11	0.75	191.00	0.15	146.00	0.06
19	42.09	130.61	518	718	0.11	0.77	194.00	0.15	144.00	0.06
20	51.52	129.11	518	718	0.11	0.75	190.00	0.15	145.00	0.06
21	39.35	126.57	518	718	0.11	0.73	195.00	0.13	144.00	0.06
22	47.63	130.76	517	718	0.11	0.77	192.00	0.16	144.00	0.06
23	39.94	128.55	515	718	0.10	0.77	194.00	0.14	143.00	0.07
24	41.99	128.45	517	718	0.11	0.76	190.00	0.15	144.00	0.06
25	48.01	128.43	518	717	0.11	0.75	190.00	0.14	144.00	0.06
26	38.35	134.08	518	718	0.11	0.77	193.00	0.15	145.00	0.07
27	35.58	130.27	517	719	0.10	0.75	195.00	0.14	146.00	0.06
28	45.22	131.08	517	719	0.11	0.76	192.00	0.15	146.00	0.06
29	47.61	130.07	517	718	0.10	0.76	194.00	0.14	144.00	0.07
30	42.90	130.90	519	719	0.12	0.75	193.00	0.15	148.00	0.07
31	50.20	128.63	520	722	0.12	0.70	202.00	0.18	152.00	0.07
32	45.42	129.62	520	724	0.12	0.71	202.00	0.21	155.00	0.08
33	46.55	132.49	520	721	0.12	0.72	202.00	0.21	150.00	0.07
34	46.95	133.73	521	722	0.12	0.71	204.00	0.20	152.00	0.08
35	56.06	129.62	521	724	0.13	0.70	203.00	0.18	156.00	0.08
36	43.08	130.81	520	722	0.12	0.70	203.00	0.21	152.00	0.07
37	36.21	135.46	521	723	0.13	0.72	204.00	0.19	154.00	0.08
38	45.62	134.72	521	723	0.12	0.72	203.00	0.20	154.00	0.08
39	46.81	134.62	520	722	0.12	0.74	202.00	0.22	153.00	0.08
40	46.84	134.71	520	723	0.13	0.73	202.00	0.20	154.00	0.08
41	41.39	133.68	521	722	0.13	0.72	204.00	0.20	153.00	0.08
42	43.09	134.26	520	723	0.12	0.73	203.00	0.21	154.00	0.08
43	50.85	130.39	520	724	0.13	0.70	203.00	0.21	156.00	0.08
44	44.85	131.95	520	722	0.12	0.72	202.00	0.19	153.00	0.07
45	44.30	135.09	520	722	0.13	0.73	202.00	0.21	153.00	0.07

Table 7.2: Selected Feature Properties Extracted from the Band Depth Values. The Area is the Sum of all Band Depth Values within the Respective Feature. The Feature Width is the Difference Between the Wavelength Values at the Upper and Lower FWHM-Values. Distance to Gauss Curve is the Root Mean Square Error (RMSE) of the Part Smaller than (Left) and Greater than (Right) the Maximum. Note that Each Line Represents one Spectral Measurement and the two Chlorophyll Absorption Features are Abbreviated According to Their Central Wavelengths as f_{460} and f_{670}.

a

	Infected	Not Infected
Infected	68.40	3.40
Not Infected	6.60	71.60

b

	Infected	Not Infected
Infected	65.60	5.60
Not Infected	9.40	69.40

Table 7.3: Error Matrix of the Obtained Classification Results for the Support Vector Machine (a) and the Neural Network (b) Models. The Rows and Columns are the Mean Values of Observations and Estimations within the 5 Repeats of the 10-fold Cross Validation, respectively.

References

Arzuaga-Cruz, E., Jimenez-Rodriguez, L.O., Velez-Reyes, M., Kaeli, D., Rodriguez-Diaz, E., Velazquez-Santana, H.T., Castrodad-Carrau, A., Santos-Campis, L.E., & Santiago, C. (2004): A MATLAB Toolbox for Hyperspectral Image Analysis. In: Geoscience and Remote Sensing Symposium, 2004. IGARSS'04. Proceedings. 2004 IEEE International, volume 7. IEEE, pp. 4839–4842.

Bacour, C., Baret, F., Béal, D., Weiss, M., & Pavageau, K. (2006): Neural Network Estimation of LAI, fAPAR, fCover and LAIxC_{ab}, from Top of Canopy MERIS Reflectance Data: Principles and Validation. *Remote Sensing of Environment*, 105, 4, 313–325.

Beleites, C., Geiger, K., Kirsch, M., Sobottka, S.B., Schackert, G., & Salzer, R. (2011): Raman Spectroscopic Grading of Astrocytoma Tissues: Using Soft Reference Information. *Analytical and Bioanalytical Chemistry*, 400, 9, 2801–2816.

Beleites, C., Salzer, R., & Sergo, V. (2013): Validation of soft classification models using partial class memberships: An extended concept of sensitivity & co. applied to grading of astrocytoma tissues. *Chemometrics and Intelligent Laboratory Systems*, 122, 12–22.

Beleites, C. & Sergo, V. (2016): hyperspec: A Package to Handle Hyperspectral Data Sets in R. R package version 0.98-20161118.
URL `http://hyperspec.r-forge.r-project.org`

Bishop, C., Liu, J., & Mason, P. (2011): Hyperspectral remote sensing for mineral exploration in pulang, yunnan province, china. *International Journal of Remote Sensing*, 32, 9, 2409–2426.

Bivand, R., Keitt, T., & Rowlingson, B. (2016): rgdal: Bindings for the Geospatial Data Abstraction Library. R package version 1.1-10.
URL `https://CRAN.R-project.org/package=rgdal`

Blanco, M. & Villarroya, I. (2002): Nir spectroscopy: A rapid-response analytical tool. *Trac-trends In Analytical Chemistry*, 21, 4, PII S0165–9936(02)00 404–1.

Breiman, L. (2001): Random forests. *Machine Learning*, 45, 1, 5–32.

Calin, M.A., Parasca, S.V., Savastru, D., & Manea, D. (2014): Hyperspectral imaging in the medical field: Present and future. *Applied Spectroscopy Reviews*, 49, 6, 435–447.

Chang, C.C. & Lin, C.J. (2011): LIBSVM. *ACM Transactions on Intelligent Systems and Technology*, 2, 3, 1–27.

Cho, M.A. & Skidmore, A.K. (2006): A new technique for extracting the red edge position from hyperspectral data: The linear extrapolation method. *Remote Sensing of Environment*, 101, 2, 181–193.

Coste, S., Baraloto, C., Leroy, C., Marcon, E., Renaud, A., Richardson, A.D., Roggy, J.C., Schimann, H., Uddling, J., & Herault, B. (2010): Assessing foliar chlorophyll contents with the SPAD-502 chlorophyll meter: A calibration test with thirteen tree species of tropical rainforest in french guiana. *Annals of Forest Science*, 67, 6, 607.

Dechant, B., Cuntz, M., Vohland, M., Schulz, E., & Doktor, D. (2017): Estimation of photosynthesis traits from leaf reflectance spectra: Correlation to nitrogen content as the dominant mechanism. *Remote Sensing of Environment*, 196, 279–292.

Féret, J.B., Gitelson, A., Noble, S., & Jacquemoud, S. (2017): PROSPECT-D: Towards modeling leaf optical properties through a complete lifecycle. *Remote Sensing of Environment*, 193, Supplement C, 204 – 215.

Filella, I. & Peñuelas, J. (1994): The red edge position and shape as indicators of plant chlorophyll content, biomass and hydric status. *International Journal of Remote Sensing*, 15, 7, 1459–1470.

Gomez, C., Rossel, R.A.V., & McBratney, A.B. (2008): Soil organic carbon prediction by hyperspectral remote sensing and field vis-nir spectroscopy: An australian case study. *Geoderma*, 146, 3-4, 403–411.

Grosse-Stoltenberg, A., Hellmann, C., Werner, C., Oldeland, J., & Thiele, J. (2016): Evaluation of continuous VNIR-SWIR spectra versus narrowband hyperspectral indices to discriminate the invasive *Acacia longifolia* within a mediterranean dune ecosystem. *Remote Sensing*, 8, 4, 334.

Haboudane, D., Miller, J.R., Tremblay, N., Zarco-Tejada, P.J., & Dextraze, L. (2002): Integrated narrow-band vegetation indices for prediction of crop chlorophyll content for application to precision agriculture. *Remote Sensing of Environment*, 81, 2-3, 416–426.

Hansen, M., DeFries, R., Townshend, J., Sohlberg, R., Dimiceli, C., & Carroll, M. (2002): Towards an operational modis continuous field of percent tree cover algorithm: Examples using avhrr and modis data. *Remote Sensing of Environment*, 83, 1-2, 303–319.

Hijmans, R.J. (2016): raster: Geographic Data Analysis and Modeling. R package version 2.5-8.
URL `https://CRAN.R-project.org/package=raster`

Jacquemoud, S. (1993): Inversion of the PROSPECT + SAIL canopy reflectance model from AVIRIS equivalent spectra: Theoretical study. *Remote Sensing of Environment*, 44, 2-3, 281–292.

Jacquemoud, S. & Baret, F. (1990): PROSPECT: A model of leaf optical properties spectra. *Remote Sensing of Environment*, 34, 2, 75 – 91.

Jacquemoud, S., Verhoef, W., Baret, F., Bacour, C., Zarco-Tejada, P.J., Asner, G.P., François, C., & Ustin, S.L. (2009): PROSPECT+SAIL models: A review of use for vegetation characterization. *Remote Sensing of Environment*, 113, S56–S66.

Kammann, C., Grünhage, L., Grüters, U., Janze, S., & Jäger, H.J. (2005): Response of aboveground grassland biomass and soil moisture to moderate long-term CO_2 enrichment. *Basic and Applied Ecology*, 6, 4, 351–365.

Kuhn, M. (2008): Building Predictive Models in R Using the caret Package. *Journal Of Statistical Software*, 28, 5, 1–26.

Kuhn, M. & Johnson, K. (2013): Applied Predictive Modeling. Springer, New York.

Lehnert, L.W., Meyer, H., Meyer, N., Reudenbach, C., & Bendix, J. (2014): A hyperspectral indicator system for rangeland degradation on the Tibetan Plateau: A case study towards spaceborne monitoring. *Ecological Indicators*, 39, 0, 54 – 64.

Lehnert, L.W., Meyer, H., Wang, Y., Miehe, G., Thies, B., Reudenbach, C., & Bendix, J. (2015): Retrieval of grassland plant coverage on the Tibetan Plateau based on a multi-scale, multi-sensor and multi-method approach. *Remote Sensing of Environment*, 164, 197–207.

Liaw, A. & Wiener, M. (2002): Classification and regression by randomForest. *R-News*, 2, 3, 18–21.

Ligges, U., Short, T., Kienzle, P., Schnackenberg, S., Billinghurst, D., Borchers, H.W., Carezia, A., Dupuis, P., Eaton, J.W., Farhi, E., Habel, K., Hornik, K., Krey, S., Lash, B., Leisch, F., Mersmann, O., Neis, P., Ruohio, J., Smith, J.O., Stewart, D., & Weingessel, A. (2013): signal: Signal Processing.
URL `http://r-forge.r-project.org/projects/signal/`

Meyer, D., Dimitriadou, E., Hornik, K., Weingessel, A., & Leisch, F. (2014): e1071: Misc Functions of the Department of Statistics (e1071), Tu Wien. R package version 1.6-2.
URL `https://CRAN.R-project.org/package=e1071`

Meyer, H., Lehnert, L.W., Wang, Y., Reudenbach, C., Nauss, T., & Bendix, J. (2017): From local spectral measurements to maps of vegetation cover and biomass on the qinghai-tibet-plateau: Do we need hyperspectral information? *International Journal of Applied Earth Observation and Geoinformation*, 55, 21–31.

Miller, J.R., Hare, E.W., & Wu, J. (1990): Quantitative characterization of the vegetation red edge reflectance 1. an inverted-gaussian reflectance model. *International Journal of Remote Sensing*, 11, 10, 1755–1773.

Mutanga, O. & Skidmore, A. (2004a): Hyperspectral band depth analysis for a better estimation of grass biomass (*Cenchrus ciliaris*) measured under controlled laboratory conditions. *International Journal of applied Earth Observation and Geoinformation*, 5, 2, 87–96.

Mutanga, O. & Skidmore, A. (2004b): Hyperspectral band depth analysis for a better estimation of grass biomass (*Cenchrus ciliaris*) measured under controlled laboratory conditions. *International Journal of applied Earth Observation and Geoinformation*, 5, 2, 87–96.

Nagler, P.L., Inoue, Y., Glenn, E., Russ, A., & Daughtry, C. (2003): Cellulose absorption index (CAI) to quantify mixed soil-plant litter scenes. *Remote Sensing of Environment*, 87, 2-3, 310 – 325.

Obermeier, W.A., Lehnert, L.W., Kammann, C.I., Müller, C., Grünhage, L., Luterbacher, J., Erbs, M., Moser, G., Seibert, R., Yuan, N., & Bendix, J. (2017): Reduced CO_2 fertilization effect in temperate C3 grasslands under more extreme weather conditions. *Nature Climate Change*, 7, 2, 137—-141.

Peñuelas, J., Filella, I., Biel, C., Serrano, L., & Savé, R. (1993): The reflectance at the 950-970 nm region as an indicator of plant water status. *International Journal of Remote Sensing*, 14, 10, 1887–1905.

Pearlman, J., Carman, S., Segal, C., Jarecke, P., Clancy, P., & Browne, W. (2001): Overview of the Hyperion Imaging Spectrometer for the NASA EO-1 Mission. In: IGARSS 2001. Scanning the Present and Resolving the Future. Proceedings. IEEE 2001 International Geoscience and Remote Sensing Symposium (Cat. No.01CH37217), volume 7. pp. 3036–3038 vol.7.

Pebesma, E., Bivand, R., & Ribeiro, P.J. (2015): Software for spatial statistics. *Journal of Statistical Software*, 63, 1.

R Core Team (2013): R: A Language and Environment for Statistical Computing (version 3.0.2). R Foundation for Statistical Computing, Vienna, Austria. (last access: 18/01/2016).
URL `http://www.R-project.org/`

Regeling, B., Laffers, W., Gerstner, A.O.H., Westermann, S., Müller, N.A., Schmidt, K., Bendix, J., & Thies, B. (2015): Development of an image pre-processor for operational hyperspectral laryngeal cancer detection. *Journal of Biophotonics*, 1–11.

Regeling, B., Thies, B., Gerstner, A.O.H., Westermann, S., Müller, N.A., Bendix, J., & Laffers, W. (2016): Hyperspectral imaging using flexible endoscopy for laryngeal cancer detection. *Sensors*, 16, 8, 1288.

Ripley, B. (1996): Pattern Recognition and Neural Networks. Cambridge University Press, Cambridge.

Schwieder, M., Leitão, P.J., Suess, S., Senf, C., & Hostert, P. (2014): Estimating fractional shrub cover using simulated EnMAP data: A comparison of three machine learning regression techniques. *Remote Sensing*, 6, 4, 3427–3445.

Sohn, Y.S. & McCoy, R.M. (1997): Mapping desert shrub rangeland using spectral unmixing and modeling spectral mixtures with TM data. *Photogrammetric Engineering and Remote Sensing*, 63, 6, 707–716.

Tucker, C.J. (1979): Red and photographic infrared linear combinations for monitoring vegetation. *Remote Sensing of Environment*, 8, 2, 127–150.

Ustin, S.L., Roberts, D.A., Gamon, J.A., Asner, G.P., & Green, R.O. (2004): Using imaging spectroscopy to study ecosystem processes and properties. *Bioscience*, 54, 6, 523–534.

Venables, W.N. & Ripley, B.D. (2002): Modern Applied Statistics with S. Springer-Verlag, New York, fourth edition.

8 Grassland ecosystem services in a changing environment: The potential of hyperspectral monitoring

This chapter is under review at *Remote Sensing of Environment*.
Submitted: 28 August 2018

Grassland ecosystem services in a changing environment: The potential of hyperspectral monitoring

Wolfgang A. Obermeier[1]*, Lukas W. Lehnert[1], Marius J. Pohl[1], Sandro Makowski Gianonni[1], Brenner Silva[1], Ruben Seibert[2], Harald Laser[3], Gerald Moser[2], Christoph Müller[2,4], Jürg Luterbacher[5,6], Jörg Bendix[1]

[1] Faculty of Geography, Philipps-University of Marburg, Deutschhausstraße 10, 35037 Marburg, Germany
[2] Institute of Plant Ecology, Justus Liebig University Giessen, Heinrich-Buff-Ring 26, 35392 Giessen, Germany
[3] Faculty of Agriculture, South Westphalia University of Applied Sciences, Lübecker Ring 2, 59494 Soest, Germany
[4] School of Biology and Environmental Science, University College Dublin, Dublin, Ireland
[5] Department of Geography, Climatology, Climate Dynamics and Climate Change, Justus Liebig University Giessen, Senckenbergstraße 1, 35390 Giessen, Germany
[6] Centre for International Development and Environmental Research, Justus Liebig University Giessen, Senckenbergstraße 3, 35390 Giessen, Germany

Abstract

Provisioning services from grassland ecosystems are strongly linked to physical and chemical grassland traits, which are affected by atmospheric CO_2 concentrations ([CO_2]s). The influences of increased [CO_2]s ([eCO_2]s) are typically investigated

in Free Air Carbon dioxide Enrichment (FACE) studies via destructive sampling methods. This traditional approach is restricted to sampling plots and harvest dates, while hyperspectral approaches provide new opportunities as they are rapid, non-destructive and cost-effective. They further allow a high temporal resolution including spatially explicit information. In this study we investigated the hyperspectral predictability of 14 grassland traits linked to forage quality and quantity within a FACE experiment in central Germany with three plots under ambient atmospheric [CO_2]s, and three plots at [eCO_2]s (∼20% above ambient [CO_2]s). We analysed the suitability of various normalisation and feature selection techniques to link comprehensive laboratory analyses with two years of hyperspectral measurements (spectral range 600 - 1600 nm). We applied partial least squares regression and found good to excellent predictive performances ($0.51 \leq$ leave one out cross-validation $R^2 \leq 0.94$), which depended on the normalisation method applied to the hyperspectral data prior to model training. Noteworthy, the models' predictive performances were not affected by the different [CO_2]s, which was anticipated due to the altered plant physiology under [eCO_2]s. Thus, an accurate monitoring of grassland traits under different [CO_2]s (present-day versus future, or within a FACE facility) is promising, if appropriate predictors are selected. Moreover, we show how hyperspectral predictions can be used e.g., within a future phenotyping approach, to monitor the grassland on a spatially explicit level and on a higher temporal resolution compared to conventional destructive sampling techniques. Based on the information during the vegetation period we show how hyperspectral monitoring might be used e.g. to adapt harvest practices or gain deeper insights into physiological plant alterations under [eCO_2]s.

Keywords Grassland, ecosystem services, forage quality, biogas potential, biochemical traits, canopy trait, hyperspectral analysis, elevated CO_2 concentrations

8.1 Introduction

Grasslands provide multiple important ecosystem services such as the supply of forage for livestock and substrate for biogas production, provision of recreational space, and carbon sequestration (Herrero et al., 2013; White et al., 2000). Grassland ecosystem services are strongly linked to physical and chemical plant traits, which are vulnerable to environmental conditions (e.g. CO_2 concentration, air temperature, water availability). Increasing atmospheric CO_2 concentration ([eCO_2]) under climate change conditions affect plant physiology through increasing the photosynthesis rate and the water use efficiency, and thus increases the aboveground biomass productivity in C3 grasslands (Ainsworth & Rogers, 2007; Ainsworth & Long, 2005; Campbell & Stafford Smith, 2000; Lee et al., 2010; McGranahan & Yurkonis, 2018; Morgan et al., 2004; Nowak et al., 2004), which is accompanied by a decreased forage N content (Ainsworth & Long, 2005; Augustine et al., 2018; Campbell & Stafford Smith, 2000; Cotrufo et al., 1998; Dumont et al., 2015; Nowak et al., 2004). From an agroeconomic perspective, forage digestibility may either remain unchanged (Dumont et al., 2015) or decreased (Augustine et al., 2018; Morgan et al., 2004), and forage quality (indicated by crude protein availability) might either be reduced (Soussana & Lüscher, 2007) or increased (McGranahan & Yurkonis, 2018). Such influences of [eCO_2]s on grassland traits, and thus, ecosystem services, are mainly investigated within free air carbon dioxide enrichment (FACE) experiments.

To estimate the ecosystem status and potential outcomes of grassland ecosystems in general and on FACE experiments, in-situ measurements of plant traits are usually performed by destructive vegetation samples, such as labour- and cost-intensive biomass cuttings for subsequent time-consuming laboratory analysis. Consequently, traditional sampling methods constrain the analysis of the grassland

traits under different [CO_2]s to certain harvest dates and sampling plots. To overcome these problems, multi- and hyperspectral approaches have proven to be advantageous due to their rapid and non-destructive sampling, allowing for high temporal resolutions with spatially explicit information at high accuracy and a reasonable price. While multi- or hyperspectral applications to grassland FACE experiments have not yet been considered, various studies have proven the feasibility of the optical delineation of physical and chemical grassland traits such as aboveground biomass (Kawamura et al., 2008; Marabel & Alvarez-Taboada, 2013; Xiaoping et al., 2011; Zhao et al., 2007), nitrogen content (Ramoelo et al., 2013), chlorophyll content (Darvishzadeh et al., 2008), leaf area index (Darvishzadeh et al., 2008), crude protein (Biewer et al., 2009; Kawamura et al., 2008; Pullanagari et al., 2012a,b, 2013; Suzuki et al., 2008; Zhao et al., 2007), crude lipids (Pullanagari et al., 2012b, 2013), crude ash (Biewer et al., 2009; Pullanagari et al., 2012a,b, 2013), neutral and acid detergent fibre (Biewer et al., 2009; Kawamura et al., 2008; Pullanagari et al., 2012a,b, 2013; Zhao et al., 2007), enzyme-soluble organic matter (Pullanagari et al., 2012a,b), and metabolizable energy which is required to derive the potential of energy extraction for ruminants (Pullanagari et al., 2013). Most of these studies applied different methods of spectral transformations, to minimize the effect of external perturbing factors e.g. soil background, illumination, and viewing geometry and/or to enhance the spectral absorption features in hyperspectral data.

To date, hyperspectral monitoring of different grassland traits under varying [CO_2]s and accompanying plant physiological alterations (e.g. within a FACE facility) have not been tested with respect to their feasibility. Therefore, it is not clear whether transfer functions derived under present-day [CO_2] conditions will accurately predict grassland traits under future atmospheric [CO_2] conditions. Difficulties may arise since the spectral delineation of plant traits might be affected by different CO_2 concentrations as a function of the altered physiology of plants under increasing [CO_2]s. For instance, an increased photosynthesis under [eCO_2]s may lead to a higher biomass for plants under [eCO_2] compared to plants grown under ambient [CO_2], despite a similar chlorophyll content (the latter is well detectable by optical sensors; e.g., Daughtry et al. 2000; Gitelson et al. 2003; Haboudane et al. 2002; le Maire et al. 2008; Maccioni et al. 2001).

We combine advanced hyperspectral measurements and data processing techniques within a FACE facility in central Germany, to set up a non-invasive monitoring approach for the most important grassland traits under different CO_2 concentrations. Here, a careful selection of methods and predictors is mandatory to enable the hyperspectral monitoring of grassland traits. The latter shall help to overcome the sampling restriction of invasive procedures to certain plots and dates, which may shed new light on the spatio-temporal dynamics of grassland traits under different CO_2 concentrations and weather conditions.

Consequently, we hypothesize that: (1a) Specific spectral transformations enable different performances for the prediction of each canopy trait, (1b) using the most suitable trait-specific transformations, each of the selected canopy traits can accurately be predicted by hyperspectral data, (2) the hyperspectral predictability of different grassland traits is biased under different [CO_2]s due to physiological alterations, and (3) higher spatial and temporal resolutions of grassland trait values (hyperspectral predictions compared to destructive sampling) enable knowledge gains e.g. to improve management practices and the understanding of biophysical plant alterations under ambient and elevated [CO_2]s.

8.2 Materials and Methods

8.2.1 Study area and sampling

Field samplings were conducted at the Environmental Monitoring and Climate Impact Research Station Linden located near Giessen, Germany (50° 32' N and 8° 41'E; 172 m a.s.l.). Here, a FACE experiment comprising six rings with 8 m in diameter is in operation on a non-grazed and extensively managed species-rich grassland under moderate climate conditions (Andresen et al., 2018; Jäger et al., 2003). The C3 vegetation is dominated by the grasses *Arrhenaterum elatius*, *Holcus lanatus* and *Poa pratensis* accompanied by forbs and legumes present at lower abundances. In three rings, the grassland vegetation has been exposed to elevated CO_2 conditions by enriching the air during daylight hours to ∼20% above the ambient [CO_2]s. The other three rings (controls) are operated under ambient

atmospheric CO_2 conditions. The six rings act as the measurement units for this study. Field data were taken in the years 2014 and 2015.

8.2.2 Biomass sampling and basic analysis

The vegetation was cut manually twice a year at approximately five centimetres above ground within four sub-plots per ring, before the end of spring (spring harvest) and at time of peak biomass accumulation in late summer (late summer harvest). The harvested aboveground biomass for each sub-plot was individually stored at 4°C and sorted by hand into three plant functional types (PFTs): grasses, forbs and legumes. One part of the sub-plot-wise biomasses for the different PFTs was oven-dried at 105°C until a constant weight was reached and weighed to determine the dry matter of each PFT. The samples from each sub-plot were proportionally mixed to one composite sample for each ring for further chemical analysis. Subsequently, the weighed PFT-wise biomass samples were grinded to 0.5 mm and used to analyse the carbon- and nitrogen-content with an elemental analyser (vario MAX, elementar Analysensysteme GmbH, Hanau, Germany). Other parts of the sorted biomass samples were oven-dried at 60°C, grinded with a cutting mill (SM 300, Retsch, Haan, Germany) to 0.5 mm, proportionally mixed, and sent to the laboratory for analysis (8.2.2.1).

8.2.2.1 Laboratory analyses of plant traits

The predried (60°C) PFT-wise biomass samples were subjected to Weende proximate analysis for estimation of fodder quality and biogas formation potential at the laboratory for forage quality, sensory evaluation and food quality at the South Westphalia University of Applied Sciences. Here, biomass samples of grasses and forbs (the latter including legumes) were analysed regarding the most important forage quality traits by near infrared (NIR) spectroscopy (Weende analyis, Verband Deutscher Landwirtschaftlicher Untersuchungs- und Forschungsanstalten 2012): dry matter (DM), crude protein, crude fibre, crude lipids, crude sugar, organic neutral detergent fibre (NDF_{om}), organic acid detergent fibre (ADF_{om}), enzyme-resistant organic matter, enzyme-soluble organic matter (ESOM). Crude ash was then defined by weighing after burning at 550°C, and fermentable

organic dry matter was derived by subtracting the crude ash content from the total dry matter. To increase comparability and to eliminate the dilution effect of moisture, all traits defined by NIR spectroscopy in the laboratory are reported in percentages of dry matter (%DM).

Subsequently, potential biological utilization was analysed with a focus on energy extraction for ruminants (metabolizable energy, net energy for lactation) and on substrate for biogas (fermentable organic matter, biogas and methane). The energy extraction for ruminants was approximated by calculating the metabolizable energy (ME) on basis of indicators for fibre ingredients and metabolization in the forestomach (Deutsche Landwirtschafts-Gesellschaft, 2013). On basis of the metabolizable energy, the net energy for lactation (NEl) was derived by considering metabolizable gross-energy (GE) and efficiency for milk production (Flachowsky et al., 2001).

The potential of substrate for biogas was analysed according to Weissbach (2008) as the fermentable organic dry matter, by subtracting the organic matter which is not biological usable under anaerobic conditions from the total organic dry matter. The yields of biogas and methane were then derived by means of stoichiometric calculations, multiplying the fermentable organic dry matter content with factors 0.8 and 0.42, respectively (Weissbach, 2008).

8.2.2.2 Upscaling to canopy average traits

For each ring, the dry matters of the different PFTs (legumes, forbs, grasses) were used as weights to upscale the PFT-wise traits measured in the laboratory for the canopy (hereinafter referred to as canopy trait). For canopy traits with a perfect correlation (Tab. 8.5), we included only one of the traits to reduce computational effort. For the energy extraction for ruminants we focused on net energy for lactation (and excluded the metabolizable energy), and for biogas potential we used methane productivity (and excluded biogas and fermentable organic matter). Moreover, due to inherent perfect correlation between enzyme-soluble organic matter and enzyme-resistant organic matter, the latter was dismissed from further analyses.

8.2.3 Hyperspectral data

Hyperspectral measurements were taken during clear-sky conditions with ImSpector V16M - eNIR (Specim Imaging Ltd., Oulu, Finland) hyperspectral scanner camera shortly before the biomass cutting in 2014 and 2015, and during the summer period of 2015. The hyperspectral scanner covers the electromagnetic radiation region from 600 to 1600 nm with a 7 nm spectral resolution (256 bands) and a 320 pixel spatial resolution. All measurements were conducted within an hour before and after local noon. For each ring, scans from two positions were performed to acquire images covering the entire plot with the sensor mounted at around 3 m height on a traverse system (Fig. 8.1). Before and after the two scans per ring, we measured the dark current (DC) and a grey spectralon (Zenith Polymer ® Diffuse Reflectance Target - 50% R, SphereOptics, Herrsching, Germany) over the full 320 pixel spatial range. Additionally, at each image scan, the grey spectralon was placed within the scanner's field of view on the ground to correct for the occurring sky conditions.

8.2.3.1 Spectral calibration

Combining the DC and spectralon measurements, we converted raw counts to reflectance values by a two-step spectral calibration procedure to eliminate distortions due to slightly differing spectral sensitivities of the sensor pixels in the scanner line. In a first calibration step, the sensor array (containing 320 pixels) was corrected using the dark current and spectralon measurements taken before and after the actual scan:

$$R1_{\lambda,c} = \frac{counts_{\lambda,c} - d_{\lambda,c}}{g1_{\lambda,c} - d_{\lambda,c}} \cdot g_{\lambda,\text{standard}} \tag{8.1}$$

Here, $R1_{\lambda,c}$ is the reflectance in band λ and column c (referring to the scan line of one pixel in the sensor array) after the first calibration step. $counts_{\lambda,c}$ are raw count values of the sensor, and $d_{\lambda,c}$ and $g1_{\lambda,c}$ are dark current and grey standard values (averages for each column and band from the measurements before and after the image scans), respectively. $g_{\lambda,\text{standard}}$ is the grey spectralon reflectance factor for band λ.

In a second calibration step, the homogenised image scenes were further spectrally calibrated to the present sky conditions using the ground-placed grey spectralon:

Figure 8.1: Hyperspectral measurement setup with the scanner mounted on a traverse system (∼3 m height) above a CO_2 enrichment ring with releasing (lower) and absorbing (higher) vent pipes. The yellow dashed lines depict the approximate field of view for one image scan.

$$R2_\lambda = R1_\lambda \cdot \frac{g_{\lambda,\text{standard}}}{g2_\lambda} \tag{8.2}$$

Here, $R2_\lambda$ is the reflectance in band λ after the second calibration step; $R1_\lambda$ is the reflectance and $g2_\lambda$ are the grey standard values (averages for each band from the spectralon placed within the image scene) in band λ after the first calibration step, respectively.

8.2.3.2 Geometric correction

Using a hyperspectral scanner (mounted on the northern end of the investigated grassland plots), the tilting of the scanner led to panoramic scale distortions where

pixels at the swath edges are larger compared to nadir pixels due to the relatively longer path length. To produce equal-area, distortion-free images, we corrected this panoramic error in along-scan and across-scan directions using information about the sensor height, sensor position, and the slit width (30 μm) as well as focal length (f = 25 mm) of the sensor lens (Richards, 2013). At first, we triangulated the sensor viewing angles for each line and column of the hyperspectral image cube. Based on the viewing angles for each pixel we generated a new raster matrix with the actual, equal-area pixel extensions. In a second step, we filled each cell of the newly created raster matrix with the corresponding reflectance values of the hyperspectral image cube to maintain a distortion-free, equal-area output.

8.2.3.3 Mean spectra for each plot

The two geometrically and spectrally corrected image cubes resulting from the two scan positions for each ring have been merged to get one image cube per ring. Due to well known differences in shaded versus sunlit reflectances (e.g. Aboutalebi et al. 2018; Zhang et al. 2015), we excluded shaded pixels on histogram basis with a threshold in the 1050 nm band where plant reflectance is very high. Thereby, also pixels containing non-organic spectra e.g. from measurement equipment were thoroughly excluded. Additionally, the spectrum for each pixel has been smoothed applying a Savitzky-Golay noise reduction filter with a filter length of nine bands (comprising 65 nm; Lehnert et al. in press). Using the geometrically and spectrally corrected image containing only sunlit pixels, we derived the mean spectra for each ring which was used for further analysis.

8.2.3.4 Predictors and feature spaces

Based on the ring-wise mean spectra, we delineated six different and widely used hyperspectral predictor feature spaces by different normalisation techniques: (1) band depth values and (2) absorption feature variables based on continuum removal, (3) the most common vegetation indices, (4) the log (1/Reflectance) and (5) the first and (6) second derivatives of the spectra. Each of the predictor spaces was based on a different method developed either to enhance the spectral absorption features and/or to minimize the effect of external perturbing factors e.g. soil background,

illumination and viewing geometry. Due to the small sample size and the common high collinearity of predictor variables in spectronomic analysis, we did not include all predictors in one feature space and rather constructed separate feature spaces for each of the transformation methods. In an additional step, the feature spaces comprising the log (1/Reflectance), the band depth values and the first and second derivatives of the spectra were further normalised by calculation of narrow band reflectance indices (NRIs), NDVI-like calculations using all possible band (predictor) combinations.

Feature spaces of absorption features and NRI band depth were derived from continuum removal transformation using a segmented hull (8.3).

$$BD_\lambda = 1 - \frac{R_\lambda}{CV_\lambda} \tag{8.3}$$

Here, R_λ and CV_λ denote the reflectance and continuum line value at wavelength λ.

For the absorption features space, we have chosen the main features at approx. 690 nm for chlorophyll, and 1045 nm, 1150 nm and 1450 nm for the water absorption, respectively. For each absorption feature, the integral and the width between lower and upper full-width-half-maximum values have been used as predictors. For the NRI band depths, normalised ratio indices (8.4) of all band depth values BD_λ (calculated in 8.3) were used.

$$NRI_{\lambda_1,\,\lambda_2} = \frac{R_{\lambda_1} - R_{\lambda_2}}{R_{\lambda_1} + R_{\lambda_2}} \tag{8.4}$$

Here, R is the reflectance or band depth (BD) at wavelength λ.

Likewise, the NRIs for the first derivative spectra (NRI 1st derivative), the second derivative spectra (NRI 2nd derivative) and the logarithm of the inverse of the reflectance (NRI $\log(1/R)$) were calculated.

Moreover, we created a feature space comprising more than 50 of the most commonly used vegetation indices (Common indices, for calculations refer to Tab. 8.1).

For computational issues, the geometric correction was performed in fortran (Gehrke, 2012); all other hyperspectral analysis was performed with CRAN R

Table 8.1: Narrowband indices tested in the present case study for their suitability to hyperspectrally predict the different grassland traits. Indices are sorted alphabetically.

Name	Formula	Reference
Boochs	D_{703}	Boochs et al. (1990)
Boochs2	D_{720}	Boochs et al. (1990)
Carter2	R_{695}/R_{760}	Carter (1994)
Carter3	R_{605}/R_{760}	Carter (1994)
Carter4	R_{710}/R_{760}	Carter (1994)
Carter5	R_{695}/R_{670}	Carter (1994)
CI	$R_{675} \cdot R_{690}/R_{683}^2$	Zarco-Tejada et al. (2003)
CI2	$R_{760}/R_{700} - 1$	Gitelson et al. (2003)
ClAInt	$\int_{600nm}^{735nm} R$	Oppelt & Mauser (2004)
D1	D_{730}/D_{706}	Zarco-Tejada et al. (2003)
D2	D_{705}/D_{722}	Zarco-Tejada et al. (2003)
Datt	$(R_{850} - R_{710})/(R_{850} - R_{680})$	Datt (1999)
Datt2	R_{850}/R_{710}	Datt (1999)
Datt3	D_{754}/D_{704}	Datt (1999)
DD	$(R_{749} - R_{720}) - (R_{701} - R_{672})$	le Maire et al. (2004)
DDn	$2 \cdot (R_{710} - R_{660} - R_{760})$	le Maire et al. (2008)
DPI	$(D_{688} \cdot D_{710})/D_{697}^2$	Zarco-Tejada et al. (2003)
GDVI_n	$(R_{800}^n - R_{680}^n)/(R_{800}^n + R_{680}^n)$*	Wu (2014)
Gitelson	$1/R_{700}$	Gitelson et al. (1999)
Gitelson2	$(R_{750} - R_{800}/R_{695} - R_{740}) - 1$	Gitelson et al. (2003)
GMI2	R_{750}/R_{700}	Gitelson et al. (2003)
LWVI_1	$(R_{1094} - R_{983})/(R_{1094} + R_{983})$	Galvão et al. (2005)
LWVI_2	$(R_{1094} - R_{1205})/(R_{1094} + R_{1205})$	Galvão et al. (2005)
Maccioni	$(R_{780} - R_{710})/(R_{780} - R_{680})$	Maccioni et al. (2001)
MSAVI	$0.5 \cdot \left(2 \cdot R_{800} + 1 - \left((2 \cdot R_{800} + 1)^2 - 8 \cdot (R_{800} - R_{670})\right)^{0.5}\right)$	Qi et al. (1994)
MSI	R_{1600}/R_{817}	Hunt & Rock (1989)
mSR2	$(R_{750}/R_{705}) - 1/(R_{750}/R_{705} + 1)^{0.5}$	Chen (1996)
MTCI	$(R_{754} - R_{709})/(R_{709} - R_{681})$	Dash & Curran (2004)
NDVI	$(R_{800} - R_{680})/(R_{800} + R_{680})$	Tucker (1979)
NDVI2	$(R_{750} - R_{705})/(R_{750} + R_{705})$	Gitelson & Merzlyak (1994)
NDWI	$(R_{860} - R_{1240})/(R_{860} + R_{1240})$	Gao (1996)
OSAVI	$(1 + 0.16) \cdot \frac{(R_{800} - R_{670})}{(R_{800} + R_{670} + 0.16)}$	Rondeaux et al. (1996)
OSAVI2	$(1 + 0.16) \cdot \frac{(R_{750} - R_{705})}{(R_{750} + R_{705} + 0.16)}$	Wu et al. (2008)
PSSR	R_{800}/R_{635}	Blackburn (1998)
PWI	R_{900}/R_{970}	Peñuelas et al. (1997)
RDVI	$(R_{800} - R_{670})/\sqrt{R_{800} + R_{670}}$	Roujean & Breon (1995)
REP_LE	Red-edge position through linear extrapolation.	Cho & Skidmore (2006)
REP_Li	$R_{re} = (R_{670} + R_{780})/2$ $700 + 40 \cdot ((R_{re} - R_{700})/(R_{740} - R_{700}))$	Guyot & Baret (1988)
SAVI	$(1 + L) \cdot (R_{800} - R_{670})/(R_{800} + R_{670} + L)$	Huete (1988)
SR	R_{800}/R_{680}	Jordan (1969)
SR1	R_{750}/R_{700}	Gitelson & Merzlyak (1997)
SR2	R_{752}/R_{690}	Gitelson & Merzlyak (1997)
SR4	R_{700}/R_{670}	McMurtrey et al. (1994)
SR5	R_{675}/R_{700}	Chappelle et al. (1992)
SR6	R_{750}/R_{710}	Zarco-Tejada & Miller (1999)
SRWI	R_{850}/R_{1240}	Zarco-Tejada et al. (2003)
Sum_Dr1	$\sum_{i=626}^{795} D_i$	Elvidge & Chen (1995)
Sum_Dr2	$\sum_{i=680}^{780} D_i$	Filella & Penuelas (1994)
Vogelmann	R_{740}/R_{720}	Vogelmann et al. (1993)
Vogelmann2	$(R_{734} - R_{747})/(R_{715} + R_{726})$	Vogelmann et al. (1993)
Vogelmann3	D_{715}/D_{705}	Vogelmann et al. (1993)
Vogelmann4	$(R_{734} - R_{747})/(R_{715} + R_{720})$	Vogelmann et al. (1993)

Note. R_λ is the reflectance at wavelength λ (nm) and D_λ is the first derivation of the reflectance value at wavelength λ (nm). L is the soil correction factor set to 0.5 in this study.
*For GDVI, indices with n = 2, 3, and 4 were derived.

statistical software (R Core Team, 2018) using the raster- (Hijmans & van Etten, 2014) and hsdar-packages (Lehnert et al., in press).

8.2.4 Statistical analyses

In general, our approach aims at finding the best statistical model (partial least squares regression) for each canopy trait based on hyperspectral data covering the harvest dates of 2014 and 2015. After the creation of the different feature spaces through spectral transformations (8.2.3.4), a careful selection of predictor variables is performed within each feature space (8.2.4.1), and the predictive performance of the final predictors is investigated for each feature space and canopy trait (8.2.4.2).

8.2.4.1 Predictors selection

Despite of the creation of separate feature spaces, the high number of predictor variables resulting from the narrow spectral band width in hyperspectral data results in highly correlated predictor variables being prone to overfitting of the models (Gowen et al., 2011; Wang et al., 2007). Here, the use of iterative variable selection approaches to reduce the number of predictors has been proven to increase the predictive power of hyperspectral data (Kawamura et al., 2008, 2006; Zhao et al., 2007). However, approaches such as recursive, backward, and forward feature selection are critically discussed especially due to a biased selection of relevant predictors (Krawczuk & Łukaszuk, 2016). Here, we apply a more recent approach that selects all relevant predictors based on random forest (Breiman, 2001), using the CRAN R package Boruta for each feature space and canopy trait (Kursa & Rudnicki, 2010).

To eliminate further collinearity that may still exist after eliminating all irrelevant predictors, we applied a subsequent step by deriving a new set of variables. Within each feature space and for each canopy trait, we used the frequently used step-wise variance inflation factor approach (VIF; CRAN R package usdm; Naimi et al. 2014) to eliminate explanatory variables with an excessive correlation. Basically, the VIF for a single predictor is calculated as the reciprocal of 1 - R^2 to all other predictors and thereby does not only include pairwise correlations but rather takes into account the correlations with all other variables (Dormann et al., 2013).

By means of a threshold (in our study a conservative VIF of 5, as suggested in Rogerson 2001), highly collinear predictors have been removed from the dataset in this step. Since the VIF changes after predictors are removed, we performed a stepwise approach by iteratively calculating the VIF for all predictors and removing the variable with the highest VIF in each step. This approach was repeated until all predictors reached values below the defined threshold. Through the selection of all relevant variables and subsequent removal of highly collinear predictors, we assembled the predictors used in the final models for each canopy trait and predictors feature space.

8.2.4.2 Final model selection

For each feature space and canopy trait, the final predictors were used to perform partial least squares regression (PLSR) using the CRAN R packages caret (Kuhn, 2008) and pls (Mevik et al., 2016). PLSR techniques transfer the information content of the predictors to independent latent vectors, which are generated with respect to a maximum representativeness of the dependent variable (Wold et al., 2001). Thereby, the number of predictors is reduced, and it is widely assumed that PLSR is insusceptible to problems of multicollinearity and overfitting even if the number of observations is low (Kawamura et al., 2008) as in our study. The PLSR models were trained by repeated cross-validation, and subsequently the model with the optimum number of latent vectors was chosen for each canopy trait and feature space. The models performances were validated by leave one out cross-validation R^2s (R^2_{LOO}) of the predicted versus observed canopy trait values. LOO was selected due to the small sample size, and its proven similar performance to validation via an independent dataset (Darvishzadeh et al., 2008). For each canopy trait, the feature space that revealed the highest R^2_{LOO} was chosen as the final PLSR model for canopy trait prediction.

To compare the overall suitability of the different feature spaces for grassland traits prediction, we also considered that only one feature space is used for the prediction of all canopy traits. Therefore, we performed a rescaling of the R^2_{LOO}s within each canopy trait by min-max normalisation and averaged all normalised R^2_{LOO}s for each feature space.

8.2.4.3 Model performance under different CO_2 concentrations

Under increasing CO_2 concentrations, plant physiology is expected to be altered, mainly by increasing the photosynthesis rate and the water use efficiency. Therefore, a bias in the hyperspectral predictability of different grassland traits in FACE experiments can be assumed. Consequently, it has to be proven whether transfer functions derived under present CO_2 concentrations can also be used in future to accurately predict grassland traits. To investigate these potential biases in the hyperspectral predictions under different CO_2 concentrations, we performed Student's t-tests on the means of the residuals in the final models for the elevated versus the ambient rings (for each canopy trait; confidence interval = 0.95).

8.2.4.4 Non-invasive trait prediction during vegetation period

To precisely adapt the management practices and to gain a deeper insight on grassland trait dynamics in the interplay of [eCO_2] and abiotic environmental factors, explicit knowledge of the spatio-temporal dynamics of the ecosystems health status and potential harvest outcomes is mandatory. Therefore, we used the final PLSR models to non-invasively predict each grassland trait on a pixel level. For each ring and measurement day, the pixel-wise grassland trait predictions were furthermore averaged to maintain a ring-wise mean canopy trait value. The predicted ring-wise mean canopy trait values were subsequently averaged within the elevated (elevated group) and the ambient treatment (ambient group), and treatment-wise mean values of selected grassland traits were plotted along with meteorological data to reveal the grassland trait dynamics in-between the harvest dates of 2015.

8.3 Results

The summary statistics of the measured canopy traits can be found in the appendix (Tab. 8.4). In general, the canopy traits revealed a good forage quality for the investigated grassland plots, indicated by net energy for lactation (> 5.8 MJ kg^{-1}), crude fibre (< 32%DM), and crude protein (> 9%DM, compare Tab. 8.4). Highest trait variances (coefficients of variation) were found for biomass followed by crude

sugar, while lowest coefficients of variation were found for dry matter followed by carbon. Strong correlations were observed for many of the grassland traits (see Tab. 8.5).

8.3.1 Performance of the different feature spaces

The analysed feature spaces revealed different performances in the prediction of the investigated canopy traits (Fig. 8.2). The feature space NRI 2nd derivative showed the best prediction performances for the highest number of canopy traits (6, organic acid detergent fibre, carbon, nitrogen, neutral acid detergent fibre, crude fibre, and crude sugar). The second best prediction results were obtained from the NRI 1st derivative feature space (5, crude ash, enzyme-soluble organic matter, methane, net energy for lactation, and crude protein). The common indices outperformed the other feature spaces only in two cases, for biomass and crude lipids. The NRI $\log(1/R)$ outperformed the other feature spaces only for dry matter. The absorption features and band depths feature spaces did not outperform the other feature spaces in the prediction of any of the canopy traits.

Similar patterns were observed for the performances of the features spaces considering the prediction of all canopy traits by only one feature space (compare Fig. 8.2o). Here, the average min-max normalised R^2_{LOO}s revealed the best performances for the NRI 2nd derivative, followed by the feature spaces NRI 1st derivative, NRI $\log(1/R)$, NRI band depths, common indices and the absorption features in descending order. All feature spaces that performed best for the predictions of at least one grassland trait, did also perform, at least one time, worse than all other feature spaces.

8.3.2 The final models for the prediction of the different canopy traits

LOO validation results of the final models for the prediction of the different canopy traits were all statistically significant (n = 23) and showed high to very high goodness of fits (compare Fig. 8.3 and Tab. 8.2). Very good validation results ($R^2_{LOO} > .8$) were observed for biomass, crude lipids, nitrogen, and dry matter,

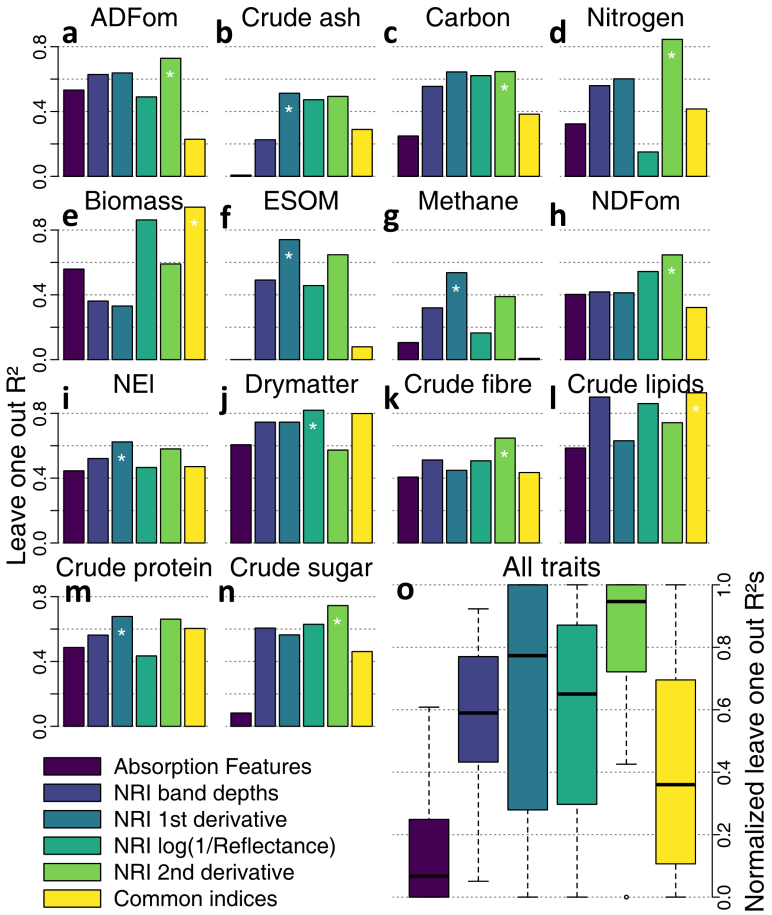

Figure 8.2: (a-n) Leave one out R^2s (R^2_{LOO}) from the best partial least squares regression models of the different feature spaces for each canopy trait. (o) Boxplots of min-max normalised R^2_{LOO}s of each feature space for the prediction of all traits. The white asterisk (a-n) denotes the feature space selected for the final predictive models (compare Fig. 8.3 and Tab. 8.2). NDF_{om} - Organic neutral detergent fibre; ADF_{om} - Organic acid detergent fibre; ESOM - Enzyme-soluble organic matter; NEl - Net energy content for lactation

while only moderate LOO validation results were derived for crude ash, methane, crude fibre ($.5 < R^2_{LOO} \leq .6$).

The models for the traits that were best predictable (biomass and crude lipids) used only common indices with predictors related to chlorophyll absorption (GDVI_4, Gitelson, REP_LE, and Sum_Dr1), and the water status of plants (LWVI_1 and PWI). Dry matter was very well predicted using the NRI $\log(1/R^2)$ and only two predictors (with wavelengths around the minor water absorption feature ~1130 nm,

Table 8.2: Summary of the used feature space and characteristics for the best partial least squares regression models on each grassland canopy trait.

Trait	Feature space	R^2_{LOO}	NRMSE (%)	No. of predictors	Predictors
ADF_{om}	NRI 2nd derivative	0.73	15.4	10	$B_{930\|810}$ + $B_{960\|910}$ + $B_{1000\|910}$ + $B_{1050\|910}$ + $B_{1070\|910}$ + $B_{1080\|910}$ + $B_{960\|920}$ + $B_{1460\|1000}$ + $B_{1030\|1010}$ + $B_{1080\|1020}$
Crude ash	NRI 1st derivative	0.51	16.0	4	$B_{1260\|1140}$ + $B_{1350\|1160}$ + $B_{1210\|1180}$ + $B_{1290\|1180}$
Carbon	NRI 2nd derivative	0.65	17.8	12	$B_{1240\|860}$ + $B_{1250\|860}$ + $B_{1030\|870}$ + $B_{1080\|870}$ + $B_{1100\|870}$ + $B_{1170\|940}$ + $B_{1180\|1000}$ + $B_{1510\|1050}$ + $B_{1510\|1060}$ + $B_{1350\|1090}$ + $B_{1490\|1090}$ + $B_{1320\|1190}$
Nitrogen	NRI 2nd derivative	0.84	10.6	12	$B_{1160\|910}$ + $B_{1510\|910}$ + $B_{1010\|920}$ + $B_{1110\|940}$ + $B_{1170\|940}$ + $B_{1090\|950}$ + $B_{1140\|1010}$ + $B_{1330\|1010}$ + $B_{1350\|1090}$ + $B_{1330\|1100}$ + $B_{1310\|1290}$ + $B_{1580\|1520}$
Biomass	Common indices	0.94	7.0	4	GDVI_4 + Gitelson + LWVI_1 + PWI
ESOM	NRI 1st derivative	0.74	12.8	9	$B_{1480\|890}$ + $B_{920\|910}$ + $B_{1180\|910}$ + $B_{970\|950}$ + $B_{1140\|950}$ + $B_{1040\|1010}$ + $B_{1300\|1120}$ + $B_{1150\|1130}$ + $B_{1570\|1140}$
Methane	NRI 1st derivative	0.54	15.9	7	$B_{970\|820}$ + $B_{1500\|830}$ + $B_{920\|910}$ + $B_{1180\|910}$ + $B_{980\|950}$ + $B_{1310\|990}$ + $B_{1040\|1020}$
NDF_{om}	NRI 2nd derivative	0.65	17.2	11	$B_{720\|640}$ + $B_{870\|660}$ + $B_{790\|710}$ + $B_{930\|710}$ + $B_{1280\|710}$ + $B_{880\|820}$ + $B_{1050\|860}$ + $B_{1600\|860}$ + $B_{1050\|880}$ + $B_{1190\|890}$ + $B_{1050\|1010}$
NEl	NRI 1st derivative	0.62	15.6	10	$B_{1590\|690}$ + $B_{1090\|770}$ + $B_{1180\|780}$ + $B_{1510\|800}$ + $B_{880\|820}$ + $B_{1150\|830}$ + $B_{1180\|850}$ + $B_{1190\|910}$ + $B_{1300\|1080}$ + $B_{1100\|1090}$
Dry matter	NRI $\log(1/R)$	0.82	11.8	2	$B_{1560\|1130}$ + $B_{1290\|1240}$
Crude fibre	NRI 2nd derivative	0.6	15.9	11	$B_{770\|710}$ + $B_{790\|710}$ + $B_{1060\|720}$ + $B_{1240\|720}$ + $B_{870\|820}$ + $B_{1110\|820}$ + $B_{1600\|850}$ + $B_{1600\|880}$ + $B_{1050\|960}$ + $B_{1240\|1100}$ + $B_{1570\|1170}$
Crude lipids	Common indices	0.93	7.7	4	GDVI_4 + LWVI_1 + REP_LE + Sum_Dr1
Crude protein	NRI 1st derivative	0.68	15.9	12	$B_{1350\|690}$ + $B_{1460\|710}$ + $B_{1310\|730}$ + $B_{1010\|750}$ + $B_{1180\|850}$ + $B_{1130\|960}$ + $B_{1190\|960}$ + $B_{1030\|1000}$ + $B_{1180\|1060}$ + $B_{1520\|1130}$ + $B_{1280\|1140}$ + $B_{1580\|1310}$
Crude sugar	NRI 2nd derivative	0.74	12.6	6	$B_{1480\|1060}$ + $B_{1160\|1140}$ + $B_{1580\|1140}$ + $B_{1200\|1150}$ + $B_{1350\|1150}$ + $B_{1550\|1320}$

Note. $B_{\lambda_1|\lambda_2}$ are NDVI-like calculations using the reflectance values in bands λ_1 and λ_2 (compare 8.4). The calculations of the different vegetation indices can be found in Section 8.2.3.4 (Tab. 8.1). All models contained 23 observations. NRMSE is the normalised root mean square error.
NDF_{om} - Organic neutral detergent fibre; ADF_{om} - Organic acid detergent fibre; ESOM - Enzyme-soluble organic matter; NEl - Net energy content for lactation

∼1250 nm, and ∼1560 nm). Carbon was well predicted by the NRI 2nd derivative and wavelengths related to biomass quantity (∼870 nm), and water absorption (∼1180 nm and ∼1245 nm). The traits which represent fodder quality (net energy for lactation) and biogas quality (methane) showed only modest R^2_{LOO}s of 0.62 and 0.54, respectively.

8.3.3 Influence of different CO_2 concentrations on hyperspectral grassland trait predictability

We did not find biases in the predictability of the different grassland traits due to different [CO_2]s (e.g. clustering of elevated rings below the PLSR regression

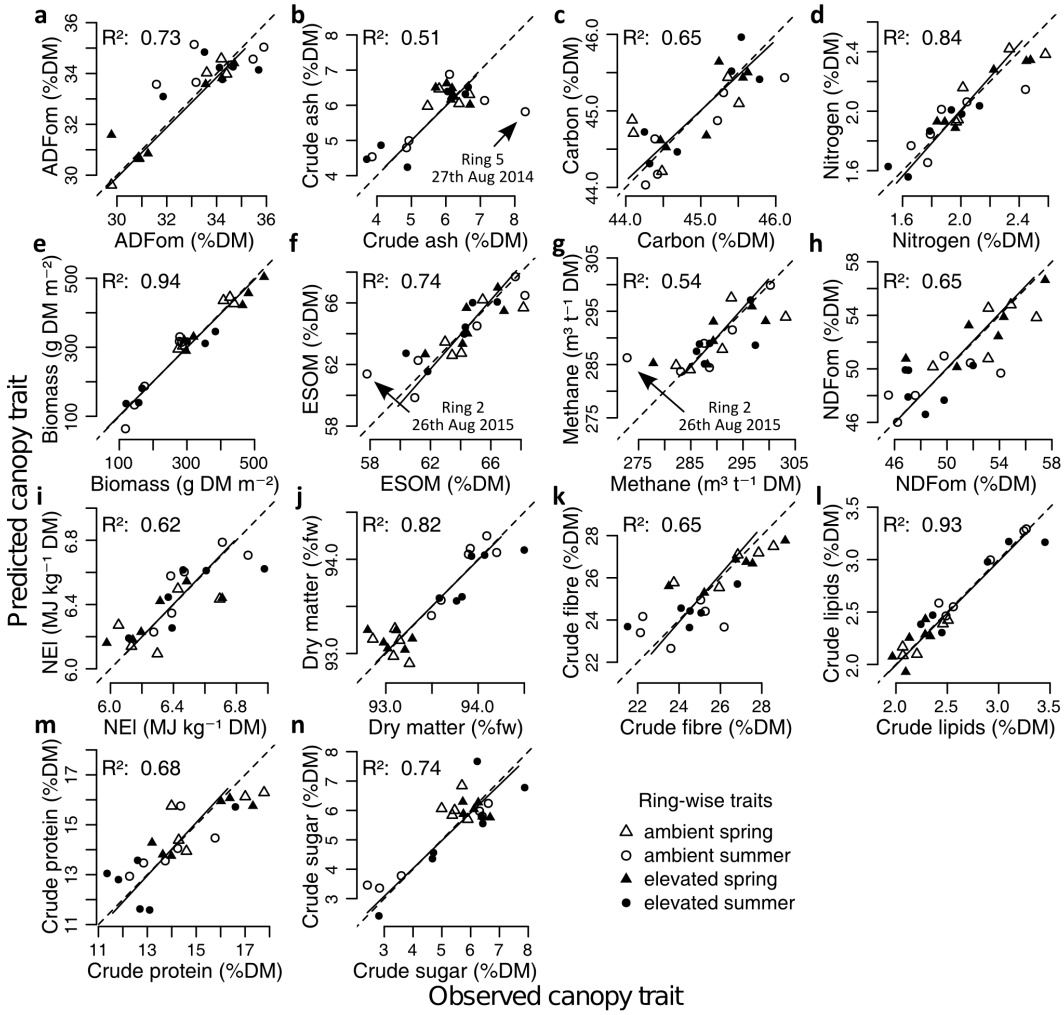

Figure 8.3: Leave one out predictions results for the best partial least squares regression models on each canopy trait. The solid and dashed lines depict the linear regression model and the 1:1 line, respectively. Outliers are marked with arrows in b), f), and g). Hyperspectral feature spaces used for the predictions can be found in Fig. 8.2 and Tab. 8.2. All regression analyses were statistically significant ($p \leq 0.001$). NDF_{om} - Organic neutral detergent fibre; ADF_{om} - Organic acid detergent fibre; ESOM - Enzyme-soluble organic matter; NEl - Net energy content for lactation

line; Fig. 8.3). In line, no significant differences were found for the means of the residuals in the final models between the predicted values in the elevated and ambient rings for any of the investigated grassland traits (Tab. 8.3). Outliers were found in three cases, for the prediction of crude ash (Ring 5 at 27th August 2014; highest measured value strongly underestimated; Fig. 8.3b), enzyme-soluble organic

matter (Ring 2 at 26th August 2015; lowest measured value strongly overestimated; Fig. 8.3f), and methane (Ring 2 at 26th August 2015; lowest measured value strongly overestimated, Fig. 8.3g).

Table 8.3: T-test statistics on the difference in the means of the final model residuals for elevated and ambient rings.

Canopy trait	p value
Nitrogen	0.70
Carbon	0.37
Biomass	0.75
Dry matter	0.97
Crude protein	0.07
Crude fibre	0.39
Crude lipids	0.73
Crude sugar	0.44
NDFom	0.98
ADFom	0.61
ESOM	0.86
Crude ash	0.99
NEl	0.85
Methane	0.07

8.3.4 Hyperspectral prediction of selected canopy traits

Based on the final PLSR models, spatially explicit pixel-wise predictions of grassland traits were possible (see Fig. 8.4 for the example of aboveground biomass under elevated CO_2 concentrations). Figure 8.4 reveals realistic aboveground biomass predictions with relatively high values for the measurement days shortly before the harvest days in 2014 and before the spring harvest in 2015. Low aboveground biomasses were observed for the measurement days ensuing the 2015 spring harvest. High within-ring variances in AGB predictions were observed for the image scenes of 27th August 2014 and 13th May 2015.

Additionally, we plotted mean values of selected grassland traits within the elevated and ambient groups for the vegetation period 2015 along with meteorological observations (Fig. 8.5). The maximum daily air temperatures were very high from the beginning of July to the mid of August with a short cooling in the last week of July. In this period, also the daily precipitation sums were very low, and only one day (19th June) revealed precipitation sums higher than 10 mm day^{-1}.

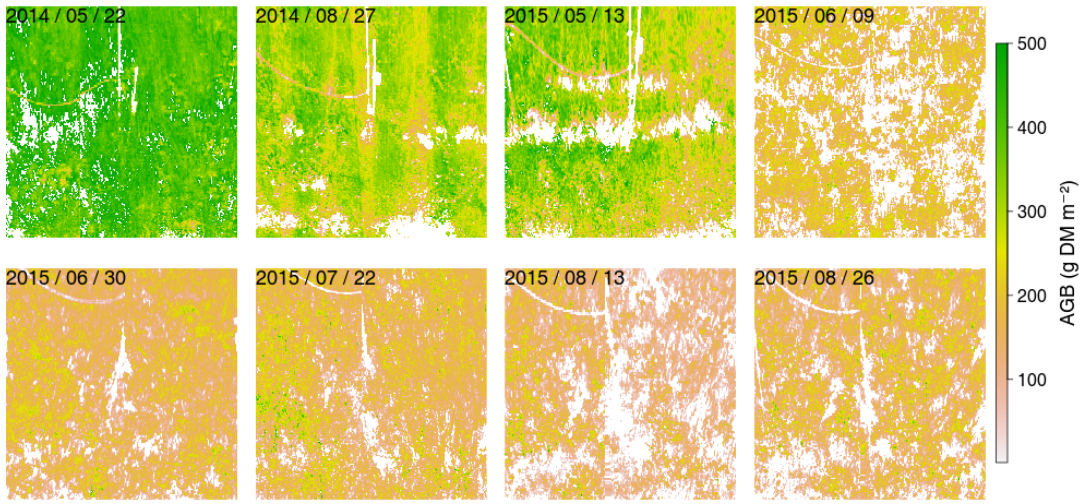

Figure 8.4: Pixel-wise, hyperspectral predictions of aboveground biomass (AGB) for one of the rings under elevated CO_2 concentrations. White areas were either excluded due to shade or measurement equipment. Scenes encompass harvest dates used to derive the predictive models (22 May 2014, 27 September 2014, 13 May 2015 and 26 September 2015) and vegetation period measurements for 2015 (interval around every three weeks; remaining ones).

Highest aboveground biomass predictions were found for the spring harvest date for both, ambient and elevated groups, with the latter showing a slightly higher AGB. In both groups, AGB recovered after the spring cuttings to a level of ∼178 g DM m^{-2}, while no increase in the AGBs occurred in the following measurement days. The biomass even decreased to ∼133 g DM m^{-2} on 13th August and slightly recovered to ∼150 g DM m^{-2} at the late summer harvest date, where AGB in the elevated group was again slightly higher compared to the ambient group. The predicted carbon content was highest at spring harvest (∼45.5% DM) and decreased with the ongoing vegetation period (minimum ∼44.8% DM at 13th August) before it distinctly increased on the last measurement day (more pronounced in the elevated compared to ambient group). Besides spring harvest, carbon content was higher in the elevated compared to the ambient group. The relative dry matter content was lowest in both groups for the spring harvest and increased in the first subsequent measurement day. Afterward, relative dry matter slightly decreased before it increased until 13th August. Subsequently, relative dry matter content slightly decreased for the late summer harvest date. At the spring harvest, dry

matter in the elevated group was slightly higher compared to the ambient group; at later measurement days the reverse relation occurred.

The predicted methane productivity was very high for the spring harvest date. After biomass cuttings, methane productivity increased until 30th June and subsequently followed a decreasing trend until the late summer harvest. Besides of the spring harvest, predicted methane productivity was slightly higher in the elevated compared to the ambient group. Predicted net energy for lactation was very low at the springs harvest date, with pronounced higher values in the elevated compared to the ambient group. In both treatment groups, NEl was higher for the first measurement after the spring harvest and subsequently decreased until 22nd July, followed by a strong increase in 13th August and only minor changes at the late summer harvest.

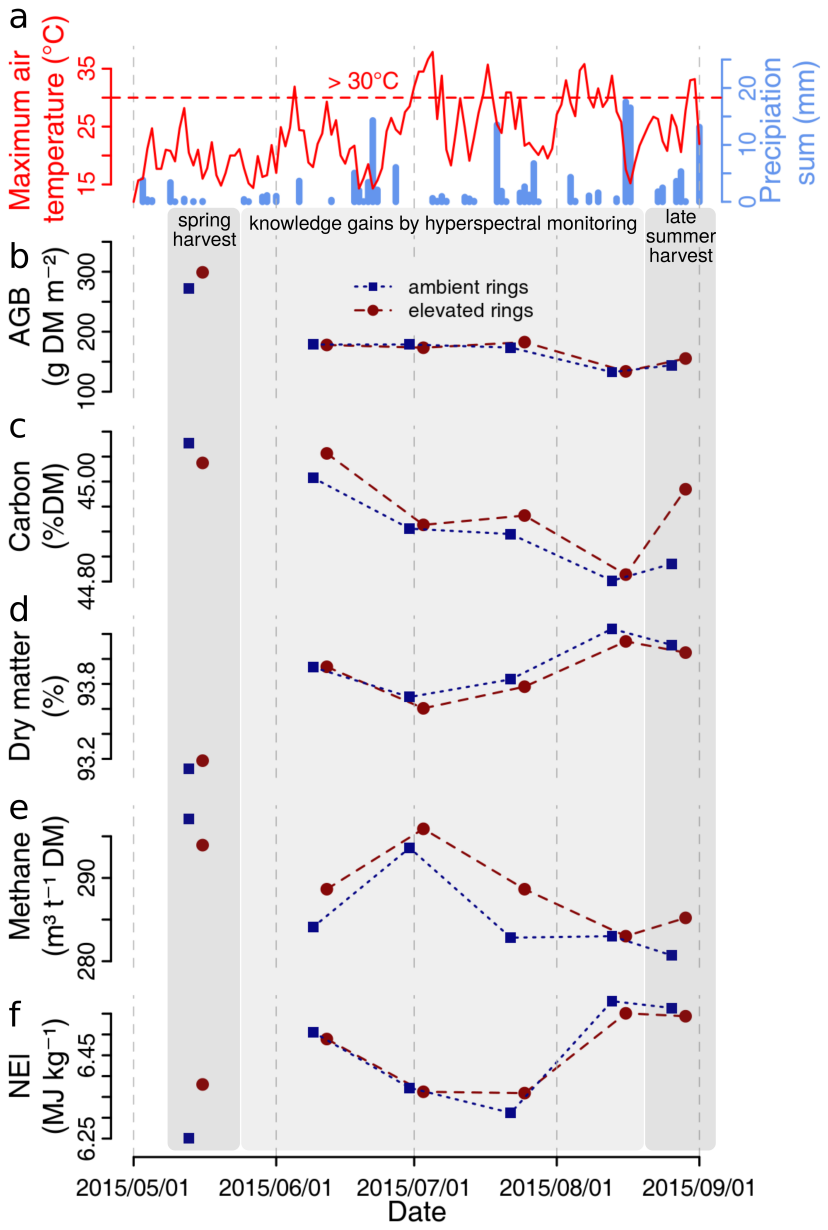

Figure 8.5: Meteorological observations (daily maximum air temperature and daily precipitation sum) and hyperspectral predictions of selected grassland canopy traits for the summer period 2015. (a) Daily maximum air temperatures and daily precipitation sums. (b-f) Mean of the predicted grassland canopy trait in the ambient and elevated groups at harvest (2015/05/13 and 2015/08/26; dark grey boxes) and during the growing period (knowledge gains by non-invasive hyperspectral approach; light grey box). Note, trait values of the elevated group are shifted by three days for readability. AGB - aboveground biomass; NEl - Net energy content for lactation

8.4 Discussion

8.4.1 Performance of the different feature spaces

In general, the validity of our approach using feature selection and elimination of multicollinearity was highlighted by good to excellent LOO validation results (Fig. 8.3). Interestingly, the common indices (available indices from literature) outperformed the other feature spaces for biomass and crude lipids. This suggests that the vegetation indices proposed in the literature can accurately predict the aboveground biomass, and their combination even increased the predictive power. For biomass, the combination of indices sensitive to chlorophyll and liquid water was not surprising given the combination of different growth stages (spring and late summer harvest) in our study. However, similar predictors were chosen for the crude lipids, which might either indicate an indirect predictability due to the strong correlation between crude lipids and aboveground biomass (r = -0.91; Tab. 8.5), or a direct reflectance response of leaf pigments as indicated in another study (Pullanagari et al., 2012b). All other grassland canopy trait predictions made use of feature spaces derived by different normalisation techniques.

Since normalisation techniques (such as derivative spectra and/or the calculation of narrowband ratio indices) are known to reduce artificial effects that may arise e.g. from different illumination conditions, we were not surprised that they improved most of the predictive models in our study combining measurements from different years and growth stages. However, given the different performances of the feature space for different grassland traits, our results reveal that it is not sufficient to predict all grassland traits by means of a single feature space comprising only one method of transformation. The NRI 2nd derivative, for example, outperformed the outer feature spaces for six out of 14 investigated grassland traits and showed the best overall performance (indicated by the normalised R^2_{LOO}s, Fig. 8.2o), while it performed worst for the prediction of dry matter and showed distinct inferior performances compared to the best performing feature spaces for biomass, methane, and crude lipids. This shows that a proper creation and selection of suitable predictor variables remains a necessary task that is needed for each grassland trait individually.

8.4.2 The final models for the prediction of the different canopy traits

The predictive performance for most of the grassland traits investigated in our study outperformed or ranged well within reported accuracies from previous studies (Buitrago et al., 2018; Homolova et al., 2013; Kawamura et al., 2008; Mutanga & Skidmore, 2003; Pullanagari et al., 2013; Zhao et al., 2007). This highlights the general suitability of hyperspectral data for monitoring of various grassland canopy traits even under different growth stages (spring and late summer harvests). However, since the selected spectral predictors in our study partly differed from previously published ones (e.g., Buitrago et al. 2018; Homolova et al. 2013; Kawamura et al. 2008; Mutanga & Skidmore 2003; Pullanagari et al. 2013; Zhao et al. 2007), we highlight, that a careful site-specific calibration is needed when using hyperspectral approaches.

8.4.3 Influence of different CO_2 concentrations on hyperspectral grassland trait predictability

Student's t-tests on the final model residuals for the elevated and the ambient rings, revealed that the final models performed well in the prediction of grassland traits irrespective of the different [CO_2]s (Tab. 8.3). This seems noteworthy, since we expected a bias in the prediction results due to an altered plant physiology under [eCO_2]s (e.g. clustering of elevated rings on one side of the regression line). We confirmed this by a t-test between the reflectance values for each band when comparing elevated and ambient group spectra, where no significant differences were found (not shown). Therefore, our results suggest, that the established relationships between hyperspectral data and grassland traits were not influenced by the different [CO_2]s. Thus, the hyperspectral monitoring of grassland traits within FACE facilities is possible, and transfer functions derived in the present seem also to be capable to accurately predict grassland traits in future (under [eCO_2]s).

8.4.4 Hyperspectral predictions of selected canopy traits

The high heterogeneity of the pixel-wise AGB predictions in two of the scenes of the presented elevated ring (Fig. 8.4) points to a major advantage of hyperspectral monitoring techniques – the spatial explicit information. Although invasive biomass samplings are usually randomly distributed, they may not properly represent the whole plot, and can not give information about the spatial distribution of the investigated grassland traits. Here, hyperspectral data leads to a clear knowledge gain.

Due to the altered plant physiology under [eCO_2]s, we exemplary investigated selected canopy traits under different [CO_2]s during the vegetation period 2015. A slightly higher biomass in the elevated compared to the ambient group at spring harvest date is in line with the expectations related to the CO_2 fertilization effect (Ainsworth & Rogers, 2007; Ainsworth & Long, 2005; Nowak et al., 2004). The absence of biomass growth during the later vegetation period can be explained by the excessive heat and dry period during July and August (similar to europe-wide observations in 2003, Ciais et al. 2005), which also prevented the plants to profit from [eCO_2] (Obermeier et al., 2018). However, the lower relative dry matter content of the plants growing under [eCO_2] for the same period may result from the increased water use efficiency, and, thus indicate an active CO_2 fertilization effect. Similarly, in the same period, the carbon content was higher in the elevated compared to the ambient rings. This suggests that plants growing under [eCO_2] and exposed to hot and dry conditions may indeed assimilate more carbon via photosynthesis and save water, while this can not be translated into an increased biomass productivity. This is in line with the new perspective on plant growth, hypothesizing that meristem activity is restricted earlier than photosynthesis by environmental conditions (Fatichi et al., 2014; Körner, 2015; Obermeier et al., 2017), and thus, that plants grown under [eCO_2] do not necessarily extend their growth but rather allocate non structural carbohydrates within the plant.

Regarding potential management practices in the investigated grassland, the peak of methane values at 30th June indicates the ideal harvest date in 2015 if the forage would be used for biogas production, while for the net energy for lactation the ideal harvest date in 2015 was around two weeks before the actual late summer

harvest (although only slightly improved compared to the actual harvest date). By finding the ideal harvest date, the increased temporal resolution of grassland trait values via hyperspectral monitoring might help farmers to optimize utilization of grasslands ecosystem services. Additionally, such timely knowledge of grassland vitality and emerging stress situations, but also of the expected yield quality and quantity, may help farmers in decision making during the vegetation period e.g. for precise fertilizer application or to adjust stocking rates, which increases profit and decreases the environmental footprint.

8.5 Conclusion

Our results clearly show that the hyperspectral prediction, and thus a non-invasive monitoring, of various grassland traits in the investigated grassland is in general feasible. However, careful creations and selections of appropriate predictor variables are needed for each canopy trait as shown by the large differences in the predictive performance of the different feature spaces. Interestingly, our results show that [eCO_2] does not lead to biases in the hyperspectral predictions of grassland traits. Consequently, the monitoring of grassland traits within a FACE facility is possible, and no indication was observed that transfer functions derived at present [CO_2]s should not be used under future [CO_2]s e.g., for phenotyping of grassland vegetation. Moreover, by monitoring selected grassland traits within a FACE experiment during the vegetation period, we highlighted how timely and spatially explicit hyperspectral data can provide new insights regarding the interacting effects of [eCO_2]s and environmental conditions on plant physiology, and help the farmers to find the ideal management practices to guarantee a proper management of the ecosystem services.

Acknowledgments

The contribution of the following individuals to the initiation, construction, installation and long-term, ongoing maintenance of the Giessen FACE experiment is gratefully acknowledged: H.-J. Jäger (deceased 2013), L. Grünhage, S. Schmidt,

8 Grassland ecosystem services in a changing environment: The potential of hyperspectral monitoring

J. Senkbeil, W. Stein, B. Lenz, J. Franz, T. Strohbusch, G. Mayer and A. Brück. Furthermore the authors want to thank S. Achilles and A. Bendix for their ongoing contributions to field sampling and S. Achilles for the help with technical aspects. This research has been funded by the LOEWE excellence cluster $FACE_2FACE$ of the Hessian State Ministry of Higher Education, Research and the Arts. We also acknowledge the long-term funding of the GiFACE infrastructure by the Hessian Agency for Nature Conservation, Environment and Geology (HLNUG).

References

Aboutalebi, M., Torres-Rua, A.F., McKee, M., Kustas, W., Nieto, H., & Coopmans, C. (2018): Behavior of vegetation/soil indices in shaded and sunlit pixels and evaluation of different shadow compensation methods using uav high-resolution imagery over vineyards. In: Autonomous Air and Ground Sensing Systems for Agricultural Optimization and Phenotyping III, volume 10664. International Society for Optics and Photonics, p. 1066407.

Ainsworth, E. & Rogers, A. (2007): The response of photosynthesis and stomatal conductance to rising [CO_2]: Mechanisms and environmental interactions. *Plant, Cell and Environment*, 30, 3, 258–270.

Ainsworth, E.A. & Long, S.P. (2005): What have we learned from 15 years of free-air CO_2 enrichment (FACE)? A meta-analytic review of the responses of photosynthesis, canopy properties and plant production to rising CO_2. *New Phytologist*, 165, 2, 351–372.

Andresen, L.C., Yuan, N., Seibert, R., Moser, G., Kammann, C.I., Luterbacher, J., Erbs, M., & Müller, C. (2018): Biomass responses in a temperate european grassland through 17 years of elevated CO_2. *Global Change Biology*, 24, 9, 3875–3885.

Augustine, D.J., Blumenthal, D.M., Springer, T.L., LeCain, D.R., Gunter, S.A., & Derner, J.D. (2018): Elevated CO_2 induces substantial and persistent declines in forage quality irrespective of warming in mixedgrass prairie. *Ecological Applications*, 28, 3, 721–735.

Biewer, S., Fricke, T., & Wachendorf, M. (2009): Development of canopy reflectance models to predict forage quality of legume-grass mixtures. *Crop Science*, 49, 5, 1917–1926.

Blackburn, G.A. (1998): Quantifying chlorophylls and caroteniods at leaf and canopy scales: An evaluation of some hyperspectral approaches. *Remote Sensing of Environment*, 66, 3, 273–285.

Boochs, F., Kupfer, G., Dockter, K., & Kühbauch, W. (1990): Shape of the red edge as vitality indicator for plants. *International Journal of Remote Sensing*, 11, 10, 1741–1753.

Breiman, L. (2001): Random forests. *Machine Learning*, 45, 1, 5–32.

Buitrago, M.F., Groen, T.A., Hecker, C.A., & Skidmore, A.K. (2018): Spectroscopic determination of leaf traits using infrared spectra. *International Journal of Applied Earth Observation and Geoinformation*, 69, 237–250.

Campbell, B. & Stafford Smith, D. (2000): A synthesis of recent global change research on pasture and rangeland production: reduced uncertainties and their management implications. *Agriculture, Ecosystems & Environment*, 82, 1-3, 39–55.

Carter, G.A. (1994): Ratios of leaf reflectances in narrow wavebands as indicators of plant stress. *International Journal of Remote Sensing*, 15, 3, 697–703.

Chappelle, E.W., Kim, M.S., & McMurtrey, J.E. (1992): Ratio analysis of reflectance spectra (RARS) - An algorithm for the remote estimation of the concentrations of chlorophyll-a, chlorophyll-b, and carotenoids in soybean leaves. *Remote Sensing of Environment*, 39, 3, 239–247.

Chen, J.M. (1996): Evaluation of vegetation indices and a modified simple ratio for boreal applications. *Canadian Journal of Remote Sensing*, 22, 229–242.

Cho, M.A. & Skidmore, A.K. (2006): A new technique for extracting the red edge position from hyperspectral data: The linear extrapolation method. *Remote Sensing of Environment*, 101, 2, 181 – 193.

Ciais, P., Reichstein, M., Viovy, N., Granier, A., Ogée, J., Allard, V., Aubinet, M., Buchmann, N., Bernhofer, C., Carrara, A., Chevallier, F., De Noblet, N., Friend, a.D., Friedlingstein, P., Grünwald, T., Heinesch, B., Keronen, P., Knohl, A., Krinner, G., Loustau, D., Manca, G., Matteucci, G., Miglietta, F., Ourcival, J.M., Papale, D., Pilegaard, K., Rambal, S., Seufert, G., Soussana, J.F., Sanz, M.J., Schulze, E.D., Vesala, T., & Valentini, R. (2005): Europe-wide reduction

in primary productivity caused by the heat and drought in 2003. *Nature*, 437, 7058, 529–533.

Cotrufo, F.M., Ineson, P., & Scott, A. (1998): Elevated CO_2 reduces the nitrogen concentration of plant. *Global Change Biology*, 4, 1, 43–54.

Darvishzadeh, R., Skidmore, A., Schlerf, M., Atzberger, C., Corsi, F., & Cho, M. (2008): LAI and chlorophyll estimation for a heterogeneous grassland using hyperspectral measurements. *ISPRS Journal of Photogrammetry and Remote Sensing*, 63, 4, 409–426.

Dash, J. & Curran, P.J. (2004): The MERIS terrestrial chlorophyll index. *International Journal of Remote Sensing*, 25, 23, 5403–5413.

Datt, B. (1999): Visible/near infrared reflectance and chlorophyll content in *Eucalyptus* leaves. *International Journal of Remote Sensing*, 20, 14, 2741–2759.

Daughtry, C.S.T., Walthall, C.L., Kim, M.S., Brown de Colstoun, E., & McMurtrey, J.E. (2000): Estimating corn leaf chlorophyll concentration from leaf and canopy reflectance. *Remote Sensing of Environment*, 74, 2, 229 – 239.

Deutsche Landwirtschafts-Gesellschaft (2013): Leitfaden zur Berechnung des Energiegehaltes bei Einzel- und Mischfuttermitteln für die Schweine- und Rinderfütterung. Stellungnahme des DLG-Arbeitskreises Futter und Fütterung. pp. 1–9.

Dormann, C.F., Elith, J., Bacher, S., Buchmann, C., Carl, G., Carré, G., Marquéz, J.R., Gruber, B., Lafourcade, B., Leitão, P.J., Münkemüller, T., Mcclean, C., Osborne, P.E., Reineking, B., Schröder, B., Skidmore, A.K., Zurell, D., & Lautenbach, S. (2013): Collinearity: A review of methods to deal with it and a simulation study evaluating their performance. *Ecography*, 36, 1, 27–46.

Dumont, B., Andueza, D., Niderkorn, V., Lüscher, A., Porqueddu, C., & Picon-Cochard, C. (2015): A meta-analysis of climate change effects on

forage quality in grasslands: specificities of mountain and mediterranean areas. *Grass and Forage Science*, 70, 2, 239–254.

Elvidge, C.D. & Chen, Z.K. (1995): Comparison of broad-band and narrow-band red and near-infrared vegetation indexes. *Remote Sensing of Environment*, 54, 1, 38–48.

Fatichi, S., Leuzinger, S., & Körner, C. (2014): Moving beyond photosynthesis: From carbon source to sink-driven vegetation modeling. *New Phytologist*, 201, 4, 1086–1095.

Filella, I. & Penuelas, J. (1994): The red edge position and shape as indicators of plant chlorophyll content, biomass and hydric status. *International Journal of Remote Sensing*, 15, 1459–1470.

Flachowsky, G., Jeroch, H., Kirchgessner, M., Pallauf, J., Pfeffer, E., Schulz, E., & Staudacher, W. (2001): Empfehlungen zur Energie- und Nährstoffversorgung der Milchkühe und Aufzuchtrinder 2001, volume 8 of *Energie- und Nährstoffbedarf landwirtschaftlicher Nutztiere*. Deutsche Landwirtschafts-Gesellschaft Verlag, Frankfurt a. M.

Galvão, L.S., Formaggio, A.R., & Tisot, D.A. (2005): Discrimination of sugarcane varieties in southeastern Brazil with EO-1 Hyperion data. *Remote Sensing of Environment*, 94, 4, 523–534.

Gao, B.c. (1996): NDWI - A normalized difference water index for remote sensing of vegetation liquid water from space. *Remote Sensing of Environment*, 58, 3, 257 – 266.

Gehrke, W. (2012): Fortran 95 Language Guide. Springer London.

Gitelson, A.A. & Merzlyak, M.N. (1997): Remote estimation of chlorophyll content in higher plant leaves. *International Journal of Remote Sensing*, 18, 12, 2691–2697.

Gitelson, A., Buschmann, C., & Lichtenthaler, H. (1999): The chlorophyll fluorescence ratio F735/F700 as an accurate measure of the chlorophyll content

in plants - Experiments with autumn chestnut and maple leaves. *Remote Sensing of Environment*, 69, 3, 296–302.

Gitelson, A., Y, G., & MN., M. (2003): Relationships between leaf chlorophyll content and spectral reflectance and algorithms for non-destructive chlorophyll assessment in higher plant leaves. *Journal of Plant Physiology*, 160, 3, 271–282.

Gitelson, A. & Merzlyak, M.N. (1994): Quantitative estimation of chlorophyll-a using reflectance spectra: Experiments with autumn chestnut and maple leaves. *Journal of Photochemistry and Photobiology B: Biology*, 22, 3, 247 – 252.

Gowen, A.A., Downey, G., Esquerre, C., & O'Donnell, C.P. (2011): Preventing over-fitting in PLS calibration models of near-infrared (NIR) spectroscopy data using regression coefficients. *Journal of Chemometrics*, 25, 7, 375–381.

Guyot, G. & Baret, F. (1988): Utilisation de la haute resolution spectrale pour suivre l'etat des couverts vegetaux. In: T.D. Guyenne & J.J. Hunt (Eds.), Spectral Signatures of Objects in Remote Sensing, volume 287 of *ESA Special Publication*. pp. 279–286.

Haboudane, D., Miller, J.R., Tremblay, N., Zarco-Tejada, P.J., & Dextraze, L. (2002): Integrated narrow-band vegetation indices for prediction of crop chlorophyll content for application to precision agriculture. *Remote Sensing of Environment*, 81, 2-3, 416–426.

Herrero, M., Havlík, P., Valin, H., Notenbaert, A., Rufino, M.C., Thornton, P.K., Blümmel, M., Weiss, F., Grace, D., & Obersteiner, M. (2013): Biomass use, production, feed efficiencies, and greenhouse gas emissions from global livestock systems. *Proceedings of the National Academy of Sciences*, 110, 52, 20 888–20 893.

Hijmans, R.J. & van Etten, J. (2014): raster: Geographic data analysis and modeling. *R package version*, 2, 8.

Homolova, L., Malenovskỳ, Z., Clevers, J.G., García-Santos, G., & Schaepman, M.E. (2013): Review of optical-based remote sensing for plant trait mapping. *Ecological Complexity*, 15, 1–16.

Huete, A. (1988): A soil-adjusted vegetation index (SAVI). *Remote Sensing of Environment*, 25, 295–309.

Hunt, E.R. & Rock, B.N. (1989): Detection of changes in leaf water-content using near-infrared and middle-infrared reflectances. *Remote Sensing of Environment*, 30, 1, 43–54.

Jäger, H.J., Schmidt, S.W., Kammann, C., Grünhage, L., Müller, C., & Hanewald, K. (2003): The University of Giessen Free-Air Carbon Dioxide Enrichment Study: Description of the Experimental Site and of a New Enrichment System. *Journal of Applied Botany*, 77, 117–127.

Jordan, C.F. (1969): Derivation of leaf-area index from quality of light on forest floor. *Ecology*, 50, 4, 663–666.

Kawamura, K., Watanabe, N., Sakanoue, S., & Inoue, Y. (2008): Estimating forage biomass and quality in a mixed sown pasture based on partial least squares regression with waveband selection. *Grassland Science*, 54, 3, 131–145.

Kawamura, S., Arakawa, M., & Funatsu, K. (2006): Development of genetic algorithm-based wavelength regional selection technique. *Journal of Computer Aided Chemistry*, 7, 10–17.

Körner, C. (2015): Paradigm shift in plant growth control. *Current Opinion in Plant Biology*, 25, 107–114.

Krawczuk, J. & Łukaszuk, T. (2016): The feature selection bias problem in relation to high-dimensional gene data. *Artificial Intelligence in Medicine*, 66, 63–71.

Kuhn, M. (2008): Building Predictive Models in R Using the caret Package. *Journal Of Statistical Software*, 28, 5, 1–26.

Kursa, M.B. & Rudnicki, W.R. (2010): Feature selection with the Boruta package. *Journal of Statistical Software*, 36, 11, 1–13.

le Maire, G., Francois, C., & Dufrêne, E. (2004): Towards universal broad leaf chlorophyll indices using PROSPECT simulated database and hyperspectral reflectance measurements. *Remote Sensing of Environment*, 89, 1, 1–28.

le Maire, G., François, C., Soudani, K., Berveiller, D., Pontailler, J.Y., Bréda, N., Genet, H., Davi, H., & Dufrêne, E. (2008): Calibration and validation of hyperspectral indices for the estimation of broadleaved forest leaf chlorophyll content, leaf mass per area, leaf area index and leaf canopy biomass. *Remote Sensing of Environment*, 112, 10, 3846 – 3864.

Lee, M., Manning, P., Rist, J., Power, S.A., & Marsh, C. (2010): A global comparison of grassland biomass responses to CO_2 and nitrogen enrichment, 2047–2056.

Lehnert, L.W., Meyer, H., Obermeier, W.A., Silva, B., Regeling, B., & Bendix, J. (in press): Hyperspectral data analysis in R: the hsdar package. *Journal of Statistical Software*.

Maccioni, A., Agati, G., & Mazzinghi, P. (2001): New vegetation indices for remote measurement of chlorophylls based on leaf directional reflectance spectra. *Journal of Photochemistry and Photobiology B: Biology*, 61, 1-2, 52 – 61.

Marabel, M. & Alvarez-Taboada, F. (2013): Spectroscopic determination of aboveground biomass in grasslands using spectral transformations, support vector machine and partial least squares regression. *Sensors*, 13, 8, 10 027–10 051.

McGranahan, D. & Yurkonis, K. (2018): Variability in grass forage quality and quantity in response to elevated CO_2 and water limitation. *Grass and Forage Science*, 73, 2, 517–521.

McMurtrey, J.E., Chappelle, E.W., Kim, M.S., Meisinger, J.J., & Corp, L.A. (1994): Distinguishing nitrogen-fertilization levels in-field corn (*Zea mays* L) with actively induced fluorescence and passive reflectance measurements. *Remote Sensing of Environment*, 47, 1, 36–44.

Mevik, B.H., Wehrens, R., & Liland, K.H. (2016): pls: Partial Least Squares and Principal Component Regression. R package version 2.6-0. URL https://CRAN.R-project.org/package=pls

Morgan, J.A., Mosier, A.R., Milchunas, D.G., LeCain, D.R., Nelson, J.A., & Parton, W.J. (2004): CO_2 enhances productivity, alters species composition, and reduces digestibility of shortgrass steppe vegetation. *Ecological Applications*, 14, 1, 208–219.

Mutanga, O. & Skidmore, A.K. (2003): Continuum-removed absorption features estimate tropical savanna grass quality in situ. In: Earsel workshop on imaging spectroscopy, volume 3. pp. 13–16.

Naimi, B., Hamm, N.A., Groen, T.A., Skidmore, A.K., & Toxopeus, A.G. (2014): Where is positional uncertainty a problem for species distribution modelling? *Ecography*, 37, 2, 191–203.

Nowak, R.S., Ellsworth, D.S., & Smith, S.D. (2004): Functional responses of plants to elevated atmospheric CO_2 – do photosynthetic and productivity data from face experiments support early predictions? *New Phytologist*, 162, 2, 253–280.

Obermeier, W.A., Lehnert, L.W., Kammann, C.I., Müller, C., Grünhage, L., Luterbacher, J., Erbs, M., Moser, G., Seibert, R., Yuan, N., & Bendix, J. (2017): Reduced CO_2 fertilization effect in temperate C3 grasslands under more extreme weather conditions. *Nature Climate Change*, 7, 2, 137—-141.

Obermeier, W.A., Lehnert, L.W., Ivanov, M.A., Luterbacher, J., & Bendix, J. (2018): Reduced summer aboveground productivity in temperate c3 grasslands under future climate regimes. *Earth's Future*, 6, 5, 716–729.

Oppelt, N. & Mauser, W. (2004): Hyperspectral monitoring of physiological parameters of wheat during a vegetation period using AVIS data. *International Journal of Remote Sensing*, 25, 1, 145–159.

Peñuelas, J., Piñol, J., Ogaya, R., & Filella, I. (1997): Estimation of plant water concentration by the reflectance water index WI (R900/R970). *International Journal of Remote Sensing*, 18, 13, 2869–2875.

Pullanagari, R.R., Yule, I.J., Hedley, M.J., Tuohy, M.P., Dynes, R.A., & King, W.M. (2012a): Multi-spectral radiometry to estimate pasture quality components. *Precision Agriculture*, 13, 4, 442–456.

Pullanagari, R.R., Yule, I.J., Tuohy, M.P., Hedley, M.J., Dynes, R.A., & King, W.M. (2012b): In-field hyperspectral proximal sensing for estimating quality parameters of mixed pasture. *Precision Agriculture*, 13, 3, 351–369.

Pullanagari, R.R., Yule, I.J., Tuohy, M.P., Hedley, M.J., Dynes, R.A., & King, W.M. (2013): Proximal sensing of the seasonal variability of pasture nutritive value using multispectral radiometry. *Grass and Forage Science*, 68, 1, 110–119.

Qi, J., Chehbouni, A., Huete, A., Kerr, Y., & Sorooshian, S. (1994): A modified soil adjusted vegetation index. *Remote Sensing of Environment*, 48, 2, 119 – 126.

Ramoelo, A., Skidmore, A., Cho, M.A., Mathieu, R., Heitkönig, I., Dudeni-Tlhone, N., Schlerf, M., & Prins, H. (2013): Non-linear partial least square regression increases the estimation accuracy of grass nitrogen and phosphorus using in situ hyperspectral and environmental data. *ISPRS Journal of Photogrammetry and Remote Sensing*, 82, 27–40.

R Core Team (2018): R: A Language and Environment for Statistical Computing. R Foundation for Statistical Computing, Vienna, Austria. (last access: 27/07/2018).
URL `https://www.R-project.org/`

Richards, J.A. (2013): Correcting and registering images. In: Remote Sensing Digital Image Analysis. Springer, pp. 27–77.

Rogerson, P. (2001): Statistical Methods for Geography. Geography / Quantitative Methods Series. SAGE Publications.

Rondeaux, G., Steven, M., & Baret, F. (1996): Optimization of soil-adjusted vegetation indices. *Remote Sensing of Environment*, 55, 2, 95–107.

Roujean, J.L. & Breon, F.M. (1995): Estimating par absorbed by vegetation from bidirectional reflectance measurements. *Remote Sensing of Environment*, 51, 3, 375–384.

Soussana, J.F. & Lüscher, A. (2007): Temperate grasslands and global atmospheric change: A review. *Grass and Forage Science*, 62, 2, 127–134.

Suzuki, Y., Tanaka, K., Kato, W., Okamoto, H., Kataoka, T., Shimada, H., Sugiura, T., & Shima, E. (2008): Field mapping of chemical composition of forage using hyperspectral imaging in a grass meadow. *Grassland science*, 54, 4, 179–188.

Tucker, C.J. (1979): Red and photographic infrared linear combinations for monitoring vegetation. *Remote Sensing of Environment*, 8, 2, 127–150.

Verband Deutscher Landwirtschaftlicher Untersuchungs- und Forschungsanstalten (2012): VDLUFA-Methodenbuch, Bd. III, Die chemische Untersuchung von Futtermitteln. 8. Erg. VDLUFA-Verlag Darmstadt, Germany.

Vogelmann, J.E., Rock, B.N., & Moss, D.M. (1993): Red edge spectral measurements from sugar maple leaves. *International Journal of Remote Sensing*, 14, 8, 1563–1575.

Wang, J., Wang, H., & Saporta, G. (2007): Discussion on importance of variable selection in pls1 modeling. In: PLS'07 5th Int. Symp. on PLS and related methods, Oslo.

Weissbach, F. (2008): Zur Bewertung des Gasbildungspotenzials von nachwachsenden Rohstoffen. *LANDTECHNIK–Agricultural Engineering*, 63, 6, 356–358.

White, A., Cannell, M.G., & Friend, A.D. (2000): CO_2 stabilization, climate change and the terrestrial carbon sink. *Global Change Biology*, 6, 7, 817–833.

Wold, S., Sjöström, M., & Eriksson, L. (2001): PLS-regression: a basic tool of chemometrics. *Chemometrics and Intelligent Laboratory Systems*, 58, 2, 109–130.

Wu, C., Niu, Z., Tang, Q., & Huang, W. (2008): Estimating chlorophyll content from hyperspectral vegetation indices: Modeling and validation. *Agricultural and Forest Meteorology*, 148, 1230–1241.

Wu, W. (2014): The generalized difference vegetation index (GDVI) for dryland characterization. *Remote Sensing*, 6, 2, 1211–1233.

Xiaoping, W., Ni, G., Kai, Z., & Jing, W. (2011): Hyperspectral Remote Sensing Estimation Models of Aboveground Biomass in Gannan Rangelands. *Procedia Environmental Sciences*, 10, 697–702.

Zarco-Tejada, P.J. & Miller, J.R. (1999): Land cover mapping at BOREAS using red edge spectral parameters from CASI imagery. *Journal of Geophysical Research: Atmospheres*, 104, D22, 27 921–27 933.

Zarco-Tejada, P.J., Pushnik, J.C., Dobrowski, S., & Ustin, S.L. (2003): Steady-state chlorophyll a fluorescence detection from canopy derivative reflectance and double-peak red-edge effects. *Remote Sensing of Environment*, 84, 2, 283–294.

Zhang, L., Sun, X., Wu, T., & Zhang, H. (2015): An analysis of shadow effects on spectral vegetation indexes using a ground-based imaging spectrometer. *IEEE Geoscience and Remote Sensing Letters*, 12, 11, 2188–2192.

Zhao, D., Starks, P.J., Brown, M.A., Phillips, W.A., & Coleman, S.W. (2007): Assessment of forage biomass and quality parameters of bermudagrass using proximal sensing of pasture canopy reflectance. *Grassland Science*, 53, 1, 39–49.

8.6 Appendix

8.6.1 Measured canopy traits

The summary statistics of the measured and calculated grassland canopy traits revealed highest within-trait-variances (coefficients of variation) for biomass, crude sugar, crude ash, crude lipids, nitrogen, and crude protein in the same order (Tab. 8.4). Lowest coefficients of variation were found for dry matter, carbon, and traits linked to the production of biogas (fermentable organic matter, biogas, methane).

Table 8.4: Descriptive statistics of ring-wise canopy traits. All ring-wise traits were calculated by biomass-weighting of the plant functional type specific trait characteristics (compare Section 8.2.2.2)

Canopy trait	Unit	Mean	Minimum	Maximum	SD	CV (%)
Nitrogen	%DM	2.01	1.50	2.58	0.29	14.38
Carbon	%DM	44.95	44.08	46.12	0.62	1.37
Biomass	g DM m^{-2}	303.61	118.30	528.10	119.60	39.39
Dry matter	%fw	93.51	92.80	94.50	0.48	0.51
Crude protein	%DM	14.33	11.35	17.78	1.83	12.75
Crude fibre	%DM	25.36	21.51	29.13	2.06	8.13
Crude lipids	%DM	2.51	1.97	3.45	0.43	16.98
Crude sugar	%DM	5.44	2.41	7.88	1.38	25.43
Organic neutral detergent fibre	%DM	50.78	45.54	57.48	3.53	6.96
Organic acid detergent fibre	%DM	33.27	29.78	35.90	1.82	5.48
Enzyme-resistant organic matter	%DM	35.88	31.75	42.20	2.64	7.36
Enzyme-soluble organic matter	%DM	64.13	57.80	68.26	2.64	4.12
Crude ash	%DM	5.85	3.70	8.30	1.08	18.41
Metabolizable energy	MJ kg^{-1}	10.70	10.07	11.52	0.38	3.52
Net energy content for lactation	MJ kg^{-1}	6.41	5.98	6.98	0.26	4.06
Fermentable organic matter	g kg^{-1}	689.72	649.52	721.84	17.20	2.49
Biogas	m^3 t^{-1}	551.78	519.61	577.47	13.76	2.49
Methane	m^3 t^{-1}	289.68	272.80	303.17	7.22	2.49

SD - standard deviation; CV - coefficient of variation; DM - dry matter; fw - fresh weight

Strong correlations were observed between many of the canopy traits (Tab. 8.5), the most important statistically significant ones are described in the following. Nitrogen showed significant positive correlations with carbon and crude protein, and a significant negative correlation with organic acid detergent fibre. Additionally, carbon was significantly positive correlated with crude lipids, crude protein, metabolizable energy and net energy for lactation, and significantly negative correlated to biomass and crude ash. For biomass, significant positive correlations were observed with crude fibre, crude sugar, organic neutral detergent fibre, and crude

ash, while carbon, dry matter, crude lipids, metabolizable energy and net energy for lactation were significantly negative correlated to biomass. The net energy for lactation showed significant positive correlations with metabolizable energy (perfect correlation, therefore excluded), crude lipids, dry matter, carbon, traits linked to biogas, and crude protein, while significant negative correlations were found with crude fibre, organic neutral detergent fibre, biomass, crude ash, crude sugar, and organic acid detergent fibre. Methane revealed significant positive correlations with fermentable organic matter (perfect correlation, therefore excluded), biogas (perfect correlation, therefore excluded), enzyme-soluble organic matter, net energy for lactation, metabolizable energy, and crude protein. Significant negative correlations for methane were found with enzyme-resistant organic matter, organic acid detergent fibre, crude fibre, organic neutral detergent fibre.

Table 8.5: Pearson product moment correlation coefficients (r) for measured, ring-wise canopy traits. Note, that the correlation matrix is split into two tables.

	Nitrogen	Carbon	Biomass	Dry matter	Crude protein	Crude fibre	Crude lipids
Carbon	0.67***						
Biomass	-0.14	-0.60**					
Dry matter	-0.33	0.25	-0.73***				
Crude protein	0.75***	0.52*	-0.17	-0.24			
Crude fibre	-0.03	-0.39	0.72***	-0.67***	-0.27		
Crude lipids	0.06	0.60**	-0.91***	0.83***	0.09	-0.64***	
Crude sugar	-0.24	-0.58**	0.69***	-0.59**	-0.33	0.36	-0.82***
NDF_{om}	0.05	-0.32	0.65***	-0.62**	-0.12	0.94***	-0.51*
ADF_{om}	-0.53**	-0.25	0.01	0.33	-0.81***	0.39	0.17
EROM	-0.13	0.22	-0.31	0.36	-0.25	0.27	0.44*
ESOM	0.13	-0.22	0.31	-0.36	0.25	-0.27	-0.44*
Crude ash	-0.21	-0.63**	0.60**	-0.58**	-0.26	0.41	-0.70***
ME	0.26	0.59**	-0.75***	0.61**	0.51*	-0.93***	0.70***
NEl	0.26	0.58**	-0.74***	0.59**	0.52*	-0.94***	0.68***
FOM	0.28	0.13	-0.02	-0.06	0.47*	-0.59**	-0.09
Biogas	0.28	0.13	-0.02	-0.06	0.47*	-0.59**	-0.09
Methane	0.28	0.13	-0.02	-0.06	0.47*	-0.59**	-0.09

	Crude sugar	NDF_{om}	ADF_{om}	EROM	ESOM	Crude ash	ME	NEl	FOM	Biogas
NDF_{om}	0.19									
ADF_{om}	-0.18	0.34								
EROM	-0.64**	0.28	0.71***							
ESOM	0.64**	-0.28	-0.71***	-1.00***						
Crude ash	0.77***	0.36	-0.08	-0.57**	0.57**					
ME	-0.56**	-0.84***	-0.46*	-0.10	0.10	-0.65***				
NEl	-0.54**	-0.84***	-0.49*	-0.14	0.14	-0.62**	1.00***			
FOM	0.29	-0.58**	-0.81***	-0.85***	0.85***	0.05	0.54**	0.57**		
Biogas	0.29	-0.58**	-0.81***	-0.85***	0.85***	0.05	0.54**	0.57**	1.00***	
Methane	0.29	-0.58**	-0.81***	-0.85***	0.85***	0.05	0.54**	0.57**	1.00***	1.00***

Statistical significance indicated with asterisks * $p < .05$, ** $p < .01$, *** $p < .001$. NDF_{om} - Organic neutral detergent fibre; ADF_{om} - Organic acid detergent fibre; EROM - Enzyme-resistant organic matter; ESOM - Enzyme-soluble organic matter; ME - Metabolizable energy; NEl - Net energy content for lactation; FOM - Fermentable organic matter

9 Conclusions and Outlook

The overall objectives of the present study were to estimate the ecosystem services provided by temperate grasslands under global change scenarios, to generally improve the monitoring of grassland ecosystem services, and to enable a better parametrization of the CFE in grasslands within climate-biogeochemical models. This resulted in three main aims, namely the assessment of the influence of environmental conditions on the CFE in grasslands, an improved assessment of potential above-ground productivity under future global change conditions, and the facilitation of a high-resolution spatio-temporal monitoring of grasslands by remote sensing techniques. To achieve these aims, the present study investigated and modelled the interacting effects of [eCO_2] and climatic drivers on grassland biomass productivity using the long-term GiFACE data (1998-2013), and explored the potential of hyperspectral techniques for an improved, non-destructive grassland monitoring providing data with high spatio-temporal resolution at low cost. The aims of the thesis resulted in three hypotheses being tested within five working packages leading to novel results and summarised in the following.

Located in a real-world environment the high correlations between environmental variables and varying CO_2 concentrations are factors which generally complicated the disentanglement of the influence of single environmental variables and the [eCO_2] on grassland above-ground productivity. Additionally, changes in the average weather conditions but also in the intensity and frequency of single extreme climatic events affect grassland productivity. To cope with this complexity different methods had to be developed, which resulted in two working packages (**WP 1** and **WP 2**) testing the following hypothesis:

H 1 The CO_2 fertilization effect is reduced under more extreme average weather conditions and after extreme climatic events

Within **WP 1**, the interacting effects of average weather conditions and varying CO_2 concentrations on above-ground biomass productivity were investigated applying the specifically developed moving subset analysis. The novelty of this method is the rejection of the factorial treatment design which dominated the analysis of FACE data since the origin of such experiments but has proven to be invalid in real-world experiments with a varying CO_2 enrichment. Instead, the novel method explores linear regression models between variables created by combinations of years with similar environmental conditions, and uses the actual [CO_2] (measured in the centre of each ring in the GiFACE experiment). Therefore, the quantification of the CFE remains robust against varying [CO_2]s which represents a clear advancement in the comparison to the conventionally used approaches (Nowak, 2017). The new approach is also applicable to other CO_2 enrichment studies, and is available to the public as CRAN R package "msaFACE" (Obermeier et al., 2016). The application of this approach to the GiFACE time series showed that the CFE was significant and strong under local average environmental conditions, but decreased as conditions became substantially wetter, drier or hotter than average. This was the first study within a single ecosystem which revealed that the greatest response to [eCO_2] has to be expected under average growth conditions to which plants have adapted in the long-term. Therefore, **part one of H 1 was confirmed**, which assumes a reduced CFE under more extreme average weather conditions.

In **WP 2**, a new method was developed linking the occurrence of single extreme climatic events to the strength of the CFE in the GiFACE. Results of this analysis based on the longest time available to date, encompassed reductions of the CFE if ECEs occurred during the growing season. The strongest decreases in the CFEs were associated with intensive and long heat waves, and could be quantified to a large extent ($\sim$30% variance of the magnitude of the CFE) by calculating the Killing Degree Days (KDDs). Thereby also **part two of H 1**, which assumes a reduced CFE when extreme climatic events occur, **was confirmed**. The results indicate that the classical carbon-centric theories, which suggest a stronger CFE at higher temperature or dryer conditions, seem only applicable within a certain range of growth conditions, when no other environmental factor except CO_2 limits the productivity. Since resource limitations by other factors than [CO_2] seem important when the range of long-term average growth conditions is exceeded, this

study suggested in line with a recent theory on plant growth (Fatichi et al., 2014; Körner, 2015), that a paradigm shift from the carbon centric view towards a more holistic perspective considering tissue formation and cell growth is urgently required.

By **confirming part one and two of H 1**, this thesis convincingly shows that the CO_2 fertilization effect is reduced under more extreme average weather conditions and after extreme climatic events, which is in clear contrast to the widely carbon-centric assumptions e.g. within numerical models.

The CFE on grassland was proven to be dependent on weather conditions. Consequently, **WP 3** investigated whether the positive influence of [eCO_2] or the potentially negative influences of the projected more extreme weather conditions will dominate above-ground biomass productivity in future, to test the following hypothesis:

H 2 Future increases in above-ground biomass productivity under elevated CO_2 concentrations more than compensate for potential biomass reductions due to global change-related environmental alterations

To estimate future grassland above-ground biomass based on the long-term experimental observations, a complex statistical approach was developed in **WP 3**. For the rings under [eCO_2] and [aCO_2] enrichment, individual statistical models on AGB were derived based on climate variables selected during an exhaustive selection approach based on the Akaike information criteria. The models were used to predict AGBs within potential future regimes by means of partial least squares regression techniques. The potential future regimes were generated by slightly modifying the ranges and relations of the selected climate variables during the experimental period. The results revealed that especially under hot and dry conditions above-ground biomass under [eCO_2] is below the average yields during the experimental period for both, rings under [eCO_2] and [aCO_2]. In contrast to the predictions of an increased future grassland productivity mainly due to [eCO_2] and warming by numerical models, the comparison of the potential future regimes with

the findings of IPCC projections revealed that grassland above-ground biomass is likely to be reduced in the mid of 21st century despite the increase in atmospheric CO_2 concentration.

Thus, the positive effect of [eCO_2] on biomass production cannot compensate for yield losses due to unfavourable environmental conditions that are likely to prevail in future, and **H 2 was rejected**.

The analysis of the long-term time series revealed strong interactions between varying CO_2 concentrations, average weather conditions (**WP 1**), single extreme climatic events (**WP 2**) and grassland above-ground productivity. However, due to the traditional, destructive sampling approach, these investigations were so far restricted to the harvest dates, and additional grassland traits have only rarely been measured due to the required cost-intensive laboratory analysis. To bridge this scale towards a spatially and temporally enhanced monitoring of multiple grassland traits, non-destructive and low-cost approaches are urgently needed. In order to meet this challenge, **WP 4** created the necessary prerequisites to enable an analysis of the predictability of different grassland ecosystem services by means of hyperspectral techniques within **WP 5**, to test the following hypothesis:

H 3 State-of-the-art remote sensing techniques enable the monitoring of grassland ecosystem services under high spatio-temporal resolutions within a FACE experiment

In **WP 4**, functions and classes were developed to manage, process, and analyse hyperspectral data with the open-source software CRAN R, and thus to provide the necessary tools for **WP 5**. Since the newly developed functions and classes greatly extend the previously existing functionalities in R, they have been made available to the public as CRAN R-package "hsdar" (Lehnert et al., in press). Within **WP 4**, a first case study showed promising results regarding the remotely sensed estimation of chlorophyll content of the vegetation within the GiFACE rings.

The newly developed functions were used within **WP 5**, for the first hyperspectral and non-destructive estimation of fourteen grassland traits related to ecosystem services within a FACE experiment. After a comprehensive preprocessing, various

hyperspectral predictors were derived by different transformation techniques and the calculation of known vegetation indices in the literature. The final predictor variables were selected by combining machine learning techniques with the variance inflation factor, and used to create predictive models between hyperspectral data and grassland traits using partial least squares regression techniques. Based on the information gained during the vegetative period it was shown how hyperspectral monitoring might be used e.g. to adapt harvest practices or gain deeper insights into physiological plant alterations under [eCO2].

Good to very good leave-one-out cross-validation results for the final models even under varying CO_2 concentrations **confirmed H 3** in that techniques for the monitoring of grassland ecosystem services under high spatio-temporal resolutions within a FACE experiment can be provided.

The analysis of the long-term data series and the hyperspectral analysis of various grassland traits revealed how complex ecosystems respond to multiple interacting factors that co-limit ecosystem processes. Therefore it is necessary to further improve the understanding of the underlying processes by in-depth analysis and to improve the integration of experimental observations into modelling efforts. Regarding the process understanding, the present thesis suggests that hyperspectral techniques could provide a remedy in future as their increased spatio-temporal resolution enables the detection of small but physiologically important differences in the response of plants, non-destructively and at low cost. Future applications of hyperspectral techniques range from phenotyping approaches within experimental sites to high temporal resolution and regional to large scale whole ecosystem assessments with satellite data once the required sensors become operational (e.g., ENMAP; Guanter et al. 2015). For an improved model parametrisation, the presented results might help ecosystem models to properly quantify the strength of the CFE, e.g., by the definition of environmental thresholds (e.g., local average conditions defined by $\pm$ 1 SD of long-term average conditions) or the implementation of new indices (e.g., KDDs). However, further and continued FACE experiments are needed because the limited number of replications and the mostly short-term duration of FACE experiments (resulting from the operational costs), as well as

their underrepresentatation in remote areas (insufficient infrastructure) hinders a global extrapolation of experimentally observed effects of [eCO_2].

In addition to the recommendations on future research needed, the results of the present studies fill an important research gap emphasised in the 5th IPCC assessment (IPCC, 2013) and can be seen as a continued wake-up call for policy makers. The provision of important ecosystem services such as forage production, biodiversity preservation and carbon storage seems uncertain in future. Grasslands might even become a carbon source much earlier than expected (e.g. Cox et al. 2000). Therefore, the increase of atmospheric [CO_2] and global warming might become accelerated, which in turn feeds back to a reduced grassland productivity, and in a vicious circle may lead to a further aggravation of the expected global changes. Alarmingly, such self-reinforcing feedback could rapidly lead to a crossing of the planetary boundary conditions for climate change and might push the Earth system into a new state (Steffen et al., 2015), possibly leading to a "Hothouse Earth" pathway even as man made emissions are reduced (Steffen et al., 2018). To counteract the foreseeable, devastating consequences of global climate change, policy makers should implement actions entailing the decarbonisation of the global economy, enhancement of biosphere carbon sinks, behavioural changes, technological innovations, new governance arrangements, and transformed social values (Heck et al., 2018; Steffen et al., 2018).

References

Cox, P.M., Betts, R.A., Jones, C.D., Spall, S.A., & Totterdell, I.J. (2000): Acceleration of global warming due to carbon-cycle feedbacks in a coupled climate model. *Nature*, 408, 184–187.

Fatichi, S., Leuzinger, S., & Körner, C. (2014): Moving beyond photosynthesis: From carbon source to sink-driven vegetation modeling. *New Phytologist*, 201, 4, 1086–1095.

Guanter, L., Kaufmann, H., Segl, K., Foerster, S., Rogass, C., Chabrillat, S., Kuester, T., Hollstein, A., Rossner, G., Chlebek, C., Straif, C., Fischer, S., Schrader, S., Storch, T., Heiden, U., Mueller, A., Bachmann, M., Mühle, H., Müller, R., Habermeyer, M., Ohndorf, A., Hill, J., Buddenbaum, H., Hostert, P., van der Linden, S., Leitão, P.J., Rabe, A., Doerffer, R., Krasemann, H., Xi, H., Mauser, W., Hank, T., Locherer, M., Rast, M., Staenz, K., & Sang, B. (2015): The EnMAP spaceborne imaging spectroscopy mission for earth observation. *Remote Sensing*, 7, 7, 8830–8857.

Heck, V., Hoff, H., Wirsenius, S., Meyer, C., & Kreft, H. (2018): Land use options for staying within the Planetary Boundaries – Synergies and trade-offs between global and local sustainability goals. *Global Environmental Change*, 49, 73–84.

IPCC (2013): Climate Change 2013: The Physical Science Basis. Contribution of Working Group I to the Fifth Assessment Report of the Intergovernmental Panel on Climate Change. *Intergovernmental Panel on Climate Change, Working Group I Contribution to the IPCC Fifth Assessment Report (AR5)(Cambridge Univ Press, New York).*

Körner, C. (2015): Paradigm shift in plant growth control. *Current Opinion in Plant Biology*, 25, 107–114.

Lehnert, L.W., Meyer, H., Obermeier, W.A., Silva, B., Regeling, B., & Bendix, J. (in press): Hyperspectral data analysis in R: the hsdar package. *Journal of Statistical Software*.

Nowak, R.S. (2017): CO_2 fertilization: Average is best. *Nature Publishing Group*, 7, 2, 101–102.

Obermeier, W., Lehnert, L., & Bendix, J. (2016): msaFACE. R package version 0.10.0.
URL `https://CRAN.R-project.org/package=msaFACE`

Steffen, W., Richardson, K., Rockström, J., Cornell, S.E., Fetzer, I., Bennett, E.M., Biggs, R., Carpenter, S.R., De Vries, W., De Wit, C.A., Folke, C., Gerten, D., Heinke, J., Mace, G.M., Persson, L.M., Ramanathan, V., Reyers, B., & Sörlin, S. (2015): Planetary boundaries: Guiding human development on a changing planet. *Science*, 347, 6223, 1259 855.

Steffen, W., Rockström, J., Richardson, K., Lenton, T.M., Folke, C., Liverman, D., Summerhayes, C.P., Barnosky, A.D., Cornell, S.E., Crucifix, M., Donges, J.F., Fetzer, I., Lade, S.J., Scheffer, M., Winkelmann, R., & Schellnhuber, H.J. (2018): Trajectories of the earth system in the anthropocene. *Proceedings of the National Academy of Sciences*, 201810 141.

Acknowledgements

This work is the result of the cooperation of many different individuals. To start with, I am very grateful to my supervisors Jörg Bendix and Lukas Lehnert for their guidance, without which this thesis would not exist in the present form. I want to deeply thank them for their helpful comments, fruitful discussions, and patience with me as well as their motivational efforts, when it was necessary. Additionally, I would like to thank all the people in the LOEWE $FACE_2FACE$ project and all the co-authors for their input to my research and at the same time for the pleasant time we shared together. I would greatly appreciate for this collaboration to maintain, and for some joint articles to follow in the future.

For the initiation, construction, installation and long-term, ongoing maintenance of the Giessen FACE experiment, I gratefully acknowledge the contribution of the following individuals: H.-J. Jäger (deceased 2013), S. Schmidt, L. Grünhage, C. Müller, G. Moser, M. Erbs, C. Kammann, J. Senkbeil, W. Stein, B. Lenz, J. Franz, T. Strohbusch, G. Mayer and A. Brück. The continued financial support of the Hessian Agency for Nature Conservation, Environment and Geology is gratefully acknowledged, since it allowed an exceptionally long data set to be obtained. Moreover, the generous funding by the LOEWE excellence cluster $FACE_2FACE$ of the Hessian State Ministry of Higher Education, Research and the Arts is gratefully acknowledged.

A special thanks goes to my colleagues at the Laboratory for Climatology and Remote Sensing at the Philipps-University of Marburg, who supported me in many situations ranging from minor everyday problems to scientific discussions or simply by reminding me to eat. Namely, I thank S. Achilles, M. Pohl, S. Makowski Gianonni, G. Curaola Fernández, S. Egli, M. Schulz, F. Rüthrich, M. Dobbermann, C. Wallis, N. Turini, C. Kolbe, K. Trachte, R. Rollenbeck, and B. Thies for their wide-ranging assistance. Moreover, I would like to thank B. Kühne-Bialozyt and C. Philippi for their constant efforts when I struggled with administrative challenges. Thanks go to the PhD commission for taking the time to read through this little book and, thus, contributing to the completion of my PhD.

Most of all, however, thank you to my family, friends and multiple flatmates for providing inspiration, ongoing patience and space.

Erklärung

Ich erkläre an Eides statt, dass ich meine Dissertation mit dem Titel

"Future ecosystem services of temperate grasslands:
bridging scales towards high-resolution spatio-temporal monitoring"

selbstständig ohne unerlaubte Hilfe angefertigt und mich dabei keinerlei anderen als der von mir ausdrücklich bezeichneten Quellen und Hilfen bedient habe.
Die Dissertation wurde in der jetzigen oder einer ähnlichen Form noch bei keiner anderen Hochschule eingereicht und hat noch keinen sonstigen Prüfungszwecken gedient.

Marburg a. d. Lahn, den 02.10.2018

Wolfgang Alexander Obermeier